A COMPUTATIONAL RE-ASSESSMENT OF SEXUAL DIMORPHISM IN THE HUMAN CRANIUM BEYOND TRADITIONAL MORPHOMETRICS: GEOMETRIC MORPHOMETRIC METHODS AND NEURAL NETWORK ANALYSIS

Antonietta Del Bove

A computational re-assessment of sexual dimorphism in the human cranium beyond traditional morphometrics: geometric morphometric methods and neural network analysis

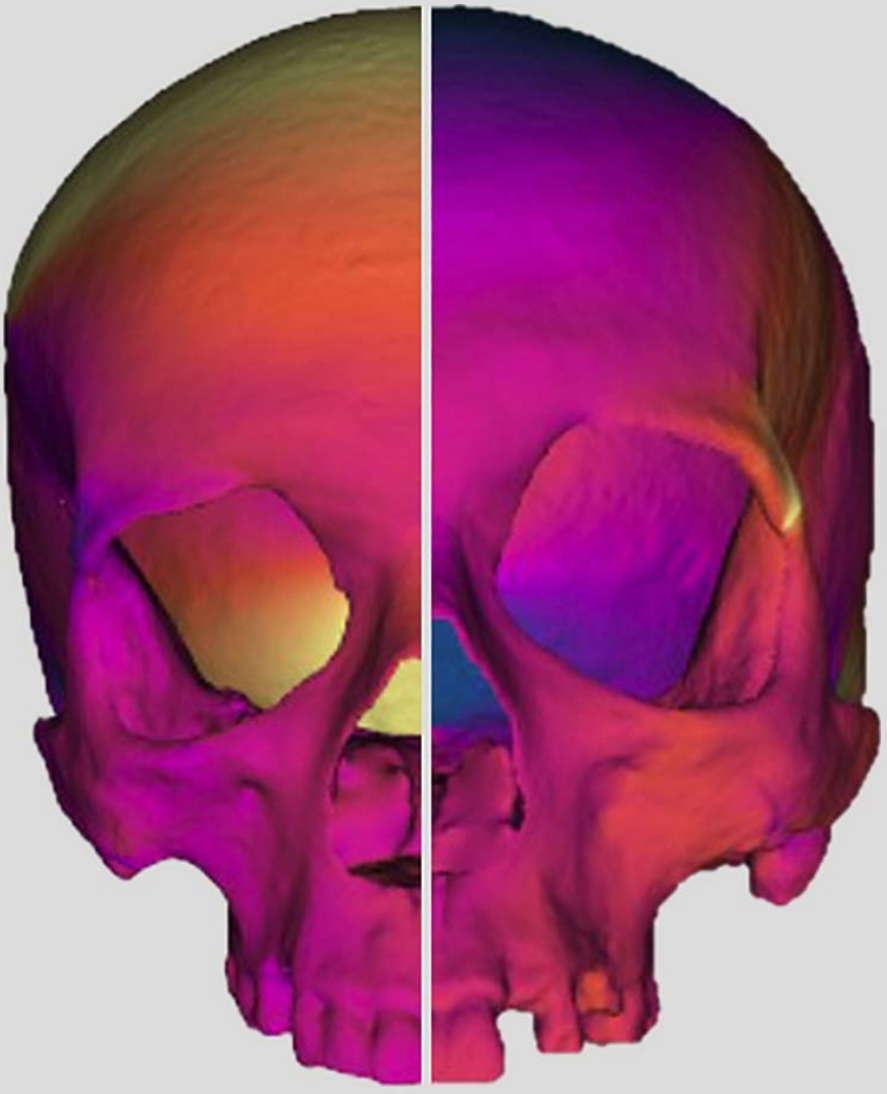

Antonietta Del Bove

- Doctoral thesis 2023 -

UNIVERSITAT ROVIRA i VIRGILI

UNIVERSITAT ROVIRA I VIRGILI
A COMPUTATIONAL RE-ASSESSMENT OF SEXUAL DIMORPHISM IN THE HUMAN CRANIUM BEYOND TRADITIONAL MORPHOMETRICS: GEOMETRIC MORPHOMETRIC METHODS AND NEURAL NETWORK ANALYSIS
Antonietta Del Bove

Antonietta Del Bove

A computational re-assessment of sexual dimorphism in the human cranium beyond traditional morphometrics: geometric morphometric methods and neural network analysis

Doctoral thesis

Supervised by
Prof. Carlos Lorenzo
Dr. Antonio Profico

UNIVERSITAT ROVIRA i VIRGILI

Tarragona
2023

UNIVERSITAT ROVIRA I VIRGILI
A COMPUTATIONAL RE-ASSESSMENT OF SEXUAL DIMORPHISM IN THE HUMAN CRANIUM BEYOND TRADITIONAL MORPHOMETRICS: GEOMETRIC MORPHOMETRIC METHODS AND NEURAL NETWORK ANALYSIS
Antonietta Del Bove

UNIVERSITAT ROVIRA i VIRGILI

FAIG CONSTAR que aquest treball, titulat “A computational re-assessment of sexual dimorphism in the human cranium beyond traditional morphometrics: geomètric morphometric methods and neural network analysis”, que presenta Antonietta Del Bove per a l’obtenció del títol de Doctor, ha estat realitzat sota la meva direcció al Departament d’Historia i Historia de l’Art d’aquesta universitat.

HAGO CONSTAR que el presente trabajo, titulado““A computational re-assessment of sexual dimorphism in the human cranium beyond traditional morphometrics: geomètric morphometric methods and neural network analysis”, que presenta Antonietta Del Bove para la obtención del título de Doctor, ha sido realizado bajo mi dirección en el Departamento de Historia e Historia del Arte de esta universidad.

I STATE that the present study, entitled“A computational re-assessment of sexual dimorphism in the human cranium beyond traditional morphometrics: geomètric morphometric methods and neural network analysis, presented by Antonietta Del Bove for the award of the degree of Doctor, has been carried out under my supervision at the Department of History and History of Art of this university.

Tarragona, 04/10/2023

El/s director/s de la tesi doctoral
El/los director/es de la tesis doctoral
Doctoral Thesis Supervisor/s

Carlos Lorenzo Merino

Antonio Profico

"I think that history appeals to you as it appealed to me when I was your age because it concerns living men and everything that concerns men, as many men as possible, all the men in the world as they come together in society, work, struggle, and improve themselves. It cannot fail to appeal to you more than anything else."

" Io penso che la storia ti piace come piaceva a me quando avevo la tua età , perchè riguarda gli uomini viventi e tutto ciò che riguarda gli uomini, quanti più uomini è possibile, tutti gli uomini del mondo in quanto si uniscono tra loro in società e lavorano e lottano e migliorano se stessi non può non piacerti più di ogni altra cosa. "

Letter to Delio, Antonio Gramsci

A mia madre,

a mio fratello

e a te Erasmo.

Index

Abstract

The primary objective of this Ph.D. dissertation is to advance the study and understanding sexual dimorphism in modern human crania. To achieve these objectives, we first explore which anatomical features are suitable for establishing sexual dimorphism. Secondly, we introduce a novel method for determining the sex of human crania.

To fulfill these aims, we apply the Geometric Morphometrics approach to a diverse geographical sample of crania. Our research encompasses three distinct studies, one focusing on the neurocranium, another on the frontal bone, and the final one on the entire cranium, involving a total of 228 individuals, both female and male.In pursuit of the second objective, we conduct a Neural Network Analysis using 10 linear measurements. We employ a craniometric worldwide dataset for this analysis.

The results derived from these four studies demonstrate the utility of both Geometric Morphometrics and Neural Network Analysis in advancing our understanding of sexual dimorphism in human crania. Specifically, our GM approach reveals that the frontal bone plays a pivotal role in elucidating morphological differences between males and females in human crania. In each study, sexual dimorphism in the frontal bone consistently exhibits significant patterns. Our analysis encompasses considerations of shape, form, and size. Within the realm of form space, the results highlight the significance of the nasal aperture and mastoid process in conveying sexual dimorphic signals. Notably, the occipital bone exhibits an entirely absent dimorphic signal, a departure from conventional literature. When we focus on the three most distinguishing dimorphic traits (glabella, supraciliary ridge, and mastoid process), we achieve an accuracy rate of 77%.

Furthermore, leveraging insights gained from anatomical studies, we develop a new method based on an extensive measurement dataset. We employ Howell's dataset for validation and training steps and the craniometric dataset from the University of Tennessee to construct a model for sex determination in complete crania. The resulting model is reproducible and exhibits an impressive accuracy rate of 84%.

Resum

L'objectiu principal d'aquesta tesi de doctorat és avançar en l'estudi i la comprensió del dimorfisme sexual en els cranis humans moderns. Per aconseguir aquests objectius, primerament explorem quines són les característiques anatòmiques adequades per establir el dimorfisme sexual. En segon lloc, introduïm un mètode innovador per determinar el sexe dels cranis humans.

Per complir aquests objectius, apliquem l'enfocament de Morfometria Geomètrica a una mostra geogràfica diversa de cranis. La nostra recerca abasta tres estudis diferents, un centrat en el neurocrani, un altre en l'os frontal i l'últim en el crani complet, amb un total de 228 individus, tant dones com homes.

A la recerca del segon objectiu, realitzem un Neural Network Analysis utilitzant 10 mesures lineals. Emprarem un conjunt de dades global per a aquest anàlisi.

Els resultats obtinguts d'aquests quatre estudis demostren la utilitat tant de la Morfometria Geomètrica com de la Neural Network Analysis en l'avanç de la nostra comprensió del dimorfisme sexual en els cranis humans. Específicament, el nostre enfocament de Morfometria Geomètrica revela que l'os frontal juga un paper fonamental en l'aclareixement de les diferències morfològiques entre el dos sexes en els cranis humans. En cada estudi, el dimorfisme sexual en l'os frontal mostra patrons consistentment significatius. La nostra anàlisi abasta consideracions de forma, estructura i mida. En l'àmbit de l'estructura (form), els nostres resultats destaquen la importància de l'obertura nasal i el procés mastoïdal en la transmissió de senyals dimòrfics sexuals. Notablement, l'os occipital mostra una senyal dimòrfica totalment absent, a diferència de la literatura convencional. Quan ens centrem en els tres trets dimòrfics més destacats (glabel·la, cresta supraorbitària i procés mastoïdal), assolim una accuracy del 77%.

A més, aprofitant les idees obtingudes d'estudis anatòmics, desenvolupem un nou mètode basat en un extens conjunt de mesures. Emprarem el conjunt de dades de Howell per a la validació i la formació, juntament amb el conjunt de dades cranimètriques de la Universitat de Tennessee, per construir un model de determinació del sexe en cranis complets. El model obtingut és reproductible i presenta una impressionant accuracy del 84%.

Resumen

El objetivo principal de esta tesis de doctorado es avanzar en el estudio y la comprensión del dimorfismo sexual en los cráneos humanos modernos. Para lograr estos objetivos, primero exploramos cuáles son las características anatómicas adecuadas para establecer el dimorfismo sexual. En segundo lugar, introducimos un método novedoso para determinar el sexo de los cráneos humanos.

Para cumplir con estos objetivos, aplicamos el enfoque de Morfometría Geométrica a una muestra de proveniencia geográficas variadas de cráneos. Nuestra investigación abarca tres estudios distintos, uno centrado en el neurocráneo, otro en el hueso frontal y el último en el cráneo completo, involucrando un total de 228 individuos, tanto mujeres como hombres.

En busca del segundo objetivo, realizamos un Neural Network Analysis utilizando 10 mediciones lineales. Empleamos un conjunto de datos global para este análisis.

Los resultados derivados de estos cuatro estudios demuestran la utilidad tanto de la Morfometría Geométrica como del Neural Network Analysis en el avance de nuestra comprensión del dimorfismo sexual en los cráneos humanos. Específicamente, nuestro enfoque de Morfometría Geométrica revela que el hueso frontal desempeña un papel fundamental en la elucidación de las diferencias morfológicas entre lo dos sexos en los cráneos humanos. En cada estudio, el dimorfismo sexual en el hueso frontal muestra patrones consistentemente significativos. Nuestro análisis abarca consideraciones de forma, estructura y tamaño. En el ámbito de la estructura, nuestros resultados resaltan la importancia de la abertura nasal y el proceso mastoideo en la transmisión de señales dimórficas sexuales. Notablemente, el hueso occipital muestra una señal dimórfica completamente ausente, a diferencia de la literatura convencional. Cuando nos enfocamos en los tres rasgos dimórficos más distintivos (glabella, cresta supraorbitaria y proceso mastoideo), alcanzamos una accuracy del 77%.

Además, aprovechando las ideas obtenidas de los estudios anatómicos, desarrollamos un nuevo método basado en un extenso conjunto de mediciones. Empleamos el conjunto de datos de Howell para la validación y el entrenamiento, junto con el conjunto de datos craniométricos de la Universidad de Tennessee, para construir un modelo de determinación del sexo en cráneos completos. El modelo resultante es reproducible y presenta una accuracy del 84%.

UNIVERSITAT ROVIRA I VIRGILI
A COMPUTATIONAL RE-ASSESSMENT OF SEXUAL DIMORPHISM IN THE HUMAN CRANIUM BEYOND TRADITIONAL MORPHOMETRICS: GEOMETRIC MORPHOMETRIC METHODS AND NEURAL NETWORK ANALYSIS
Antonietta Del Bove

1. Introduction

1.2 State of the art

Sexual dimorphism refers to physical differences between individuals of the same species (Fairbairn, 1997) and it is a popular topic among naturalists, biologists, physical anthropologists, and paleoanthropologists. In biological anthropology, the interest in studying sexual dimorphic traits has a twofold meaning: i) understanding the mechanisms, and external and internal factors involved in the process of emergence of sexual dimorphic traits; ii) developing and applying a method able to identify sex from skeletal elements. Among humans, sexual dimorphism has been the subject of ongoing discussion, particularly with regard to differences in primary and secondary sex characteristics and sexual behavior. It is important to note that sexual dimorphism is distinct from gender, which refers to the social and cultural roles and behaviors associated with an individual. Gender is a social construct that can vary based on culture, time period, ethnicity, religion, and sexual orientation (Frayer & Wolpoff, 1985; Gentile, 1993; Glucksmann, 1981). Sexual dimorphism (SD) has been studied for a long time, but many questions remain unanswered. This chapter has multiple aims. The first part will focus on the overview of previous studies on the human cranium SD. The second part will investigate the new methodologies applied to the study of SD. Lastly, the current state of knowledge and limitations of current methods in detecting sex from the human skull will be described. Irrespective of specific fields such as physical anthropology, forensic anthropology, and bio-archaeology, the determination of an individual's sex through the analysis of human remains constitutes a pivotal aspect within these disciplines (Cattaneo & Grandi, 2004; Duday, 2009; Lozano et al., 2021; Lugli et al., 2020; White & Folkens, 2005). In the domain of forensics, sex identification is indispensable for reconstructing the identities of victims; in archaeology, it aids in reconstructing the demographic composition of ancient populations; and in biology, it contributes to characterizing intraspecific morphological variations attributed to sexual dimorphism (Stewart, 1979; Ubelaker

& DeGaglia, 2017). However, distinct methodologies are employed across the various anthropological domains. For instance, forensic practices are guided by national laws and regulations, while in archaeology, the level of uncertainty is relatively lower and contingent on the preservation state of skeletal remains.

1.2 Tracing the history of investigation of Sexual Dimorphism in the human cranium.

Fig. 1. Skeleton of a female individual, the letters indicate the anatomical regions that differ between the two sexes. Original drawing by Felix Platter, De corporis humani structura (1583), Book 3 (Stolberg, 2003).

The study of skeletal differences between sexes began in the 16th century with the Age of Enlightenment. The pioneering work of Andreas Vesalius in 1543, *"De humani corporis fabrica libri septem"* (On the fabric of the human body), may be considered one of the first comparisons between the two forms of skeletons (Vesalius et al., 1973). Another work by Felix Platter, *"De corporis humani structura et usu libri III"* in 1583, described peculiar features of the female skeleton (Stolberg, 2003) with an important drawing that highlighted the differences between female and male skeletons. The increase in the investigation occurred in the 17th century with Albinus (1749), Ackermann (1788), and others, in correspondence with the publication of important anatomy manuals (Schiebinger, 2015).

While differences between sexes were noted during the 17th century, it took much longer than expected to develop a method to reconstruct the sex from the inspection of skeletal remains. In the 1800s, anthropologists began to develop a method to establish sex based on cranial measurements. Later, in 1830, Morton assigned sex to his collection according to cranial capacity (Lewis et al., 2011). However, the first real breakthrough may have been Dureau's publication, which claimed 90% accuracy in establishing sex (Giles & Elliot, 1963). Moving into the 1900s, with forensic cases, there were more reports of studies clearly identifying human remains as belonging to women or men (Harrington, 1911).

In 1919, Hrdliča published an article about the differences in the male and female skulls, providing a method for sex estimation. Hrdliča (1919) starts his work "*Someday it may be possible to write on the actual state of anthropometry in general, and on the many individual modifications of and tendencies in the same which are outside of international agreements; but what the student of the branch in this country needs now are simple, practical, well-tested instructions for his guidance in work which is rapidly increasing*". The method proposed was based on differences in measurements of the cranial vault between males and females and, some differences in shapes between the two sexes.

The research on sexual dimorphism focuses on investigating the anatomical differences in skull structures between males and females. This thesis specifically examines the cranium (excluding the mandible), which includes the neurocranium and splanchnocranium (see Materials and Methods). Before delving into the anatomical characteristics that distinguish the sexes in the cranium, it is crucial to acknowledge the inherent complexity of this structure. Comprising eight bones (frontal, parietal, temporal, occipital, sphenoid, and ethmoid bones), the human cranium serves multiple functions. Firstly, it provides protection for the brain and sensory organs. Additionally, it serves as a structural support for the face and contains the initial segments of the digestive and respiratory systems (Werner Platzer, 2014).The morphology of the cranium is shaped and influenced by several factors such as age (Urban et al., 2016), ancestry, diet, epigenetic traits, pathology, and sex, (Ackermann, 2002; González-José et al., 2005; Guglielmino-Matessi et al., 1979; Lieberman et al., 2000).

Glossary of defined terms	
SEX ASSESSMENT	the term indicates the assessment of sex without scientific rigor based on morphological assessment practices. Defined by Spradley and Jantz (2011) as "morphological traits with no estimable error rates, classification rates, or any associated statistics"(Spradley & Jantz, 2011).
SEX DETERMINATION	determination or establish means to assign the sex exactly. It is used to talk about results that are 100% accurate or very close, for example, DNA analysis.
SEX ESTIMATION	the terminology estimating is used when dealing with metric methods of measuring bones such as the femur, humerus, etc. For metric methods, it is possible to calculate the rate error (Moore, 2013; Spradley & Jantz, 2011).
QUALITATIVE METHOD:	defines a method based on appearance, size, and aspect. It would be more appropriate to talk about the morphological method. It is the same as the "non-metric method". A proper alternative is called that methodologies "Morphological Method".
MORPHOSCOPIC/MACROSCOPIC	defines method based on the presence or absence of some feature, or degree of development of a particular character. Macroscopic is a more recent technical term (Hefner, 2009), while morphoscopic is an original term introduced in the XVIII century (A. Christensen et al., 2014; Dirkmaat, 2012).
QUANTITATIVE METHOD	is a contrary of qualitative, defines a method based on a metric. In the case of SD for example is applied in the case of measurement of the neck of the length's femur or humerus.

Fig. 2. Glossary of the terms commonly used in physical anthropology to refers to sexual dimorphism studies.

One of the most extensively investigated aspects of sexual dimorphism pertains to size differences between the two sexes. It is a recurrent observation to find references in literature that associate a gracile skull with females and a robust skull with males (Cattaneo & Grandi, 2004). However, when delving into intraspecific variations beyond mere size discrepancies, it becomes imperative to acknowledge that cranial morphology inherently encompasses variations stemming from diverse factors. These factors encompass allometric influences, hierarchical integration among distinct cranial bones, and microevolutionary processes arising from a complex interplay of multiple influences (Bruner, 2007; Von Cramon-Taubadel, 2014). Situated within the confines of this thesis, which is inherently dedicated to the methodical examination and meticulous analysis of the influence exerted

by sexual dimorphism upon the intricate architecture of the cranial structure, it is crucial to emphasize that the impact of sexual discrepancies is not uniformly distributed across the entirety of the cranium. Additionally, not all anatomical attributes are equally prone to the effects of these variations, with a conspicuous level of intraspecific variability determining the degree to which these distinctions manifest (Relethford, 1994).Among the principal accomplishments achieved within this thesis, a noteworthy feat is the creation of a cranial cartography structured within the framework of sexual dimorphism. The arsenal of diverse quantitative methodologies employed, including geometric morphometry, has served to illuminate the fact that the configuration of cranial traits is not universally subject to alteration due to sexual dimorphism. This study further establishes that specific traits have been influenced in ways distinct from those detailed in previous literature. Moreover, our research substantiates that the amalgamation of the most dimorphic traits yields sex estimations that are not only more precise but also more efficacious. This confluence of findings significantly enriches our comprehension of the intricate interplay between sexual dimorphism and the morphology of the cranial structure, thus substantially contributing to the advancement of knowledge within this domain. Broca, one of the most influential physical anthropologists and anatomists of the last century in his work identified the following anatomical elements as the most sexual dimorphic: glabella, frontal curve, frontal eminence, superciliary arch, supraorbital lines, the inion, occipital lines, occipital condyles, styloid process, mastoid apophysis, and sulcus of digastric muscle for the neurocranium and the cranial base. For the splanchnocranium, the dimorphic features recognized by Broca are the infraorbital margin, canine fossa, palatine bone, size of teeth, and nasal cavity (Broca, 1875).

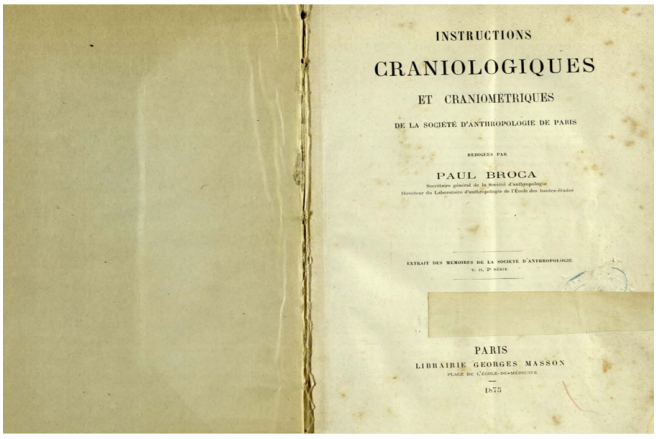
INSTRUCTIONS
CRANIOLOGIQUES
ET CRANIOMETRIQUES
DE LA SOCIÉTÉ D'ANTHROPOLOGIE DE PARIS
PAUL BROCA
PARIS
LIBRAIRIE GEORGES MASSON
1875

Fig. 3. Broca's Original copy of the first page of " Instructions craniologiques et craniometriques" in 1875.

Acsadi and Nemeskeri (1970) proposed a method to identify sex based on the visual inspection of skeletal elements. The Acsadi-Nemeskeri method is a scoring system used in the day-to-day work of the laboratory. It is based on the definition of the degree of expression or presence/absence of certain cranial features to determine whether an individual is male or female. The scoring system developed by Acsadi and Nemeskeri was the standard methodology used to distinguish sex based on cranial features. Acsadi and Nemeskeri's method identifies five specific anatomical features and defines the particular characteristics that should be evaluated to assign a score. These morphological traits are not general but rather specific and must be assessed based on their degree of development, which differs between sexes. The method also provides detailed instructions for the positioning of the skull before the assessment is made by the operators, anthropologists, technicians, and scholars (Buikstra & Ubelaker, 1994; Ubelaker, 2021). For example, in the case of the nuchal crest, it should be observed in a lateral position, and any roughness in the area of muscle attachment should be identified through touch. Similarly, the skull should be positioned in a lateral view of the glabella. In the case of the mastoid process, the volume of the

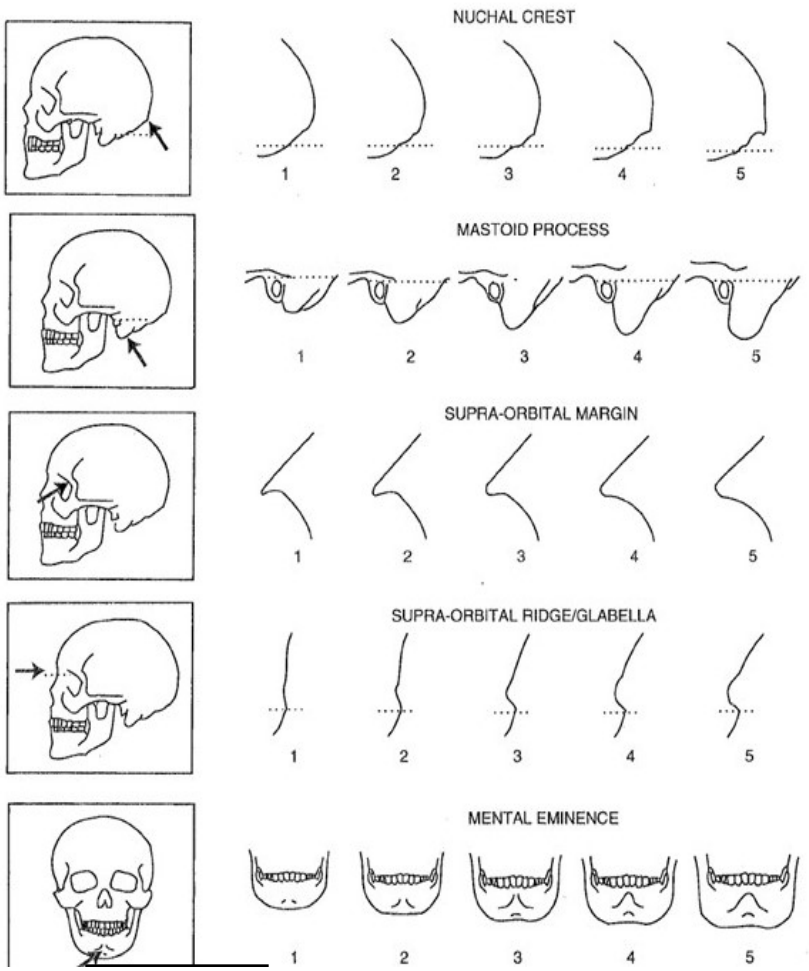

Fig. 4. Fig. 4. Scoring system by Acsadi e Nemeskeri, 1970

process should be considered, rather than its length. Finally, to evaluate the score of the supraorbital margin, the thickness should be assessed using the feel of one's finger. Twenty years after the Acsadi & Nemeskeri method, another milestone work in physical anthropology was published, "The Standards for data collection from human skeletal remains", edited by Jane E. Buikstra and Douglas H. Ubelaker in 1994 (Buikstra & Ubelaker, 1994). The Standards were developed to improve the collection and identification of Native American skeletal remains and to facilitate the repatriation process (Walrath et al., 2004).

The document includes a comprehensive review of skeletal morphologies, as well as defined landmarks and metric traits. It provides a compendium of approaches for establishing and assessing the ages and sexes of individuals being examined. In terms of sex determination from the skull, the Standards provide a more detailed review of the Acsadi & Nemeskeri method.

The first attempt to use morphometrics to identify sex from the skeletal collection is the work developed by Gilles & Elliot (1963). They proposed a mathematical model (multivariate linear discriminant analysis) to classify sex as a set of linear cranial measurements. They collected a sample of skulls with known sex and acquired a series of measurements, including cranial capacity, bizygomatic diameter, and basion-bregma height to build a predictive model. This method proved to be a significant improvement over the previous

qualitative methods, as it relied on objective measurements rather than subjective assessments of anatomical features. However, it still had limitations, such as the requirement for a large sample of skulls with known sex and the potential for variation within a population that could affect the accuracy of the predictions. Subsequently, recent studies mainly followed two approaches. The first is the morphological approach, as previously explained, based on score system techniques for the various morphological features (Pinto et al., 2016; Walker, 2008; Walrath et al., 2004). The second is the morphometric approach based on the application of statistical methods on a set of shape variables (Birkby, 1966; Claudio et al., 2008). Linear measurements offer the advantage of simplicity in replication. The measurement procedure is comparably cost-effective, necessitating only the utilization of a caliper or digital landmarks for acquisition. Nonetheless, they are constrained by the inherent limitation of reducing the multidimensional concept of three-dimensional form into a quantification confined to two dimensions, namely linear measurements. This transition inevitably results in a diminution of intricate morphological intricacies during the analytical process. Quantifying shape in a measurable way is a problem with a long history, dating back to D'Arcy Thompson's work in the early 20th century (Richtsmeier et al., 1992). The objective of studies during that time was to capture the geometry of an object, rather than simply describe a few variables (Blackith & Reyment, 1971; Rohlf & Leslie, 1993).

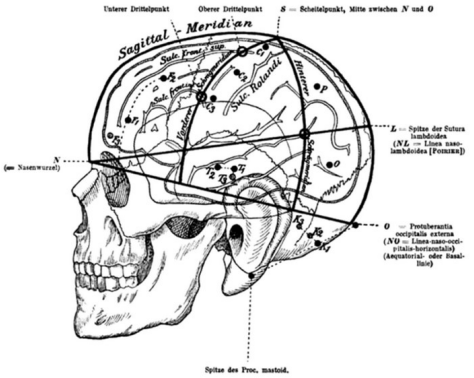

Fig. 5. Example of craniometric measurements by Neisser and Pollack' Mitt Grenzgeb, 1904 (Serletis & Glenn Pait, 2016)

Over the last decade, the use of geometric morphometrics and 3D techniques, which were previously only used in medical analyses, have emerged as a new application for anthropologists to complement traditional anthropology (Weber, 2015). The field of Geometric Morphometrics (GM) emerged through the combination of morphological shape description with statistical analysis (Adams et al., 2004; O'Higgins, 2000; Rohlf & Marcus, 1993). By integrating GM with statistical analysis, it becomes possible to visualize the pattern of shape variations among different shapes or groups of shapes. Mathematically, the shape is defined as all sets of geometric features of an object except its size, position, and orientation (Dryden & Mardia, 1998; Kendall, 1977).

As techniques have progressed, using landmarks has been considered a more stable method. Landmarks refer to the Cartesian coordinates (x, y, and z) of anatomical points that respect the rule of biological homology. Homology refers to anatomical points that correspond across all individuals and are related to the concepts of development and evolution. In 1843, Owell and subsequently Boyden 1943 defined homology as a concept denoting structural similarity. It was only following the publication of "On the Origin of Species" that the definition evolved to encompass "structural similarity resulting from selection for common ancestry" (Wood S.W., 1995).

The analysis involves considering 2 or 3-dimensional biological coordinates and removing variables that are correlated with scale, position, and rotation before conducting the analysis (Bookstein, 1991; Rohlf & Marcus, 1993). To understand how shapes are compa-

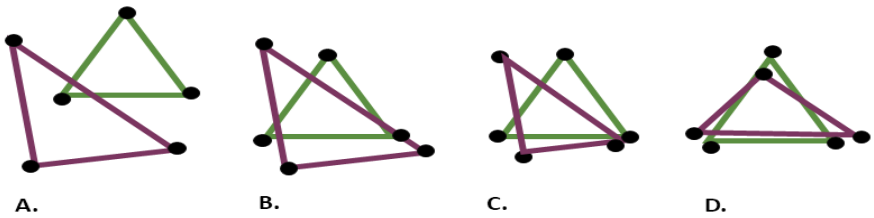

Fig. 6. The three steps of Procrustes superimposition: translation to a common origin, scaling to unit centroid size, and rotation to minimize the sum of squared Euclidean distances among the homologous landmarks. The resulting landmark coordinates are called Procrustes shape coordinates. A: raw landmarks, B: centered landmarks, C: centered and scaled landmarks, and D: centered scaled, and rotated landmarks.

red, it is essential to mention Procrustes Analysis (GPA). GPA is used to minimize the difference in landmark configurations. The method consists of translation, rotation, and after scaling each configuration of landmarks subtracting a central size (Rohlf & Slice, 1990).

The GM analysis could be in 2D or in 3D, depending on the technique of acquisition for example X-Ray, computed tomography (CT scan), or models via photogrammetry. The development of virtual anthropology in the last 20 years represents a revolution (Weber, 2001). Nowadays, is relatively easy to focus on the acquisition of a 3D model of each anatomical bone or trait. The principal manner to acquire 3D models in anthropology in the last years is with the use of photogrammetry, laser scanners, CT scan, and, micro CT scan. All of that allows us to create a digital version of the skeletal element (Profico et al., 2019; Uldin, 2017; Weber, 2015). It is not surprising that GM has been widely used to answer many questions about SD. The progress of research can be illustrated by advances in methodology, from craniometric analyses of entire crania (Franklin et al., 2005; Kranioti et al., 2008) to more focused studies of specific traits such as the os petrous (Wahl & Graw, 2001), foramen magnum (Kanchan et al., 2013), mastoid process, or 2D analyses, such as studies of the occipital and temporal bones (Boucherie et al., 2022), frontal bone (Čechová et al., 2019), mastoid process (Saini et al., 2012), brow ridge, and chin (Garvin & Ruff, 2012), and later views of cranial traits (Gonzalez et al., 2011), as well as the cranial base (Lestrel et al., 2005). With the introduction and use of 3D models, studies have increased for all cranial traits (Abdel Fatah et al., 2014; Dereli et al., 2018; Franklin et al., 2007; Green & Curnoe, 2009; Kelley & Tallman, 2022). Of course, 3D modeling has also been applied to single traits, such as studies of the palate and cranial base (Chovalopoulou et al., 2013; Rooppakhun et al., 2010), craniofacial morphology (Bejdová et al., 2018; Bigoni et al., 2010; Chovalopoulou et al., 2016; Hennessy et al., 2002), cortical thickness of cranial bones (Lillie et al., 2016), and, the neurocranium (Chovalopoulou et al., 2016).

In the field of Science and Engineering, the use of artificial intelligence (AI) provides an alternative solution (Monson et al., 2018). AI is a broad term that includes different approaches, such as Machine Learning, Deep Learning, and Neural Network Analysis. Machine Learning and Deep Learning are both categories of AI. In brief, Machine Learning is an AI method that can automatically adapt with little human intervention. On the other hand, Deep Learning is a type of Machine Learning that employs artificial neural networks to simulate how the human brain learns (Alpaydin, 2020; Bishop, 2006; Patterson & Gibson, 2017). Recently, AI has been increasingly applied to solve dilemmas in physical anthropology (Cao et al., 2022; Lo et al., 2023; Nikita & Nikitas, 2020). Techniques like Machine Learning and Deep Learning enable the solution of problems such as regression, classification, and clustering. For instance, in literature, AI is utilized to solve questions about ancestry classification (Hefner & Ousley, 2014; Navega et al., 2015). Similarly, AI has been used to address sexual dimorphisms, such as determining the sex from the analysis of the femur bone (Curate et al., 2017; du Jardin et al., 2009), sex estimation of the length of bones in the Asian population (Darmawan et al., 2015), differences of the morphology of the patella between sexes (Mahfouz et al., 2007)(Navega et al., 2015), dimorphic differences in tarsal bone and the coxal bone between sexes. However, to apply these methods, a large dataset is required since the aim of AI is to develop an algorithm that can learn from data and verify other datasets after training (Alpaydin, 2020; Bishop, 2006). One limitation of AI is the use of the black box method, which makes it challenging to understand for non-experts in the field (Bishop, 2006). Machine Learning Machine Learning and Neural Network analysis have been utilized to address the problem of sex classification of the skull ((Bewes et al., 2019; Cappella et al., 2020; Gao et al., 2018)). Most studies employ large datasets of linear measurements (Pozzi et al., 2020), or CT scans and 3D models (Bewes et al., 2019; Gao et al., 2018). For example, a study conducted on a specific Italian population using Linear Discriminant Analysis and Machine Learning methods achieved an accuracy of approximately 70% (Pozzi et al., 2020). Another study by Bewes et al. (2019) shows how the Neural Network Analysis could be used with the CT scan images for the study of SD.

1.3 Sexual differences in human cranial morphology

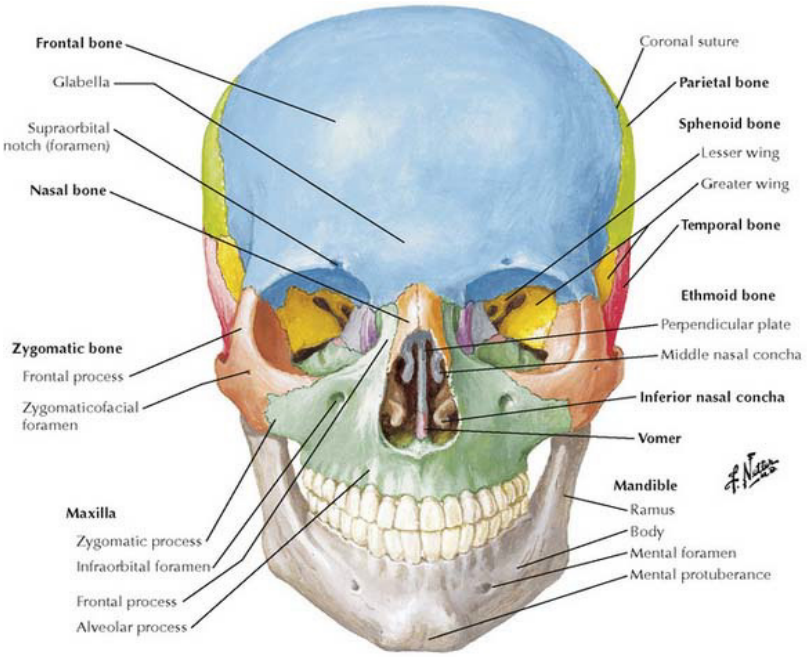

Fig. 7. Anatomical image of the skull by Netter, Atlas of Human Anatomy 6th ed. 2008.

This paragraph describes the dimorphic features of the skull as described in the literature, which are divided into macro-regions of interest: the craniofacial area or splanchnocranium, calvarium, and cranial base. More studies in the literature focus on the region of the frontal bone (glabella and supraorbital ridges) and the mastoid process, as these anatomical traits are considered key factors for estimating the sex of individuals.

However, for a long time, the principal differences between male and female crania were considered to be robustness and size (Broca, 1875; Garvin et al., 2014). Females were generally considered to have less robust crania than males. Recent studies have shown that robustness cannot be used as a discriminant factor for sex estimation, as an individual's size is correlated with factors such as diet, health, provenance, and genetics (Bhola et al., 2011). In addition, different populations are characterized by different mean cranial sizes.

The neurocranium macro area is the cranial region most studied when the aim is the identification of sex. The most diagnostic region to identify SD from the analysis of the frontal bone is the glabellar region it is considered the most dimorphic anatomical trait (Bejdová et al., 2018; Chovalopoulou et al., 2016; Walker, 2008). The glabella is a landmark located in the center of the frontal bone, between the supraorbital margins. Ubelaker (1994) defines the glabella as "the most anterior point on the frontal bone, usually above the frontonasal suture". Before the age of 14 years, the glabella was flat, but after that,

it showed a protuberance in males but not in females (Anzelmo et al., 2015). To evaluate the glabella using the traditional method (Acsádi and Nemeskeri., 1970; Walker, 2008), it must be analysed in the lateral view. With GM approaches an effort was made to evaluate the deformation of two in the extremes of shape variation obtained by Thin-plate spines (TPS). In males, the protuberances are more pronounced for the entire magnitude while in females only along the caudal end (Perlaza, 2014).

The frontal bone is more dimorphic than other bones in the cranium (Čechová et al., 2019). The orbital region has also been extensively investigated for sexual dimorphism. Morphologically, the thickness of the orbital margin's upper part can be used to determine sex, with a sharper margin indicating females and a more rounded edge indicating males (Acsádi & Nemeskéri, 1970; Graw et al., 1999; Walker, 2008). The orbital shape outline is also considered dimorphic in some studies (Bigoni et al., 2010; Canci & Minozzi, 2005; White & Folkens, 2000). It is also noted that male orbits are shorter than female orbits, with the male edges placed more superiorly and posteriorly. Female orbits are considered slightly larger (Bejdová et al., 2018). The deeper and more pronounced orbit in males is attributed to the more developed brow ridge in males (Gonzalez et al., 2011). Bigoni highlights the different positions of the orbits between sexes, with males parallel to the frontal plane and females slightly angled in the sagittal plane (Bigoni et al., 2010). However, some publications using GM declare that the orbits are not reliable anatomical traits to distinguish sex (Bigoni et al., 2010; Chovalopoulou et al., 2016), while others confirm the opposite (Lidstone, 2011).

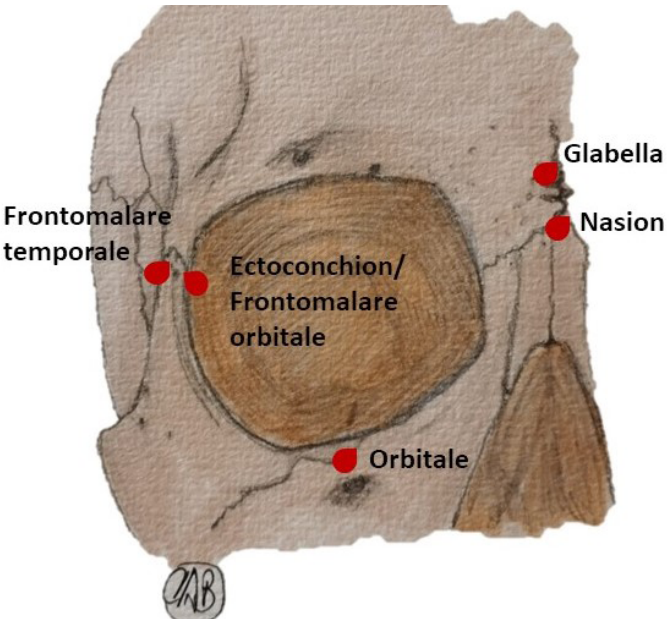

Fig. 8. Frontal bone with the landmark used during the Gm analysis. (Drawing by A. Del Bove)

The shape outline of the orbits, whether rounded or squared, is also controversial, with studies only finding differences between populations (Garvin et al., 2014; Garvin & Ruff, 2012). The supraorbital ridges are a key anatomical feature for sex estimation in craniometry. While classical morphometric studies already identified differences in size and shape of the supraorbital ridges between males and females, more recent approaches using geometric morphometrics have demonstrated that the difference in size between the sexes increases the accuracy of sex estimation by up to 80% (Garvin & Ruff, 2012). Moreover, the dimorphic signal in the supraorbital ridges appears to be stable and consistent across different populations, making it a reliable indicator of sex in forensic and archaeological contexts.

In terms of cranial measurements, males have a shorter distance between the right and left frontotemporale, while the distance between the frontomalare temporale and the frontotemporale orbitale (also known as Ectoconchion) is wider. This could be attributed to the positioning of three points, glabella, frontomalare temporale, and frontotemporale orbital, which are sharper in women (Chovalopoulou et al., 2016). Frontomalare temporale is a landmark localized in the most lateral point on the frontomalare suture, frontotemporale is a landmark positioned in temporal lines in the most anteromedial position on the frontal, and the frontotemporale orbitale or ectoconchion is the landmark in the intersection of the most anterior surface of the lateral border of the orbit in the suture between the frontal bones and zygomatic bone (Ubelaker & DeGaglia, 2017). The hypothesis proposes that the higher protrusion of the glabella in males causes swelling in "lateral transects" not found in females. The thickness of the orbits, on the other hand, is believed to be a response to the different development of brow ridges and glabella protuberances between the sexes (Garvin & Ruff, 2012).

Furthermore, research has revealed that the temporal lines in the area of the frontal bone display a moderately more concave shape in females, whereas the midsagittal line has a sharper angle in the bregma region in males. It is noteworthy that the profile of the frontal bone has traditionally been characterized as vertical in females and horizontal in males (Čechová et al., 2019).

According to Bigoni (2010), the neurocranium of females is more spherical along the midsagittal line, while in males, the bregma landmark is positioned higher. The upper and middle face area is marked by size variations that serve as the most reliable indicators of sexual dimorphism. Typically, males have wider faces than females (Bigoni et al., 2010). Among these characteristics, the zygomatic bone contributes considerably to the increase in facial width and is usually wider and higher in males than in females. Statistically significant differences were found for both sex and population signals in the zygomatic bone through multivariate analysis of variance. The geometric morphometric approach used to study the zygomatic bone revealed that in males, the inferior margin is expanded more in the inferior and frontal directions than in females, resulting in greater shape variance. The

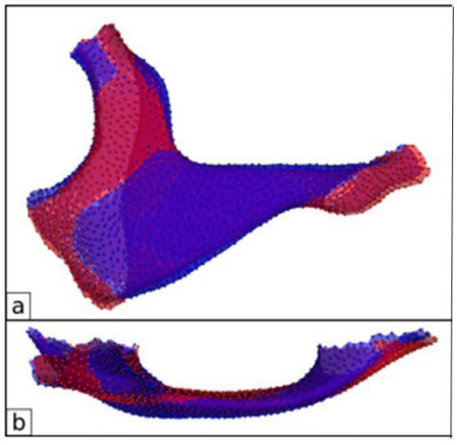

Fig. 8. Shape differences between male and female average shapes (exaggerated by factor 2; (a) lateral view; (b) viewed from superior. Blue: male; red: female.

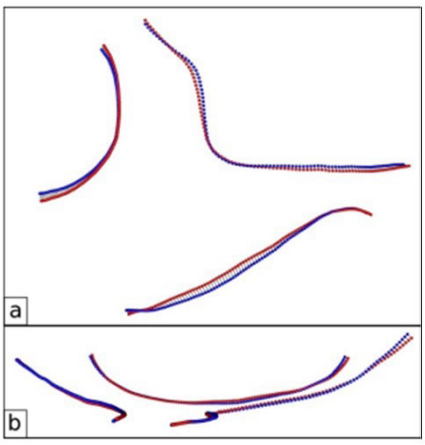

Fig. 9. Differences between male and female average curve shapes (exaggerated by factor 2; (a) lateral view; (b) viewed from superior. Blue: male; red: female.

Fig. 9. Shape variations of the result of the study of zygomatic bone (Schlager & Rüdell, 2017)

curvature of the arch (Fig. 9) is also stronger in males, with a more pronounced bowing in the direction of the temporal. Additionally, the zygomatic bone in males is wider in the vertical position (Schlager & Rüdell, 2017). However, some studies suggest that the zygomatic bone may be less dimorphic than the supraorbital ridges and glabella regions. For example, correct sex estimation using the zygomatic bone ranges from 60.12% to 68.2% (Gonzalez et al., 2011).

Moving to the facial region, the nasal region is another area of interest. Due to its high variability among populations, the signal of sexual dimorphism in the nasal region may be more controversial or more closely correlated to population variation than other cranial traits (Chovalopoulou et al., 2016). Bigoni (2010) analysed the distance from the landmark nasion and the nasospinale and found slight slippage at the anterior face in males.

In addition, the nasal region of males tends to have a narrower and deeper nasal aperture, while females have a wider nasal base aperture around the medial base of the aperture. The accuracy of this method is around 77%. Lopez et al. (2009) confirmed differences in shape by analysing mixed "ancestry" populations from Brazil, noting that the nasal aperture is higher in males than in females across all groups. That confirms the hypothesis that the signal of population genetic composition is stronger than the signal of sexual dimorphism in the nasal region (Gustafsson et al., 2007; Safont et al., 2000).

The height of the internal maxillary sinus shows the same signal of sexual dimorphism with an accuracy greater than 70% (Paknahad et al., 2017). However, there is a lack of specific literature on the external part of the maxilla for sexual dimorphism.

In the lateral view, the signal of sex differentiation of the mastoid process in the temporal bones is highly pronounced, as supported by multiple studies (Acsádi & Nemeskéri, 1970; Ubelaker, 2021; Walker, 2008). The mastoid process serves as a reliable anatomical marker for sexual dimorphism in the cranium. Many studies have consistently employed mastoid process volume to classify individuals by sex. The mastoid process in females is less prominent; in males is bigger, larger, and more robust (Acsádi & Nemeskéri, 1970; Broca, 1875; Christensen et al., 2014; Garvin & Ruff, 2012b; Stewart, 1979; Ubelaker & DeGaglia, 2017; Walker, 2008; White & Folkens, 2005; Wilkinson, 2004). It is noteworthy that the mastoid process undergoes significant ontogenetic development, being absent in neonatal stages and gradually appearing during the first year of life. Recent studies have employed morphometrics analysis to capture variations in mastoid process shape. The underlying hypothesis posits differential growth rates between girls and boys, resulting in size discrepancies during adulthood (Petaros et al., 2015). Another hypothesis suggests that differences in musculature between males and females, particularly in the sternocleidomastoid, splenius *capitis*, and longissimus *capitis* muscles, may contribute to the observed variations (Paiva & Segre, 2003). Certain studies have defined a mastoid triangle, which involves measuring the distances between three fixed landmarks: Mastoidale (lower point of the mastoid process), Asterion (junction of the occipital, temporal, and parietal bones), and Porion (upper margin of each ear canal). The distances from Porion to Mastoid have demonstrated statistical significance in sex discrimination, with an accuracy rate of approximately 70% (Kemkes & Göbel, 2006).

In the posterior region of the cranial bones, the occipital protuberance, specifically the external occipital protuberance located at the highest point known as the inion, is of particular interest. Differences between males and females are described based on the

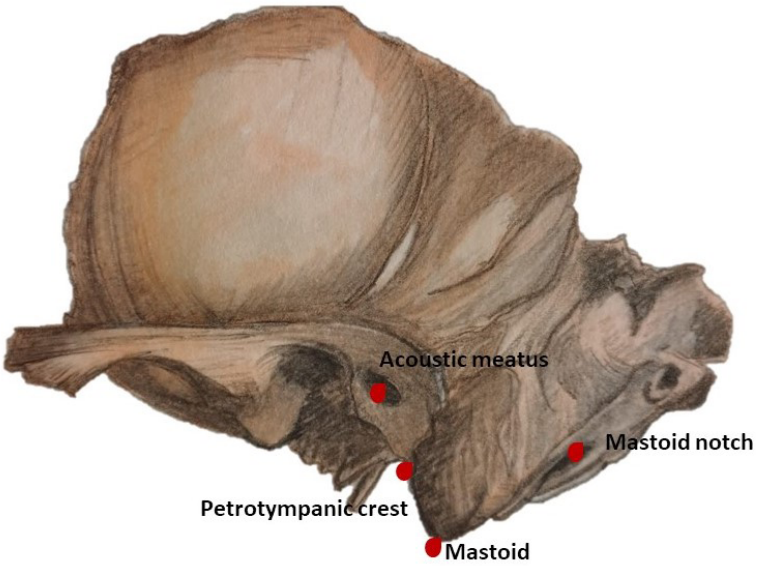

Fig. 10. Part of the temporal bone with the mastoid process (Drawing by A. Del Bove)

projection of this protuberance, which corresponds to the attachment point of the nuchal and trapezius muscles, as well as the nuchal ligament. Females typically exhibit rugosity in this area, while males display pronounced and well-defined nuchal lines with a hooked and externally prominent appearance.

The literature shows some disagreements regarding the statistical significance of occipital protuberances and their correlation with sexual dimorphism (Krüger et al., 2015). However, there are studies supporting this correlation (Gapert et al., 2009; Gapert & Last, 2008; Gülekon & Turgut, 2003; Holland, 1986; Hsiao et al., 2010; Isaza et al., 2014; Macaluso, 2011; Nikita & Michopoulou, 2018). The challenge in defining the shape of the nuchal crest is more determined by sexual dimorphic signals or biomechanical stress. That is because the nuchal area, where ligaments are attached, is responsible for head rotation and increased activity. Notably, some intriguing studies have linked variations in nuchal crest development to running capacity (Swindler & Wood, 1973) studies focused on gender differences in labor, as observed in hunter-gatherer populations (Hoover & Thomas, 2022). Another parameter to consider is the length from lambda to inion, which is typically greater in males (Olivier, 1975). Which results in long occipital bones for male individuals. Within the cranial base, two dimorphic traits of interest are the foramen magnum and the occipital condyles. The foramen magnum is a large aperture that serves as a passageway connecting the central nervous system, encompassing the brain and spinal cord, with the skull. Its maximum development occurs around the age of 7, reflecting early dimorphic developmental patterns preceding the onset of puberty (Scheuer & Black, 2000). A smaller length is typically associated with females, while a wider length is observed in males (Catalina-Herrera, 1987; Dean Holland, 1986; Zdilla et al., 2017). Although the foramen magnum is often utilized for metric evaluation,

the assessment of the occipital condyles is frequently overlooked. In terms of morphological parameters, females tend to exhibit a shorter bicondylar breadth compared to males (Dean Holland, 1986; Gangrade et al., 2013; Kunar & Nagar, 2014; Macaluso, 2011; Sholapurkar et al., 2017). Similar to the nuchal crest, the presence of bio-mechanical factors is evident in the occipital condyles, as they are directly influenced by movements of the first cervical vertebra, facilitating head rotation, flexion, and extension. Asymmetry between the right and left condyles can be attributed to handedness uses (Uysal et al., 2005). In this regard, studies suggest that dimorphic traits in occipital condyles are correlated with differences in activity or bio-mechanical stresses (Gapert et al., 2009; Marino, 1995; Wescott & Moore-Jansen, 2001), such as gender-based divisions of labor (Hoover & Thomas, 2022).

1.4 Problematic synthesis: where we are and where we should go

The primary objective of anthropologists is to investigate cranial morphology and discern the signal of sexual dimorphism while considering the influence of various factors, including ancestry, age, diet, and genetic factors. However, disentangling the specific effects of sexual dimorphism from these complex variables poses significant challenges in anthropological studies (Smith et al., 2021).

In comparison to other primates, the degree of sexual dimorphism in humans is generally less pronounced (Fleagle, 2013). Consequently, differentiating between sexes based solely on specific bone regions in humans is not straightforward. Furthermore, the literature emphasizes that cranial features exhibit a more nuanced nature compared to other skeletal elements, where sexual dimorphism is more readily apparent, such as in the pelvis (Fischer & Mitteroecker, 2017). As a result, it becomes a natural inquiry to question the binomial nature of sexual dimorphism, leading to overlapping traits between sexes, even when results are examined through descriptive statistical analyses.

In the examination of sexual dimorphism and its impact on morphological differences between males and females, it is crucial to acknowledge the potential distortions introduced by each variable. Among these variables, the age of individuals included in the study sample holds significant importance. Age plays a critical role in the investigation of sexual dimorphism, with a focus on adult age ranges in many studies. However, caution must be exercised when including older individuals, particularly older than 60 years old, as age-related changes can introduce bias. Additionally, tooth loss in maxillary traits can further contribute to alterations in cranial morphology (Velemínská et al., 2021).

These complexities underline the need for careful consideration and controlled methodologies when analyzing sexual dimorphism in cranial morphology. As mentioned earlier, it is important to recognize that not all cranial traits develop at the same age. For instance, the development of the foramen magnum ceases at a particular age, while other traits, such as the glabella, begin to develop after puberty (Scheuer & Black, 2000). This emphasizes the significance of considering the ontogenesis of sexual dimorphism. However, it is unfortunate that compared to the literature focusing on sexual dimorphism in adults,

there remains limited research on the timing of puberty for sex determination in young individuals. This is primarily due to the challenges posed by different growth models of hormones in males and females during this developmental stage (Worthman, 1995).

Ancestry, referring to the geographical region of origin of individuals, is another crucial factor in the study of human morphology (Christensen & Crowder, 2009; Dunn et al., 2020). Currently, ancestry is often categorized into European, Asian, and African, as these represent the major geographic regions of ancestral origin (Digangi & Hefner, 2015).

Evolutionary processes such as gene flow and genetic drift contribute to the diversification of human populations. The recognition of ancestry is typically accomplished through the morpho-macroscopic or metric analysis of specific traits. It is widely accepted that relying on a single diagnostic trait for determining ancestry is not sufficient, and instead, multiple traits must be considered when examining unidentified human remains (Digangi & Hefner, 2015). However, there is an exception for the shovel-shaped incisors found in the Asian population, as this trait demonstrates a high discrimination rate of 70-85% (Hefner, 2009; Scott & Turner, 1997; Rhine, 1990).

It is important to note that forensic anthropology has raised doubts about the concept of ancestry. In a letter to the editor of the Journal of Forensic Science, experts have expressed concerns about defining specific groups based on assumed clear laws of heredity. They argue that not considering the movements of people complicates the classification of ancestry. Moreover, the letter serves as a political manifesto, highlighting the unfortunate presence of discrimination in the field of forensics (Bethard & DiGangi, 2020).

While their concerns are relevant to current forensic practices, we believe that until all anthropological disciplines universally adopt alternative approaches, it is reasonable to consider ancestry as a biological factor indicative of an individual's origin. Many traits used to determine the population of origin are also the same traits investigated for sexual dimorphisms, such as the zygomatic arch, nasal aperture, and alveolar prognathism (Caple et al., 2018). As mentioned earlier in the description of the anatomical features of the skull, this can sometimes lead to confusion when distinguishing traits influenced by sex from those influenced by geographic variation. Additionally, it has been noted in the literature that the growth rate differs not only between sexes but also among populations (Ashizawa et al., 2005).

Another significant aspect of research on sexual dimorphism in populations is that many of the methods discussed in the literature are tailored to specific populations. For instance, the Ubelaker method,i.e. which serves as the foundation for skeletal identification, was originally developed for a particular population. This is influenced by two factors:

Firstly, conducting research on a global scale is challenging to execute. Although the use of 3D models has made it more feasible in recent times, not all repositories provide open access to such data, which restricts the availability of comprehensive worldwide samples.

Secondly, research tends to be more focused and specific because the accuracy of findings increases when studying a restricted population or sample, compared to attempting to generalize findings to the entire global population. However, this can create challenges when attempting to evaluate populations that are unknown or differ from those for which the methods were initially developed.

Furthermore, the proliferation of studies in recent scientific literature on sexual dimorphism has led to the accumulation of more information and specific findings. While this contributes to a deeper understanding of sexual dimorphism, it also poses challenges when comparing results obtained using different methodologies and specific populations.

In conclusion, the specific nature of population-based research methods and the increasing number of studies focusing on sexual dimorphism create both advantages and difficulties in terms of obtaining comprehensive and comparable results across different populations.

2. Main object

Despite the considerable body of literature addressing Sexual Dimorphism (SD) in humans, numerous aspects of this phenomenon remain ambiguous, leaving several questions unanswered. A notable observation from previous reviews is the disproportionate emphasis on investigating SD within specific anatomical regions, rather than examining the entire cranium comprehensively. Additionally, existing research often concentrates on limited geographic populations or restricted areas of study. Consequently, it has become increasingly difficult to develop a novel quantitative methodology capable of accurately determining the sex of human crania, comparable in accuracy to DNA analysis.

The primary objective of this thesis is to contribute to the study of Sexual Dimorphism in the entire cranium of *Homo sapiens* using innovative approaches. By building upon novel methodologies compared to previous studies, we aim to identify the specific regions of the cranium exhibiting sexual dimorphism. Additionally, we seek to determine the consistency of previously identified dimorphic points in the literature and ascertain whether they exhibit variations influenced by secondary factors. A crucial goal of the thesis is to create a comprehensive map of sexual dimorphism in the human cranium, encompassing diverse populations without specific limitations.

To achieve these objectives, we employed samples from various repositories known to belong to individuals of different sexes from populations spanning the 19th and 20th centuries. Two methodologies were used to address these research objectives: the Geometric Morphometrics Approach and Neural Network Analysis (refer to Chapter 3 for details).

These selected methodologies align with our objective of identifying traits associated with Sexual Dimorphism with enhanced accuracy. A novel approach utilizing linear mea-

surements analysis was also developed to establish a new method for determining sex in human remains. Both approaches reflect the inherent necessity in scientific research for new quantitative methods that offer measurable accuracy and reproducibility.

2.1 Specific objectives

This thesis consisted of four distinct sessions, each with its own set of objectives.

I) Sexual dimorphism in the **Neurocranium**

Objective: Utilize *a non-priori* method to analyse the entire neurocranium and identify the anatomical regions that exhibit the most pronounced sexual dimorphism. Additionally, thanks of union to Geometric morphometric and virtual anthropology, aim to visually represent the differences in shape variation between males and females within these regions.

Publication paper: detection of sexual dimorphism in the neurocranium at local scale. Antonietta Del Bove, Antonio Profico, Carlos Lorenzo. *2019 IMEKO TC4 International Conference on Metrology for Archaeology and Cultural Heritage, MetroArchaeo 2019*, 2019, pp. 571–575.

Presented in the following meeting: ESHE Meeting 2019. Title of poster: Sexual dimorphism in the human calvarium: a Geometric Morphometric approach. Authors: Antonietta Del Bove, Antonio Profico, Ana Bucchi, Carlos Lorenzo.

II) Sexual Dimorphism in the **Frontal Bone**

Objective: Using a geometric morphometric approach, this study aimed to analyse the main anatomical traits of the human frontal bone. The objectives of this research were two-fold: firstly, to explore the variations in frontal bone morphology between males and females, and secondly, to identify the specific regions of the frontal bone that display sexual dimorphism.

Publication paper: A geometric morphometric approach to the study of sexual dimorphism in the modern human frontal bone. Del Bove, A., Profico, A., Riga, A., Bucchi, A., Lorenzo, C. *American Journal of Physical Anthropology*, 2020, 173(4), pp. 643–654.

(Presented in the following meeting) Conference: XXIII congress dell'Associazione Antropologica Italiana. 2019 Geometric Morphometric analysis of the sexual dimorphism in human frontal bone. Authors: Antonietta Del Bove, Antonio Profico, Carlos Lorenzo.

ESHE meeting 2018. Sexual dimorphism in human frontal bone: a landmark-based approach. Authors: Antonietta Del Bove, Antonio Profico, Carlos Lorenzo.

III) Sexual dimorphism in the **entire crania** and creation of a new map of sexual dimorphism anatomical traits.

Objective: in that work we explore the possibility of studying sexual dimorphism at a local scale, building a model to measure the accuracy of each small portion of the cranium to obtain a self-explained 3D map of accuracy.

Publication paper accepted: Mapping sexual dimorphism signal in the human cranium. Antonietta Del Bove, Lumila Menéndez, Giorgio Manzi, Jacopo Moggi Cecchi, Carlos Lorenzo, Antonio Profico in *Scientific Report.*

Presented in the following meeting: ESHE 2020. Automatic detection of sexual dimorphic traits in the human cranium. Antonietta Del Bove, Antonio Profico & Carlos Lorenzo.

IV) Neural network Analysis approach: a new method to establish the sex in human modern **crania**.

Objective: To address the limitations associated with a specific population, we have devised a neural network approach that embraces inclusivity by accommodating diverse populations. The primary objective of our research is to employ extensive training and testing datasets from various sources, with a particular emphasis on prioritizing the probability of estimation rather than absolute accuracy. The significance of this work lies in its provision of a versatile estimation method that can be easily applied to different datasets, irrespective of ancestral backgrounds. Furthermore, our study highlights the potential of quantitative, algorithm-based estimation of sex based on cranial features, placing a greater emphasis on probability as a priority over accuracy. In addition, we present a comprehensive, step-by-step protocol for the application of machine learning-based predictions, aimed at addressing fundamental issues within the field of physical anthropology.

Publication paper: A Generalised Neural Network Model to Estimate Sex from Cranial Metric Traits: A Robust Training and Testing Approach. Del Bove, A., Veneziano, A. *Applied Sciences*, 2022, 12(18), 9285.

Presented in the following meeting: ESHE 2023. Unravelling sexual dimorphism in human crania: in-depth exploration using Neural Networks Antonietta Del Bove, Antonio Profico, Carlos Lorenzo, Alessio Veneziano.

UNIVERSITAT ROVIRA I VIRGILI
A COMPUTATIONAL RE-ASSESSMENT OF SEXUAL DIMORPHISM IN THE HUMAN CRANIUM BEYOND TRADITIONAL MORPHOMETRICS: GEOMETRIC MORPHOMETRIC METHODS AND NEURAL NETWORK ANALYSIS
Antonietta Del Bove

3. Materials and Methods

In order to accomplish the objectives of this thesis work, the focus was solely on the collection of human crania. The sample used in this study was obtained from various repositories acquired throughout the course of the Ph.D. research. The acquisition of materials occurred at different stages, specifically to address the specific objectives of each single paper.

It is important to note that not all individuals were included in every paper, and the analysis of cranial morphology varied across different papers. To avoid redundancy and unnecessary repetition of information already present in each paper, the material section of this chapter provides a comprehensive overview of the entire sample, augmenting the incomplete information provided in the respective material sections of each paper.

The chapter is divided into two parts: the first part delves into the GM approach, while the second part explores the NNA. Both sections are centred around the examination of sexual dimorphism. In the first section, the focus is on the research paper concerning the neurocranium, while in the second section, the study shifts its attention to the frontal bone. The third section encompasses the study of the entire cranium. The last work is included in the second part due to its emphasis on developing a new methodology for determining sex through Neural Network Analysis.

Part 1:

3.1.1 Samples and repositories

The whole sample comes from different repositories:

i. Anthropological Museum of University of Florence (Italy)

ii. Anthropological Museum "G. Sergi" of University of Rome Sapienza (Italy)

iii. Smithsonian National Museum of Natural History (USA)

iv. The digital collection NESPOS (The Neanderthal Tools, EU program "Digi-cult") (Germany)

v. Museum of Natural Science, Universidad nacional de la Plata (Argentina)

vi. The New Mexico Decedent Image Database (USA)

A deliberate selection criterion was applied for methodological rigor, including only adult individuals of known sex and devoid of pathological diseases that could influence cranial morphology. The sample comprised a total of 228 individuals, with 112 females and 116 males, ensuring a balanced representation of both sexes (Table 1)

Table 1

Complete study sample

Numer of identification	Sex	Repositories	Age of death	3D modelling	Population
F0007	Female	UNIFI	-	Photogrammetry	Sardinian
F0023	Female	UNIFI	-	Photogrammetry	Sardinian
F0131	Female	UNIFI	24	Photogrammetry	Florentine
F0165	Female	UNIFI	23	Photogrammetry	Florentine
F0313	Female	MDLP	-	Ct scan	Mapuche
F0314	Female	MDLP	-	Ct scan	Mapuche
F0315	Female	MDLP	-	Ct scan	Mapuche
F0316	Female	MDLP	-	Ct scan	Mapuche
F0317	Female	MDLP	-	Ct scan	Mapuche
F0323	Female	MDLP	-	Ct scan	Mapuche
F0343	Female	MDLP	-	Ct scan	Chubut
F0345	Female	MDLP	-	Ct scan	Chubut
F0356	Female	MDLP	-	Ct scan	Chubut
F0368	Female	MDLP	-	Ct scan	Pampa Grande
F0369	Female	MDLP	-	Ct scan	Pampa Grande
F0372	Female	MDLP	-	Ct scan	Pampa Grande

F0378	Female	MDLP	-	Ct scan	Pampa Grande
F0405	Female	UNIFI	30	Photogrammetry	Florentine
F0414	Female	UNIFI	30	Photogrammetry	Florentine
F0418	Female	UNIFI	26	Photogrammetry	Florentine
F0730	Female	UNIFI	34	Photogrammetry	Florentine
F0840	Female	Terry C.	32	Ct scan	North American
F0860	Female	UNIFI	43	Photogrammetry	Florentine
F0868	Female	UNIFI	38	Photogrammetry	Florentine
F0870	Female	UNIFI	35	Photogrammetry	Florentine
F0872	Female	UNIFI	-	Photogrammetry	Florentine
F0880	Female	UNIFI	31	Photogrammetry	Florentine
F0886	Female	Oloriz C.	59	Ct scan	Spanish
F0906	Female	Terry C.	22	Ct scan	North American
F0921	Female	Terry C.	38	Ct scan	North American
F0929	Female	Terry C.	20	Ct scan	North American
F0970	Female	Terry C.	21	Ct scan	North American
F100229	Female	NMDID	31	Ct scan	no Hispanic
F100263	Female	NMDID	51	Ct scan	no Hispanic
F100442	Female	NMDID	34	Ct scan	no Hispanic
F100487	Female	NMDID	28	Ct scan	no Hispanic
F100516	Female	NMDID	55	Ct scan	no Hispanic
F100541	Female	NMDID	49	Ct scan	Hispanic Latin
F101106	Female	NMDID	42	Ct scan	no Hispanic
F101356	Female	NMDID	41	Ct scan	no Hispanic
F101377	Female	NMDID	24	Ct scan	no Hispanic
F1015	Female	Terry C.	41	Ct scan	North American
F101798	Female	NMDID	50	Ct scan	no Hispanic
F103668	Female	NMDID	27	Ct scan	Native american
F104103	Female	NMDID	38	Ct scan	Hispanic Latin
F104125	Female	NMDID	27	Ct scan	Hispanic Latin
F104719	Female	NMDID	42	Ct scan	Hispanic Latin
F1052	Female	Terry C.	48	Ct scan	North American
F105208	Female	NMDID	31	Ct scan	Unknow
F105294	Female	NMDID	40	Ct scan	Hispanic Latin
F105475	Female	NMDID	42	Ct scan	Hispanic Latin
F106044	Female	NMDID	39	Ct scan	Hispanic Latin
F106212	Female	NMDID	22	Ct scan	Hispanic Latin
F1064	Female	Terry C.	33	Ct scan	North American
F107434	Female	NMDID	23	Ct scan	Native american
F108398	Female	NMDID	37	Ct scan	Native american
F109148	Female	NMDID	27	Ct scan	Native american
F111392	Female	NMDID	49	Ct scan	Native american
F1135	Female	Terry C.	62	Ct scan	North American
F115842	Female	NMDID	40	Ct scan	Native american
F1197	Female	Oloriz C.	30	Ct scan	Spanish
F1199	Female	Oloriz C.	39	Ct scan	Spanish

F1306	Female	Terry C.	36	Ct scan	North American
F1333	Female	Terry C.	33	Ct scan	NorthAmerican
F1360	Female	UNIFI	50	Photogrammetry	Florentine
F1370	Female	UNIFI	20	Photogrammetry	Florentine
F1381	Female	UNIFI	31	Photogrammetry	Florentine
F1383	Female	UNIFI	28	Photogrammetry	Florentine
F1384	Female	UNIFI	30	Photogrammetry	Florentine
F1405	Female	UNIFI	38	Photogrammetry	Florentine
F1411	Female	UNIFI	26	Photogrammetry	Florentine
F1419	Female	UNIFI	26	Photogrammetry	Florentine
F1428	Female	Oloriz C.	77	Ct scan	Spanish
F1517	Female	UNIFI	-	Photogrammetry	Sardinian
F1523	Female	UNIFI	-	Photogrammetry	Sardinian
F1552	Female	UNIFI	-	Photogrammetry	Sardinian
F1553	Female	UNIFI	-	Photogrammetry	Sardinian
F1763	Female	UNIFI	39	Photogrammetry	Florentine
F1764	Female	UNIFI	44	Photogrammetry	Florentine
F1771	Female	UNIFI	24	Photogrammetry	Florentine
F1777	Female	UNIFI	24	Photogrammetry	Florentine
F1785	Female	UNIFI	23	Photogrammetry	Florentine
F1786	Female	UNIFI	39	Photogrammetry	Florentine
F1790	Female	UNIFI	20	Photogrammetry	Florentine
F2535	Female	UNIROMA1	-	Photogrammetry	Mod Roman
F2537	Female	UNIROMA1	-	Photogrammetry	Mod Roman
F2538	Female	UNIROMA1	-	Photogrammetry	Mod Roman
F2539	Female	UNIROMA1	-	Photogrammetry	Mod Roman
F2540	Female	UNIROMA1	-	Photogrammetry	Bolognesi
F2541	Female	UNIROMA1	-	Photogrammetry	Bolognesi
F2543	Female	UNIROMA1	-	Photogrammetry	Bolognesi
F2544	Female	UNIROMA1	-	Photogrammetry	Bolognesi
F2545	Female	UNIROMA1	-	Photogrammetry	Bolognesi
F2546	Female	UNIROMA1	-	Photogrammetry	Bolognesi
F2547	Female	UNIROMA1	-	Photogrammetry	Bolognesi
F2548	Female	UNIROMA1	-	Photogrammetry	Bolognesi
F2550	Female	UNIROMA1	-	Photogrammetry	Bolognesi
F2551	Female	UNIROMA1	-	Photogrammetry	Bolognesi
F2552	Female	UNIROMA1	-	Photogrammetry	Bolognesi
F2553	Female	UNIROMA1	-	Photogrammetry	Bolognesi
F4874	Female	UNIFI	49	Photogrammetry	Syracusan
F4880	Female	UNIFI	37	Photogrammetry	Syracusan
F4883	Female	UNIFI	-	Photogrammetry	Syracusan
F4884	Female	UNIFI	32	Photogrammetry	Syracusan
F4895	Female	UNIFI	34	Photogrammetry	Syracusan
F5795	Female	UNIFI	-	Photogrammetry	Sardinian
F5799	Female	UNIFI	-	Photogrammetry	Sardinian
F5800	Female	UNIFI	-	Photogrammetry	Sardinian

F5838	Female	UNIFI	-	Photogrammetry	Sardinian
F5867	Female	UNIFI	-	Photogrammetry	Sardinian
F5874	Female	UNIFI	-	Photogrammetry	Sardinian
F5937	Female	UNIFI	-	Photogrammetry	Sardinian
M0001	Male	UNIFI	-	Photogrammetry	Sardinian
M0004	Male	UNIFI	-	Photogrammetry	Sardinian
M0006	Male	UNIFI	-	Photogrammetry	Sardinian
M0015	Male	UNIFI	-	Photogrammetry	Sardinian
M0021	Male	UNIFI	-	Photogrammetry	Sardinian
M0022	Male	UNIFI	-	Photogrammetry	Sardinian
M0258	Male	UNIFI	-	Photogrammetry	Sardinian
M0260	Male	UNIFI	-	Photogrammetry	Sardinian
M0263	Male	UNIFI	-	Photogrammetry	Sardinian
M0265	Male	UNIFI	-	Photogrammetry	Sardinian
M0306	Male	MDLP	-	Ct scan	Mapuche
M0307	Male	MDLP	-	Ct scan	Mapuche
M0308	Male	MDLP	-	Ct scan	Mapuche
M0310	Male	MDLP	-	Ct scan	Mapuche
M0326	Male	MDLP	-	Ct scan	Chubut
M0327	Male	MDLP	-	Ct scan	Chubut
M0339	Male	MDLP	-	Ct scan	Chubut
M0340	Male	MDLP	-	Ct scan	Chubut
M0341	Male	MDLP	-	Ct scan	Chubut
M0344	Male	MDLP	-	Ct scan	Chubut
M0370	Male	MDLP	-	Ct scan	Pampa Grande
M0380	Male	MDLP	-	Ct scan	Pampa Grande
M0412	Male	UNIFI	20	Photogrammetry	Florentine
M0419	Male	UNIFI	33	Photogrammetry	Florentine
M0734	Male	UNIFI	25	Photogrammetry	Florentine
M0735	Male	UNIFI	35	Photogrammetry	Florentine
M0794	Male	UNIFI	-	Photogrammetry	Florentine
M0830	Male	Oloriz C. UNIFI	28	Ct scan	Spanish
M0855	Male	UNIFI	36	Photogrammetry	Florentine
M0864	Male	Terry C.	42	Ct scan	North American
M0869	Male	Oloriz C.	42	Ct scan	Spanish
M0874	Male	UNIFI	22	Photogrammetry	Florentine
M0878	Male	UNIFI	36	Photogrammetry	Florentine
M100099	Male	NMDID	50	Ct scan	Hispanic Latin
M100144	Male	NMDID	47	Ct scan	no Hispanic
M100148	Male	NMDID	58	Ct scan	Hispanic Latin
M100169	Male	NMDID	20	Ct scan	no Hispanic
M100205	Male	NMDID	43	Ct scan	no Hispanic
M100221	Male	NMDID	34	Ct scan	Hispanic Latin
M100247	Male	NMDID	-	Ct scan	no Hispanic
M100284	Male	NMDID	47	Ct scan	Hispanic Latin

M100309	Male	NMDID	37	Ct scan	no Hispanic
M100371	Male	NMDID	46	Ct scan	Hispanic Latin
M100389	Male	NMDID	36	Ct scan	Hispanic Latin
M100418	Male	NMDID	35	Ct scan	no Hispanic
M100543	Male	NMDID	25	Ct scan	Native american
M100967	Male	NMDID	33	Ct scan	no Hispanic
M101121	Male	NMDID	50	Ct scan	Native american
M101378	Male	NMDID	47	Ct scan	Hispanic Latin
M101599	Male	NMDID	26	Ct scan	Hispanic Latin
M102436	Male	NMDID	37	Ct scan	Native american
M102965	Male	NMDID	23	Ct scan	Native american
M103044	Male	NMDID	39	Ct scan	Native american
M103205	Male	NMDID	29	Ct scan	Native american
M103634	Male	NMDID	43	Ct scan	Native american
M103640	Male	NMDID	31	Ct scan	Native american
M1068	Male	Oloriz C.	48	Ct scan	Spanish
M1112	Male	Oloriz C.	23	Ct scan	Spanish
M1168	Male	Terry C.	33	Ct scan	North American
M1187	Male	Oloriz C.	40	Ct scan	Spanish
M1192	Male	Oloriz C.	67	Ct scan	Spanish
M1280	Male	Terry C.	75	Ct scan	North American
M1282	Male	Oloriz C.	66	Ct scan	Spanish
M1293	Male	Terry C.	51	Ct scan	North American
M1363	Male	UNIFI	44	Photogrammetry	Florentine
M1368	Male	UNIFI	66	Photogrammetry	Florentine
M1385	Male	UNIFI	26	Photogrammetry	Florentine
M1386	Male	UNIFI	28	Photogrammetry	Florentine
M1387	Male	UNIFI	27	Photogrammetry	Florentine
M1393	Male	UNIFI	20	Photogrammetry	Florentine
M1395	Male	UNIFI	24	Photogrammetry	Florentine
M1399	Male	UNIFI	21	Photogrammetry	Florentine
M1400	Male	UNIFI	23	Photogrammetry	Florentine
M1403	Male	UNIFI	30	Photogrammetry	Florentine
M1406	Male	UNIFI	16	Photogrammetry	Florentine
M1410	Male	UNIFI	57	Photogrammetry	Florentine
M1412	Male	UNIFI	35	Photogrammetry	Florentine
M1428	Male	UNIFI	35	Photogrammetry	Florentine
M1429	Male	UNIFI	36	Photogrammetry	Florentine
M1430	Male	UNIFI	60	Photogrammetry	Florentine
M1432	Male	UNIFI	35	Photogrammetry	Florentine
M1433	Male	UNIFI	50	Photogrammetry	Florentine
M1505	Male	UNIFI	-	Photogrammetry	Sardinian
M1507	Male	UNIFI	-	Photogrammetry	Sardinian
M1508	Male	UNIFI	-	Photogrammetry	Sardinian
M1518	Male	UNIFI	-	Photogrammetry	Sardinian
M1525	Male	UNIFI	-	Photogrammetry	Sardinian

M1533	Male	UNIFI	-	Photogrammetry	Sardinian
M1535	Male	UNIFI	-	Photogrammetry	Sardinian
M1537	Male	UNIFI	-	Photogrammetry	Sardinian
M1756	Male	UNIFI	41	Photogrammetry	Florentine
M1770	Male	UNIFI	44	Photogrammetry	Florentine
M1773	Male	UNIFI	24	Photogrammetry	Florentine
M1774	Male	UNIFI	43	Photogrammetry	Florentine
M1781	Male	UNIFI	50	Photogrammetry	Florentine
M1789	Male	UNIFI	23	Photogrammetry	Florentine
M2524	Male	UNIROMA1	-	Photogrammetry	Bolognesi
M2525	Male	UNIROMA1	-	Photogrammetry	Bolognesi
M2526	Male	UNIROMA1	-	Photogrammetry	Bolognesi
M2527	Male	UNIROMA1	-	Photogrammetry	Bolognesi
M2528	Male	UNIROMA1	-	Photogrammetry	Bolognesi
M2529	Male	UNIROMA1	-	Photogrammetry	Bolognesi
M2530	Male	UNIROMA1	-	Photogrammetry	Bolognesi
M2531	Male	UNIROMA1	-	Photogrammetry	Bolognesi
M2532	Male	UNIROMA1	-	Photogrammetry	Bolognesi
M2533	Male	UNIROMA1	-	Photogrammetry	Bolognesi
M4835	Male	UNIFI	60	Photogrammetry	Syracusan
M4839	Male	UNIFI	64	Photogrammetry	Syracusan
M4843	Male	UNIFI	56	Photogrammetry	Syracusan
M4848	Male	UNIFI	66	Photogrammetry	Syracusan
M4849	Male	UNIFI	-	Photogrammetry	Syracusan
M4850	Male	UNIFI	64	Photogrammetry	Syracusan
M4852	Male	UNIFI	36	Photogrammetry	Syracusan
M4858	Male	UNIFI	28	Photogrammetry	Syracusan
M4861	Male	UNIFI	19	Photogrammetry	Syracusan
M4862	Male	UNIFI	21	Photogrammetry	Syracusan
M4882	Male	UNIFI	36	Photogrammetry	Syracusan

3.1.2 A brief overview of the collections

Most of the acquired collections span the past two centuries, with one notable exception being The New Mexico Decedent Image Database (NMDID) (Edgar et al., 2020), which is more recent. Each collection provides valuable information, particularly regarding the sex of the individuals. In certain cases, additional details such as age at the time of death (categorized as an adult, sub-adult, or older than 60 years old), cause of death, and the recorded age at the time of death are also available.

Specifically, at the Anthropological Museum of the University of Florence in Italy, three distinct collections were acquired, originating from different regions of Italy. These collections, namely the Syracusans from Sicily, the Sardinians from Sardinia, and the Florentines from Tuscany, were procured from the museum through various means, beginning in the late 19th century and continuing thereafter (Moggi Cecchi & Stanyon, 2014).

The Sardinians collection is a unique amalgamation that was directly donated by Paolo Mantegazza (1831-1910) during his tenure as the Director of the Anthropological Museum of Florence. It was further enriched through an acquisition by Cipriani in 1934.

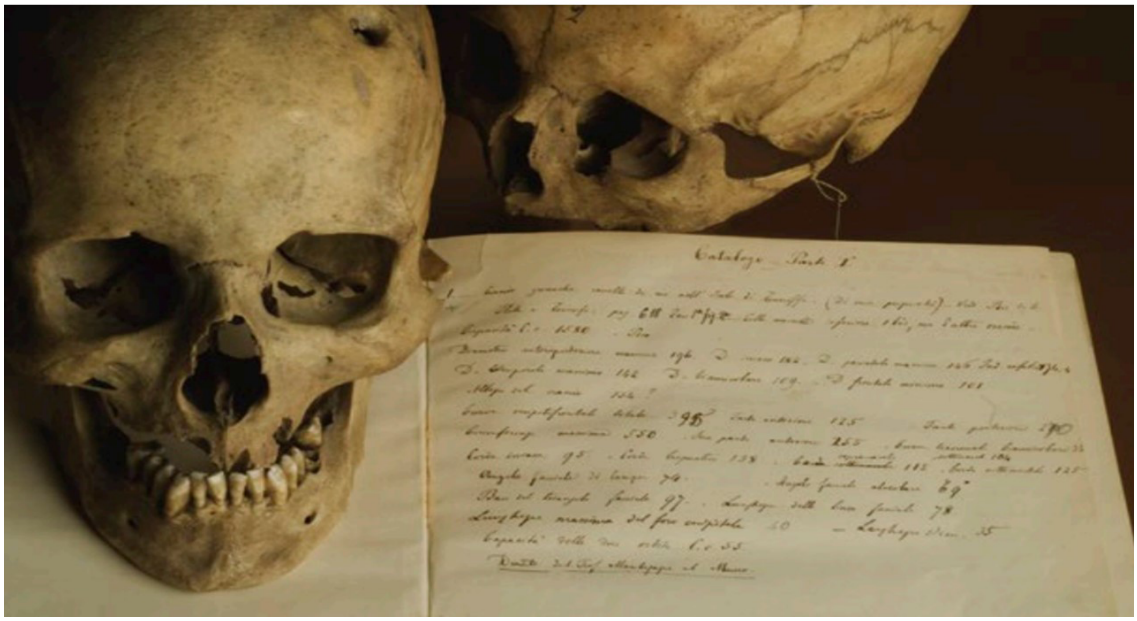

Fig.11. The first page of the Chronological catalog of the National Museum of Anthropology in Florence. (1870) in: Le collezioni antropologiche/Anthropological collections, (Moggi Cecchi & Stanyon, 2014).

The Florence collection originates from the renowned Santa Maria Nuova Hospital in Florence, which held significant prominence within the city. Historically, families of lesser means would often leave the bodies of their deceased loved ones at the hospital.

The Syracusans collection, on the other hand, was acquired from the cemetery of the Sicilian city (Moggi Cecchi & Stanyon, 2014). It is worth noting that the museum offers the opportunity to access the original catalog in digital format. This catalog provides detailed information about the acquisition process, including the full names of individuals, item conditions, acquisition dates, donor information, and other pertinent details.

In Rome, was acquired the "Bolognesi" collection from the G. Sergi Anthropological Museum at the University "La Sapienza" (web.uniroma1.it/polomuseale/museo-antropologia). This collection, although small, is part of a larger collection shared between the Universities of Rome and Bologna (Rubini & Scarani, 1989).

It is important to note that the skulls available on the NESPOS online repository represent only a fraction of the extensive Oloriz collection. Federico Aguilera Oloriz, a distinguished Doctor and Professor of Anatomy at the University of Madrid in Spain played a pivotal role in establishing museums of comparative osteology during the early 20th century (Guirao Piñeyro & Guirao Pérez, 2008). Alongside other influential figures such as Paolo Mantegazza in Florence, they contributed significantly to these museums by acquiring numerous collections. Similar to the Florence collection, Oloriz's collection consists of unclaimed deceased individuals from the General Madrid Hospital. For the purpose of this thesis, my focus was exclusively on the crania accessible through open access on NESPOS.

The Terry Anatomical Collection is housed in the Department of Anthropology at the Smithsonian Institute. Robert J. Terry assembled it during his tenure as a professor of anatomy at the Medical School in St. Louis, Missouri (1899-1941). Similar to previous cases, this collection was derived from donating bodies to medical schools to avoid burial costs (Hunt & Albanese, 2005).The Terry collection is remarkably comprehensive, encompassing a wide range of factors. It consists of over 1700 individuals, accompanied by complete biological information, ancestral background, and details about the post-mortem processing of the corpses. While not the entire collection is available in 3D format, a portion of the collection's skulls was made accessible through the efforts of Lynn Copes in her Ph.D. dissertation titled "Comparative and Experimental Investigations of Cranial Robusticity in Mid-Pleistocene Hominins" scanned more than 705 individuals, including some previously described specimens from the Terry collection (Copes, 2012).

The inclusion of individuals from the Terry Anatomical Collection provides a valuable resource for research due to the inherent variability resulting from their mixed ancestry, which reflects the genetic composition typically found in the United States population, encompassing both African and European genetic influences. This characteristic holds particular significance for studies seeking to account for the diverse human variability observed in contemporary populations. For convenient access to the three-dimensional (3D) data associated with these individuals (https://www.lynncopes.com/human-ct-scans.html; Hunt & Albanese, 2005).

Another noteworthy addition to the available databases is the New Mexico Decedent Image Database (NMDID). This database contains whole-body computed tomography (CT) scans of over 15,000 individuals who passed away between 2010 and 2017. Each individual's metadata file provides comprehensive information encompassing 60 variables that cover demographics, medical history, and hospital procedures. The NMDID project was established in 2010, specifically focusing on investigating deaths resulting from firearms injuries, drug poisoning, and childhood-related causes (Edgar et al., 2020).

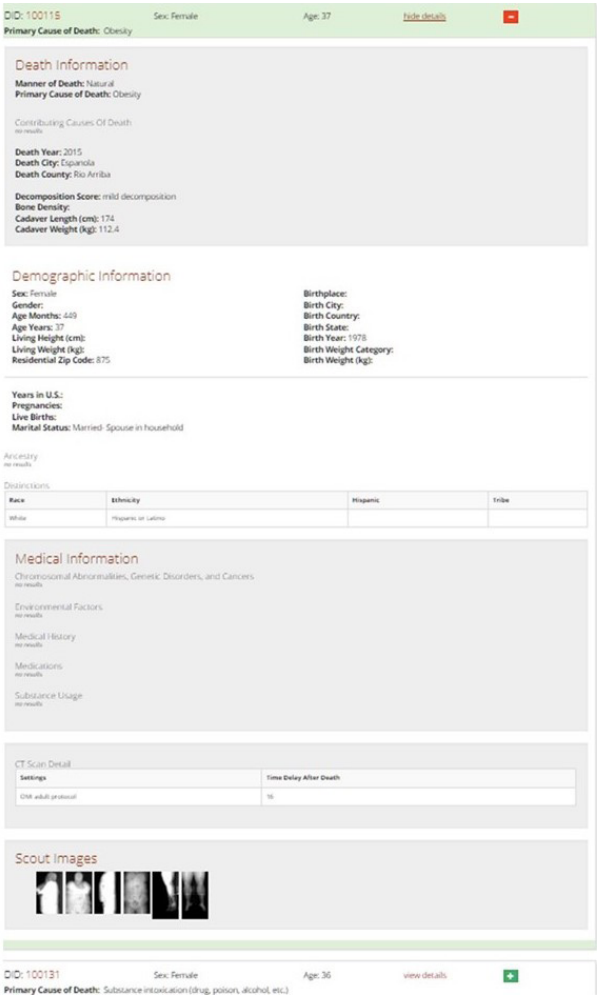

Fig. 12 Example of NMDID's database with biological information and scout images.

The Osteological collection housed at the National Museum of Natural Science de la Plata in Argentina, within the Faculty of Natural Science, offers another valuable resource for research. This collection primarily represents individuals from Native American, showcasing the region's unique genetic diversity. The collection's diversity is influenced by various factors such as genetic drift resulting from population isolation and geographical distances (Manel et al., 2003). This diversity within the collection significantly enhances the overall sample, providing researchers with a broader representation of the population (Castro et al., 2009).

Furthermore, the collection encompasses individuals from different populations, including Azul, Mapuche, and Pampa Grande, further adding to its variability. Additionally, the collection includes specimens obtained through various means, including naturalistic expeditions, sales, exchanges, donations, and the exhumation of burials. This multi-sourced acquisition process contributes to the collection's richness and provides researchers with a wider range of samples to study. Overall, the Osteological collection of the de National Museum of Natural Science la Plata offers a diverse and comprehensive dataset that serves as a valuable resource for researching populations from South America (Castro et al., 2009).

3.1.3 Data acquisition

The data collection process involved obtaining 3D models of each cranium's external surface using photogrammetry and segmentation (Thi Porter et al., 2016; Weber, 2015). Three collections were acquired during research visits to Italy via photogrammetry. These collections were sourced from the Anthropological Museum of Florence and the Anthropological Museum of Roma Sapienza. The photogrammetry process was conducted using Agisoft Photoscan professional.

Fig. 13. Photos during the photogrammetry process at the University of Florence and in the Anthropological Museum of Florence UNIFI.

The cranium's external surface was acquired using segmentation software in the CT-scan collection case. Instead, if permission to physically access the collection was granted, the 3D models of the external surface were obtained using photogrammetry. Detailed information regarding the acquisition methods for each cranium can be found in Table 1.

The use of both photogrammetry and segmentation techniques allowed for comprehensive and accurate capture of the external surface of the cranium, facilitating subsequent analysis and measurements in the study (Bucchi et al., 2020).

To create a 3D model of each cranium, I captured three sets of photographs covering a 360-degree view, resulting in a total of 120 high-resolution images. It is generally recommended to have a minimum of one photograph every 30 degrees to ensure a sufficiently complete model. Instead of using an automated turntable to calculate the angle, I manually captured 30 photos for each set, meeting the software's requirements for generating a point cloud. The photographs were taken using a Nikon D60 camera (insert camera specifications), and the cranium was illuminated using cold lights within a lightbox setup.

In my analysis, the teeth did not significantly impact the research objectives; therefore, I did not focus extensively on capturing high-resolution details of the dental region. Addi-

tionally, to ensure the preservation of the human cranium, I decided not to use a matting spray that could enhance the texture resolution of the models. While creating 3D models with texture can be useful for applications such as museums, it is not a requirement for geometric morphometrics analysis, which is the primary focus of this study.

The software procedure involved several phases in creating the 3D models.

1)Firstly, the photographs were aligned to reconstruct the spatial position of each photo around the object.

2)A mask was then created by extracting the object from the background using the "import mask" function.

3) A dense point cloud was generated by calculating depth information for each photo based on the camera positions. This was done with high-quality settings and aggressive depth filtering to maximize the number of pixels positioned in 3D space.

4) Subsequently, a mesh was constructed using polygons to define the structural reconstruction of the object. Each vertex in the mesh was defined by Cartesian coordinates (X, Y, and Z).

5) To combine multiple chunks of the cranium into a single model, the alignment process called "merge chunks" was applied. This alignment was performed automatically.

6) The final step involved reconstructing the texture of the model using the pixel information from the photos.

It is important to note that the 3D models obtained through photogrammetry were not automatically scaled. The scaling was performed manually using previous measurements taken with callipers, and the scale was adjusted using Amira software. The exported format for the models was ".ply".

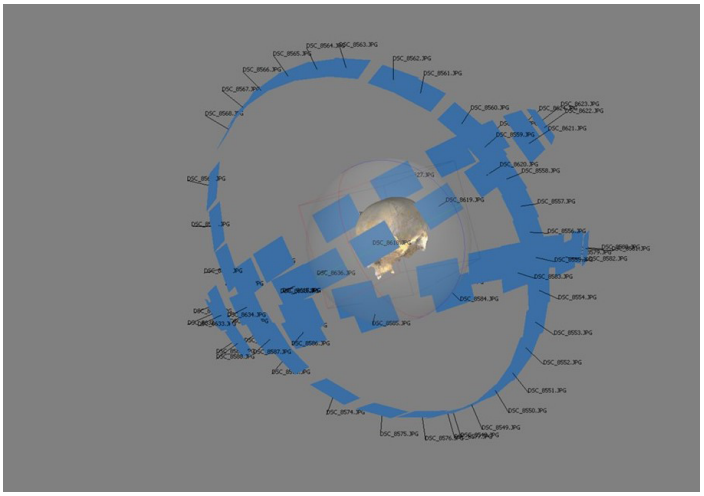

Fig. 14. Photogrammetry of the cranium, combining the single chunks to elaborate the 3D model.

In contrast, the process of creating 3D models from computer tomography (CT) data was entirely different from photogrammetry. This method was applied to samples obtained from open repositories such as the Oloriz Collection (NESPOS) and the New Mexico Decedent Image Database.

Computed Tomography (CT-scan) is commonly used in paleoanthropological and anthropological studies to capture volumetric images of human remains. While X-rays had been used for studying Neanderthals as early as 1905, the invention of CT by Godfrey

Hounsfield in 1972 greatly enhanced the resolution and utilization of this technique in physical anthropology (Hounsfield, 1973). CT-scan provides higher-resolution cross-sectional images, allowing researchers to explore the internal structures of human remains with greater detail, unaffected by conservation methods (Wu & Schepartz, 2009).

The CT scan procedure involves extracting a 3D model from the ".dicom" file, which is known as the 3D reconstruction procedure. CT scans produce 2D slices of anatomical features represented in a grayscale known as the Hounsfield scale. Each scanned material, such as bones, soft tissues, and organs, renders a different shade of grey depending on its density. While each slice provides only a 2D visualization, the resolution depends on the distance between each slice (typically around 4 mm in medical CT scans). By utilizing medical software like Materialize Mimics, Avizo, and 3D Slicer, a series of 2D slices can be processed to generate a 3D model (Weber, 2015).

For the segmentation of the CT scans, I used the Mimics software and followed a specific protocol to obtain the 3D model of the external surface saved in ".ply" format.

1. The CT scans were opened in dicom format, and for the NMDID's CT scans, which covered the entire body, they were divided into two or three portions: upper part (head and thorax), lower part, and in some cases, the head was isolated. To optimize computer RAM usage and facilitate the extraction of the head bone, I applied a "Crop Mask" to limit the area of interest.
2. The next stage involved calibrating the "thresholding" process. While some software offers predefined threshold settings for bones, teeth, soft tissues, etc., it was necessary to manually calibrate the thresholds to refine the 3D model generation.
3. Segmentation of the mandible was crucial because its natural temporomandibular joint has the surface of the two bones (temporal and mandibular) very close to each other. To separate them, I utilized the "split mask" option in Mimics, and in some specific slices, I manually segmented the bones using the "Edit Mask" function.
4. The final step involved reviewing the 3D preview of the segmented mask, ensuring the desired segmentation result, and saving and exporting it in .ply format for further analysis.

3.1.4 Landmarks and semilandmarks configuration

To capture the complete shape of the 3D models, we utilized a configuration of landmarks. Landmarks were collected in 3D space, and to enhance the coverage of the shape, we incorporated semilandmarks patches on the surface. The entire landmark configuration consisted of 50 landmarks (Table 2). The configuration of landmarks followed three different types, as defined by Bookstein (1997).

Type 1 landmarks were positioned on the surface of tissues near each other. These landmarks aimed to capture specific anatomical features and their spatial relationships.

Type 2 landmarks, although not strictly like type 1, were also used to represent geometric constructs such as points of maximum curvature or other local morphogenetic processes. These landmarks provided information about shape variations related to specific morphological characteristics.

Type 3 landmarks were placed on external points of the object, such as intersections or centroid points. These landmarks were selected to capture overall shape information and provide reference points for analysing shape changes.

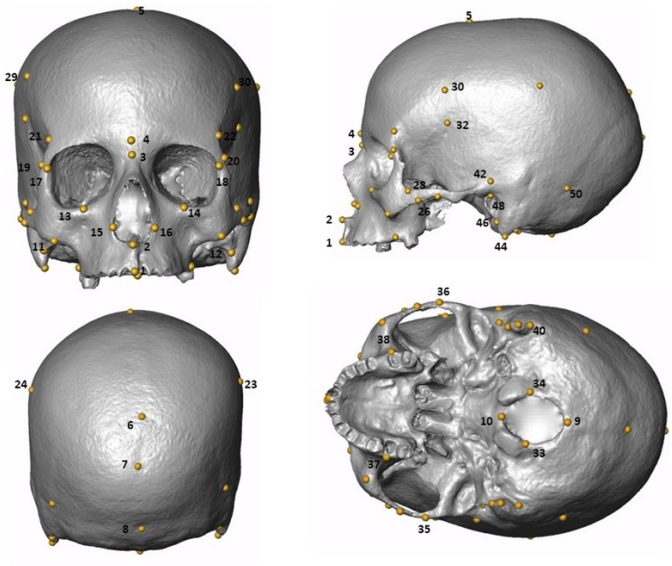

Fig. 15. Landmark configuration in the entire cranium.

By incorporating these different types of landmarks, our configuration aimed to comprehensively capture the shape variations present in the 3D models.

In geometric morphometrics, type 1 landmarks are often considered the most reliable landmarks. Compared to type 2 and type 3 landmarks, which may involve more subjective interpretations or geometric constructs, type 1 landmarks are typically more consistent and less prone to measurement error or variability (Bookstein, 1997).

Table 2. List of cranial landmarks used for the study of the entire cranium.

Numbers	Landmarks	Type of Landmark	Definition
1	Prosthion	1	The most anterior point in the midline on the alveolar process of the maxillae.
2	Nasospinale	1	The point where a line drawn between the inferior most point of the nasal aperture crosses the midsagittal plane.
3	Nasion	1	The point of intersection between the frontonasal suture and the midsagittal plane.
4	Glabella	1	The most anterior midline point on the frontal bone, usually above the frontonasal suture.
5	Bregma	1	The ectocranial midline point where the coronal and sagittal sutures intersect.
6	Lambda	1	The ectocranial midline point where the sagittal and lambdoid sutures intersect.
7	Opisthocranion	3	Instrumentally determined most posterior points of the skull not on the external occipital protuberance.
8	External occipital protuberance crest	2	Is a highly variable median line or crest that passes between the right and the left nuchal musculature.
9	Opisthion	1	Midline point at the posterior margin of the foramen magnum.

10	Basion	1	Midline point on the anterior margin of the foramen magnum.
11-12	Zygomatic process inf.	2	Inferior point of zygomatic process.
13-14	Zygomatic process sup.	2	Superior point of zygomatic process.
15-16	Alare	2	The most lateral points on the nasal aperture in a transverse plane.
17-18	Ectoconchion	1	The intersection of the most anterior surface of the lateral border of the orbit.
19-20	Frontomalare temporale	1	The most laterally positioned point of the fronto-malar suture.
21-22	Frontotemporale	1	The point where the temporal line reaches its most anteromedial position on the frontal.
23-24	Eurion	3	Ectocranial points on opposite sides of the skull that form the termini of the line of greatest cranial breadth.
25-26	Inferior temporal process	2	Inferior point where the zygomatic process joints with the temporal bone to form the zygomatic arch.
27-28	Superior temporal process	2	Superior point where the zygomatic process joints with the temporal bone to form the zygomatic arch.
29-30	Stephanion	1	Point where the upper temporal line cuts the coronal suture.
31-32	Pterion	1	Is located on the side of the skull, just behind the temple, where the frontal, parietal, temporal and sphenoid bones join together.
33-34	Foramen magnum lateral point	1	Most lateral points on the foramen magnum aperture in a transverse plane.
35-36	Zygion	2	Most lateral points on the zygomatic arch.

37-38	Ectomolare	1	Most lateral points on the outer surface of the alveolar borders of the maxilla.
39-40	Mastoid notch	1	Most inferior point on juxta-mastoid crests.
41-42	Auricolare	1	Point on the lateral aspect of the root of the zygomatic process at the deepest incur-vature.
43-44	Mastoid	1	Extreme point mastoid pro-cess.
45-46	Petrotympanic crest	1	Lateral origin of petrotym-panic crest.
47-48	Acoustic meatus	1	Internal acoustic meatus.
49-50	Asterion	1	The posterior point end of the parietomastoid suture.

Table.3 List of landmarkS used for the frontal bones

Landmark number	Landmark
1	Nasion
2	Glabella
3	Bregma
4-5	Ectoconchion
6-7	Frontomalare temporale
8-9	Frontotemporale
10-11	Stephanion
12-13	Pterion

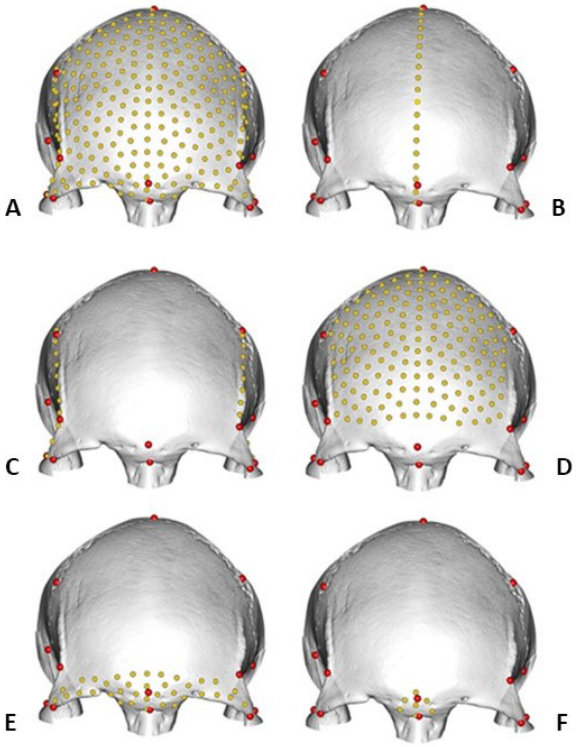

Fig. 16. Semi-landmark configuration of frontal bone; the frontal bone was divided into 6 modules: A: entire bone, B: midsagittal lines, C: temporal lines, D: squama, E: supraorbital ridges and, F: glabella.

The placement of landmarks was conducted using Amira software, and the resulting landmark coordinates were imported into R using the "read.amira.dir" function from the Arothron package (Profico et al., 2021). The specific configuration of semilandmarks varied depending on the requirements of each research paper, such as focusing on neurocranium patches, entire frontal bones, or specific anatomical areas of the frontal bone, such as the squama or entire crania.

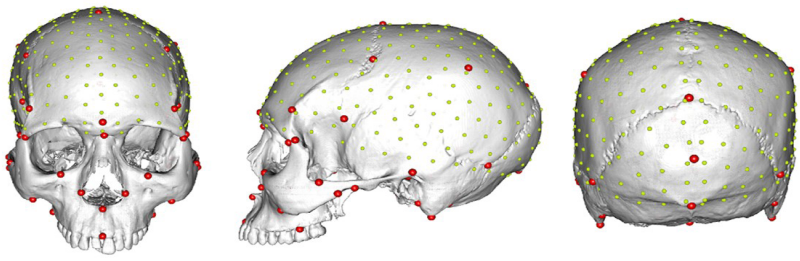

Fig. 17. Semilandmark configuration of the neurocranium. The patch was realized with the use of 500 equidistant sliding semilandmarks.

To create the semilandmarks configuration, an initial patch of semilandmarks was generated in Amira or Viewbox software. Each semilandmark was equidistant from the adjacent ones. Once the patch was created, it was superimposed on all other specimens using R. In order to consider the semilandmarks as landmarks in the geometric morphometric (GM) analysis, the summed squared deviations between each individual and a reference form needed to be minimized (Sampson et al., 1996). To achieve this, a sliding procedure was performed using the Morpho package (Schlager, 2017) in R.

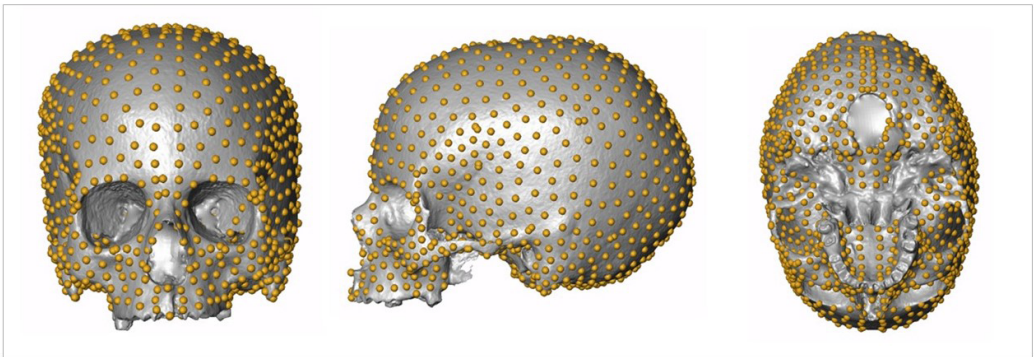

Fig. 18. Semilandmark configuration of the entire cranium.

3.2 Part 2:

3.2.1 Sample and repositories

In order to conduct the last research, which involved studying a new method based on linear measurements of crania, we utilized datasets obtained from open repositories. Instead of directly collecting the linear measurements ourselves, we employed two pre-existing open datasets. As detailed in the subsequent chapter on results, it is crucial to utilize different datasets during the process of Neural Network Analysis. This approach ensures that the performance of the model is evaluated using external sources, thereby avoiding any overlapping. The first dataset we utilized is the well-known Howell craniometric dataset.

The craniometric dataset used in this study was sourced from an open-access dataset available at https://web.utk.edu/~auerbach/HOWL.htm (Howells, 1973, 1989, 1995). This dataset consists of measurements obtained from 2524 human crania, representing 28 different populations. The sex of crania was estimated by Howells (Howells, 1973). From this original dataset, a subset of 10 craniometric measurements was carefully selected. These measurements were chosen to capture key cranial shape characteristics while incorporating knowledge of sexually dimorphic traits from existing literature y after different tests. The decision to utilize a subset of measurements was motivated by the need to reduce the number of variables, minimize redundancy, and optimize computational efficiency, as the modeling process can be computationally intensive.

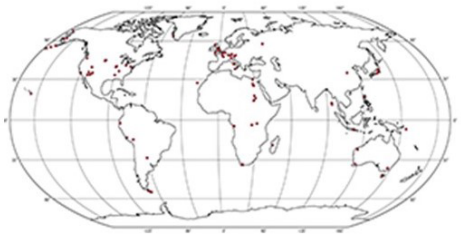

Fig. 19. Howell's sample of provenience (https://web.utk.edu/~auerbach/DATA.htm)

The Howells dataset served as the training and validation set for this study. For testing purposes, a separate dataset of craniometric measurements from the University of Tennessee (UT) Dataset for forensic anthropology in the United States was utilized. The

UT dataset comprises 36 craniometric measurements recorded from 1396 individuals of mixed ancestry (Jantz & Moore-Jansen, 1988).3.2.

The UT dataset originated in 1986 and was funded by the National Institute of Justice. It is widely recognized as one of the most comprehensive datasets in the field. The dataset includes various data points such as birthplace, medical history, occupation, stature, weight, cranial and postcranial metrics, suture closure details, perimortem trauma, epigenetic traits, and dental macro-wear analysis. It is important to note that only cases with available sex information were included in the analysis. The measurements in the UT dataset were collected by a different anthropologist affiliated with a separate institution.

3.2.2 Data preparation

In our study, we utilized a set of 10 craniometric measurements to evaluate our model, as shown in Table 4. Prior to the training phase, we removed observations that exceeded three standard deviations from the mean of the last measurement among the 10 variables. However, in the testing phase, we decided not to remove the same cases as we aimed to reflect real-world scenarios. Instead, we excluded individuals with missing data in more than 5 out of the 10 measurements. For cases with missing data below 50%, we estimated the values using Additive

Table 4. list of measurements to modelling the analysis.

Measurements	Abbreviation	Definition
Biauricular breadth	AUB	Shortest distance across the roots of the zygomatic processes
Basion-bregma height	BBH	Linear distance from basion to bregma
Glabella-occipital length	GOL	Linear distance from glabella to opisthcranion
Mastoid height	MDH	Linear distance between porion and mastoidale points
Nasal breadth	NLB	Maximum breadth of the nasal aperture
Nasal height	NLH	Height from the nasion to the lowest point on the rim of nasal aperture
Orbit breadth	OBB	Linear distance from dacryon to ectoconchion points
Orbit height	OBH	Linear distance between the superior and inferior margins of the orbits, measured perpendicularly to orbital breadth
Lambda-opisthion chord	OCC	Linear distance from lambda to opisthion along the mid-sagittal plane
Bizygomatic breadth	ZYB	Maximum breadth across the zygomatic arches, perpendicular to the mid-sagittal plane

Regression from the "Hmisc" package in R (Harrell & Dupont, 2022). Additionally, we adjusted the measurements to the geometric mean using the Mosimann transformation (Mosimann, 1970). To represent the size of the sample, we included the geometric mean as an additional measurement. The table provided includes details of the individuals, their provenances, and the repositories involved in each phase of the modelling process.

3.3.1. Geometric Morphometrics Analysis

Geometric morphometrics (GM) is a statistical approach used to study shape and size variations and their correlations with other variables (Claude, 2008). GM is widely employed in biological research due to the fundamental role that shape plays in understanding biological phenomena. Shape differences in various biological fields are assessed through comparisons and observations (Adams et al., 2004). Morphometrics provides a quantitative framework for evaluating these differences, making it a branch of mathematical shape analysis. One of the strengths of morphometrics lies in its ability to offer precise and accurate descriptions of shapes, while also employing rigorous statistical analyses. Furthermore, the visualization capabilities of GM are instrumental in effectively presenting the results. It is important to note that GM is a discipline guided by strict rules and principles, ensuring methodological rigor in shape analysis (Adams et al., 2004; Rohlf & Marcus, 1993).

3.3.2 Basic Rules and fundamental principles of GM

In geometric morphometrics (GM), shape analysis focuses on the information about objects or specimens while disregarding factors such as location, scale, and rotation effects (D. Kendall, 1977). After acquiring shape information using landmarks and semi-landmarks, one of the fundamental analyses in GM is the **General Procrustes Analysis** (GPA). The purpose of GPA is to calculate shape differences by employing Procrustes distances. The primary goal of GM is to accurately assess these shape differences while ignoring size variations (Gower, 1975; Kendall, 1977; Rohlf & Slice, 1990).

The GPA protocol involves a process called "registration", which standardizes the size, position, and orientation of landmark coordinates. This is achieved by scaling, translating, and rotating individual landmark configurations using their centroid, which is the arithmetic mean of all landmark coordinates (Mitteroecker et al., 2013). By aligning the configurations to their centroid and minimizing the squared distances between equivalent landmarks across all specimens, the Procrustes distances are minimized (Mardia et al., 1979).

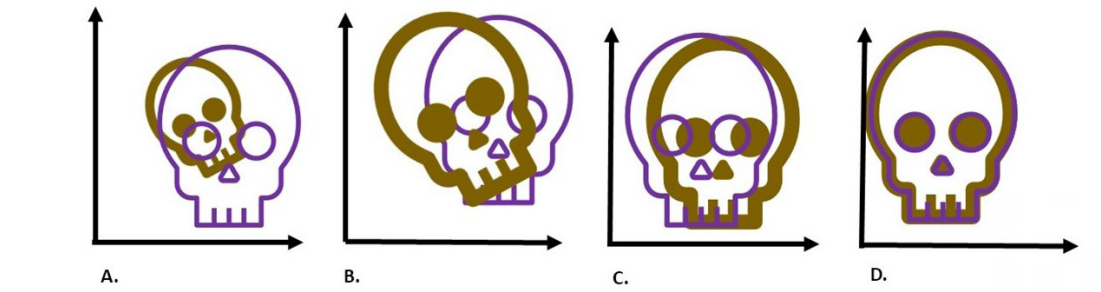

Fig. 20. A: raw landmarks, B: centered landmarks, C: centered and scaled landmarks, and D: centered scaled, and rotated landmarks (Mitteroecker & Gunz, 2009)

Scaling in GM is commonly performed using the Centroid size (Cs, (Mitteroecker et al., 2013), which is calculated as the square root of the sum of squared distances between a set of landmarks and their centroid. To ensure comparability between configurations, each configuration is standardized to a scale of 1 by dividing the raw landmark coordinates by the centroid size (Mitteroecker & Gunz, 2009).

During the alignment process, the specimens are initially aligned to a reference specimen that is arbitrarily chosen. Each configuration is then adjusted to minimize the distances between corresponding landmarks. After fitting all specimens to the reference, the sample mean of each coordinate (x, y, z) is calculated. In subsequent iterations, the configurations are aligned to the mean shape, which is recomputed based on the aligned configurations from the previous iteration. This iterative process continues until the sum of residuals, representing the differences between the aligned configurations and the mean shape, reaches a minimum. Typically, convergence is achieved after 3-5 iterations. The "shape coordinates" refer to the registered landmark positions after alignment, and they are ready for statistical analysis to compare shape variations across specimens in a standardized manner.

In the provided script, the "ProcSym" function from the "Morpho" package in R Studio (Schlager, 2017) is used for all work packages of GM aproach. This function performs the Procrustes superimposition and generates specimens in Kendall's shape space. Kendall's shape space is a manifold of a hypersphere (Dryden & Mardia, 1993; D. G. Kendall, 1984).

When shape variations are relatively small, the distribution of landmarks points on the shape manifold tends to be concentrated. In such cases, it is possible to approximate the region of shape space occupied by these points as planar. This planar approximation allows for the application of multivariate analyses using linear models (Dryden & Mardia, 1993). By projecting the tangent-projected shape variables onto the tangent space, researchers can perform statistical analyses assuming linearity within the chosen approximation.

The tangent-projected shape variables obtained from the tangent space projection method are then subjected to relevant statistical analyses based on the objectives of the study. These analyses may include regression analysis, analysis of variance (ANOVA), principal component analysis (PCA), or other appropriate multivariate statistical methods. The goal is to explore relationships, assess significance, and derive meaningful interpretations

regarding the investigated shape variables in relation to the research question or hypothesis.

In addition to shape analyses, centroid size differences are of considerable interest as they allow for the examination of how shape varies in relation to centroid size in allometric studies. Centroid size can be incorporated as an additional column in the shape coordinate data matrix, either independently or in combination with shape data. This approach enables the analysis of size and shape differences or the assessment of covariance with other factors using established multivariate methods, as demonstrated in studies by Mitteroecker et al. (2004) and Mitteroecker et al. (2013).

By including centroid size as a covariate, researchers can explore the interplay between size and shape and their associations with other relevant factors. This approach has been successfully employed in studies utilizing standard multivariate methods, as demonstrated by works such as (Chatzigianni & Halazonetis, 2009; Pujol et al., 2016). These statistical analyses allow for a comprehensive examination of size and shape differences or their joint influence on various biological phenomena.

It is important to note the distinction between "shape space" and "form space." In this context, "shape space" refers to the space without the information of size (centroid size), while "form space" (also known as size-and-shape space) includes both size and shape variables (Mitteroecker et al., 2004). Literally, Form in GM refers to the geometric properties' invariant only to translation and rotation.

Getting the form space is possible in two manners, standardizing the raw landmark configurations for position and orientation as is the usual Procrustes analysis but not standardizing the size (Dryden & Mardia, 1993). Or, augmenting the Procrustes shape coordinate with the natural logarithm of central size (log CS) as an additional variable (Mitteroecker et al., 2004).

This section provides a brief overview of the methods employed in the study. For more comprehensive details, please refer to the respective papers and scripts available in the repositories. The methodologies described here are general in nature, as each paper had its specific methodology tailored to address its individual objectives.

To conduct the statistical analysis, we utilized R Studio (R Core Team, 2022). R Studio is an open-source tool that serves as an integrated development environment (IDE) for the R programming language. It facilitates interaction with R by offering various features, including code completion and debugging capabilities.

R, the programming language employed in this study, is widely recognized for its applications in statistical computing, data analytics, and scientific research. It is extensively used by statisticians, data analysts, and researchers for data management, manipulation, analysis, and visualization purposes.

One of the fundamental principles in Geometric Morphometrics (GM) is that **landmark coordinates** are inherently multivariate in nature, distinguishing them from conventional morphometric data. Multivariate methods in GM serve two primary purposes: classification and ordination. Classification techniques, such as cluster analysis, are commonly employed to group specimens based on their shape characteristics (Landau et al., 2011). On the other hand, ordination methods involve arranging objects along one or more axes,

with Principal Component Analysis (PCA) being a prominent example. PCA, for example, enables the identification of the primary sources of shape variation by maximizing the explained variance in the data. (Klingenberg & McIntyre, 1998; Klingenberg et al., 2002).

In GM, shape variables are treated as having the same metrical unit, facilitating the analysis based on the covariance matrix. It is crucial to preserve the Procrustes metric, which ensures the meaningful comparison of shapes. The statistical methods employed in GM, regardless of whether the data is two-dimensional or three-dimensional, rely on the same underlying algebraic principles. The Covariance Matrix landmark coordinates are used to construct a covariance matrix. This matrix represents the shape variation among the specimens. However, it is worth noting that all statistical analyses in GM involve the inversion of the landmark variance-covariance matrix. To perform such inversion, the number of cases should ideally exceed the number of variables, a condition that is not always met in modern morphometric studies.

To sum the principal multivariate analysis in GM are Multivariate Regression, PCA, CVA, Partial Least Squared, Multivariate Analysis of the Variance and etc.

Principal Component Analysis (PCA) is a statistical method used for descriptive purposes to capture the diversity of specimens in terms of their shape characteristics. It is primarily employed as a tool for data description rather than hypothesis testing. PCA generates new variables through linear combinations of the original variables. These new variables, known as principal components, allow for visual analysis and exploration of variation among individuals. In the context of geometric shape variables, different specimens exhibit varying degrees of overlap in specific regions of an organism or structure. This occurs because shape variables are not biologically or statistically independent; instead, they are influenced by common processes that generate variation. Overlapping regions represent anatomical regions with shared functional, developmental, and genetic connections.

To address the challenge of interpreting models of covariation and variation, PCA aims to simplify patterns and facilitate data interpretation through a graphical approach. Principal components are linear combinations of the original variables that are independent of one another. This simplification of patterns assists in uncovering the underlying structure of the data and facilitates the interpretation of complex variations.

One advantage of PCA is the ability to represent the three principal components (PCs) that account for 90% of the overall variation in a single plot, rather than separately. And, also the plot allows the visualization of clusters of individuals within the plot. However, it is important to exercise caution in interpreting these clusters, as their presence does not necessarily indicate the existence of statistically distinct entities. It is crucial to be mindful of potential misinterpretations and avoid making unfounded inferences about separate statistical categories based solely on the presence of clusters. When considering the geometry of PCA, it is helpful to envision the distribution of analyzed values as an ellipse in the coordinate plane. The PCA process aims to describe the positions of individuals within this ellipse. One of the initial steps in PCA is determining the direction of individuals along the axes. This is done based on the second axis, which represents the maximum amount of total variance. The outcome of PCA is determined by the orthogonal projection of individuals along the Principal Component Scores (PCs), providing a representation of

their positions within the ellipse. PCs as formally the basis for a new coordinate system in the ellipse. Variance calculated is mean in statistics the squared sum of the mean of the distances of individuals from the mean. To conclude the PCA is a descriptive analysis able to show if the data present the covariance. In the results, the plots of PCA were made in R studio (more details in the script).

Prior to commencing the statistical analysis, a **sensitivity test** was meticulously conducted to assess the reproducibility of the landmark configurations. This test involved four rounds of data collection, each spaced one week apart, utilizing the identical configuration of 50 landmarks as employed in the analysis of the entire crania.

Subsequently, in order to quantify the error associated with the acquisition of cranial landmarks, the Procrustes Anova (Fruciano, 2016) was executed. This analysis was performed four times, utilizing randomly selected subsamples consisting of 8 individuals in each iteration. Detailed results stemming from these assessments can be found in the paper about the entire crania in the third session of the results.

Linear Discriminant Analysis (LDA) is an analysis formulated by Fisher in 1936. Its main objective is the quantification and visualization of shape differences between groups or categories. In GM, it is widely used to understand the factors that contribute to shape variation (McLachlan, 2004). As well as being an obvious tool to aid in the identification of species, populations and to make comparisons. It also allows targeting the effects of specific variables in the shape. LDA is based on the finding of the projection hyperplane that minimize the interclass variance and maximized the distance between the projection mean of the classes. To perform the LDA we used PCs as dependent variables and the logCS and sex are considered as independent variables (Klingenberg, 2016).

The statistical analysis was performed in shape and form space (the log of the central size is added as a variable during the GPA). That is to investigate both the answer, the shape with the information relative only to the morphology, and in the form to evaluate the impact of the size variable. Analysis of variance (ANOVA) was used to evaluate the influence of sex on shape and size. For the analysis, we used Procrustes ANOVA of the package “geomorph” (Adams et al., 2019).

Analysis of variance is a set of statistical techniques that are part of inferential statistics, which allow one to compare two or more groups of data by calculating and comparing the variability within these groups with the variability between the groups (only the difference in outcomes is of interest).

The variances in the analysis are calculated as the mean squares, obtained by dividing the sums of squares by the appropriate degrees of freedom. The degrees of freedom for variance calculations are determined by the number of groups minus one and the number of individuals minus the number of groups. The statistical significance of the study is assessed through the comparison of two variances using a ratio. Importantly, this ratio remains unaffected by certain alterations made to the experimental observations. Specifically, adding a constant to all observations or multiplying all observations by a constant does not impact the significance of the results. Thus, the statistical significance determined by the ANOVA is independent of constant biases, scaling errors, and the units used to express the observations. The F value, in this context, represents the ratio between the explained and unexplained variances, providing an indication of

the extent to which the observed data can be accounted for by the experimental factors.

The application of **Partial Least Squares (PLS)** was utilized solely in the study of frontal bone to analyze the modularity of the block. In this context, the term "block" pertains to distinct traits of frontal bones that were examined.

Partial Least Squares analysis (PLS) is a powerful statistical method that enables the quantification and visualization of the covariation between two or more sets of variables, commonly referred to as "blocks." When applied within a morphometric context, PLS calculates the linear combination of two sets or "blocks" of shape variables, typically represented by two landmark sets. The primary objective of PLS in this context is to maximize the explained covariance between these two blocks of shape variables. By doing so, PLS facilitates the identification of meaningful patterns and relationships between the shape variables within the blocks, allowing researchers to gain valuable insights into the covariation of anatomical structures represented by the landmarks.

The Partial Least Squares analysis (PLS) results in pairs of singular axes, the covariation between these blocks can be quantified for each pair of axes by calculating Pearson's correlation coefficient between the scores of each block (Hollander et al., 2013). To assess the significance of this association, the estimated value is compared to a distribution of values obtained by randomly permuting the individuals in one block, a process repeated 1000 times. If the estimated covariation exceeds a predetermined threshold, such as 5% of the permuted values, the association is deemed statistically significant at the 5% level, with a p-value less than 0.05 (Bookstein et al., 2003).

In the application of Partial Least Squares (PLS) to landmark data for studies of modularity and integration in work package II, General Procrustes Analysis (GPA) is initially performed separately for each block of landmarks. Subsequently, PLS is conducted between these blocks of data. The alignment of the two blocks of landmarks is achieved through Procrustes superimposition for each species. Performing GPA separately for each block is essential, as conducting a common superimposition for the entire dataset before running the PLS analysis could lead to an overestimation of the percentage of covariance between blocks. This overestimation arises from the introduction of covariance between all specimens and across all landmarks, particularly among the more contiguous ones.

The output of the PLS analysis consists of a series of plots displaying pairs of singular axes. These axes demonstrate the association between the two blocks of landmarks. Furthermore, the proportion of total covariance explained by each pair of axes is computed. Additionally, PLS allows for the calculation of the proportion of total variance in each block that is explained by each singular axis for that specific block (Cardini, 2019).

A strong association between blocks does not necessarily indicate that a large proportion of the variance of each block is explained by the analysis. Thus, blocks can be strongly associated, but this association may account for a large or a small proportion of variance in each block. A strong and highly significant association that accounts for a very small proportion of the total variance in one or other block, while being statistically significant, might have little real morphological or biological meaning. For the visualization of the patterns of association resulting from PLS, the mean of each block is warped along each singular axis, and the two warpings are presented.

Morphological integration pertains to the extent of correlation observed among various

traits within an organism, encompassing functional, developmental, and genetic aspects (Olson & Miller, 1985). In our study, we focused on analyzing the integration among diverse modules comprising the frontal bone and explored their associations in relation to sexual dimorphism. Integration refers to the extent of interconnection observed among various traits within an organism, reflecting their coordinated development and functional relationships. This integration ensures that different parts of the organism work together efficiently to fulfill specific functions. On the other hand, modularity explores the presence of subdivisions or modules within an organism, where certain traits demonstrate stronger integration among themselves compared to other traits. These modules maintain a level of independence from each other while contributing to the overall function and structure of the organism.

In summary, integration emphasizes the interconnectedness of traits, while modularity identifies distinct functional units within an organism that operate with some degree of autonomy. Both concepts contribute to our understanding of how biological systems are organized and adapted to meet specific ecological demands.

3.3.3 Neural Network Analysis

Neural Network Analysis (NNA) is a branch of artificial intelligence that seeks to replicate the functioning of the human brain by employing interconnected neurons. These neurons receive input values and calculate the results using an activation function. The architecture of the network, including the arrangement of neurons, the direction of flow, and the distribution of layers, is crucial for NNA analysis. In our study, we utilized the H2O package in R (LeDell et al., 2022) to implement NNA, specifically opting for a Feed-Forward Neural Network (Attia et al., 2022).

The Feed-Forward Neural Network operates in a unidirectional manner, with data flowing only in the forward direction and not backtracking. The network consists of layers comprising nodes or neurons, connected by links. In the input layer, the data (features) are introduced into the network. For our analysis, the parameter tuning data were divided into 10 training and validation datasets (Mueller & Massaron, 2021; Witten et al., 2016).

The hidden layers form the intermediate part of the network, where the input data undergo transformations to extract relevant features. This leads to the final part of the network represented by the output layer. During the hidden layer, the algorithm assesses the performance of models on the validation sets, enabling the selection of the best-performing model.The output layer receives the processed data from within the network and produces results based on the learned patterns and relationships (Feng & Lu, 2019).

In our NNA analysis, we utilized a non-linear activation function. The process involved training the model using the combined dataset of training and validation sets to obtain the best-performing model. The performance of the best model was then evaluated using a separate test dataset. A crucial aspect of NNA is parameter tuning, which involves considering various factors that influence the network and affect its performance. The selection and adjustment of these parameters significantly impact the algorithm's effectiveness (Svozil et al., 1997).

One approach to parameter tuning is the "brute force" method, where the training algo-

rithm is executed multiple times with different combinations of parameters. Validation of the models is crucial in this process. Furthermore, to enhance the complexity of the model, one can consider increasing the number of nodes and layers. However, it is essential to note that a more complex model does not necessarily guarantee better performance. Overfitting is a potential challenge that arises when the algorithm excessively captures intricate details and replicates them during the prediction phase. This often occurs when there is redundant information or when the training and validation sets overlap, leading to high variance in estimates (Del Bove, Veneziano, 2022).

An essential concept in NNA is the definition of an epoch. Each epoch represents a learning cycle encompassing each model's training and validation phases. In our study, a maximum of 1000 epochs were set. During the validation phase, predictions were compared to the output. Additionally, cross-validation of Howell's data was performed during the training and validation processes. A total of 98 models were trained and evaluated 10 times. After generating multiple models during the parameter tuning process, we carefully examined each model's performance to identify the one with the best results. This selection allowed us to construct the final model, which represents the optimal approach for analyzing sex detection. Once the final model was obtained, it demonstrated the ability to generalize its predictive power effectively.

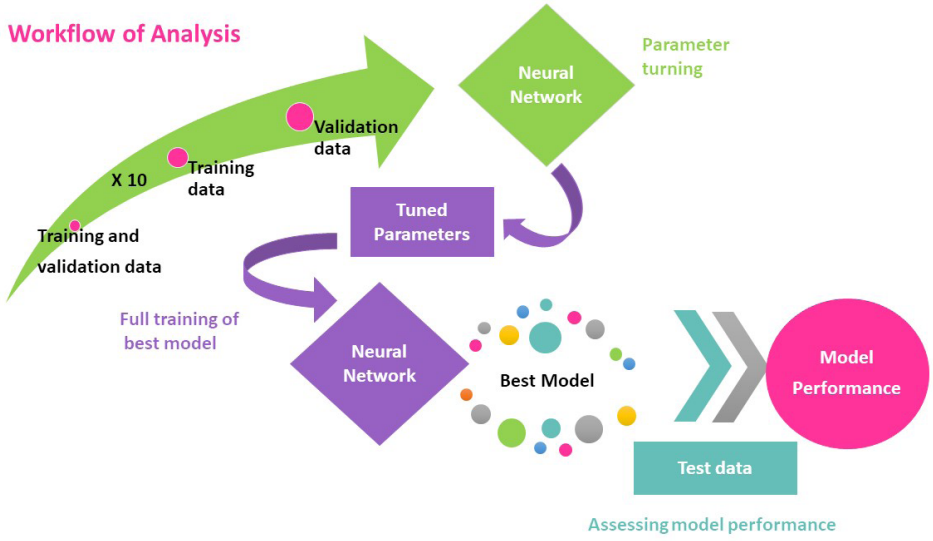

Fig. 21. Workflow of NNA.

3.4 Open Science

Open Science encompasses a scientific practice that promotes collaboration, enrichment, contribution, and verification of research processes through the availability of research, data, and methods in a freely accessible manner. Adhering to the principles of Open Science, the majority of the work presented in this thesis was conducted with a focus on reproducibility. This involves providing open access to experimental elements to facilitate research replication. To achieve this, the data (including landmarks, semilandmarks, linear measurements, and crania meshes) as well as the analysis scripts were published and made available. The analyses performed throughout the thesis were conducted using the open-source software R. The scripts for all work packages, with the exception of work package 1, were published with a Digital Object Identifier (DOI) and can be accessed through the Zenodo repository (DOI: 10.5281/zenodo.3940597; DOI: 10.5281/zenodo.7933169). The script for work package IV is available on GitHub at the following URL: https://github.com/AlessioVeneziano/Papers/tree/d51af94816ab57e02e3e9b5bf6e387fb4c3aae42/DelBove_%26_Veneziano_2022.

Fig. 22. Open Science rules Source : Australian National Data Service (ANDS)

4. Results

This section presents the findings of each studies as outlined in Chapter 2. The results adhere to the same organizational structure of the objectives. To preserve the original format and comply with the copyright policies of each respective journal, we present the complete papers in their original form.

4.1 Results about the study of sexual dimorphism in the neurocranium

In this section, we present the results of the I. session about the study of sexual dimorphism of the neurocranium titled "Sexual Dimorphism in the Neurocranium," which resulted in the publication titled "Detection of Sexual Dimorphism in the Neurocranium at a Local Scale."

The study focuses on exploring the morphology of the neurocranium concerning sexual dimorphism. Geometric Morphometrics (GM) method was applied to analyze a sample of 164 individuals, using a configuration of 50 landmarks and a patch of 500 semilandmarks to capture the external surface of the neurocranium. Multivariate Analysis was employed, and the novelty lies in applying the analysis to a single group of semilandmarks to investigate the anatomical response to sexual dimorphism.

Initially, Principal Component Analysis (PCA) demonstrated substantial overlap between both sexes (Fig. 2). The results identified a "Best Dimorphic Patch," wherein only the semilandmarks with a p-value < 0.05 were classified as dimorphic. Linear Discriminant Analysis (LDA) and shape variation analysis revealed that the anatomical regions most affected by sexual dimorphism were the frontal bones, with a lesser influence from the eminence of parietal bones (Fig. 3 and Fig. 4).

The accuracy of dimorphism detection for the entire neurocranium was determined to be 0.79, and the precision of discrimination was 78% for females and 83% for males.

2019 IMEKO TC-4 International Conference on
Metrology for Archaeology and Cultural Heritage
Florence, Italy, December 4-6, 2019

Detection of sexual dimorphism in the human neurocranium at local scale

Antonietta Del Bove[1,2], Antonio Profico[3], Carlos Lorenzo[1,2]

[1] *Catalan Institute of Human Paleoecology and Social Evolution (IPHES), Tarragona (Spain)*
[2] *Area de Prehistòria, Universitat Rovira i Virgili (URV), Tarragona (Spain)*
antoniadelbove@gmail.com; clorenzo@iphes.cat
[3] *PalaeoHub, Department of Archaeology,University of York, York (United Kingdom)*
antonio.profico@uniroma1.it

***Abstract* – In physical anthropology sexual dimorphism refers to the morphological differences observed in female and male individuals belonging to the same species. In the human cranium a number of anatomical traits are known to be sexual dimorphic. In this work, we present a geometric morphometric approach to automatically detect the most sexual dimorphic on skeletal collections. We applied the workflow on the human neurocranium and we defined, without an a priori definition of modules, which portions are most sexually dimorphic. We used a large sample of sex-known human 3D skulls to analyse the rate of sexual dimorphism found in the human neurocranium. We applied the Procrustes ANOVA on the best dimorphic patch found using the proposed workflow. We calculated the accuracy in discriminating sex in a sex-known sample by using our proposed model and the traditional approach.**

I. INTRODUCTION

The study of archaeological populations is a crucial step to reconstruct the lifestyles in the past. In addition, the morphological analysis of human remains returns essential information about the biological profile of populations. In bio-archaeology, the recognition of sex is essential to increase our knowledge about the culture of ancient populations, their funerary rituals and their gender concepts e.g. [1], [2]. In physical anthropology the analysis of sexual dimorphic traits is performed by distinguishing males and females by a visual assessment or metric estimation [3].

Standard anthropological approaches briefly associate a score to masculine and feminine morphology at specific anatomical traits. Optionally a weight could be associated to the score of skeletal features[4]–[6][7]. On the human neurocranium the traits taken into account include the morphology of the glabellar region, the supraorbital torus, frontal eminence, bregma, parietal eminence, mastoid shape and size, neurocranial architecture and frontotemporal constriction.

In the last years, a number of papers focused on the use of innovative shape analysis (Geometric Morphometrics, GM) method to classify a human specimen as male or female [8]–[10]. GM is a landmark-based method and it requires the definition a priori of the anatomical traits under investigation by acquiring the geometrical topology in the sample. In GM the anatomical region is described by the acquisition of anatomical (landmarks) and geometrical (semilandmarks) points [11]. The use of semilandmarks requires a sliding step to establish the geometric correspondence of the semilandmarks by removing the effect of the arbitrary initial spacing minimizing the TPS bending energy between each individual and the Procrustes mean shape [12]. The neurocranium shape can be analysed to investigate the human variability and the principal axes of variations can be used as input to classify the specimens regarding to categorical variables as the sex. In this paper, we present a GM based approach capable to identify locally which portions of skeletal surface are most sexual dimorphic. We tested the approach on a large collection of sex-known human specimen analysing the neurocranial morphology. This approach does not require an a priori definition of anatomical modules. It discretizes the surface in triangles and it analyse locally the entire topology calculating through a Procruste ANOVA [13] which triangles are related to a categorical variable: sex in our case study.

II. DIGITAL ACQUISITION

The arising of Virtual Anthropology development of computerized technologies based on X-rays, structured-light, and photogrammetry, allows us to acquire and digitally process osteological collections. Further analytical tools based on statistical and multivariate methods for the study of skeletal variability allow an assessment of evolutionary and

functional of human collections. The sample used in this study consists of acquisition via CT-scan and photogrammetry. X-ray tomography provides a series of 2D slices spaced by a constant distance which defines the resolution of the scan. Information about the radio density of the object comes from attenuation of radiation, resulting from absorption and scattering, caused by the object itself. By setting a proper radio density range is set, it is possible to calculate a 3D model [14], [15][16]. Photogrammetry is a method able to reconstruct 3D model starting from the acquisition of multiple images. Via photogrammetry the operator acquires a series of images of the specimen in different views. The collected images are then aligned, a sparse point cloud is generate allowing the calculation of a 3D model [17]. The quality of the models acquired thorough CT-scan and photogrammetry are comparable. Usually 3D model acquired via photogrammetry required post-production steps as smoothing and decimation [18].

III. MATERIALS AND METHODS

The sample size consisted of 163 crania (75 female and 88 male) belonging to four digital osteological repositories: i) the Lynn Copes digital Collection [19], [20], ii) the Museum of Anthropology "G. Sergi" from Sapienza University of Rome [21], iii) the Oloriz Collection from Spain and iv) the Anthropological Museum of Florence (University of Florence) [22]. The collections consisted of 3D models of crania of adult specimens of known-sex. The 3D models were obtained via photogrammetry and via CT scan as explained in the "Digital Acquisition" section. Each 3D model composing the sample of study has been decimated to 500.000 facets; no smoothing algorithm has been applied in order to avoid loss of anatomical information[23].

On each specimen, we collected 50 landmarks (Table 2) placed on the entire cranial morphology by using Avizo software (version 7). We defined on a specimen, chosen as reference, a net of geometric points (semi-landmarks). The patch of semi-landmarks consists of 500 bilateral and symmetric points.

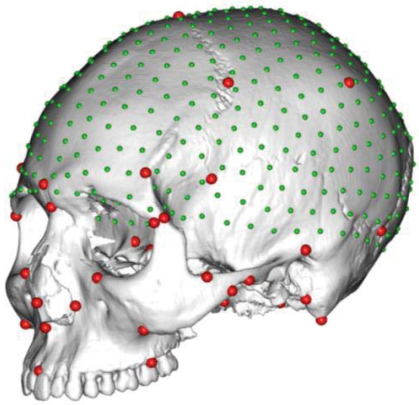

Fig. 1. Landmark (red) and semi-landmarks (green) shown on the reference specimen (grey).

We analysed the shape of the entire neurocranial region by performing a PCA on the scaled and rotated landmark and semi-landmark configuration after the Generalized Procrustes Analysis. We reported in figure 2 the PCA of the first two PC scores.

Methodological design

We devised an approach to detect dimorphic sexual signal into a very small local scale. First, we built a triangulation starting from the entire semi-landmark configuration (500 points); second, we performed on the three vertices composing each triangle of the triangulation a Procrustes ANOVA test (function procD.lm of the geomorph R package) [13] and we calculated at each triangle the p-value and the R-squared value.

We built a semi-landmark patch by using only the vertices belonging to those triangles presenting a p-value lower than 0.05. The semi-landmark patch so defined is the best sexual dimorphic patch (BDP) in the neurocranium.

By using the procedure described below, we are able to find morphological patches responding to categorical variables as sex in this study. We tested the goodness of fit of the procedure by creating 1000 random patches formed by N contiguous semi-landmarks of the same size of the BDP. The connection between semi-landmarks has been extrapolated from the triangulation of the entire set of semi-landmarks. At each iteration we calculated the R-squared value. We counted the number of iterations in which the R-squared value is lower than that observed in the BDP and we divided by the number of total observed values (number of iterations + BDP). In this way, we properly defined the p-value.

Detection of sexual dimorphism in BDP

On the entire neurocranium and in the BDP we performed a Linear Discriminant Analysis (LDA) considering in the model the 75% of the shape information (PCscores), the Centroid Size (CS) and the sex variable. Subsequently, we calculated the accuracy of the model to discriminate, within the sample, the female and the male individuals.

IV. RESULTS

The PCA performed on the landmark and semi-landmark configurations highlights the presence of an overlapping between female and male morphology. The first two PC scores accounts for 37.61% of the total variance.

We calculated at each triangle of the triangulated patch of semi-landmark (500 vertices and 952 facets) the relation between shape and sex variable. For each triangle we extracted the p-value and R-squared after applying the Procruste ANOVA. We selected only the vertices belonging to the facets associated to a p-value lower than 0.05. This collection of vertices defined the Best Sexual Dimorphic Patch (BDP). As stated in the section "*Methodological design*" we calculated the Procrustes ANOVA on the BDP and on 1000 random contiguous patches sampled with same number of semi-landmarks (N=208). In Figure 4 is reported the R-squared distribution for the random patches. These values are bracketed between 0.010 and 0.018. The R-squared calculated on the BDP is equal to 0.029 and statically significantly lower than random patches (p-value = 0.001).

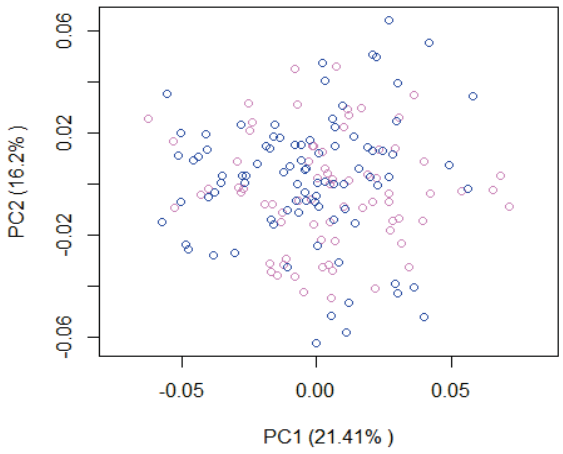

Fig, 2. PCA of the first two principal components performed on the entire neurocranium. Female and male specimens are reported in violet and blue respectively.

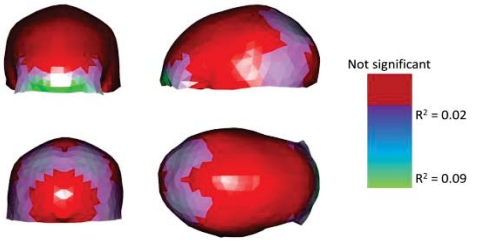

Fig. 3. Detection of local sexual dimorphism in the human neurocranium. In red triangles not sexual dimorphic (p-value greater than 0.05). The gradient of sexual dimorphism is reported in a colour gradient ranged from violet (low sexual dimorphism) to green (high sexual dimorphism).

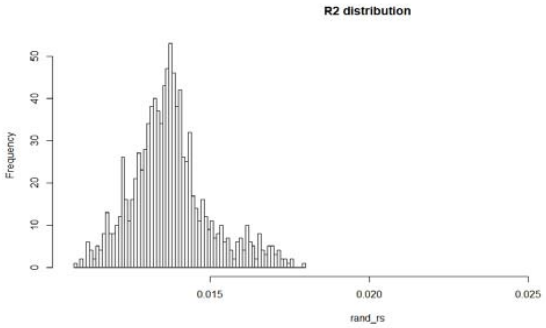

Fig. 4. Histogram showing the distribution of R-squared calculated on random and contiguous semi-landmark patches. The vertical line indicates the R-squared calculated on the best dimorphic patch.

The linear discriminant analysis performed on the entire neurocranium shows an accuracy equals to 0.79, while the precision to discriminate correctly females and males is equal to 75% and 83% respectively.

The same analysis performed on the BDP return a value of accuracy equals to 0.84. The precision to correct identify females is equal to 82%, the precision to classify male specimens is equal to 85%.

V. DISCUSSION

The study on sexual dimorphism landmark-based traditionally requires the definition of a model to be tested against the sex variable. For what concerns the skull the rate of expression of some anatomical feature

are easily recognisable such as development of supraorbital torus, the glabellar region, presence of the frontal eminence, orbital margin shape, shape of the zygomatic bone, mastoid size, the nuchal crest. In detail for the neurocranium only a few numbers of landmarks are detectable. For this reason, until now a quantitative approach is not possible. We overcome this issue by using a semi-landmark approach without a definition of modulus a priori.

Our results show as the neurocranium is not entirely sexual dimorphic despite in literature its globular architecture is associated to female morphology. We found as the major anatomical traits sexual dimorphic are found in correspondence with the supraorbital torus, the frontal-temporal constriction, the parietal eminence. We need to consider that the sample used in this study coming from different populations and the population affinity variable should influence the neurocranium morphology in some traits more than sex variable.

The advantage of using the approach reported in this study, is the chance to visualize the shape variations of the modules found related to sexual dimorphism only, deleting all the shape information not directly related to sexual dimorphism (fig. 5). In addition, a more extensive study of the entire cranial morphology could be taken as reference by physical anthropologists to correctly detect sex in sex-unknown archaeological populations.

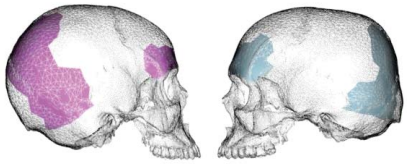

Fig. 5. Shape variations associated to the best dimorphic patch in females (left) and males (right)

VI. CONCLUSION

The potentiality of synergy between advances in technology (Virtual Anthropology) and shape analyse (Geometric Morphometrics) techniques has been shown in this case-study. Traditionally, physical anthropologists analyse the "real" skeletal collections in order to extrapolate information about the population as sex, age, paleopathology. This case-study showed as the use of digital models instead of physic ones could be a real alternative way to infer on the life history of human populations.

VII. ACKNOWLEDGMENTS

We are grateful to Prof. J. Moggi Cecchi and Dr. M. Zavattaro (Museum of Anthropology of Florence), Prof. G. Manzi (Museum of Anthropology of Rome "G. Sergi"), Dott. Tommaso Mori from University of Tubingen and Dr. L. E. Copes for sharing with us the osteological collections. This study is partially funded by the research projects of MICINN-FEDER (PGC2018-093925-B-C32), the AGAUR (SGR 2017-1040) and the URV (2018PFR-URV-B2-91) projects at IPHES-URV.

REFERENCES

[1] C. Hedenstierna-Jonson *et al.*, "A female Viking warrior confirmed by genomics," *Am. J. Phys. Anthropol.*, vol. 164, no. 4, pp. 853–860, Dec. 2017.

[2] G. A. Pearson, "Of Sex and Gender," *Science (80-.).*, vol. 274, no. 5286, p. 324g–329, Oct. 1996.

[3] E. DiGangi and M. Moore, *Research Methods in HUman Skeletal Biology*. 2013.

[4] P. L. Walker, "Sexing skulls using discriminant function analysis of visually assessed traits," *Am. J. Phys. Anthropol.*, vol. 136, no. 1, pp. 39–50, 2008.

[5] G. Acsádi and J. Nemeskéri, "History of human life span and mortality," 1970.

[6] J. Buikstra and D. Ubelaker, "Standards for data collection from human skeletal remains: Proceedings of a seminar at the Field Museum of Natural History (Arkansas Archaeology," *Fayetteville Arkansas Archaeological Survey*. 1994.

[7] T. D. White and P. A. Folkens, *The Human Bone Manual.* Elsevier, 2005.

[8] L. Bigoni, J. Velemínská, and J. Brůžek, "Three-dimensional geometric morphometric analysis of cranio-facial sexual dimorphism in a Central European sample of known sex," *HOMO- J. Comp. Hum. Biol.*, vol. 61, no. 1, pp. 16–32, 2010.

[9] P. E. Lestrel, E. Kanazawa, and C. A. Wolfe, "Sexual dimorphism using elliptical Fourier analysis: shape differences in the craniofacial complex," *Anthropol. Sci.*, vol. 119, no. 3, pp. 213–229, 2010.

[10] A. Rosas and M. Bastir, “Thin-plate spline analysis of allometry and sexual dimorphism in the human craniofacial complex,” *Am. J. Phys. Anthropol.*, vol. 117, no. 3, pp. 236–245, 2002.
[11] F. Bookstein, B. Chernoff, and R. Elder, “Morphometrics in evolutionary biology: the geometry of size and shape change, with examples from fishes,” 1985.
[12] P. Gunz and P. Mitteroecker, “Semilandmarks: a method for quantifying curves and surfaces,” *Hystrix, Ital. J. Mammal.*, pp. 1–77, 2013.
[13] D. C. Adams and E. Otárola-Castillo, “Geomorph: An r package for the collection and analysis of geometric morphometric shape data,” *Methods Ecol. Evol.*, vol. 4, no. 4, pp. 393–399, 2013.
[14] Y. Livnat, Han-Wei Shen, and C. R. Johnson, “A near optimal isosurface extraction algorithm using the span space,” *IEEE Trans. Vis. Comput. Graph.*, vol. 2, no. 1, pp. 73–84, Mar. 1996.
[15] G. W. Weber, “Virtual anthropology,” *Am. J. Phys. Anthropol.*, vol. 156, no. S59, pp. 22–42, 2015.
[16] G. W. Weber, “Virtual anthropology (VA): A call forGlasnost in paleoanthropology,” *Anat. Rec.*, vol. 265, no. 4, pp. 193–201, Aug. 2001.
[17] C. Nicolae, E. Nocerino, F. Menna, and F. Remondino, “Photogrammetry applied to problematic artefacts,” *Int. Arch. Photogramm. Remote Sens. Spat. Inf. Sci. - ISPRS Arch.*, vol. 40, no. 5, pp. 451–456, 2014.
[18] A. Profico *et al.*, “Virtual Anthropology and its Application in Cultural Heritage Studies,” 2018.
[19] L. Copes, “Comparative and Experimental Investigations of Cranial Robusticity in Mid-Pleistocene Hominins,” Arizona State University, 2012.
[20] D. R. Hunt and J. Albanese, “History and demographic composition of the Robert J. Terry anatomical collection,” *Am. J. Phys. Anthropol.*, vol. 127, no. 4, pp. 406–417, Aug. 2005.
[21] M. Rubini and P. Scarani, “Studio antropologico e patologico su 38 crani di individui deceduti durante la prima metà del XIX secolo presso il manicomio dell’ospedale di S. Orsola in Bologna. Patologie associate e variabilità dei caratteri metrici e discontinui.,” *Riv. di Antropol.*, vol. LXVII, pp. 273–2986, 1989.
[22] J. Moggi Cecchi and R. Stanyon, “The Anthropological and Ethnological Collections Il Museo di Storia Naturale,” vol. V, no. December, 2014.
[23] A. Veneziano, F. Landi, and A. Profico, “Surface smoothing, decimation, and their effects on 3D biological specimens,” *Am. J. Phys. Anthropol.*, vol. 166, no. 2, pp. 473–480, Jun. 2018.

4.2 Results about the study of sexual dimorphism in human frontal bone

That result is focused on the analysis of the frontal bone and was published in the American Journal of Physical Anthropology under the title "A geometric morphometric approach to the study of sexual dimorphism in the modern human frontal bone." In this study, we delved into how sexual dimorphism impacts the frontal bone of modern humans. The sample comprised 161 individuals from European and North American populations.

We tested three main questions in this paper

1. Are dimorphic traits present in all frontal bones in a similar manner?
2. Is size (CS - Centroid Size) a significant factor in the study of sexual dimorphism?
3. Is the sexual dimorphism detected in each trait of the frontal bone (glabella, frontal squama, supraorbital ridges) correlated with factors of integration and modularity?

To address these hypotheses, we employed the following analyses:

1. General Procrustes Analysis (GPA) to assess size in form space and shape space.
2. Analysis of Variance (ANOVA) to evaluate the influence of sex on frontal bone traits.
3. Linear Discriminant Analysis (LDA) to calculate the accuracy of the model in classifying individuals based on sex.
4. Partial Least Squares (PLS) analysis to investigate the modularity between modules.

Through our analyses, we aimed to gain valuable insights into the patterns of sexual dimorphism in the frontal bone and its association with factors such as size and integration. The findings presented in the published paper have illuminated the intricate interplay of shape variations within the frontal bone and their significance in sexual dimorphism among modern human populations. The results pertaining to size indicated that it may not be universally relevant for the entire frontal bone, but its importance varies across different analyzed modules (as indicated in Table 3).

However, we observed a notable improvement in accuracy when we considered the Centroid Size (CS) in form space, as shown in Table 4. Particularly, the module of supraorbital ridges exhibited the highest success rate for sexual dimorphism classification, with an accuracy of 86±1%. Additionally, our Partial Least Squares (PLS) analysis revealed correlations, such as the glabella showing a low degree of association with the squama and temporal lines.

Furthermore, through our shape variation analysis, we were able to visually represent the extremes of shape variations in the frontal bone between males and females, depicted in Fig. 2. This visualization provided valuable insights into the nature and magnitude of shape differences between the sexes.

Overall, the comprehensive results obtained through our geometric morphometric approach have significantly contributed to our understanding of sexual dimorphism in the frontal bone among modern human populations. The combination of size, shape, and integration analyses has shed light on the intricate relationships between these factors and sexual dimorphism, further advancing our knowledge.

Received: 23 November 2019 | Revised: 28 August 2020 | Accepted: 13 September 2020
DOI: 10.1002/ajpa.24154

RESEARCH ARTICLE

American Journal of PHYSICAL ANTHROPOLOGY WILEY

A geometric morphometric approach to the study of sexual dimorphism in the modern human frontal bone

Antonietta Del Bove[1,2] | Antonio Profico[3] | Alessandro Riga[4,5] | Ana Bucchi[1,2] | Carlos Lorenzo[1,2]

[1]Àrea de Prehistòria, Facultat de Lletres, Universitat Rovira i Virgili, Tarragona, Spain
[2]Catalan Institute of Human Paleoecology and Social Evolution IPHES, Tarragona, Spain
[3]PalaeoHub—Department of Archaeology, University of York, York, UK
[4]Department of Biology, University of Florence, Florence, Italy
[5]Laboratory of Archaeoanthropology, SABAP-FI, Scandicci, Italy

Correspondence
Antonietta Del Bove, Àrea de Prehistòria, Facultat de Lletres, Universitat Rovira i Virgili, Tarragona, Spain.
Email: antoniadelbove@gmail.com

Funding information
Agència de Gestió d'Ajuts Universitaris i de Recerca, Grant/Award Number: 2017 SGR 1040; Consejo Superior de Investigaciones Científicas, Grant/Award Number: PGC2018-093925-B-C32

Abstract

Objectives: We analyzed the main anatomical traits found in the human frontal bone by using a geometric morphometric approach. The objectives of this study are to explore how the frontal bone morphology varies between the sexes and to detect which part of the frontal bone are sexually dimorphic.

Materials and methods: The sample is composed of 161 skulls of European and North American individuals of known sex. For each cranium, we collected 3D landmarks and semilandmarks on the frontal bone, to examine the entire morphology and separate modules (frontal squama, supraorbital ridges, glabellar region, temporal lines, and mid-sagittal profile). We used Procrustes ANOVAs and LDAs (linear discriminant analyses) to evaluate the relation between frontal bone morphology and sexual dimorphism and to calculate precision and accuracy in the classification of sex.

Results: All the frontal bone traits are influenced by sexual dimorphism, though each in a different manner. Variation in shape and size differs between the sexes, and this study confirmed that the supraorbital ridges and glabella are the most important regions for sex determination, although there is no covariation between them. The variable size does not contribute significantly to the discrimination between sexes. Thanks to a geometric morphometric analysis, it was found that the size variable is not an important element for the determination of sex in the frontal bone.

Conclusion: The usage of geometric morphometrics in analyzing the frontal bone has led to new knowledge on the morphological variations due to sexual dimorphism. The proposed protocol permits to quantify morphological covariation between modules, to calculate the shape variations related to sexual dimorphism including or omitting the variable size.

KEYWORDS
sexual dimorphism, frontal bone, geometric morphometrics, LDA

1 | INTRODUCTION

Determination of sex is a crucial in all branches of physical anthropology. Many standards for building biological profiles, such as those for age, stature, and body mass estimation, are sex-specific (e.g., Brooks & Suchey, 1990; Formicola & Franceschi, 1996; Garvin & Ruff, 2012; Scheuer & Black, 2000; Trotter & Gleser, 1951). In forensic anthropology, correctly sexing an individual can drastically reduce possible matches of missing persons (DiGangi & Moore, 2013). In bio-archaeology, sexing individuals can provide unexpected insights into the culture of ancient populations, their funerary rituals, and their gender concepts (Hedenstierna-Jonson et al., 2017; Pearson, 1996). In

palaeoanthropology, size variation among specimens of early *Homo* has been alternatively interpreted as related to taxonomic differences or to sexual dimorphism (Plavcan, 2012; Spoor et al., 2007; Wood, Li, & Willoughby, 1991).

The difference between the sexes in terms of body size and shape, development, and behavior is called sexual dimorphism (DiGangi & Moore, 2013). In *Homo sapiens*, sexual dimorphism in the skeleton arises during growth and is determined and influenced by many genetic and environmental factors, such as hormones, development, and nutrition (Buikstra & Ubelaker, 1994; Frayer & Wolpoff, 1985; Lorenzo, Carretero, Arsuaga, Gracia, & Martínez, 1998; Steyn & Yaşar İşcan, 1998; Walrath, Turner, & Bruzek, 2004).

Physical anthropologists use sexually dimorphic traits in the skeleton to distinguish males and females through visual assessment or metric estimation (DiGangi & Moore, 2013). Sex assessment by visual inspection is widely used because, when highly dimorphic traits such as the pelvis are observable, it is fast and, if applied by trained scholars, its accuracy can reach more than 90% (Phenice, 1969; Ubelaker & Volk, 2002). In other circumstances, for example, when skeletal remains are incomplete or poorly preserved, measurement-based methods estimate sex are preferable (Spradley & Jantz, 2011). Many approaches to sex estimation have been developed, both on cranial and postcranial elements, based on single measurements and multivariate techniques (i.e., Konigsberg, Algee-Hewitt, & Steadman, 2009; Saini et al., 2011; Spradley & Jantz, 2011), or using a geometric morphometric (GM) approach (Bigoni, Velemínská, & Brůžek, 2010; Bytheway & Ross, 2010; Franklin, Oxnard, O'Higgins, & Dadour, 2007; Gonzalez, Bernal, & Perez, 2011; Kimmerle, Ross, & Slice, 2008; Perlaza, 2014; Pretorius, Steyn, & Scholtz, 2006; Rmoutilová, Dupej, Velemínská, & Brůžek, 2017).

1.1 | GMs and sex estimation

Since the first studies applying discriminant functions to linear measurements on skulls (Giles & Elliot, 1963; Uytterschaut, 1986), many authors have felt the need to find new quantitative methods to distinguish between sexes (i.e. Luo, Wang, Zhang, & Congbo, 2018; Small, Schepartz, Hemingway, & Brits, 2018; Suazo Galdames, Perez Russo, Zavando Matamala, & Luiz Smith, 2009). Among them, a number of scholars opted for a GM approach, and applied it to mandibles (Franklin et al., 2007), pelves (Bytheway & Ross, 2010; Rmoutilová et al., 2017), and skulls (Bigoni et al., 2010; Gonzalez et al., 2011; Kimmerle et al., 2008; Pretorius et al., 2006). In the last decades, GM proved itself to be a powerful tool for studying shape variation and its relationship to other variables like sex and population (Adams, Rohlf, & Slice, 2004; Baylac & Friess, 2005; Gunz et al., 2004; Rohlf & Leslie, 1993; Weber, 2015).

The GM method allows for the study of specific anatomical regions/traits by defining a set of geometric points (i.e., landmarks and semilandmarks). Through the study of the geometry of anatomical traits paired with multivariate statistical analyses, we can analyze shape components in detail, independent of dimensions, and relate changes therein to sex differences and other variables (Bookstein, 1989).

1.2 | Sexual dimorphism in the frontal bone

One of the elements most used for sexing individuals is the skull, considered by some anthropologists to be the second-most dimorphic area after the pelvis (but see discussion in Spradley & Jantz, 2011). In the human skull, morphological differences due to sexual dimorphism are recognizable in different anatomical regions, with males generally having a more robust appearance (Buikstra & Ubelaker, 1994; Frayer & Wolpoff, 1985; Walker, 2008).

The cranium is a complex structure organized in modules. From a morphological point of view, a module is defined as a within integrated unit and modules could be integrated and/or modular each other due to the interactions between them (Esteve-Altava, Diogo, Smith, Boughner, & Rasskin-Gutman, 2015; Klingenberg, 2014).

In accordance with "the Palimpsest Model of Covariation Structure" proposed by Hallgrímsson et al. (2009) the phenotype is influenced by the covariation between modules. Subsequently, the study of the pattern of integration between the parts composing the structure under investigation is determinant to interpret the morphological variations and differences in the light of functional and adaptive processes. The analysis of the pattern of covariation between sub-modules belonging to the same bone has been studied far less than the relation between bones.

The frontal bone, which is the focus of this article, is one of the most sexually dimorphic anatomical areas of the human cranium (Acsádi & Nemeskéri, 1970; Buikstra & Ubelaker, 1994). It is one of the largest cranial bones and represents part of the interface between the neurocranium and the upper face, articulating with the parietals, nasals, maxillae, sphenoid, ethmoid, lacrimal, and zygomatic bones (Bruner, Athreya, De La Cuétara, & Marks, 2013; White & Folkens, 2005).

In addition to frontal bone morphology, physical anthropologists analyze the size and shape of specific anatomical regions such as the supraorbital ridges, the frontal squama, the glabellar region, and the temporal lines during sex determination (Acsádi & Nemeskéri, 1970; Walker, 2008). Studies have found consistent differences in frontal bone morphology between females and males (Bulut, Petaros, Hizliol, Wärmländer, & Hekimoglu, 2016; Garvin & Ruff, 2012; Perlaza, 2014; Petaros, Garvin, Sholts, Schlager, & Wärmländer, 2017; Shearer, Sholts, Garvin, & Wärmländer, 2012). The frontal bone in males is more inclined, whereas in females it appears more vertical and rounded (Bulut et al., 2016). In general, the brow ridge and supraorbital region are the most sexually dimorphic areas of the frontal bone; specifically, supraorbital ridges in males tend to be extended inferiorly as compared to the relatively flat appearance of females (Garvin & Ruff, 2012; Perlaza, 2014; Shearer et al., 2012). The glabellar region has also been suggested in the literature as being a good proxy for sex assessment, as it is much larger in males (Perlaza, 2014; Petaros et al., 2017).

In this article, we propose a workflow developed in R (R Core Team, 2020) for the study of sexual dimorphism using a GM approach. The main purpose of this study is to analyze differences in shape and size in the frontal bone due to sexual dimorphism and to highlight how the frontal bone varies between the sexes in *Homo sapiens*. In detail, we tested the following hypotheses: (i) the human frontal bone shows a uniform degree of sexual dimorphism; (ii) in the frontal bone, the size of anatomical modules (i.e., supraorbital ridges, frontal squama, glabella, frontal profile, and temporal lines) has a relationship with the sexual dimorphism signal; and (iii) in the frontal bone the degree of sexual dimorphism detected is related to the pattern of integration and modularity between modules.

We measured how sexual dimorphism affects frontal bone morphology analyzing five different a priori anatomical modules (i.e., supraorbital ridges, frontal squama, glabella, frontal midsagittal profile, and temporal lines) by placing on them a set of curves or surface semilandmarks and we calculated the pattern of integration and modularity between the five modules defined on the frontal bone. These modules are those commonly investigated by physical anthropologists in assigning sex-to-sex-unknown collection. We also propose a standardized protocol for quantifying sexual dimorphism in the frontal bone to produce shape variations related only to sexual dimorphism, that can act as a standard for the detection of sex in osteological collection. For maximum certainty regarding the relationship between form and sex, we used only specimens of known sex; however, this markedly reduced our ability to use a global sample and prevented us from looking at interpopulation variability.

2 | MATERIALS AND METHODS

2.1 | Sample

The sample size consisted of 161 crania (74 females and 87 males) belonging to four digital osteological repositories: (i) the Lynn Copes digital Collection (Black Americans) from the Anthropology department at the National Museum of Natural History, Washington, DC (Copes, 2012); (ii) the Museum of Anthropology "G. Sergi" from Sapienza University of Rome (Rubini & Scarani, 1989); (iii) the Oloriz Collection in Spain; and iv) the Anthropological Museum of Florence (University of Florence) (Moggi Cecchi & Stanyon, 2014) (Table 1). The collections consisted of 3D models of crania of adult specimens of known sex. The 3D models were obtained via photogrammetry and CT scan.

2.2 | Data acquisition

In the case of samples obtained via photogrammetry, we used Agisoft PhotoScan software (version 1.4) to build 3D models.

On each specimen, we collected 13 fixed landmarks (Table 2) placed on the entire frontal bone using Avizo software (Version 7). The anatomical traits belonging to the frontal bone were defined by placing semilandmarks sets. The average distance calculated on the mean shape between each semi-landmark and its neighborhood (the closest 10 semilandmarks) is 1.06 ± 0.11 mm.

We opted to record the frontal midsagittal profile (19 points) and the temporal lines (22 points) by acquiring three curves. The frontal midsagittal profile starts from the frontonasal suture (i.e., *nasion*) to the coronal suture (i.e., *bregma*). The two temporal lines start from zygomaticofrontal suture (i.e., *frontomalare temporale*) to the coronal suture (i.e., *stephanion*; Figure 1). Before shape analysis, the R package Morpho was used to slide the curves to minimize bending energy (Schlager, 2017).

We defined frontal squama (161 semilandmarks), supraorbital ridges (36 semilandmarks), and glabellar regions (7 semilandmarks) by building a unique symmetric reference template. Subsequently, we

TABLE 1 List of collection used in this study

Population	Repository	Total	Females	Males
Fiorentini	A	58	27	31
Sardi	A	29	12	17
Siracusani	A	16	5	11
Bolognesi	B	26	16	10
Oloriz	C	11	3	8
Terry collection	D	21	11	10

Abbreviations: A, Museum of Anthropology and Ethnology, University of Florence; B, Museum of Anthropology "G. Sergi" from Sapienza University of Rome; C, Nespos repository and D, Terry Collection of the National Museum of Natural History, Washington, DC.

TABLE 2 List of cranial landmarks with definitions (White & Folkens, 2005).

Numbers	Landmarks	Definition
1	Nasion	The midline point where the two nasal bones and the frontal intersect
2	Glabella	The most anterior midline point on the frontal bone
3	Bregma	The ectocranial point where the coronal and sagittal sutures intersect
4–5	Ectoconchion	The most lateral point on the orbital margin
6–7	Frontomalare temporale	The point where the frontozygomatic suture crosses the temporal line
8–9	Frontotemporale	The point where the temporal line reaches its most anteromedial position on the frontal
10–11	Stephanion	The point where the coronal suture crosses the temporal line
12–13	Pterion	The point, where the frontal, temporal, parietal, and sphenoid meet on the side of the vault

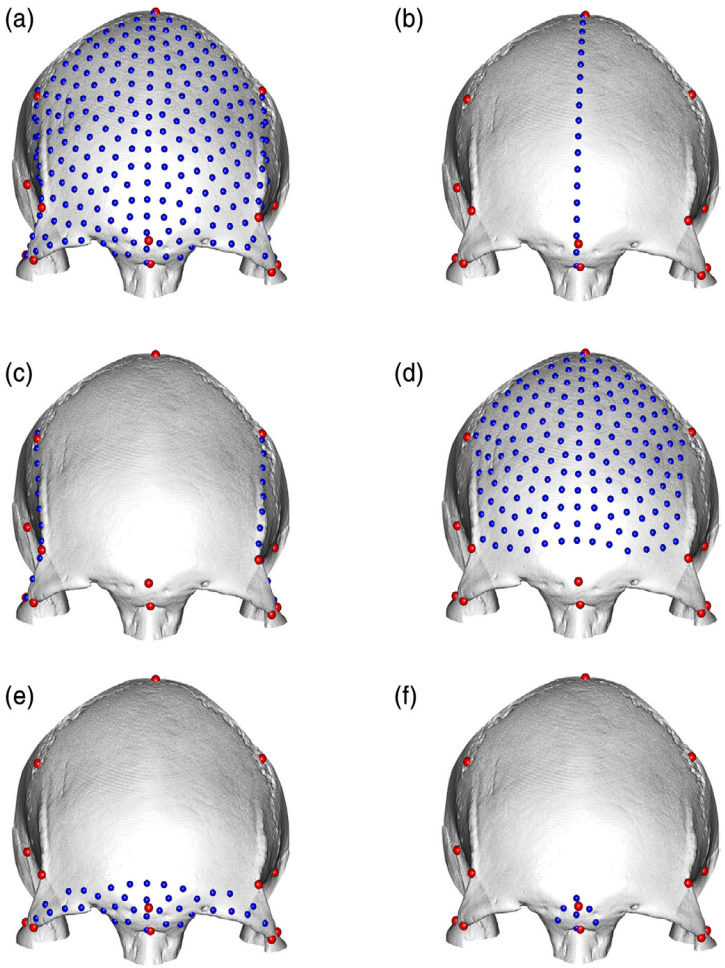

FIGURE 1 Landmark and semilandmark configurations used in this study. In red anatomical landmarks, in blue surface semilandmarks and curves. The modules tested are as follows: entire frontal shape (a), mid-sagittal profile (b), temporal lines (c), frontal squama (d), supraorbital ridges (e), glabellar region (f)

split the entire slid semilandmark patch into three sub-modules: one for each anatomical trait (Figure 1). The sliding procedure was performed by sliding the entire patch (Morpho R package).

2.3 | Linear discriminant analysis, integration, modularity, and shape variations

The morphology of the entire frontal bone was analyzed by performing a PCA on the semilandmarks sets after generalized procrustes analysis (GPA). We performed the analysis in the shape and form space (the log of the centroid size [CS] is added as variable to the coordinates after the GPA) in order to investigate the relation between sex and frontal bone morphology including and excluding the size variable.

We evaluated the influence of sex on shape and size by using the Procrustes ANOVA embedded in the geomorph R package (Adams, Collyer, & Kaliontzopoulou, 2019).

In addition, we performed an linear discriminant analysis (LDA) using PC scores (defined as 95% of the shape information) as dependent variable; the log of the Centroid Size (logCS) and sex are considered as independent variables. We used the logCS as a proxy for the actual size of the anatomical regions under investigation. Subsequently, we calculated the accuracy of the model in classifying individuals based on sex by designing a bootstrap procedure (1,000 iterations). At each iteration, we randomly sampled 100 individuals, at the end of the iterative procedure we calculated the mean accuracy and the standard deviation of the model in discriminating sex.

We calculated the pattern of integration and modularity among all the combinations (10 pairs of comparisons) of the five

morphological modules defined on the frontal bone in the female and male sample. We evaluated integration within the frontal bone by applying a partial least square (PLS) between two modules at a time (Rohlf & Corti, 2000). We considered as signal of integration the correlation coefficient between PLS scores of the first PLS axis. The modularity between modules (Adams, 2016; Klingenberg, 2009, 2013) has been assessed by calculating the covariance ratio (CR) between pairs of modules.

For each morphological module defined in the frontal bone, we built the shape variations associated to female and male morphology. We consider as shape the first PC scores accounting the 95% of the total explained variance. On each PC, we test differences in means between females and males applying the T-Student test. In the definition of the shape variation of each module, we considered only the PC scores statistically different between male and female groups summing their contribution. Though canonical variate analysis (CVA) produces a high degree of accuracy, we used PCA because CVA standardizes total variance by the within-group variance, thus altering the pattern of differentiation among groups (Renaud, Dufour, Hardouin, Ledevin, & Auffray, 2015).

3 | RESULTS

3.1 | Procrustes ANOVA

Results from the Procrustes ANOVA show that variables "sex" and "size" are significantly related to the morphology of the entire frontal bone and its sub-modules (frontal squama, supraorbital ridges, glabellar region, temporal line, and frontal mid-sagittal profile) except for the relation between size and temporal lines in the shape space (Table 3). The inclusion of "size" in the shape variable increases the R^2 in all the modules tested.

The interaction between "sex" and "size" is not significant in all the investigated modules. This means that the significances observed for the independent variables "sex" and "size" is not due to their interaction.

3.2 | Linear discriminant analysis

The results of the LDA differ depending on whether CS is included in the analysis. Accuracy and precision in sex estimation are usually higher when CS is excluded (Table 4). The best success in discriminating sexes was achieved by LDAs on the "supraorbital ridges" when size is excluded with 86 ± 1% success rate. The "temporal lines" in both shape space and form spaces show the worst rate of success with 63 and 69%, respectively. In sum, when size is excluded from the analysis only the "supraorbital ridges" (86%) show higher or equal success rate in discriminating sex than the entire frontal bone morphology (82%). In the form space only the "supraorbital ridges" (85%) shows a level of accuracy higher than the entire frontal bone (80%; Figure 2).

3.3 | Integration and modularity in the frontal bone

In the PLS analysis, the "glabella" shows in males and females a low degree of covariation with the "squama" and the "temporal lines" (PLS-corr = .29, p = .30 in females and PLS-corr = .34, p = .03; Table 5). Instead, we observed in females a moderate degree of covariation between "glabella" and "supraorbital ridges" (PLS-corr = .89, p<.01) and a low degree of covariation between these two modules in males (PLS-corr = .74, p < .01). The test of modularity between all the combinations possible with the five modules show a general pattern of integration (the CR is close to 1) except in the comparison between "glabella and squama" (CR = 0.77, p < .01 in females, and CR = 0.82, p < .01 in males), "glabella and temporal lines" (CR = 0.79, p < .01 in

TABLE 3 Summary of the results of procrustes ANOVA performed on the semilandmark configurations after GPA in the shape and form space

Shape space	R^2 (sex)	p-value	R^2 (size)	p-value	R^2 (sex*size)	p-value
Entire	**.030**	**.001**	**.034**	**.001**	.004	.627
Glabella	**.074**	**.001**	**.106**	**.001**	.008	.198
Squama	**.023**	**.011**	**.062**	**.001**	.003	.698
Midsagittal profile	**.039**	**.002**	**.058**	**.001**	.002	.770
Supraorbital ridges	**.025**	**.002**	**.021**	**.010**	.004	.728
Temporal lines	**.024**	**.025**	.017	.065	.001	.914
Form space	R^2 (sex)	p-value	R^2 (size)	p-value	R^2 (sex*size)	p-value
Entire	**.078**	**.001**	**.400**	**.001**	.002	.627
Glabella	**.076**	**.001**	**.450**	**.001**	.005	.198
Squama	**.056**	**.001**	**.501**	**.001**	.001	.698
Midsagittal profile	**.098**	**.001**	**.642**	**.001**	.001	.770
Supraorbital ridges	**.090**	**.001**	**.595**	**.001**	.001	.728
Temporal lines	**.086**	**.001**	**.457**	**.001**	.001	.914

Note: Statistically significant results in bold.

TABLE 4 Precision and accuracy (expressed as percentage) calculated on the modules defined in the frontal bone in classifying sex in the shape space and form space

Shape Space	Accuracy upper	Accuracy mean	Accuracy lower	Precision female upper	Precision female mean	Precision female lower	Precision male upper	Precision male mean	Precision male lower
Entire	81.996	81.784	81.572	81.993	81.743	81.493	82.120	81.897	81.674
Glabella	78.755	78.556	78.357	76.308	76.079	75.850	80.876	80.659	80.442
Squama	73.469	73.273	73.077	71.777	71.543	71.309	74.841	74.639	74.437
Midsagittal profile	79.129	78.912	78.695	77.154	76.891	76.628	80.932	80.697	80.462
Supraorbital ridges	85.721	85.545	85.369	85.075	84.837	84.599	86.344	86.146	85.948
Temporal lines	62.827	62.633	62.439	59.929	59.490	59.051	64.330	64.124	63.918
Form Space	**Accuracy upper**	**Accuracy mean**	**Accuracy lower**	**Precision Female upper**	**Precision Female mean**	**Precision Female lower**	**Precision Male upper**	**Precision Male mean**	**Precision Male lower**
Entire	80.083	79.879	79.675	78.293	78.053	77.813	81.454	81.247	81.040
Glabella	73.657	73.467	73.277	71.220	71.002	70.784	75.675	75.456	75.237
Squama	73.075	72.872	72.669	70.625	70.367	70.109	75.136	74.934	74.732
Midsagittal profile	76.570	76.371	76.172	76.413	76.198	75.983	76.710	76.488	76.266
Supraorbital ridges	85.104	84.913	84.722	83.306	83.064	82.822	86.700	86.506	86.312
Temporal lines	69.712	69.494	69.276	67.533	67.265	66.997	71.385	71.165	70.945

females, and CR = 0.78, $p < .01$ in males). Despite the CR being close to 1 when the modularity test is performed between "glabella" and "supraorbital ridges", the *p*-value is not statistically significant (Figure 3).

3.4 | Shape analysis

When looking at the entire set of semilandmarks, males are characterized by an antero-posteriorly elongated frontal bone; the temporal lines are closer to the midsagittal plane than in females, and the frontal squama are oriented horizontally. The frontal squama in females are shorter than those observed in males and their orientation, as noted above, is vertical on females and horizontal in males. Compared to males, the central superior margin of the supraorbital ridges of females are slightly expanded as compared to males. The glabellar region in females is related to horizontal expansion of the frontal bone and appears more vertically elongated, while males have a protruded glabellar region. Temporal lines in females are shorter vertically and restricted laterally, because the intersection between the coronal suture and the stephanion is positioned lower and anteriorly.

The frontal midsagittal profile in males is horizontal and a bulging is detectable at the level of the glabellar region. The female profile is vertical and short. In females, bulging is visible in the frontal eminence and the glabellar portion appears deflated. Additionally, midsagittal lines emphasize the male-horizontal and female-vertical feature of frontal bone. The male frontal bone morphology is characterized by an expansion of the squama in the anterior portion and by the presence of longer temporal lines. The supraorbital ridge in males is expanded laterally and reduced medially in correspondence of the glabella.

4 | DISCUSSION

The approach used in this study was specifically designed to encompass all the steps made by physical anthropologists during sex determination. In fact, the frontal bone shape was acquired in its entirety. In the analysis, we considered both local (module) and whole morphologies. A great advantage to using GM is the decomposition of the variance along single and independent shape variables. For each defined module, we took into consideration only the PC scores which were statistically significant for sex discrimination. The use of a sample of individuals of known sex eliminated researcher subjectivity in sex determination, and so the accuracy values are reliable. In addition, this approach may be used by other researchers on other anatomical regions.

We built six pairs (female and male) of shape variations (entire morphology + five modules) adding in each pair only the PC scores separating female from male individuals. The results of these shape variations are specifically related to morphological differences due to sexual dimorphism and could supply clear guidelines for sex determination of specimens of unknown sex.

This study, through a GM approach, demonstrates that sexual dimorphism significantly influences the morphology of the frontal bone in all the modules analyzed. Frontal bone morphology is influenced by both sex and size. Analyzing sexual dimorphism in each trait can help us understand how specific differences are due to sexual dimorphism. From the shape variations, most of the differences

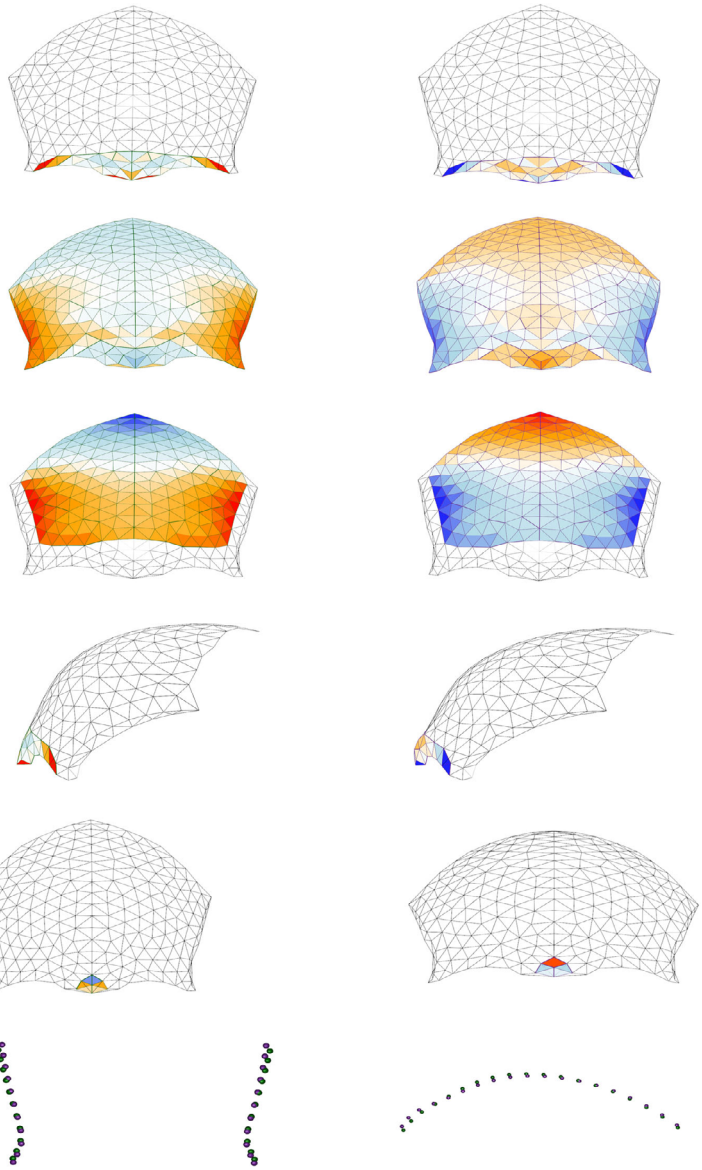

FIGURE 2 Shape variation associated to the female (left) and male (right) morphology for each module considered in this study. Warm colors are associated to regions characterized by local contraction (of area), cold colors indicate local expansion of area. In the first four rows, the shape variations related to the female morphology are reported on the left, those related to the male morphology on the right. The shape variations of the temporal lines and mid-sagittal profile related to the female and male morphology are shown respectively in dark green and violet

between sexes in the squamous regions are found in the frontal eminence, in agreement with a prior study on the inclination of frontal bone (Bulut et al., 2016). The morphology of the supraorbital ridges is different in female and male specimens and is particularly important for detecting sex differences between males and females (Table 4). In females the supraorbital ridges is flattened medially while in males it is well-developed medially. The degree of shape variation of the frontal bone demonstrates that the supraorbital ridges is particularly important for detecting sex differences between males and females. In the literature, the glabella is often held to be the most informative trait for determining sex in osteological collections. Using this variable, our models were 79% (excluding CS) and 73% (including CS) accurate at predicting sex, indicating that this anatomical trait is a good indicator of sex. Many studies (Acsádi & Nemeskéri, 1970; Buikstra & Ubelaker, 1994; White & Folkens, 2005) have indicated that the glabellar region is expanded in males and contracted in females. A recent

TABLE 5 Results of the PLS (integration) and CR (modularity) analyses

Female	PLS corr	PLS *p*-value	CR corr	CR *p*-value
Glabella versus squama	.29	.30	**.77**	**<.01**
Glabella versus midsagittal profile	**.79**	**.02**	1.01	.06
Glabella versus supraorbital ridges	**.89**	**<.01**	.97	.07
Glabella versus temporal lines	.32	.16	**.79**	**<.01**
Squama versus midsagittal profile	**.79**	**<.01**	**.89**	**<.01**
Squama versus supraorbital ridges	**.67**	**<.01**	**.86**	**<.01**
Squama versus temporal lines	**.95**	**<.01**	**.94**	**<.01**
Midsagittal profile versus supraorbital ridges	**.63**	**<.01**	**.77**	**<.01**
Midsagittal profile versus temporal lines	**.43**	**<.01**	**.79**	**<.01**
Supraorbital versus temporal lines	.61	.16	**.88**	**<.01**
Males	**PLS-corr**	**PLS-*p*-value**	**CR-corr**	**CR-*p*-value**
Glabella versus squama	**.34**	**.03**	**.82**	**<.01**
Glabella versus midsagittal profile	**.61**	**<.01**	**.98**	**.03**
Glabella versus supraorbital ridges	**.74**	**<.01**	1.01	.20
Glabella versus temporal lines	.24	.45	**.78**	**<.01**
Squama versus midsagittal profile	**.71**	**<.01**	**.92**	**<.01**
Squama versus supraorbital ridges	**.56**	**<.01**	**.89**	**<.01**
Squama versus temporal lines	**.95**	**<.01**	**.94**	**<.01**
Midsagittal profile versus supraorbital ridges	**.64**	**<.01**	**.88**	**<.01**
Midsagittal profile versus temporal lines	**.47**	**<.01**	**.82**	**<.01**
Supraorbital versus temporal lines	**.45**	**.01**	**.89**	**<.01**

Note: On the first column are shown the pairs of tested modules in males and females. Statistically significant results are in bold.

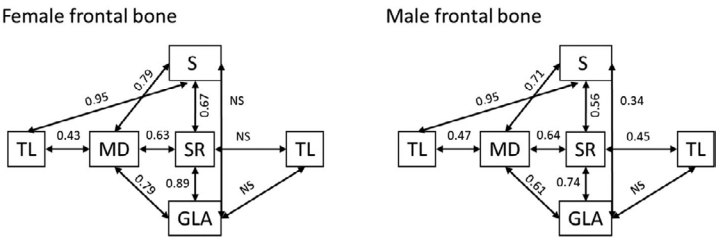

FIGURE 3 Network of integration between the modules defined in the frontal bone. The numbers indicate the correlation coefficients between the PLS scores of the first PLS axis (NS, result not statistically significant). On the left and right the networks for respectively female and male subsamples. GLA, glabella; MD, midsagittal profile; S, squama; SR, supraorbital ridges; TL, temporal lines

article about the inclination of the glabella (Petaros et al., 2017) suggests that the morphology of the glabellar region is related to the population variable. The five modules investigated in this work show a low level of integration (Table 5), except for a clear signal of morphological integration between the frontal squama and the temporal lines, suggesting that the sexual dimorphic signal we observed in the glabellar region and in the supraorbital ridges is not due to the covariation between these two modules.

Unexpectedly, the visual perception that the anatomical traits of the frontal bone in males appear bigger than those in females is not confirmed by both Procrustes ANOVA and LDA. From Procrustes ANOVA (Table 3) the interaction between the variables sex and size is not statistically significant in both shape and size space indicating the level of the sex variable does not depend on the size variable. In addition, in the LDA analysis the inclusion of size led to the reduction of the accuracy except for the "temporal lines." These findings are also confirmed when comparing the predicted sexes from the LDA analysis by using separately the variables size and shape. The percentage of the specimens correctly classified by sex in both analyses ranged between 28.57 and 54.66% (entire = 46.58%, glabellar region = 47.82%, squama = 28.57%, midsagittal profile = 43.48%, supraorbital ridge = 54.66%, temporal lines = 34.16%). This confirms that the variable size should be treated with caution in sexing archaeological collections basing on frontal bone morphology.

In sum, these results reject the hypothesis that human frontal bone shows a uniform signal of sexual dimorphism. The results reject the hypothesis that the variable size increases the accuracy in detecting sex. Last, the hypothesis that "in the frontal bone the degree

TABLE 6 Summary of previous studies on the sexual dimorphism signal found in the frontal bone

Anatomical region	Methodology	Number of individuals	Accuracy	Reference
Supraorbital ridges	T-test on 3D volume	128	NA	Shearer et al., 2012
Frontal bone inclination	Trait scoring	413	76.1% 81.1% 74.8% 66.3%	Petaros et al., 2017
2D sagittal profile on the glabellar region and supraorbital regions	LDA	60	84.31%	Perlaza, 2014
Entire frontal bone	LDA	160	77.5 %	Bulut et al., 2016
Supraorbital ridges	Cross-validation LOOCV	119	91.6%, 79.8%	Garvin & Ruff, 2012
Entire frontal bone	Cross-validation	103	83.49% 86.41%	Čechová et al., 2019
Glabellar region	Trait scoring	90	84.0 % 86.0 %	Çelbiş, İşcan, Soysal, & Çağdir, 2001

of sexual dimorphism detected is related to the pattern of integration and modularity between modules" is falsified because the two most dimorphic modules "glabella" and "supraorbital ridges" are not strongly integrated (Table 5).

Prior research has demonstrated that ancestry interacts with sex in shaping cranial morphology. Not all traits are subject to the influence of ancestry, nor are they affected equally: for example, the glabellar region, the nuchal crest, and the temporal lines show significant correlations between sex and ancestry (Bakken, Dale, & Schork, 2011; Garvin, Sholts, & Mosca, 2014; Jurda & Urbanová, 2016). Our study used only samples from individuals of known sex, which reduced our ability to investigate ancestry in a worldwide sample; moreover, the primary focus of our research was on the use of GM methodologies to study sexual dimorphism.

The shape variation of temporal lines shows how the morphology of this region is different in female and male individuals. Temporal lines in males are longer and narrower than in females. The different lengths of the temporal lines in females and males is linked to differences in the position of the stephanion. The accuracy of the model based on the temporal lines is equal to 63% (without CS), but when CS is taken into account the accuracy increases to 69% (Table 4), suggesting that size is an important factor in determining sexual differences.

Analyses of the mid-sagittal profile are relatively simple because its morphology is easily observable in lateral view. The sex shape variation model for this module highlights as the projection of the frontal mid-sagittal along the frontal squama is vertical in females and horizontal in males, confirming previous studies (Bigoni et al., 2010; Rosas & Bastir, 2002).

One goal of this study was to create a scale of importance of single traits in determining sex; based on the accuracy of our models when size is excluded, the supraorbital ridges (86%) is the most dimorphic trait, followed by the glabella (79%), the midsagittal profile (79%), the squama (73%), and lastly the temporal lines (63%). If the size is included in the analysis the supraorbital ridges (85%) is the most dimorphic trait followed by the midsagittal profile (76%), the glabella (73%), the squama (73%), and the temporal lines (69%).

Importantly, this study has allowed us to reconsider which traits of the frontal bone are most critical for determining sex. Through GM, it is possible to bypass the variables and consider the importance of traits individually. Thanks to the methodological approach we designed it is possible to investigate in detail the contribution of both shape and size in discriminating sex in osteological collections. We confirmed the previous literature (Table 6) about the importance of analyzing the supraorbital ridges and the glabellar region in classifying sex-unknown osteological individuals. On the contrary, we found that the size of the morphological traits of the frontal bone is not statistically related with sex in the sample we investigated; the only exception is found in the supraorbital ridges with a slight increment in detecting males (86% excluding size and 87% including size).

The same methodological approach on the entire cranium subdivided in modules should be considered by physical anthropologists to update the trait scores used in the classification of specimens as females or males. In addition, another advantage of a GM approach is the opportunity to build 3D models specifically accounting for sexual dimorphism as we demonstrated in this case study.

5 | CONCLUSION

We want to emphasize that one of the most important outcomes of this study has been an updated hierarchy of importance of sexually dimorphic areas of the frontal bone (supraorbital ridges, glabellar region, midsagittal profile, frontal squama, and temporal lines). Specifically, the supraorbital ridge region impacts more than

entire frontal bone. The results of this study suggest that size differences in the frontal bone modules between males and females should be reconsidered as an important factor in sexing individuals.

ACKNOWLEDGMENTS

The authors thank two anonymous reviewers for their insightful comments that helped improving our manuscript. This project has received funding from the Agència de Gestió d'Ajuts Universitaris i de Recerca (Grant n° 2017 SGR 1040) and the Economía y Competitividad Consejo Superior de Investigaciones Científicas (Grant n° PGC2018-093925-B-C32). The authors thank the curator and institutions that permitted access to the cranial collections. The authors are grateful to Prof. J. Moggi Cecchi and Dr. M. Zavattaro (Museum of Anthropology of Florence), Prof. G. Manzi (Museum of Anthropology of Rome "G. Sergi"), and Dr. L. E. Copes for sharing with us the osteological collections.

AUTHOR CONTRIBUTIONS

Antonietta Del Bove: Conceptualization; data curation; formal analysis; investigation; methodology; writing-original draft; writing-review and editing. **Antonio Profico:** Conceptualization; formal analysis; methodology; project administration; software; supervision; writing-original draft; writing-review and editing. **Alessandro Riga:** Investigation; writing-original draft; writing-review and editing. **Ana Bucchi:** Methodology; validation; writing-review and editing. **Carlos Lorenzo:** Conceptualization; methodology; project administration; supervision; writing-original draft; writing-review and editing.

CONFLICT OF INTEREST

The authors declare no conflict of interest.

DATA AVAILABILITY STATEMENT

Code and full data are available on Zenodo (10.5281/zenodo.3940597).

ORCID

Antonietta Del Bove https://orcid.org/0000-0001-6620-4514
Antonio Profico https://orcid.org/0000-0003-2884-7118
Ana Bucchi https://orcid.org/0000-0002-1247-230X

REFERENCES

Acsádi, G., Nemeskéri, J., & Balás, K. (1970). History of human life span and mortality (pp. 113–135). Budapest: Akadémiai Kiadó.

Adams, D. C. (2016). Evaluating modularity in morphometric data: Challenges with the RV coefficient and a new test measure. *Methods in Ecology and Evolution*, *7*(5), 565–572 https://doi.org/10.1111/2041-210X.12511

Adams, D., Collyer, M., & Kaliontzopoulou, A. (2020). "Geomorph: Software for geometric morphometric analyses. R package version 3.2.1." https://cran.r-project.org/package=geomorph

Adams, D. C., Rohlf, F. J., & Slice, D. E. (2004). Geometric morphometrics: Ten years of progress following the 'revolution' geometric morphometrics: ten years of progress following the 'revolution'. *Italian Journal of Zoology*, *71*, 5–16 https://doi.org/10.1080/11250000409356545

Bakken, T. E., Dale, A. M., & Schork, N. J. (2011). A geographic cline of skull and brain morphology among individuals of European ancestry. *Human Heredity*, *72*(1), 35–44 https://doi.org/10.1159/000330168

Baylac, M., & Frieß, M. (2005). Fourier descriptors, Procrustes superimposition, and data dimensionality: an example of cranial shape analysis in modern human populations. In Modern morphometrics in physical anthropology (pp. 145–165). Boston, MA: Springer.

Bigoni, L., Velemínská, J., & Brůžek, J. (2010). Three-dimensional geometric morphometric analysis of cranio-facial sexual dimorphism in a central European sample of known sex. *HOMO-Journal of Comparative Human Biology*, *61*(1), 16–32 https://doi.org/10.1016/j.jchb.2009.09.004

Bookstein, F. L. (1989). Principal warps: Thin-plate splines and the decomposition of deformations. *IEEE Transactions on Pattern Analysis and Machine Intelligence*, *11*(6), 567–585 https://doi.org/10.1109/34.24792

Brooks, S., & Suchey, J. M. (1990). Skeletal age determination based on the Os Pubis: A comparison of the Acsádi-Nemeskéri and Suchey-Brooks methods. *Human Evolution*, *5*(3), 227–238 https://doi.org/10.1007/BF02437238

Bruner, E., Athreya, S., De La Cuétara, J. M., & Marks, T. (2013). Geometric Variation of the Frontal Squama in the Genus Homo: Frontal Bulging and the Origin of Modern Human Morphology. *American Journal of Physical Anthropology*, *150*(2), 313–323 https://doi.org/10.1002/ajpa.22202

Bulut, O., Petaros, A., Hizliol, I., Wärmländer, S. K. T. S., & Hekimoglu, B. (2016). Sexual dimorphism in frontal bone roundness quantified by a novel 3D-based and landmark-free method. *Forensic Science International*, *261*, 162.e1–162.e5 https://doi.org/10.1016/j.forsciint.2016.01.028

Bytheway, J. A., & Ross, A. H. (2010). A geometric morphometric approach to sex determination of the human adult Os Coxa. *Journal of Forensic Sciences*, *55*(4), 859–864 https://doi.org/10.1111/j.1556-4029.2010.01374.x

Čechová, M., Dupej, J., Brůžek, J., Bejdová, Š., Horák, M., & Velemínská, J. (2019). Sex estimation using external morphology of the frontal bone and frontal sinuses in a contemporary Czech population. *International Journal of Legal Medicine*, *133*(4), 1285–1294. https://doi.org/10.1007/s00414-019-02063-8

Çelbiş, O., İşcan, M. Y., Soysal, Z., & Çağdir, S. (2001). Sexual diagnosis of the glabellar region. *Legal Medicine*, *3*(3), 162–170 https://doi.org/10.1016/S1344-6223(01)00025-6

Copes, L. E. (2012). *Comparative and experimental investigations of cranial robusticity in mid-pleistocene hominins*, Ph.D Dissertation, Anthropology, Arizona State University.

DiGangi, E., & Moore, M. L. (2013). *Research methods in human skeletal biology*, Waltham, MA: Academic Press. https://doi.org/10.1016/B978-0-12-385189-5.11001-5

Esteve-Altava, B., Diogo, R., Smith, C., Boughner, J. C., & Rasskin-Gutman, D. (2015). Anatomical networks reveal the musculoskeletal modularity of the human head. *Scientific Reports*, *5*, 8298.

Formicola, V., & Franceschi, M. (1996). Regression equations for estimating stature from long bones of early Holocene European samples. *American Journal of Physical Anthropology*, *100*(1), 83–88 https://doi.org/10.1002/(SICI)1096-8644(199605)100:1<83::AID-AJPA8>3.0.CO;2-E

Franklin, D., Oxnard, C. E., O'Higgins, P., & Dadour, I. (2007). Sexual dimorphism in the Subadult Mandible: Quantification using geometric morphometrics. *Journal of Forensic Sciences*, *52*(1), 6–10 https://doi.org/10.1111/j.1556-4029.2006.00311.x

Frayer, D. W., & Wolpoff, M. H. (1985). Sexual dimorphism. *Annual Review of Anthropology*, *14*(1), 429–473 https://doi.org/10.1146/annurev.an.14.100185.002241

Garvin, H. M., & Ruff, C. B. (2012). Sexual dimorphism in skeletal Browridge and Chin morphologies determined using a new quantitative method. *American Journal of Physical Anthropology*, *147*(4), 661–670 https://doi.org/10.1002/ajpa.22036

Garvin, H. M., Sholts, S. B., & Mosca, L. A. (2014). Sexual dimorphism in human cranial trait scores: Effects of population, age, and body size. *American Journal of Physical Anthropology*, *154*(2), 259–269. https://doi.org/10.1002/ajpa.22502

Giles, E., & Elliot, O. (1963). Sex determination by discriminant function analysis of Crania. *American Journal of Physical Anthropology*, *21*(1), 53–68 http://www.ncbi.nlm.nih.gov/pubmed/13947858

Gonzalez, P. N., Bernal, V., & Perez, S. I. (2011). Analysis of sexual dimorphism of craniofacial traits using geometric morphometric techniques. *International Journal of Osteoarchaeology*, *21*(1), 82–91 https://doi.org/10.1002/oa.1109

Gunz, P., Mitteröcker, P., Seidler, H., Weber, G. W., Prossinger, H., & Schäfer, K. (2004). Virtual anthropology: The digital evolution in anthropological sciences. *Journal of Physiological Anthropology and Applied Human Science*, *20*(2), *69*–80 https://doi.org/10.2114/jpa.20.69

Hallgrímsson, B., Jamniczky, H., Young, N. M., Rolian, C., Parsons, T. E., Boughner, J. C., & Marcucio, R. S. (2009). Deciphering the palimpsest: studying the relationship between morphological integration and phenotypic covariation. *Evolutionary Biology*, *36*(4), 355–376 https://doi.org/10.1007/s11692-009-9076-5

Hedenstierna-Jonson, C., Kjellström, A., Zachrisson, T., Krzewińska, M., Sobrado, V., Price, N., … Storå, J. (2017). A female viking warrior confirmed by genomics. *American Journal of Physical Anthropology*, *164*(4), 853–860 https://doi.org/10.1002/ajpa.23308

Jurda, M., & Urbanová, P. (2016). Sex and ancestry assessment of brazilian crania using semi-automatic mesh processing tools. *Legal Medicine*, *23*, 34–43 https://doi.org/10.1016/j.legalmed.2016.09.004

Kimmerle, E. H., Ross, A., & Slice, D. (2008). Sexual dimorphism in America: geometric morphometric analysis of the craniofacial region. *Journal of Forensic Sciences*, *53*(1), 54–57 https://doi.org/10.1111/j.1556-4029.2007.00627.x

Klingenberg, C. P. (2009). Morphometric integration and modularity in configurations of landmarks: tools for evaluating a priori hypotheses. *Evolution & Development*, *11*(4), 405–421 https://doi.org/10.1111/j.1525-142X.2009.00347.x

Klingenberg, C. P. (2013). Cranial integration and modularity: insights into evolution and development from morphometric data. *Hystrix, the Italian Journal of Mammalogy*, *24*(1), 43–58 https://doi.org/10.4404/hystrix-24.1-6367

Klingenberg, C. P. (2014). Studying morphological integration and modularity at multiple levels: concepts and analysis. *Philosophical Transactions of the Royal Society B: Biological Sciences*, *369*(1649), 20130249.

Konigsberg, L. W., Algee-Hewitt, B. F. B., & Steadman, D. W. (2009). Estimation and evidence in forensic anthropology: Sex and race. *American Journal of Physical Anthropology*, *139*(1), 77–90 https://doi.org/10.1002/ajpa.20934

Lorenzo, C., Carretero, J. M., Arsuaga, J. L., Gracia, A., & Martínez, I. (1998). Intrapopulational body size variation and cranial capacity variation in Middle Pleistocene humans: the Sima de los Huesos sample (Sierra de Atapuerca, Spain). *American Journal of Physical Anthropology: The Official Publication of the American Association of Physical Anthropologists*, *106*(1), 19–33 https://doi.org/10.1002/(SICI)1096-8644(199805)106:1<19::AID-AJPA2>3.0.CO;2-8

Luo, H., Wang, J., Zhang, S., & Congbo, M. (2018). The application of frontal sinus index and frontal sinus area in sex estimation based on lateral Cephalograms among Han nationality adults in Xinjiang. *Journal of Forensic and Legal Medicine*, *56*(January), 1–4 https://doi.org/10.1016/j.jflm.2017.12.014

Moggi-Cecchi, J., & Stanyon, R. (2014). Il Museo di Storia Naturale dell'Universitá degli Studi di Firenze: volume V: le collezioni antropologiche ed etnologiche. Il Museo di Storia Naturale dell'Universitá degli Studi di Firenze, 1–331.

Pearson, G. A. (1996). Of sex and gender. *Science*, *274*(5286), 328–329.

Perlaza, N. A. (2014). Sex determination from the frontal bone: A geometric morphometric study. *Journal of Forensic Sciences*, *59*(5), 1330–1332 https://doi.org/10.1111/1556-4029.12467

Petaros, A., Garvin, H. M., Sholts, S. B., Schlager, S., & Wärmländer, S. K. T. S. (2017). Sexual dimorphism and regional variation in human frontal bone inclination measured via digital 3D models. *Legal Medicine*, *29* (October), 53–61 https://doi.org/10.1016/j.legalmed.2017.10.001

Phenice, T. W. (1969). A newly developed visual method of sexing the Os pubis. *American Journal of Physical Anthropology*, *30*, 297–302.

Plavcan, J. M. (2012). Body size, size variation, and sexual size dimorphism in early Homo. *Current Anthropology*, *53*(Suppl. 6), S409–S423. https://doi.org/10.1086/667605

Pretorius, E., Steyn, M., & Scholtz, Y. (2006). Investigation into the usability of geometric morphometric analysis in assessment of sexual dimorphism. *American Journal of Physical Anthropology*, *129*(1), 64–70 https://doi.org/10.1002/ajpa.20251

R Core Team. (2020). *R: A language and environment for statistical computing*. Vienna: R Foundation for Statistical Computing https://www.R-project.org

Renaud, S., Dufour, A. B., Hardouin, E. A., Ledevin, R., & Auffray, J. C. (2015). Once upon multivariate analyses: When they tell several stories about biological evolution. *PloS One*, *10*(7), e0132801 https://doi.org/10.1371/journal.pone.0132801

Rmoutilová, R., Dupej, J., Velemínská, J., & Brůžek, J. (2017). Geometric morphometric and traditional methods for sex assessment using the posterior ilium. *Legal Medicine*, *26*(May), 52–61 https://doi.org/10.1016/j.legalmed.2017.03.004

Rohlf, F. J., & Corti, M. (2000). Use of two-block partial least-squares to study covariation in shape. *Systematic Biology*, *49*(4), 740–753 https://doi.org/10.1080/106351500750049806

Rohlf, J. F., & Leslie, F. M. (1993). A revolution morphometrics. *Trends in Ecology & Evolution*, *8*(4), 129–132. https://doi.org/10.1016/0169-5347(93)90024-J

Rosas, A., & Bastir, M. (2002). Thin-plate spline analysis of allometry and sexual dimorphism in the human craniofacial complex. *American Journal of Physical Anthropology*, *117*(3), 236–245 https://doi.org/10.1002/ajpa.10023

Rubini, M., & Scarani, P. (1989). Studio Antropologico e Patologico Su 38 Crani Di Individui Deceduti Durante La Prima Metà Del XIX Secolo Presso Il Manicomio Dell'ospedale Di S. Orsola in Bologna. Patologie Associate e Variabilità Dei Caratteri Metrici e Discontinui. *Rivista Di Antropologia*, *LXVII*, 273–2986.

Saini, V., Srivastava, R., Rai, R. K. M. D., Shamal, S. N., Singh, T. B., & Tripathi, S. K. M. D. (2011). An osteometric study of northern Indian populations for sexual dimorphism in craniofacial region. *Journal of Forensic Sciences*, *56*(3), 700–705 https://doi.org/10.1111/j.1556-4029.2011.01707.x

Scheuer, L., & Black, S. M. (2000). *Developmental Juvenile Osteology*. San Diego: Academic Press.

Schlager, S. (2017). Morpho and Rvcg—Shape analysis in R. In *Statistical Shape and Deformation Analysis* (pp. 217–256). In Zheng G, Li S, Szekely G (eds.) Academic Press, Elsevier. https://doi.org/10.1016/B978-0-12-810493-4.00011-0

Shearer, B. M., Sholts, S. B., Garvin, H. M., & Wärmländer, S. K. T. S. (2012). Sexual dimorphism in human Browridge volume measured from 3D models of dry crania: A new digital morphometrics approach. *Forensic Science International*, *222*(1–3), 1–5 https://doi.org/10.1016/j.forsciint.2012.06.013

Small, C., Schepartz, L., Hemingway, J., & Brits, D. (2018). Three-dimensionally derived interlandmark distances for sex estimation in intact and fragmentary crania. *Forensic Science International*, *287*, 127–135 https://doi.org/10.1016/j.forsciint.2018.02.012

Spoor, F., Leakey, M. G., Gathogo, P. N., Brown, F. H., Antón, S. C., McDougall, I., … Leakey, L. N. (2007). Implications of new early homo fossils from Ileret, East of Lake Turkana, Kenya. *Nature*, *448*(7154), 688–691 https://doi.org/10.1038/nature05986

Spradley, M. K., & Jantz, R. L. (2011). Sex Estimation in Forensic Anthropology: Skull versus Postcranial Elements. *Journal of Forensic Sciences*, *56*(2), 289–296 https://doi.org/10.1111/j.1556-4029.2010.01635.x

Steyn, M., & Yaşar İşcan, M. (1998). Sexual dimorphism in the Crania and Mandibles of South African Whites. *Forensic Science International*, *98*(1–2), 9–16 https://doi.org/10.1016/S0379-0738(98)00120-0

Suazo Galdames, I. C., Perez Russo, P., Zavando Matamala, D. A., & Luiz Smith, R. (2009). Sexual dimorphism in the foramen magnum dimensions. *International Journal of Morphology*, *27*(1), 21–23. https://doi.org/10.4067/s0717-95022009000100003

Trotter, M., & Gleser, G. C. (1951). Trends in stature of American Whites and Negroes Born between 1840 and 1924. *American Journal of Physical Anthropology*, *9*(4), 427–440 https://doi.org/10.1002/ajpa.1330090404

Ubelaker, D. H., & Volk, G. D. (2002). A test of the Phenice method for the estimation of sex. *Journal of Forensic Sciences*, *47*(1), 19–24.

Uytterschaut, T. (1986). Sexual Dimorphism in Human Skulls. A Comparison of Sexual Dimorphism in Different Populations. *Human Evolution*, *1*(3), 243–250.

Ubelaker, D. H., & Buikstra, J. E. (1994). Standards for data collection from human skeletal remains. Arkansas Archaeological Survey Research, *44*, 206.

Walker, P. L. (2008). Sexing skulls using discriminant function analysis of visually assessed traits. *American Journal of Physical Anthropology*, *136*(1), 39–50 https://doi.org/10.1002/ajpa.20776

Walrath, D. E., Turner, P., & Bruzek, J. (2004). Reliability test of the visual assessment of cranial traits for sex determination. *American Journal of Physical Anthropology*, *125*(2), 132–137 https://doi.org/10.1002/ajpa.10373

Weber, G. W. (2015). Virtual Anthropology. *American Journal of Physical Anthropology*, *156*(S59), 22–42 https://doi.org/10.1002/ajpa.22658

White, T. D., & Folkens, A. P. (2005). *The Human Bone Manual*, San Diego, USA: Academic Press.

Wood, B. A., Li, Y., & Willoughby, C. (1991). Intraspecific variation and sexual dimorphism in cranial and dental variables among higher primates and their bearing on the hominid fossil record. *Journal of Anatomy*, *174*, 185–205.

How to cite this article: Del Bove A, Profico A, Riga A, Bucchi A, Lorenzo C. A geometric morphometric approach to the study of sexual dimorphism in the modern human frontal bone. *Am J Phys Anthropol*. 2020;173:643–654. https://doi.org/10.1002/ajpa.24154

4.3 Result about the study of sexual dimorphism in the entire crania.

Prior to this work, our analyses were focused on specific anatomical regions of the cranium, such as the neurocranium and frontal bone. However, in this new study, we sought to comprehensively analyze the entire cranium, encompassing all previously noted dimorphic traits from the literature (e.g., glabella, supraorbital ridges, mastoid process, zygomatic) as well as previously unexplored traits, without distinction. Our primary objective was to create a new map of traits that are influenced by the sexual dimorphism signal in the human cranium. Currently, this work is undergoing the peer-review process at the "Scientific Reports" journal, under the title "Mapping Sexual Dimorphism Signal in the Human Cranium."

The sample for this study comprised 228 individuals from various repositories. To capture the entire cranium anatomy, we collected 50 fixed landmarks and 500 pairs of bilateral semilandmarks.

To create the dimorphism map, we utilized the results obtained from the accuracy of the linear discriminant analysis (LDA). We conducted the LDA in both form and shape spaces to assess the potential impact of size on the dimorphic patterns. Additionally, we aimed to investigate whether cranial allometry interacts with sexual dimorphism.The findings revealed that size was not statistically significant, but the accuracy in form space exhibited a more pronounced increase compared to shape space. The trajectories of allometry for females and males were similar, but the differences became more apparent when considering the size of females and males.

Our research successfully validated sexual dimorphism in specific regions, namely the glabellar region, supraorbital torus, and mastoid size. Additionally, noteworthy differences between sexes were observed in the upper and medial sections of the orbital margin. Distinctive variations in nasal size and shape were also identified between males and females, a crucial factor to consider in sexual identification analyses. However, it is essential to clarify that the level of projection of the external occipital protuberance was found to be more closely associated with cranial size rather than sexual dimorphism.

Overall, our study provides a comprehensive and detailed map of traits affected by sexual dimorphism in the human cranium, shedding new light on the complex interplay between anatomical variations and gender differences in the cranium.

Mapping sexual dimorphism signal in the human cranium

Antonietta Del Bove*[1,2], Lumila Menéndez[3,4], Giorgio Manzi[5], Jacopo Moggi Cecchi[6], Carlos Lorenzo[1,2], Antonio Profico[7]

1. University Rovira i Virgli, Department of History and History of Arts. Avinguda de Catalunya 35, 43002 Tarragona, Spain.
2. Catalan Institute of Human Paleoecology and Social Evolution (IPHES-CERCA), Zona Educacional 4, Campus Sescelades URV (Edifici W3), 43007 Tarragona, Spain.
3. University of Bonn. Department of Anthropology of the Americas Oxfordstraße 15, 53111 Bonn, Germany.
4. University of Vienna. Department of Evolutionary Biology. Djerassiplatz 1, 1030 Vienna, Austria
5. Department of Environmental Biology, Sapienza University of Rome, Rome 00185, Italy +39 06 4991 2442.
6. Department of Biology, University of Florence. Via del Proconsolo, 12, 50122, Italy 0552757746.
7. Department of Biology, University of Pisa, Via Luca Ghini, 13 56126 Pisa Pisa 56126, Italy. Tel. 050.2211310.

Abstract

The study of sexual dimorphism in human crania has important applications in the fields of human evolution and human osteology. Current, the identification of sex from cranial morphology relies on manual visual inspection of identifiable anatomical features, which can lead to bias due to user's expertise. We developed a landmark-based approach to automatically map the sexual dimorphism signal on the human cranium. We used a sex-known sample of 228 individuals from different geographical locations to identify which cranial regions are most sexually dimorphic taking into account shape, form and size. Our results, which align with standard protocols, show that glabellar and supraciliary regions, the mastoid process and the nasal region are the most sexually dimorphic traits (with an accuracy of 73%). The accuracy increased to 77% if they were considered together. Surprisingly the occipital external protuberance resulted to be not sexually dimorphic but mainly related to variations in size. Our approach here applied could be expanded to map other variable signals on skeletal morphology.

Introduction

Modern humans, compared to other primates, exhibit a lower level of sexual dimorphism [1,2]Sexual dimorphism consists of phenotypic differences between females and males driven by genetic and physiological factors [3]. The study of sexual dimorphism has a long tradition in forensic anthropology and bioarchaeology. For example, in forensic anthropology the application of laboratory protocols to identify sex permits the reconstruction of the identity of missing persons. In bioarchaeology, classifying sex from skeletal remains belonging to archeological populations is fundamental in reconstructing paleodemography, and it allows for the interpretation of gender-related cultural aspects such as division of labor and funerary behavior [4].

Among skeletal regions, the pelvis is the most dimorphic anatomical structure in our species, showing a percentage of accuracy in detecting sex close to 100%[5–8]. However, the cranium has been the most frequently prioritized skeletal structure in archaeological and paleoanthropological contexts [9,10]. Several studies[11–14] have developed methods aiming to increase as much as possible the accuracy in determining sex from the analysis of cranial bones.

Physical anthropologists assign the sex based on the analysis of cranial remains, mainly focusing on differences in morphology of a list of anatomical traits [15–17]. From all three references, the hyperfemale cranial morphology is characterized by the presence of: i) a smoothed nuchal plane and an external occipital protuberance not developed, ii) a small and narrow mastoidal process, iii) a sharp and thin supra-orbital margin beside the concave morphology of the posterior border, iv) a smoothed glabellar region without anterior projection. In contrast, the hypermale cranial morphology shows: i) nuchal lines and pronounced external occipital protuberance, ii) a very large mastoidal process, iii) a rounded and blunted supra-orbital margin with a flat or inferiorly projected posterior border, iv) a massive glabellar region with a marked anterior projection.

The scoring system used to characterize sex from cranial morphology takes into account variations in the size and shape of the glabella, mastoidal process, occipital crest, and orbital margin. On average, female individuals are smaller in cranial size and overall more gracile compared to males; however, only a few studies have focused on analyzing variations in cranial size at the interpopulation level [12,18]. In addition, the inclusion of size as a variable in sex identification leads to issues related to the overlapping of the signal due to both sexual dimorphism and cranial allometry.

Biological anthropology has been drastically changed thanks to the introduction of new methods of investigation. Since the foundation of virtual anthropology[19], we are witnessing an increase in new strategies to identify sex by using geometric morphometric methods[13,14,20–23], beside the application of machine/deep learning[12,24–26],3D modeling techniques[27,28] and linear measurements [29,30].

Most of the recent works focusing on cranial differences between sexes agree that sexual dimorphism signal is more marked if the analyses are performed on single populations than on a worldwide sample [25,31–33]. Despite the vast literature on this topic, protocols used day to day to classify individuals by sex are limited to empirical and visual morphological approaches.

Furthermore, skeletal variation is influenced by additional factors such as subsistence strategies[34,35] and nutritional patterns that may have a significant impact on level of sex hormones [36]. Within this framework, geographical provenance assumes

a pivotal role in increasing the diversification and understanding of the impact of sexual dimorphism on skeletal morphology [37,38]. Numerous studies employing geometric morphometrics have explored sexual dimorphism at population level [39–44].

In this paper, we apply a landmark-based method to map the signal due to sexual dimorphism in the human cranium of a mixed ancestry sample. Our novelty approach, despite traditional methods in assessing sexual dimorphism on the entire cranial morphology or single bone elements, analyzes the accuracy in discriminating sex at a local level. In that case "local" means a small area defined by 10 contiguous semilandmarks discernible from the bone macro area usually analyzed (fig. 3). The use of geometric morphometric methods permits to convert 3D models of human crania into a dense cloud of shape variables acquiring with high precision variations in shape and size. This information is used to build a model at the local level to measure the accuracy in discriminating sexes. In detail, the accuracy is measured by linear discriminate analysis treating each small portion of the cranium as an independent unit. One of the great advantages of studying sexual dimorphism at a local scale is the chance to build self-explained 3D maps of accuracy in detecting sex. We used part of the sample as a training set and the remaining part as a test dataset to avoid issues related to overfitting.

Here, we map the signal of sexual dimorphism on the human cranium using a mixed ancestry sample of 228 individuals. In detail, we test the following hypotheses: 1. Landmark-based methods effectively identify cranial sexually dimorphic traits that align with the anatomical characteristics typically outlined in literature utilizing conventional approaches. Hypothesis 1 is tested by applying linear discriminant analysis on shape and form variables from landmark-based methods. 2. Cranial allometry does not interact with sexual dimorphism. Hypothesis 2 is tested by comparing the allometric trajectories of males and females with differences in shape commonly attributed to sexual dimorphism.

Results

Cranial morphology in relation to sexual dimorphism and size

We performed a Principal Component Analysis (PCA) on the entire cranial form on sex known individuals belonging to different populations (Table S1). The first two PC scores account for 48.43% of the total variance (PC1=37.41%; PC2=11.02%) (Fig. 1). The proportion of total variance associated with sex and size is equal to 0.079 and 0.37, respectively. The interaction between sex and size is not statically significant. Along the PC1 female (F) and male (M) individuals are largely overlapped. However, the means of females and males are statistically different ($t = -7.12$, p-value <0.001; meanF = -0.020; meanM = 0.019).

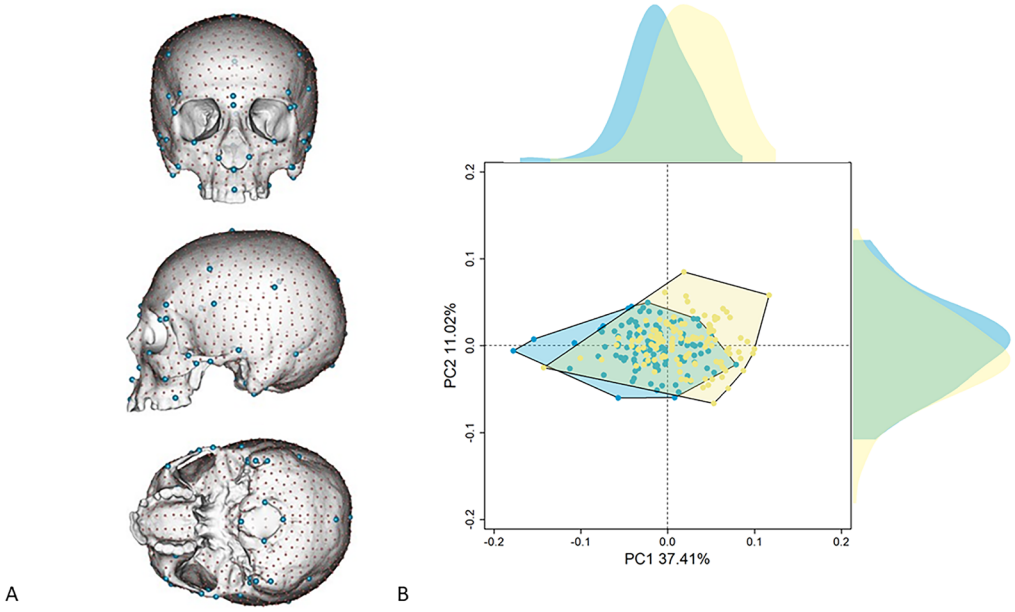

Fig. 1. Cranial form in relation to sex. Landmark (in blue) and semilandmark (in red) configurations used to describe cranial variations (A); Principal Component Analysis (PCA) of cranial form on female (light blue) and male (yellow) individuals (see the top margin of PCA figures). On the top of the PCA plot, we displayed density plots of PC1 and PC2 pooled by sex (B).

The surface warpings built along PC1 show differences mainly related to the pattern of cranial robusticity/gracilization (Fig. 2). At negative values the frontal squama is more horizontally oriented, the morphology of the supraorbital region is less robust, the supero-lateral margin of the orbit is thinner, the zygomatic bone is more gracile in shape, the mastoid processes are smaller and the parietal bones are more rounded. At positive values, we observe an opposite pattern (Fig. 2). Morphological variations detected by PC1 are almost completely related to cranial size ($AdjR^2 = 0.98$) and only partially to sexual dimorphism ($AdjR^2 = 0.18$).

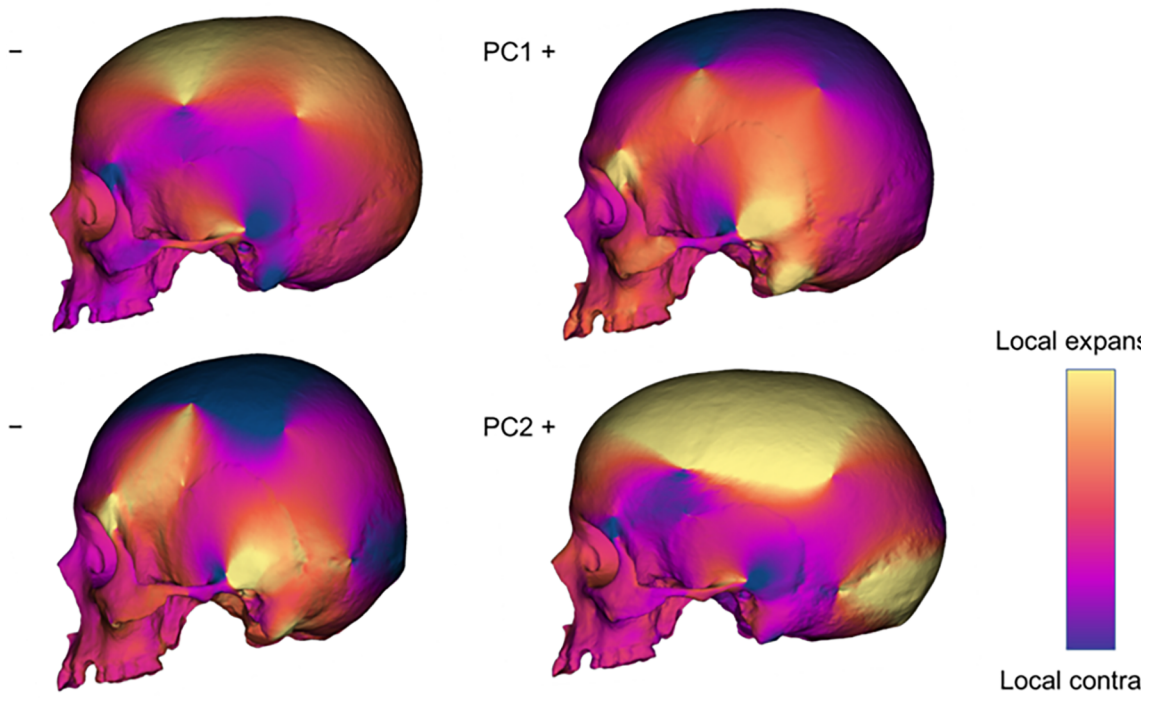

Fig. 2.Cranial form variations along PC1 and PC2. Surfaces warping built at the extreme values of the first two principal components. The colors of the form variations represent relative differences in area compared to the mean shape. Warm and cool colors indicate regions that are expanded and contracted, respectively, compared to the mean shape.

The PC2 detects differences in the overall cranial architecture (dolichocephaly vs brachycephaly). At negative values, the cranium is shorter and higher; at positive values, the neurocranium is elongated anteroposteriorly (Fig. 2). On PC2 the form variations are not related to sexual dimorphism nor to centroid size.

Three-dimensional mapping of sexual dimorphism

3D maps of accuracy were performed by applying Linear Discriminant Analysis (LDA) to define sex as an independent variable, and the PC scores in the shape space and the form space as dependent variables (Fig. 3 and Table 1). A third mapping was performed using the centroid size only as a dependent variable. In the shape space, the central portion of the supraorbital torus, including the glabellar region and part of the frontal squama, resulted to be the most suitable region of the cranium for sexual classification (maximum accuracy equal to 76%) (Fig. 4A). In the shape-and-size space the mastoid processes, the central region of the frontal squama including the supraorbital ridges and the medial portion of the zygomatic bone are the cranial parts showing the highest values of accuracy in classifying sex (accuracy ranged between 71% and 74%) (Fig. 4B). When the centroid size is the only dependent variable used, the mastoid processes and the inferior and lateral portion of the nasal aperture show the highest values of accuracy (ranging between 67% and 70%) (Fig. 4C) (see Table 1 for full results).

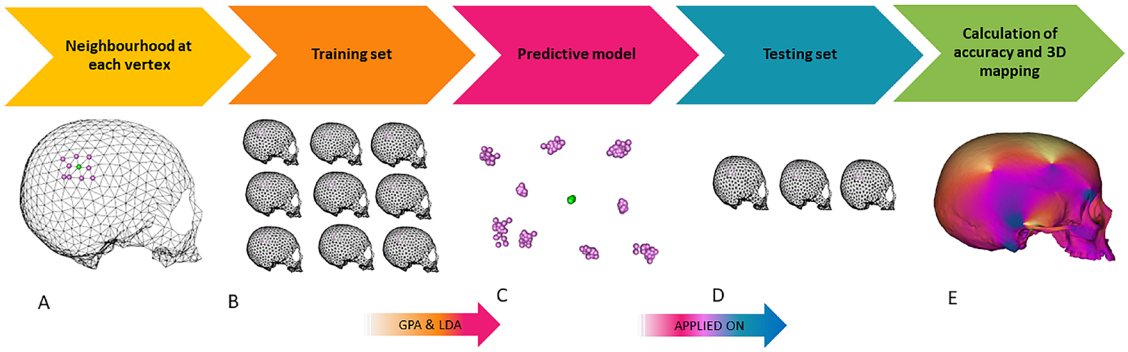

Fig. 3. Workflow to map sexual dimorphism:

A. Calculate a neighborhood of 10 points around each semilandmark.

B. Use part of the sample (70%) as a training set.

C. Perform Generalized Procrustes Analysis (GPA) on the training set.

D. Apply the predictive model to the testing set.

E. Calculate accuracy for each set (B-D) and repeat the process 100 times, randomly defining the training and testing sets.

C. At the end of the iterative process, calculate the average accuracy value associated with each semilandmark.

E. Convert the average accuracy values into a 3D color map.

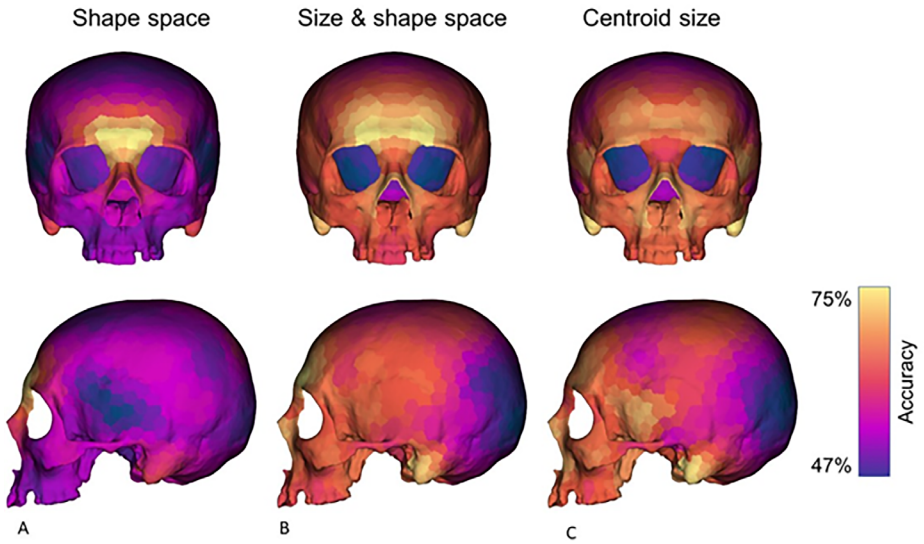

Fig. 4. Percentages of accuracy mapped on a 3D model of the cranium. The predictive model has been built using PC scores calculated in the shape (A) and the shape-and-size (B) space as variables. A third model has been run using only the centroid size (C). Warm and cool colors indicate regions that respectively show high and low accuracy in discriminating sex.

Table 1. Accuracy values for detecting sex from cranial shape, form and size. At each iteration, the PC scores are used until the 90% of the variance to define the linear discriminant model (Tot = entire sample, F = female, M = male).

	Shape			Size and shape			Centroid size		
	Tot	F	M	Tot	F	M	Tot	F	M
Entire set	0.66	0.65	0.67	0.73	0.71	0.76	0.71	0.69	0.73
Glabellar and supraciliary region	0.73	0.70	0.77	0.68	0.66	0.72	0.63	0.61	0.66
Frontal bone	0.70	0.68	0.71	0.71	0.68	0.74	0.65	0.63	0.67
Mastoid process	0.64	0.63	0.65	0.73	0.72	0.75	0.70	0.68	0.72
Nasal region	0.67	0.65	0.68	0.73	0.71	0.75	0.63	0.61	0.65
Combined	0.71	0.71	0.71	0.77	0.80	0.75	0.71	0.73	0.70

We created a 3D map of accuracy based only on the Italian population to evaluate potential differences based on the structure of the sample under investigation. 3D maps of accuracy based on the Italian population overlap well with the 3D maps built respectively both on the entire sample and the entire sample without the Italian population (Supplementary Fig. S1). According to the previous analysis, in the shape space, the medial-inferior portion of the frontal bone resulted to be the most dimorphic region of the cranium. In the form space, instead, the frontal bone and the mastoid processes are the most dimorphic. Lastly, if only the centroid size is considered, the mastoid processes resulted to be the most dimorphic region of the cranium. These results are confirmed by a correlation test between the average values of accuracy calculated per semilandmark. The correlations between the Italian population and the entire sample in the shape space, form space, and size are all significant and equal respectively to 0.49, 0.85, and 0.84 (Supplementary Fig. S2). In the shape space, when the correlation is calculated by subsetting the values of accuracy by selecting values equal or higher than the third quantile (>= 0.63), the value of accuracy increases to 0.75. We replicated the same analysis considering as a comparison the entire sample without the Italian population. The correlations between the Italian population and the comparison sample in the shape space, form space, and size are all significant and equal respectively to 0.38, 0.72 and 0.69. In the shape space, the correlation, subsetting the values of accuracy by selecting values equal or higher than the third quantile (>= 0.63), is equal to 0.74 (Supplementary Fig. S2).

Geometric morphometric analyses on the most dimorphic cranial regions

The PCA on the most dimorphic trait identified is glabellar region in the shape space is reported in figure 5. The two sexes are slightly separated along PC2 (15.40%), even if the female group is almost completely contained within the male variability ($t = 5.32$, p-value <0.001; meanF = 0.007; meanM = -0.007). Variations along PC1 are related to the general structure of the medial-inferior portion of the frontal bone. At negative values, the region of supraorbital torus is narrow and elongated superior-inferiorly. This pattern is opposite at positive values of PC1. Shape variations associated with PC2 are related to sexual dimorphism. At negative values of PC2, the supraorbital ridges are well developed with the presence of supraorbital depression. At positive values, the region in correspondence with the supraorbital torus is flattened, and the upper medial portion of the orbital arch is more rounded.

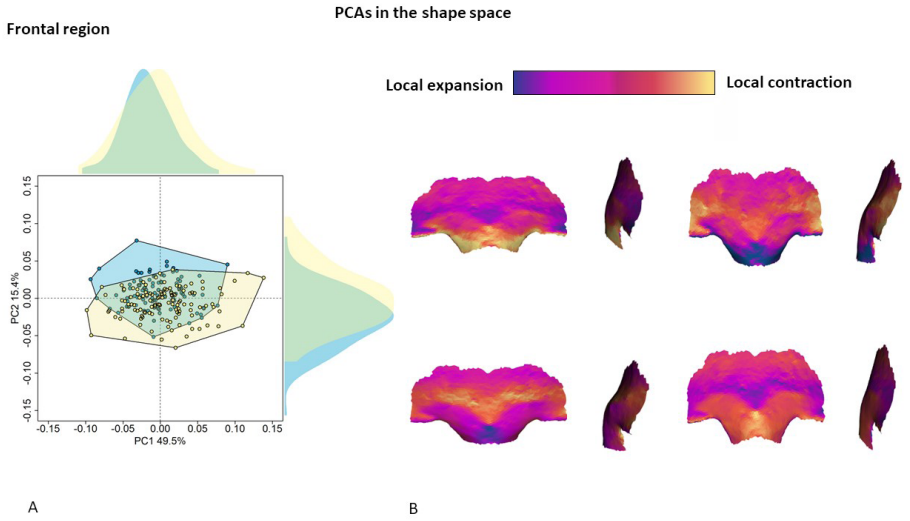

Fig. 5. Shape variations of the supraorbital and glabellar regions. Principal Component Analysis (PCA) of the most prominent dimorphic region identified in the shape space (A). In the plot, female and male individuals are represented in light blue and yellow, respectively. The shape variations (B) are computed at the extremes of PC1 and PC2. These shape variations are compared to the mean shape: cold and warm colors indicate local contraction and expansion, respectively.

On average, female individuals possess an expanded glabellar region, and the middle portion of the supraorbital ridges is reduced. On the contrary, in males, the glabellar region is inflated, the central region of supraorbital ridges is more robust and the supraorbital depression well defined.

In the form space (Fig.6), three different cranial modules resulted to be the best in discriminating sex: the inferior portion of the frontal bone, the nasal region, and the mastoid processes. The PCA on the inferior portion of the frontal bone shows variations linked to the general structure of this region. At negative values of PC1 (50.67%), the frontal squama and the upper medial orbital arch are wide and influenced by allometry ($R2 = 0.93$, p-value < 0.001). PC2 (26.41%) detects variations attributable to sexual dimorphism ($R2 = 0.17$, p-value < 0.001). At positive values of PC2: i) the glabellar region is inflated, ii) the frontal squama is rounded and iii) the supraciliary arches are less developed. At negative values of the same principal component, the surface warping shows the presence of the supraorbital region developed with a supratoral sulcus. In addition, at negative values the angle between the medial margin of the orbit and the supraorbital arch is obtuse.

The PCA on the nasal region shows variations mainly linked to the shape and size of the piriform aperture. At negative values of PC1 (50.46%), the piriform aperture is wide, particularly in the middle part. The lateral portion of the nasal region is more enlarged than the medial part. PC2 (20.44%) detects variations associated with the height of the nasal region. At negative values, the nasal aperture is higher and the two lateral margins form a more acute angle. On the contrary, the nasal region is short and wide at positive values. The proportion of variance of PC1 and PC2 associated with sex is equal to 0.06 (p-value $z < 0.001$) and 0.13 (p-value $z < 0.001$), respectively.

The PC1 of the PCA performed on the variations in size and shape of the mastoid processes shows a clear pattern linked to allometry ($R2 = 0.97$, p-value $z < 0.001$). However, about 20% of the variance of PC1 is significantly associated with sex ($R2 = 0.20$, p-value < 0.001) and this proportion of variance is entirely associated also with size. At negative values of PC1, the mastoid process is bigger, and its posterior inferior margin is more expanded. The length of the anterior margin of the mastoid process intercepted by PC2 is not related to sex or to size.

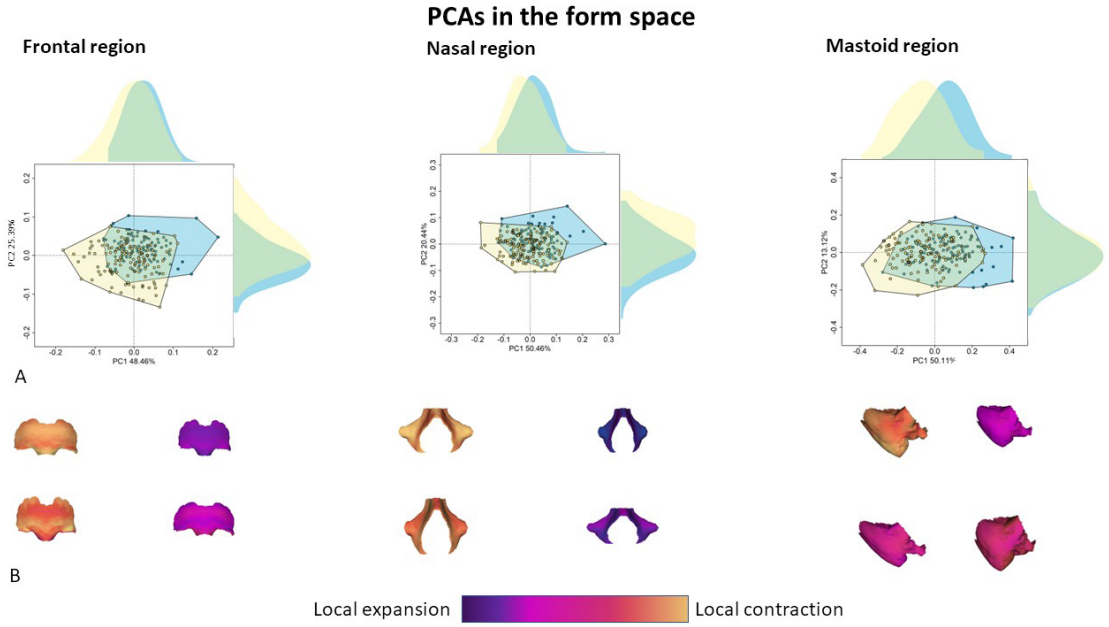

Fig. 6. Best dimorphic traits of the human cranium in the form space. Principal Component Analysis (PCA) of the most prominent dimorphic region identified in the form space (A). In the plot, female and male individuals are represented in light blue and yellow, respectively. The form variations (B) are computed at the extremes of PC1 and PC2. These form variations are compared to the mean shape: cold and warm colors indicate local contraction and expansion, respectively.

Sexual dimorphism and cranial allometry in males and females

We analyzed and compared cranial allometric trajectories in males and females by performing multivariate regression on landmark and semilandmark data after Procrustes registration. The centroid size (the square root of the sum of squared distances between each landmark and the centroid) was used as an independent variable and the landmark and semilandmark (after a GPA in the shape and size space) coordinates as dependent variables. The angle between the allometric trajectories in males and females is equal to 10.12°. However, the differences between the trajectories resulted were not statistically significant after performing a permutation test (1000 permutations, p-value = 0.532). Since the angle divergence between the two allometric trajectories is not significant we performed two separate multivariate regressions, one for each biological sex.

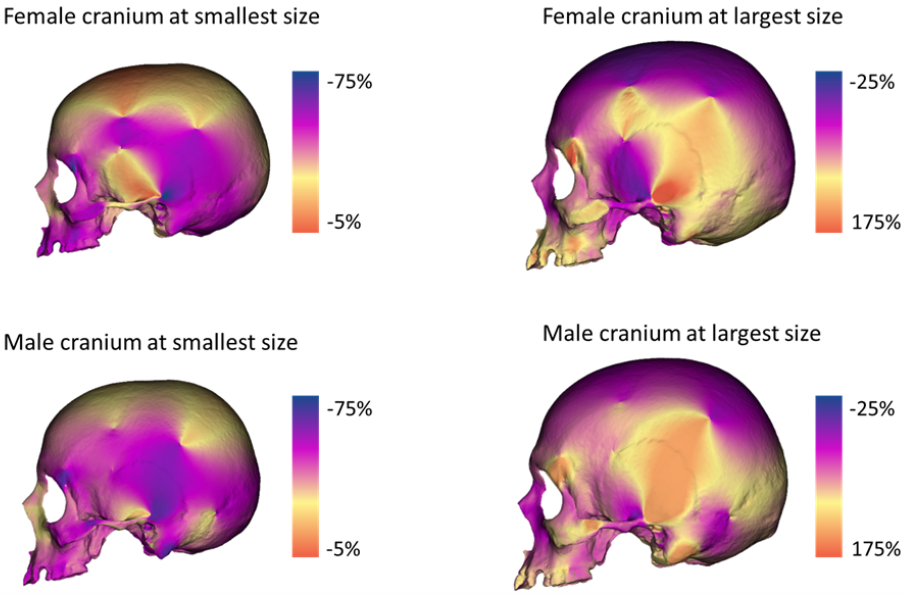

Fig. 7. Cranial allometry in females and males. Differences in cranial morphology of the two allometric trajectories. Color maps indicate local variations in area between centroid size extremes in female and male allometric trajectories. Cold colors indicate relative contraction, while warm colors indicate relative expansion.

The allometric trajectories in both sexes shared a similar pattern of form changes from small to large size. From small to large cranial size, the inferior part of the parietal bone (temporal fossa) increases in area as well as the mastoid region (Fig.7). The expansion of the mastoid process is more accentuated in the male trajectory. At small size the superior part of the cranial calotte is relatively more expanded than at large cranial size. Concerning the facial complex, at small cranial size, the nasal region relatively expanded, as well as the zygomatic process and supraorbital arch. From the posterior view, the region between the lambda and inion is relatively more expanded in males than females at large cranial size [45].

Discussion

In this study, we identified the cranial regions presenting a higher signal for sexual dimorphism by performing a series of LDA on small portions of the external surface of the cranium. Each LDA is statistically independent of others since a GPA step is run at each iteration. When the variable cranial size is excluded from the analysis (shape space) the medial-inferior portion of the frontal bone resulted to be the most suitable cranial region for sex classification. Shape variations of this area agree with standard protocols commonly used in sex determination from cranial remains [12,31,46]. In females, the supraorbital torus is less developed, the glabellar region is more expanded, and the angle between the median and superior margin of the orbit is narrower than in males. On the contrary, on average, males possess a robust supraorbital region with a well-defined supratoral sulcus.

The morphological variations of these anatomical features in males and females are the same as described in traditional anthropology protocols[15,46,47]. However, the accuracy of this area is limited to 78.00%. The inclusion of centroid size in LDA analysis reveals which are the three different cranial regions that vary the most in shape and size between the sexes: i) the medio-inferior portion of the frontal bone, ii) the nasal cavity and iii) the mastoid processes. These three regions show respectively 73.00%, 72.00% and 78.00% of accuracy in sex classification.

From the form variation performed on the medial-inferior part of the frontal bone, it is noticeable that in males, the angle between the medial margin of the orbit and the supraorbital arch is acute. This is partially in agreement with standard protocols describing the male orbital shape as less rounded than the one observed in females[22,48]. On average, males exhibit a larger and narrower piriform aperture than females. Nevertheless, this anatomical feature, noted in the literature, is not described in standard protocols as related to sexual dimorphism [13,49]. Concerning the mastoid process, we found, in agreement with standard protocols, that males possess larger mastoid processes[50–54]. However, our results suggest that differences in the mastoid shape are not related to sexual dimorphism.

Our results show that the cranial form is more influenced by size differences than by sexual dimorphism. Allometry dominates the first axis of cranial form variation, and the results of sexual dimorphism change drastically if the variable cranial size is included or excluded from the analysis[55,56]. If the cranial size is included in the analysis, the nasal region and the mastoid processes resulted to be significantly related to sexual dimorphism. The comparison between the allometric trajectories of males and females highlights that they diverge from each other, despite those differences not being statistically significant. More importantly, when the cranial morphology is predicted at a large size in both sexes the external occipital protuberance is well-developed. From standard protocols, this anatomical feature is listed as related to sexual dimorphism probably because on average the male cranium is larger than that observed in females. Therefore, the inclusion of the external occipital protuberance projection in traditional protocols of sex determination may lead to a systematic bias in sex identification, especially when individuals from different populations are being compared. The 3D maps of sexual dimorphism are confirmed by analysing only the individuals from the Italian skeletal collections (see

Supplementary Fig 1 and 2). The vectors of values of accuracy calculated per semilandmark on the Italian population and the entire sample (including and excluding Italian individuals) are statistically significant suggesting no differences in the identification of sexual dimorphic cranial traits in analysing single populations or mixed ancestry samples.

In conclusion, the application of advanced landmark-based methods shows the potentiality of displaying, at a local scale, which regions of the cranium are related to certain factors. Our study confirms that the glabellar region, the supraorbital torus, and mastoid size are sexually dimorphic. However, only the upper and medial portions of the orbital margin differ significantly between sexes. We found that nasal size and nasal shape are different in males and females, and it should be considered when conducting sexual identification analysis. On the contrary, the level of projection of the external occipital protuberance is linked to the cranial size and not strictly to sexual dimorphism.

Materials and methods

Sample of study

The total number of individuals analyzed in this study is 228 sex known individuals (112 females and 116 males). The sample consists of different repositories (see Table S1). We considered only adult individuals without any pathology that can affect cranial morphology. In detail, the repositories defining the sample of study are: i) Lynn Copes Digital Collection from the Anthropology Department - National Museum of Natural History, Washington DC [57]; ii) Museum of Anthropology " G. Sergi" - Sapienza University of Rome[58]; iii) Oloriz Collection - Virtual CT collection of the Museo Nacional de Ciencias Naturales, Universidad Complutense de Madrid; iv) Anthropological Museum of Florence (University of Florence)[59]; v) Museum of La Plata (UNLP), Buenos Aires, Argentina[60] and, the New Mexico Decedent Image Database (NMDID, https://nmdid.unm.edu/)[61]. All the repositories consist of computerized tomography scans with the exception of the photogrammetric models from the repositories of Rome and Florence. The photogrammetric models have been obtained by using the software Agisoft PhotoScan.

Landmark and semilandmark sets

We acquired 10 median landmarks and 20 pairs of bilateral landmarks (Table S2) for a total of 50 landmarks by using 3D Slicer[62]. In addition, we added 500 pairs of bilateral surface semilandmarks to the landmark configuration. We defined the template of surface semilandmarks by applying K-means clustering on the set of vertices of the right side of the cranial surface of a reference specimen (female individual; ID:4884). Subsequently, the left set of semilandmarks has been specified by applying the function *rotonmat* of the package Morpho[63], using the cranial landmarks as reference for

rigid rotation. After performing the sliding procedure[13], we symmetrized the entire set of landmarks and semilandmarks to remove the asymmetric component from the analysis. Landmark data has been standardized by applying Generalized Procrustes Analysis (GPA). The average inter-landmark (and semilandmark) distance is equal to 8.73 ± 1.59 mm. To assess the error in the positioning of cranial landmarks, we performed Procrustes ANOVA (according to Fruciano, 2016[64]) by landmarking eight individuals four times each. The repeatability percentage turned out to be equal to 97.87%.

Multivariate statistics

Geometric morphometric analyses are performed in the shape and form space (the log of centroid size has added a variable to the matrix of shape variables before applying principal component analysis, PCA). Variations among landmark and semilandmark coordinates after GPA have been analyzed by PCA. The accuracy in correctly classifying female and male individuals has been measured by Linear Discriminant Analysis (LDA). We calculated the values of accuracy in each LDA analysis by performing a permutation test, randomly defining each permutation training and testing set. The training and testing sets are represented respectively by 70% and the 30% of the sample. LDA analysis has been performed on i) the entire set of variables (landmarks plus semilandmarks), ii) the cranial modules resulted from the automatic mapping of sexual dimorphism, taking into consideration shape, size & shape and size. The last set of analyses includes the application of LDA on the combined modules that emerged from single sessions of the analysis in the shape space, size & shape space and cranial size (see [65]Profico et al., 2019 for methodological specifications). Values of accuracy in detecting sex have been calculated for entire sample and separately for female and male intra-groups. Each value is calculated by running 1’000 iterations by defining at each iteration the training (70% of the sample) and testing set (30% of the sample).

Code and R data are available on Zenodo (10.5281/zenodo.8304736) [66].

Mapping sexual dimorphism

We propose a landmark-based statistical approach to map a signal associated with a categorical variable (biological sex in this case) onto the landmark configuration. The protocol divides the entire configuration into parts defined by 10 anatomical/geometric points. Each part consists of contiguous points centered on each point of the starting dataset. For each set of 10 points, part of the individuals (70%) is used as a training set and the remaining individuals (30%) as a testing set and the accuracy is evaluated by permutation test. In summary, on each landmark/semilandmark, we define a set of 10 points among landmarks and semilandmarks (1050 sets). For each set of 10 points, the value of accuracy is evaluated by permuting (nperm=100) individuals in randomly defining training and testing datasets. Each map of sexual dimorphism has requested 105’000 (1050x100) LDA analyses.

Validation of the model at population model

The results from the workflow shown in Fig. 3 has been corroborated by applying the same procedure to the Italian population (*sensu lato*) here represented by Florentine, Roman, Sardinian anthropological collections. In detail, we calculated the accuracy per semilandmark in classifying sex running 100 iterations on each neighbourhood (total of 1050) splitting the Italian population (130 individuals) into a training (70% of the number of individuals) and testing set (30% of the number of individuals) for a total of 105'000 linear discriminant analysis (100x1'050). 3D maps of accuracy based on the Italian population have been compared with the 3D maps of the entire sample (including Italian population) and the entire sample without the Italian population. The analysis has been repeated three times in the shape space, size and shape space and by using only the centroid size. Furthermore, we calculated the correlation of the values of accuracy between the Italian population and the entire sample and between the Italian population and the entire sample without the individuals from Italian anthropological collections.

References

1. Plavcan, J. M. Sexual dimorphism in primate evolution. *Am J Phys Anthropol* **Suppl 33**, 25–53 (2001).

2. Fischer, B., Grunstra, N. D. S., Zaffarini, E. & Mitteroecker, P. Sex differences in the pelvis did not evolve de novo in modern humans. *Nat Ecol Evol* **5**, 625–630 (2021).

3. Rigby, N. & Kulathinal, R. J. Genetic Architecture of Sexual Dimorphism in Humans. *Journal of Cellular Physiology* vol. 230 2304–2310 Preprint at https://doi.org/10.1002/jcp.24979 (2015).

4. Lozano, M. *et al.* Argaric craftswomen: Sex-based division of labor in the Bronze Age southeastern Iberia. *J Archaeol Sci* **127**, (2021).

5. Bass, W. M. & Birkby, W. H. *Exhumation: The Method Could Make the Difference*. *FBI Law Enforcement Bulletin* vol. 47 (1978).

6. Spradley, M. K. & Jantz, R. L. Sex estimation in forensic anthropology: Skull versus postcranial elements. *J Forensic Sci* **56**, 289–296 (2011).

7. Bytheway, J. A. & Ross, A. H. A geometric morphometric approach to sex determination of the human adult os coxa. *J Forensic Sci* **55**, 859–864 (2010).

8. Bilfeld, M. F. *et al.* Human Coxal Bone Sexual Dimorphism and Multislice Computed Tomography: Geometric Morphometric Analysis of 65 Adults. *J Forensic Sci* **57**, 578–588 (2012).

9. Bidmos, M. A. & Asala, S. A. Discriminant Function Sexing of the Calcaneus of the South African Whites. *J Forensic Sci* **48**, 2003104 (2003).

10. Suazo Galdames, I. & Zavando, D. Age Effect in the moprhological traits performance determination in human skulls and mandibles . *Int. J. Morphol.* **30**, 296–301 (2012).

11. Cappella, A. *et al.* Sexual Dimorphism of Cranial Morphological Traits in an Italian Sample: A Population-Specific Logistic Regression Model for Predicting Sex. *Biology (Basel)* **11**, (2022).

12. Del Bove, A. & Veneziano, A. A Generalised Neural Network Model to Estimate Sex from Cranial Metric Traits: A Robust Training and Testing Approach. *Applied Sciences (Switzerland)* **12**, (2022).

13. Schlager, S. & Rüdell, A. Sexual Dimorphism and Population Affinity in the Human Zygomatic Structure—Comparing Surface to Outline Data. *Anatomical Record* **300**, 226–237 (2017).

14. Del Bove, A., Profico, A., Riga, A., Bucchi, A. & Lorenzo, C. A geometric morphometric approach to the study of sexual dimorphism in the modern human frontal bone. *Am J Phys Anthropol* (2020) doi:10.1002/ajpa.24154.

15. Acsádi, G. & Nemeskéri, J. History of human life span and mortality. (1970).

16. Buikstra, J. & Ubelaker, D. Standards for data collection from human skeletal remains: Proceedings of a seminar at the Field Museum of Natural History (Arkansas Archaeology. *Fayetteville Arkansas Archaeological Survey* Preprint at http://scholar.google.com/scholar?hl=en&btnG=Search&q=intitle:Standards+for+Data+Collection+-from+Human+Skeletal+Remains+Proceedings+of+a+Seminar+at+the+Field+Museum+of+Natural+History#0 (1994).

17. Walker, P. L. Sexing skulls using discriminant function analysis of visually assessed traits. *Am J Phys Anthropol* **136**, 39–50 (2008).

18. Garvin, H. M., Sholts, S. B. & Mosca, L. A. Sexual dimorphism in human cranial trait scores: Effects of population, age, and body size. *Am J Phys Anthropol* **154**, 259–269 (2014).

19. Weber, G. W. Virtual anthropology (VA): A call forGlasnost in paleoanthropology. *Anat Rec* **265**, 193–201 (2001).

20. Musilová, B., Dupej, J., Brůžek J, Bejdová Š & Velemínská. Exocranial surfaces for sex assessment of the human cranium. *J- Forensic science* **297**, 364–369 (2019).

21. Perlaza, N. A. Sex Determination from the Frontal Bone: A Geometric Morphometric Study. *J Forensic Sci* **59**, 1330–1332 (2014).

22. Pretorius, E., Steyn, M. & Scholtz, Y. Investigation into the usability of geometric morphometric analysis in assessment of sexual dimorphism. *Am J Phys Anthropol* **129**, 64–70 (2006).

23. Teodoru-Raghina, D., Perlea, P. & Marinescu, M. Forensic anthropology from skeletal remains to ct scans: A review on sexual dimorphism of human skull. *Romanian Journal of Legal Medicine* Preprint at https://doi.org/10.4323/rjlm.2017.287 (2017).

24. Bewes, J., Low, A., Morphett, A., Pate, F. D. & Henneberg, M. Artificial intelligence for sex determination of skeletal remains: Application of a deep learning artificial neural network to human skulls. *J Forensic Leg Med* **62**, 40–43 (2019).

25. Imaizumi, K. *et al.* Development of a sex estimation method for skulls using ma-

chine learning on three-dimensional shapes of skulls and skull parts. *Forensic Imaging* **22**, 200393 (2020).

26. Pozzi, Raffone, Belcastro & Camilleri-Carter. Sex estimation in cranial remains: A comparison of machine learning and discriminant analysis in Italian populations. *bioRxiv* 2020.04.30.071597 (2020) doi:10.1101/2020.04.30.071597.

27. Bulut, O., Petaros, A., Hizliol, İ., Wärmländer, S. K. T. S. & Hekimoglu, B. Sexual dimorphism in frontal bone roundness quantified by a novel 3D-based and landmark-free method. *Forensic Sci Int* **261**, 162.e1-162.e5 (2016).

28. Shearer, B. M., Sholts, S. B., Garvin, H. M. & Wärmländer, S. K. T. S. Sexual dimorphism in human browridge volume measured from 3D models of dry crania: A new digital morphometrics approach. *Forensic Sci Int* **222**, 1–6 (2012).

29. Petaros, A., Sholts, S. B., Slaus, M., Bosnar, A. & Wärmländer, S. K. T. S. Evaluating sexual dimorphism in the human mastoid process: A viewpoint on the methodology. *Clinical Anatomy* **28**, 593–601 (2015).

30. Casado, A. M. Quantifying Sexual Dimorphism in the Human Cranium: A Preliminary Analysis of a Novel Method. *J Forensic Sci* **62**, 1259–1265 (2017).

31. Kelley, S. R. & Tallman, S. D. Population-Inclusive Assigned-Sex-at-Birth Estimation from Skull Computed Tomography Scans. *Forensic Sciences* **2**, 321–348 (2022).

32. Milella, M., Giovanna Belcastro, M., Zollikofer, C. P. E. & Mariotti, V. The effect of age, sex, and physical activity on entheseal morphology in a contemporary Italian skeletal collection. *Am J Phys Anthropol* **148**, 379–388 (2012).

33. Garcovich, D., Albert Gasco, L., Alvarado Lorenzo, A., Aiuto, R. & Adobes Martin, M. Sex estimation through geometric morphometric analysis of the frontal bone: an assessment in pre-pubertal and post-pubertal modern Spanish population. *Int J Legal Med* **136**, 319–328 (2022).

34. Von Cramon-Taubadel, N. Measuring the effects of farming on human skull morphology. *Proceedings of the National Academy of Sciences of the United States of America* vol. 114 8917–8919 Preprint at https://doi.org/10.1073/pnas.1711475114 (2017).

35. Katz, D. C., Grote, M. N. & Weaver, T. D. Changes in human skull morphology across the agricultural transition are consistent with softer diets in preindustrial farming groups. *Proc Natl Acad Sci U S A* **114**, 9050–9055 (2017).

36. Gabory, A., Attig, L. & Junien, C. Sexual dimorphism in environmental epigenetic programming. *Molecular and Cellular Endocrinology* vol. 304 8–18 Preprint at https://doi.org/10.1016/j.mce.2009.02.015 (2009).

37. Harvati, K. & Weaver, T. D. Human cranial anatomy and the differential preservation of population history and climate signatures. *Anat Rec A Discov Mol Cell Evol Biol* **288A**, 1225–1233 (2006).

38. Ubelaker, D. H. & DeGaglia, C. M. Population variation in skeletal sexual dimorphism. *Forensic Sci Int* **278**, 407.e1-407.e7 (2017).

39. Milella, M., Franklin, D., Belcastro, M. G. & Cardini, A. Sexual differences in human cranial morphology: Is one sex more variable or one region more dimorphic? *Anatomical Record* **304**, (2021).

40. Cappella, A. *et al.* Preliminary study on sexual dimorphism of metric traits of cranium and mandible in a modern Italian skeletal population and review of population literature. *Leg Med* **44**, (2020).

41. Ramamoorthy, B., Pai, M. M., Prabhu, L. V., Muralimanju, B. V. & Rai, R. Assessment of craniometric traits in South Indian dry skulls for sex determination. *J Forensic Leg Med* **37**, 8–14 (2016).

42. Ekizoglu, O. *et al.* Assessment of sex in a modern Turkish population using cranial anthropometric parameters. *Leg Med* **21**, 45–52 (2016).

43. Green, H. & Curnoe, D. Sexual dimorphism in Southeast Asian crania: A geometric morphometric approach. *HOMO- Journal of Comparative Human Biology* **60**, 517–534 (2009).

44. Franklin, D., Freedman, L. & Milne, N. Sexual dimorphism and discriminant function sexing in indigenous South African crania. *HOMO- Journal of Comparative Human Biology* **55**, (2005).

45. Smith, O. A. M. *et al.* 3D Modeling of craniofacial ontogeny and sexual dimorphism in children. *Anatomical Record* **304**, 1918–1926 (2021).

46. Čechová, M. *et al.* Sex estimation using external morphology of the frontal bone and frontal sinuses in a contemporary Czech population. *Int J Legal Med* 16–19 (2019) doi:10.1007/s00414-019-02063-8.

47. Garvin, H. M. & Ruff, C. B. Sexual dimorphism in skeletal browridge and chin morphologies determined using a new quantitative method. *Am J Phys Anthropol* **147**, 661–670 (2012).

48. Bejdová, Š., Dupej, J., Krajíček, V., Velemínská, J. & Velemínský, P. Stability of upper face sexual dimorphism in central European populations (Czech Republic) during the modern age. *Int J Legal Med* **132**, 321–330 (2018).

49. Bastir, M., Godoy, P. & Rosas, A. Common features of sexual dimorphism in the cranial airways of different human populations. *Am J Phys Anthropol* **146**, 414–422 (2011).

50. Kemkes, A. & Göbel, T. Metric Assessment of the 'Mastoid Triangle' for Sex Determination: A Validation Study. *J Forensic Sci* **51**, 985–989 (2006).

51. Bernal, V. Size and shape analysis of human molars: Comparing traditional and geometric morphometric techniques. *HOMO- Journal of Comparative Human Biology* **58**, 279–296 (2007).

52. Claudio, I., Galdames, S., Alejandra, D., Matamala, Z. & Smith, R. L. *Sex Determination Using Mastoid Process Measurements in Brazilian Skulls*. *Int. J. Morphol* vol. 26 (2008).

53. de Paiva, L. A. S. & Segre, M. Sexing the human skull through the mastoid process. *Rev Hosp Clin Fac Med Sao Paulo* **58**, 15–20 (2003).

54. Sumati, V. V. G. & Phatak, A. Determination of sex from the mastoid process. *J Anat Soc India* **59**, 222–228 (2010).

55. Urban, J. E. *et al.* Evaluation of morphological changes in the adult skull with age and sex. *J Anat* **229**, 838–846 (2016).

56. Rosas, A. & Bastir, M. Thin-plate spline analysis of allometry and sexual dimorphism in the human craniofacial complex. *Am J Phys Anthropol* **117**, 236–245 (2002).

57. Copes, L. Comparative and Experimental Investigations of Cranial Robusticity in Mid-Pleistocene Hominins. (Arizona State University, 2012).

58. Rubini, M. & Scarani, P. Studio antropologico e patologico su 38 crani di individui deceduti durante la prima metà del XIX secolo presso il manicomio dell'Ospedale di S. Orsola in Bologna. Patologie associate e variabilità dei caratteri metrici e discontinui. *Riv. di Antropol.* **LXVII**, 237–298 (1989).

59. Moggi Cecchi, J. & Stanyon, R. The Anthropological and Ethnological Collections Il Museo di Storia Naturale. **V**, (2014).

60. Castro, J. C. *et al. ACTUALIZACIÓN DEL CATÁLOGO Y DE LAS CONDICIONES DE CONSERVACIÓN DE LAS COLECCIONES DE LA DIVISIÓN ANTROPOLOGÍA, FACULTAD DE CIENCIAS NATURALES Y MUSEO, UNLP*. (2009).

61. Edgar, H. J. H. *et al.* New Mexico Decedent Image Database. (2020).

62. Fedorov, A. *et al.* 3D Slicer as an image computing platform for the Quantitative Imaging Network. *Magn Reson Imaging* **30**, 1323–1341 (2012).

63. Schlager, S. Morpho and Rvcg – Shape Analysis in R. in *Statistical Shape and Deformation Analysis* 217–256 (Elsevier, 2017). doi:10.1016/B978-0-12-810493-4.00011-0.

64. Fruciano, C. Measurement error in geometric morphometrics. *Development Genes and Evolution* vol. 226 139–158 Preprint at https://doi.org/10.1007/s00427-016-0537-4 (2016).

65. Profico, A. *et al.* Seeing the wood through the trees. Combining shape information from different landmark configurations. *Hystrix* **30**, (2019).

66. Profico, A. & Del Bove, A. Code to reproduce data in 'Mapping sexual dimorphism signal in the human cranium'.

Acknowledgements

The authors thank the curator and institutions that permitted access to the cranial collections. The authors are grateful to the Museum of Anthropology of Florence, Museum of Anthropology of Rome "G. Sergi", Museum of La Plata and, Dr. L. E. Copes for sharing with us the osteological collections. CL obtained an ICREA Academy distinction. We would like to express our gratitude to the editor (Dr Vera Weisbecker) and two anonymous reviewers for their insightful comments, which have helped us significantly improve the paper.

Funding

- Martí-Franquès Research grants Programme. Doctoral grants. 2020PmF-PIPF-43.
- Ajuts per donar suport a les activitats dels grups de recerca de Catalunya (SGR-Cat 2021) Funder: Agència de Gestió d'Ajuts Universitaris i de Recerca (AGAUR) Period: 01/01/2022 - 31/12/2024 Reference Code: 2021 SGR 01239 (double filiation IPHES-URV Group).
- Eco-Social behavior of the Sierra de Atapuerca Hominins during Quaternary, VI. Funder: Ministerio de Ciencia e Innovación Period: 01/09/2022 –31/08/2025 Reference Code: PID2021-122355NB-C32

Data availability

The authors used different repositories to share different types of data. The Lynn Copes Digital Collection (Ct scan) from the Anthropology Department National Museum of Natural History Washington DC. were deposited at https://www.lynncopes.com/human-ct-scans.html. The NMDID, on the other hand, was deposited in https://nmdid.unm.edu/ , which is a database managed by the Office of the Medical Investigator, University of New Mexico that archives and distributes. And, Oloriz Collection - Virtual CT collection of the Museo Nacional de Ciencias Naturales was deposited in Nespos (the project actually expired).

As a commitment to transparency and reproducibility, All research data and code publicly available via Zenodo repository (10.5281/zenodo.8304736).

Author contributions

Conceptualization: ADB, AP, CL, JM, GM, LM

Methodology: ADB, AP, CL

Investigation: ADB, AP, CL, JM, GM, LM

Visualization: ADB, AP, CL, JM, GM, LM

Supervision: AP, CL

Writing—original draft: ADB, AP, CL, JM, GM, LM

Writing—review & editing: ADB, AP, CL, LM

Competing interests

The authors declare no competing interests' should be given.

UNIVERSITAT ROVIRA I VIRGILI
A COMPUTATIONAL RE-ASSESSMENT OF SEXUAL DIMORPHISM IN THE HUMAN CRANIUM BEYOND TRADITIONAL MORPHOMETRICS: GEOMETRIC MORPHOMETRIC METHODS AND NEURAL NETWORK ANALYSIS
Antonietta Del Bove

Supplementary information

Mapping sexual dimorphism signal in the human cranium.

Antonietta Del Bove*[1,2], Lumila Menéndez[3,4], Giorgio Manzi[5], Jacopo Moggi Cecchi[6], Carlos Lorenzo[1,2], Antonio Profico[7]

Figure S1

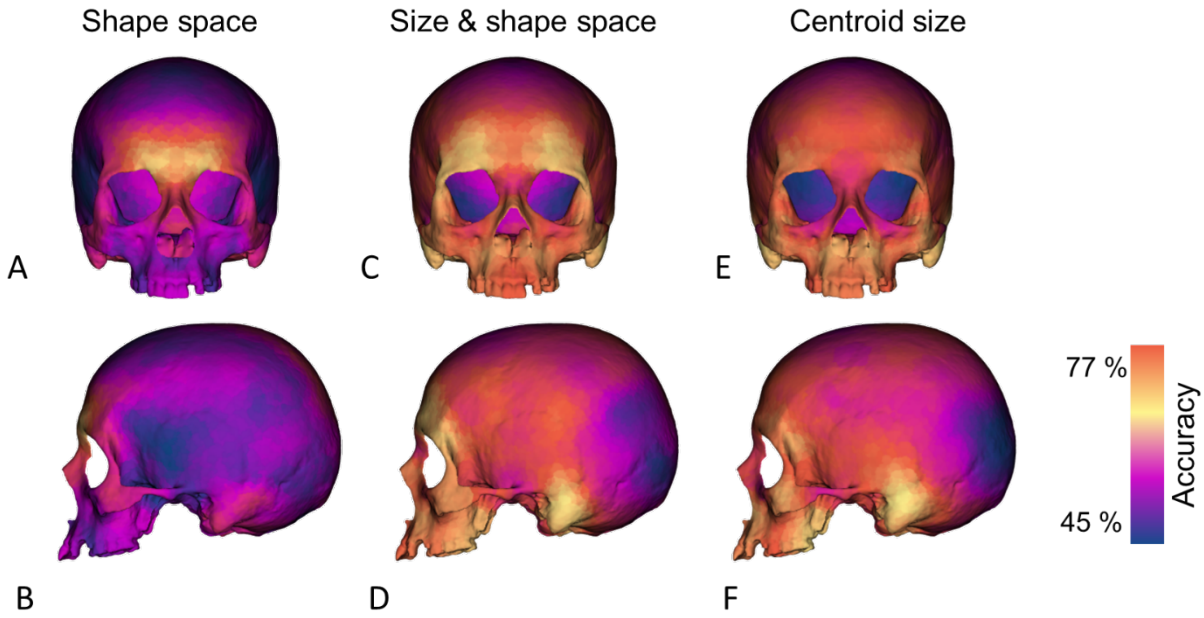

Fig. S1. Percentages of accuracy mapped on a 3D model of the cranium for the Italian sample. The predictive model has been built using as variables the PC scores calculated in the shape (A, B) and the shape-and-size (C, D) space. A third model has been run using only the centroid size (E, F). Warm and cool colors indicate which regions respectively show high and low accuracy in discriminating sex.

Figure S2

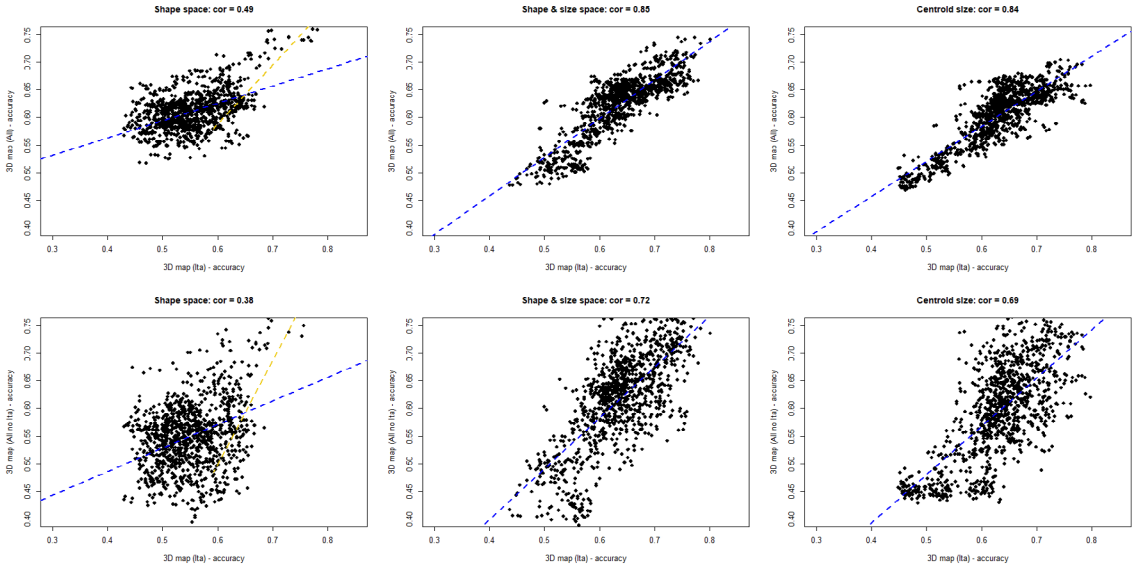

Fig. S2. Correlation analysis between the accuracy values per semilandmark in classifying sex within the Italian population and the full and partial sample.

First row: correlation plots (shape space on the left, shape, and size space in the middle, centroid size on the right) between the accuracy values within the Italian population (x-axis) and the full sample (y-axis). Second row: correlation plots (shape space on the left, shape and size space in the middle, centroid size on the right) between the accuracy values within the Italian population (x-axis) and the partial sample (excluding Italian individuals) on the y-axis.

Blue and orange dashed lines represent, respectively, the least-squares regression lines calculated on the entire dataset and only on the subset of observations with high accuracy values (75th percentile).

Table S1

Complete study sample

SEX	ID	Origin	Age of death	Population	Ancestry
F	7	Italy	-	Sardinian	European
F	23	Italy	-	Sardinian	European
F	131	Italy	24	Florentine	European
F	165	Italy	23	Florentine	European
F	348	South America	-	Azul	Native American
F	347	South America	-	Azul	Native American
F	350	South America	-	Azul	Native American
F	351	South America	-	Azul	Native American
F	355	South America	-	Azul	Native American
F	379	South America	-	Azul	Native American
F	1120	South America	-	Chubut	Native American
F	1131	South America	-	Chubut	Native American
F	1268	South America	-	Chubut	Native American
F	17688	South America	-	Pampa Grande	Native American
F	17695	South America	-	Pampa Grande	Native American
F	17703	South America	-	Pampa Grande	Native American
F	17735	South America	-	Pampa Grande	Native American
F	405	Italy	30	Florentine	European
F	414	Italy	30	Florentine	European
F	418	Italy	26	Florentine	European
F	730	Italy	34	Florentine	European
F	840	North America	32	North America	North America
F	860	Italy	43	Florentine	European
F	868	Italy	38	Florentine	European
F	870	Italy	35	Florentine	European
F	872	Italy	-	Florentine	European
F	880	Italy	31	Florentine	European
F	886	Spain	59	Spanish	European
F	906	North America	22	North America	North America
F	921	North America	38	North America	North America
F	929	North America	20	North America	North America
F	970	North America	21	North America	North America
F	100229	New Mexico	31	no Hispanic	Unknown
F	100263	New Mexico	51	no Hispanic	Unknown

F	100442	New Mexico	34	no Hispanic	Unknown
F	100487	New Mexico	28	no Hispanic	Unknown
F	100516	New Mexico	55	no Hispanic	Unknown
F	100541	New Mexico	49	Hispanic Latin	Unknown
F	101106	New Mexico	42	no Hispanic	Unknown
F	101356	New Mexico	41	no Hispanic	Unknown
F	101377	New Mexico	24	no Hispanic	Unknown
F	1015	North America	41	North America	Unknown
F	101798	New Mexico	50	no Hispanic	Unknown
F	103668	New Mexico	27	Native American	Unknown
F	104103	New Mexico	38	Hispanic Latin	Unknown
F	104125	New Mexico	27	Hispanic Latin	Unknown
F	104719	New Mexico	42	Hispanic Latin	Unknown
F	1052	North America	48	North America	North America
F	105208	New Mexico	31	Native American	Unknown
F	105294	New Mexico	40	Hispanic Latin	Unknown
F	105475	New Mexico	42	Hispanic Latin	Unknown
F	106044	New Mexico	39	Hispanic Latin	Unknown
F	106212	New Mexico	22	Hispanic Latin	Unknown
F	1064	North America	33	North America	Unknown
F	107434	New Mexico	23	Native American	Unknown
F	108398	New Mexico	37	Native American	Unknown
F	109148	New Mexico	27	Native American	Unknown
F	111392	New Mexico	49	Native American	Unknown
F	1135	North America	62	North America	North America
F	115842	New Mexico	40	Native American	Unknown
F	1197	Spain	30	Spanish	European
F	1199	Spain	39	Spanish	European
F	1306	North America	36	North America	North America
F	1333	North America	33	North America	North America
F	1360	Italy	50	Florentine	European
F	1370	Italy	20	Florentine	European
F	1381	Italy	31	Florentine	European
F	1383	Italy	28	Florentine	European
F	1384	Italy	30	Florentine	European
F	1405	Italy	38	Florentine	European
F	1411	Italy	26	Florentine	European
F	1419	Italy	26	Florentine	European
F	1428	Spain	77	Spanish	European
F	1517	Italy	-	Sardinian	European
F	1523	Italy	-	Sardinian	European
F	1552	Italy	-	Sardinian	European
F	1553	Italy	-	Sardinian	European
F	1763	Italy	-	Florentine	European
F	1764	Italy	39	Florentine	European

F	1771	Italy	44	Florentine	European
F	1777	Italy	24	Florentine	European
F	1785	Italy	23	Florentine	European
F	1786	Italy	39	Florentine	European
F	1790	Italy	20	Florentine	European
F	2535	Italy	-	Roman	European
F	2537	Italy	-	Roman	European
F	2538	Italy	-	Roman	European
F	2539	Italy	-	Roman	European
F	2540	Italy	-	Roman	European
F	2541	Italy	-	Roman	European
F	2543	Italy	-	Roman	European
F	2544	Italy	-	Roman	European
F	2545	Italy	-	Roman	European
F	2546	Italy	-	Roman	European
F	2547	Italy	-	Roman	European
F	2548	Italy	-	Roman	European
F	2550	Italy	-	Roman	European
F	2551	Italy	-	Roman	European
F	2552	Italy	-	Roman	European
F	2553	Italy	-	Roman	European
F	4874	Italy	49	Syracusan	European
F	4880	Italy	37	Syracusan	European
F	4883	Italy	-	Syracusan	European
F	4884	Italy	32	Syracusan	European
F	4895	Italy	34	Syracusan	European
F	5795	Italy	-	Sardinian	European
F	5799	Italy	-	Sardinian	European
F	5800	Italy	-	Sardinian	European
F	5838	Italy	-	Sardinian	European
F	5867	Italy	-	Sardinian	European
F	5874	Italy	-	Sardinian	European
F	5937	Italy	-	Sardinian	European
M	1	Italy	-	Sardinian	European
M	4	Italy	-	Sardinian	European
M	6	Italy	-	Sardinian	European
M	15	Italy	-	Sardinian	European
M	21	Italy	-	Sardinian	European
M	22	Italy	-	Sardinian	European
M	258	Italy	-	Sardinian	European
M	260	Italy	-	Sardinian	European
M	263	Italy	-	Sardinian	European
M	265	Italy	-	Sardinian	European
M	318	South America	-	Azul	Native American
M	319	South America	-	Azul	Native American
M	320	South America	-	Azul	Native American

M	331	South America	-	Azul	Native American
M	1014	South America	-	Chubut	Native American
M	1016	South America	-	Chubut	Native American
M	1110	South America	-	Chubut	Native American
M	1111	South America	-	Chubut	Native American
M	1112	South America	-	Chubut	Native American
M	1122	South America	-	Chubut	Native American
M	17697	South America	-	Pampa Grande	Native American
M	17739	South America	-	Pampa Grande	Native American
M	412	Italy	20	Florentine	European
M	419	Italy	33	Florentine	European
M	734	Italy	25	Florentine	European
M	735	Italy	35	Florentine	European
M	794	Spain	-	Spanish	European
M	830	North America	28	North America	North America
M	855	Italy	36	Florentine	European
M	864	North America	42	North America	North America
M	869	Spain	42	Spanish	European
M	874	Italy	22	Florentine	European
M	878	Italy	36	Florentine	European
M	100099	New Mexico	50	Hispanic Latin	Unknown
M	100144	New Mexico	47	no Hispanic	Unknown
M	100148	New Mexico	58	Hispanic Latin	Unknown
M	100169	New Mexico	20	no Hispanic	Unknown
M	100205	New Mexico	43	no Hispanic	Unknown
M	100221	New Mexico	34	Hispanic Latin	Unknown
M	100284	New Mexico	47	Hispanic Latin	Unknown
M	100309	New Mexico	37	no Hispanic	Unknown
M	100371	New Mexico	46	Hispanic Latin	Unknown
M	100389	New Mexico	36	Hispanic Latin	Unknown
M	100418	New Mexico	35	no Hispanic	Unknown
M	100543	New Mexico	25	Native American	Unknown
M	100967	New Mexico	33	no Hispanic	Unknown
M	101121	New Mexico	50	Native American	Unknown
M	101378	New Mexico	47	Hispanic Latin	Unknown
M	101599	New Mexico	26	Hispanic Latin	Unknown
M	102436	New Mexico	37	Native American	Unknown
M	102965	New Mexico	23	Native American	Unknown
M	103044	New Mexico	39	Native American	Unknown
M	103205	New Mexico	29	Native American	Unknown
M	103634	New Mexico	43	Native American	Unknown
M	103640	New Mexico	31	Native American	Unknown
M	1068	Spain	48	Spanish	European
M	1112	Spain	23	Spanish	European
M	1168	North America	33	North America	North America
M	1187	Spain	40	Spanish	European

M	1192	Spain	67	Spanish	European
M	1280	North America	75	North America	North America
M	1282	Spain	66	Spanish	European
M	1293	North America	51	North America	North America
M	1363	Italy	44	Florentine	European
M	1368	Italy	66	Florentine	European
M	1385	Italy	26	Florentine	European
M	1386	Italy	28	Florentine	European
M	1387	Italy	27	Florentine	European
M	1393	Italy	20	Florentine	European
M	1395	Italy	24	Florentine	European
M	1399	Italy	21	Florentine	European
M	1400	Italy	23	Florentine	European
M	1403	Italy	30	Florentine	European
M	1406	Italy	18	Florentine	European
M	1410	Italy	57	Florentine	European
M	1412	Italy	35	Florentine	European
M	1428	Italy	35	Florentine	European
M	1429	Italy	36	Florentine	European
M	1430	Italy	60	Florentine	European
M	1432	Italy	35	Florentine	European
M	1433	Italy	50	Florentine	European
M	1505	Italy	-	Sardinian	European
M	1507	Italy	-	Sardinian	European
M	1508	Italy	-	Sardinian	European
M	1518	Italy	-	Sardinian	European
M	1525	Italy	-	Sardinian	European
M	1533	Italy	-	Sardinian	European
M	1535	Italy	-	Sardinian	European
M	1537	Italy	-	Sardinian	European
M	1756	Italy	41	Florentine	European
M	1770	Italy	44	Florentine	European
M	1773	Italy	24	Florentine	European
M	1774	Italy	43	Florentine	European
M	1781	Italy	50	Florentine	European
M	1789	Italy	23	Florentine	European
M	2524	Italy	-	Roman	European
M	2525	Italy	-	Roman	European
M	2526	Italy	-	Roman	European
M	2527	Italy	-	Roman	European
M	2528	Italy	-	Roman	European
M	2529	Italy	-	Roman	European
M	2530	Italy	-	Roman	European
M	2531	Italy	-	Roman	European
M	2532	Italy	-	Roman	European
M	2533	Italy	-	Roman	European

M	4835	Italy	60	Syracusan	European
M	4839	Italy	64	Syracusan	European
M	4843	Italy	56	Syracusan	European
M	4848	Italy	66	Syracusan	European
M	4849	Italy	-	Syracusan	European
M	4850	Italy	64	Syracusan	European
M	4852	Italy	36	Syracusan	European
M	4858	Italy	28	Syracusan	European
M	4861	Italy	19	Syracusan	European
M	4862	Italy	21	Syracusan	European
M	4882	Italy	36	Syracusan	European

4.4 Results of the new method based on linear measurements of the entire crania with the use of NNA .

The research paper titled "A Generalised Neural Network Model to Estimate Sex from Cranial Metric Traits: A Robust Training and Testing Approach," published in Applied Science, stands as a unique contribution in its exploration of various analytical techniques. In this study, we specifically employed Neural Network Analysis to achieve our objectives. Furthermore, we utilized two extensive open repositories of linear measurements to develop the model.

The primary focus of this work was two-fold. Firstly, we aimed to create a reliable model capable of estimating sex based on only 10 linear measurements of the cranium. This model was intended to be a valuable tool for sex estimation in anthropological and bio-archaeological studies. Secondly, we sought to establish standardized guidelines for applying this approach to different applications within the fields of anthropology and bio-archaeology.

Our selection of 10 linear measurements was based on prior literature indicating their relevance in identifying sexual dimorphism. Through rigorous training and testing, we achieved an impressive accuracy rate of 84% for the model. A notable advantage of this model is its a-population specificity, enhancing its applicability to diverse populations. However, it is important to acknowledge that the model is limited to cases where the same set of measurements is available, making it unsuitable for fragmented samples.

This research represents a significant advancement in the study of sexual dimorphism in the cranium and demonstrates the potential of Neural Network Analysis in this domain. The development of a robust and standardized model paves the way for enhanced sex estimation in anthropological and bio-archaeological investigations while providing a valuable framework for future applications in related fields.

applied sciences

MDPI

Article

A Generalised Neural Network Model to Estimate Sex from Cranial Metric Traits: A Robust Training and Testing Approach

Antonietta Del Bove [1,2] and Alessio Veneziano [3,*]

[1] Departament d'Historia i Història de l'Art, Universitat Rovira i Virgili, Avinguda de Catalunya 35, 43002 Tarragona, Spain
[2] Institut Català de Paleoecologia Humana i Evolució Social (IPHES-CERCA), Edifici W3, Campus Sescelades URV, Zona Educational 4, 43007 Tarragona, Spain
[3] Department of Archaeology, University of Cambridge, Downing Street, Cambridge CB2 3DZ, UK
* Correspondence: av620@cam.ac.uk or veneziano.alessio@gmail.com

Featured Application: The method presented can be used to estimate sex attributes from a small set of cranial metric traits.

Abstract: The morphology of the human cranium allows for reconstructing important information about the identity of an individual, such as age, ancestry, sex, and health status. The estimation of sex from morphology is a key component of the work of physical anthropologists, and in the last decade, the field has witnessed an increase in the use of novel algorithm-based methodologies to tackle the aforementioned task. Nevertheless, several limitations (e.g., small training/testing sample size, training-test data relatedness, limited population inclusiveness, overfitting) have hampered the application of such methods as a standardised procedure in the field. Here, we propose a population-inclusive protocol for estimating sex from a small set of cranial metric traits (10 measurements) based on a neural network architecture trained to maximise the probability of sex attribution and prevent overfitting. The cross-validation returned an accuracy of 86.7% $\pm$ 0.02% and log loss of 0.34 $\pm$ 0.03. The protocol developed was tested on data unrelated to that of the training and validation phase and returned an estimated accuracy of 84.3% and log loss of 0.348. The model and the related code to use it are made publicly available.

Keywords: sexual dimorphism; neural network analysis; human cranium; physical anthropology; protocol

Citation: Del Bove, A.; Veneziano, A. A Generalised Neural Network Model to Estimate Sex from Cranial Metric Traits: A Robust Training and Testing Approach. *Appl. Sci.* **2022**, *12*, 9285. https://doi.org/10.3390/app12189285

Academic Editor: Kevin M. Kelly

Received: 29 June 2022
Accepted: 10 September 2022
Published: 16 September 2022

1. Introduction

One fundamental task of physical anthropologists is that of reconstructing the biological identity of human remains from the incomplete information provided by the skeleton or parts of it [1]. Available methods to establish the sex from the skeleton include protocols based on the visual inspection of morphological traits differing between males and females or quantitative methods often relying on linear measurements used to discriminate between sexes by means of specific algorithms. Such methods have been successfully applied to attribute sex from several different elements within the human skeleton (i.e., femur [2], humerus [3], pelvis [4], teeth [5], talus and calcaneus [6], upper limb [7], and the metacarpal bones [8]). To achieve the highest accuracy, the analysis of the most dimorphic skeletal regions is desirable, such as the coxal bone and other post-cranial elements [9]; when these are not available, another useful source of information is found in the cranium [1,10]. Some important sources of information regarding sexual dimorphism in the human cranium reside in the occipital protuberance, the mastoid process, and the glabellar region [11,12], among others. To provide a standardised approach, potentially less prone to individual bias, it is essential to refine the quantitative methodologies currently available, defining their limitations and establishing the expected performance achievable. In traditional anthropology, a common procedure for estimating sex from the cranium uses a scoring

system of morphological traits evaluated visually [11,13]. Despite being a straightforward and practical method, the success of these traditional approaches depends directly on the experience of the observer, and errors due to subjectivity tend to be higher than in quantitative methods [14,15]. To overcome such obstacles, the use of quantitative measurements and algorithm-based methods have received considerable attention in the last decades.

Previous studies have highlighted the challenges of extrapolating sex information from cranial morphology and variability. The cranium, by its own nature, is a sum of multivariate factors, such as ontogeny, ageing, diet, genetics, epigenetics, and pathologies [16], and it is, therefore, difficult to isolate sex-related information from those confounding factors. Another great challenge comes from the relationship between morphology and ancestry. For example, some studies define small and gracile skulls as females, while the attributes of a large size and robust appearance are associated with males [12,17,18]. These differences cannot be applied to humans *tout court* because the association between the robust/gracile appearance is never perfectly binary: depending on the population, it is possible to find small males and robust females and overlapping morphological variability between sexes is common in modern humans [16], as it is the general overlapping among populations [19]. These circumstances led several authors to focus their studies on individual populations [20–24], which produce results that can hardly be extrapolated to the whole human variability.

The last few decades have witnessed a remarkable development in quantitative methods such as geometric morphometrics and machine learning, which have been successfully applied to Biological and Forensic Anthropology [25–27]. Those methods have triggered a tremendous growth in the search for new quantitative solutions to the problem of estimating sex from the human skeleton [19,28–31]. In particular, machine learning (ML) provides a flexible approach to estimating attributes such as sex from skeletal measurements—an approach adopted more and more in the field [25–32].

All too often, though, algorithm-based studies addressing sex estimation from the human cranium suffer from a lack of "generalisability" and the absence of a solid testing framework. Part of the issue derives from the use of only limited human variability, for example, during the training phase of the ML applications: as mentioned above, studies on individual populations, or groups of populations, have been prioritised [29,32,33], probably because of the difficulty of accessing worldwide data of known sex [34]. Furthermore, testing is often performed on samples too small to provide statistical reliance [35–37], and those samples are often part of the same body of data (e.g., collected by the same observer, belonging to the same population/group) used during the training phase [38], which potentially limits the population-inclusive application of the estimation achieved.

The shortcomings of previous approaches are not only limited to the source and size of the sample. The number of variables considered can be problematic for several reasons. Cranial variables can be highly correlated with each other because of morphological integration [24], and this can make the dataset redundant. The more the number of variables, the higher the redundancy, which increases the risk of overfitting (i.e., when the prediction performs well on the training data but cannot generalise on unseen data [39]). Furthermore, the use of several variables can become problematic when dealing with incomplete cranial remains, a common occurrence with archaeological and forensic material.

An additional limitation is the over-reliance on "accuracy" as a measure of performance. The accuracy of an estimation reflects the proportion of cases correctly assigned to their class: in a binary situation, such as the estimation of sex, the accuracy is computed by counting how many males and females are identified as males or females, respectively. Quantitative algorithms, though, provide the estimation in terms of probability, and, in a binary case, observation is attributed to a class if it has a probability higher than 0.5 for that class, although the threshold can be different. Therefore, accuracy does not account for the probability of the estimation (its "strength", in other words) because the same result is obtained regardless of whether the probability of an observation being male or

female is 0.51 or 0.99. The usefulness of accuracy is dependent on where we set the cut-off probability [40].

The result of the abovementioned limitations is that, as of today, we lack a clear understanding of the potential of quantitative applications for the estimation of sex from the human cranium. In fact, although previous applications have fuelled research on the subject, the training and testing frameworks they used were prone to potential bias to an extent difficult to pinpoint, thus limiting their use as standardised methods for estimating sex. Here, we try to overcome those limitations using a population-inclusive neural network approach based on large training and testing datasets from different sources, requiring a limited number of traits and maximising the probability of estimation rather than accuracy. The advances produced by this work are three-fold: (I) it provides an estimation easy to transfer to other datasets, regardless of ancestry; (II) it clarifies the potential of quantitative, algorithm-based estimation of sex from human crania, maximising probability over accuracy; (III) it presents a step-by-step protocol for the application of ML-based predictions to solve basic problems in the field of physical anthropology.

2. Materials and Methods

2.1. The Datasets

Machine learning applications make use of three sets of data, namely *Training*, *Validating*, and *Testing*. The training set is used to provide the algorithm with "learning material", on which it iteratively improves its performance to build an optimal model; the performance during training is assessed on the validating set; finally, the testing set is an external source of data for evaluating the ability of the model to generalise its performance. This work relies on two sources of cranial measurements: Howell's craniometric dataset [41–43] and the University of Tennessee (UT) Database for Forensic Anthropology in the United States [44]. Here, Howell's data is used during the training and validation steps, while the UT Forensic dataset is used for testing. Howell's dataset consists of 82 craniometric measurements recorded on 2524 human crania from 30 populations with worldwide distribution. The UT Database for Forensic Anthropology includes 36 craniomandibular variables recorded on 1396 individuals of mixed ancestry (identified or unidentified) from forensic cases (from 1962 to 1991) in the United States.

2.2. Data Preparation

Ten craniometric measurements were selected from the datasets, and their definitions are reported in Table 1. The measurements were chosen to represent most of the morphology of the human cranium using only a reduced number of variables (to reduce redundancy across measurements); at the same time, the measurements were chosen to account for some cranial traits previously associated with high levels of sexual dimorphism in modern humans (e.g., mastoid and orbital shape [1,45,46]. The measurements are shown in Figure 1. Only adult individuals were included in the analysis. The sex attribution in Howell's dataset is not known with certainty but is estimated based on non-metric traits by the same William Howell, using a procedure described in [43]. Although it is not ideal to train the model on specimens whose sex is estimated, this choice was necessary due to the difficulties of finding cranial metric datasets of suitable size and with worldwide representation; therefore, this limitation may be reflected in the final model. To balance population representation within the dataset, we removed populations including only one or the other sex. In the UT database, sex information is based on direct identification or on soft tissue estimation—only individuals whose sex is identified directly are included in our dataset—thus, the sex of the individuals included in this dataset is known. To avoid biases during the training and testing phases, in both datasets, the female and male sample size was balanced by randomly reducing the male subsample (originally more abundant).

Table 1. Cranial measurements used in the analysis, abbreviations, and definitions.

Measurement	Abbreviation	Definition
Biauricular breadth	AUB	The shortest distance across the roots of the zygomatic processes
Basion-bregma height	BBH	The linear distance from basion to bregma
Glabella-occipital length	GOL	The linear distance from glabella to opisthocranion along the midsagittal plane
Mastoid height	MDH	The linear distance between porion and mastoidale points
Nasal breadth	NLB	The maximum breadth of the nasal aperture
Nasal height	NLH	The height from the nasion to the lowest point on the rim of the nasal aperture
Orbit breadth	OBB	The linear distance from dacryon to ectoconchion points
Orbit height	OBH	The linear distance between the superior and inferior margins of the orbits, measured perpendicularly to orbital breadth
Lambda-opisthion chord	OCC	The linear distance from lambda to opisthion along the mid-sagittal plane
Bizygomatic breadth	ZYB	The maximum breadth across the zygomatic arches, perpendicular to the mid-sagittal plane

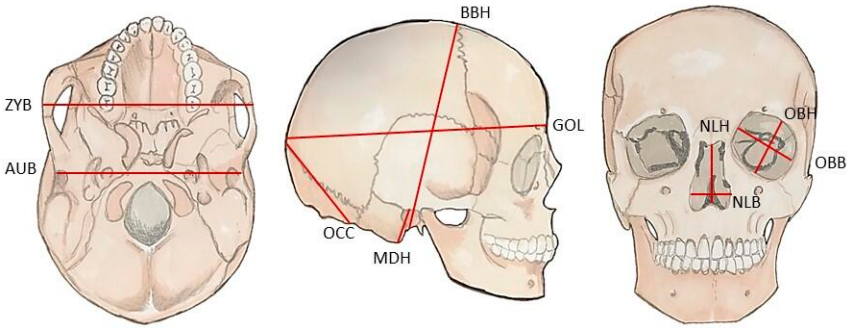

Figure 1. Graphical representation of the 10 cranial measurements used in the analysis. The measurements respect the anthropological standard established by Howells [36]. Definitions are provided in Table 1. (ZYB: bizygomatic breadth; MDH: mastoid height; AUB: biauricular breadth; OBH: orbit height; GOL: glabella-occipital length; NLB: nasal breadth; OCC: lambda-opisthion chord; OBB: orbit breadth; BBH: basion-bregma height; NLH: nasal height).

To account for outliers in Howell's dataset, all the observations that exceed three standard deviations from the mean of at least one of the 10 measurements were removed. Outliers were not removed from the UT dataset because it constitutes the test data and because of the need for evaluating the performance of the eventual model on a realistic variability of the human cranium. Missing data were present in the subset obtained for the UT dataset; those individuals missing 50% of data or more (at least 5 out of 10 measurements) were discarded from the dataset. The other incomplete observations were estimated using Additive Regression, performed using the R package "Hmisc" [47]. The percentage of missing data in each measurement did not exceed 7.9%. In both datasets, the 10 linear measurements were adjusted for the isometric effect of size using Mosimann transformation, which weighs each measurement on the geometric mean of all measurements [48]. The geometric mean was included as an additional measurement in both datasets to explicitly represent size. The measurements were then standardised by z-score transformation (scaled to zero mean and unit variance).

The transformed measurements are henceforth referred to as *features*, in line with the current use in machine learning applications. The final size of Howell's dataset is 2292 individuals, including 1146 females and 1146 males; the final UT dataset consists of 606 individuals, 303 females and 303 males. Each dataset includes 11 metric features generated from 10 measurements. Specifics of the sample are also reported in Table 2.

Table 2. Details of the sample used. Source, population (if known), and sex attribution are reported. Sample sizes refer to the datasets after the transformations operated for the scopes of the current study.

Dataset	Source	Population	Sex (F:M)
Training and Validation	William W. Howell's craniometric dataset	Ainu	38:46
		Andaman	31:33
		Arikara	27:36
		Atayal	17:26
		Australia (aboriginals)	49:50
		Berg	53:53
		Buriat	54:45
		Bushman	46:39
		Dogon	51:45
		Easter Island	37:42
		Egypt (600–200 B.C.)	53:53
		Eskimo	55:43
		Guam	27:28
		Hainan	38:43
		Mokapu	49:45
		Moriori	51:54
		Japan (North)	32:52
		Japan (South)	41:45
		Norse (medieval)	54:52
		Peru	55:49
		Santa Cruz	51:47
		Tasmania (aboriginals)	42:40
		Teita	50:32
		Tolai	54:49
		Zalavar (medieval)	45:49
		Zulu	46:50
Test	University of Tennessee Database for Forensic Anthropology in the United States	Ancestry unknown	303:303

2.3. The Classification Algorithm

The Machine Learning application presented here is a classification task, with the ultimate target of finding a model capable of attributing sex based on a limited number of metric cranial features. The steps followed in the procedure described below are summarised in Figure 2. The implementation of the classification task was performed using the open-source Machine Learning platform "H2O" through the R interface package "h2o" [49].

The sex-classification model was implemented using a feedforward neural network [50], consisting of an input layer (that introduces the features into the network), one or more hidden layers (that transform the input features), and an output layer (the last layer that receives the data processed within the network and produces a result). Each layer is made of nodes (also called neurons or perceptrons), which are the network's computational units. Every time an input travels to a node of the hidden layers, it is multiplied by some weight, which modifies the influence of that input on the output. At each node of the hidden layers, multiple weighted input features arrive and are combined by an activation function, whose output is a new input to another hidden layer or to the output layer. In this work, we use a

non-linear activation function (see Table 3) to allow the output model to identify non-linear patterns in the differences between females and males.

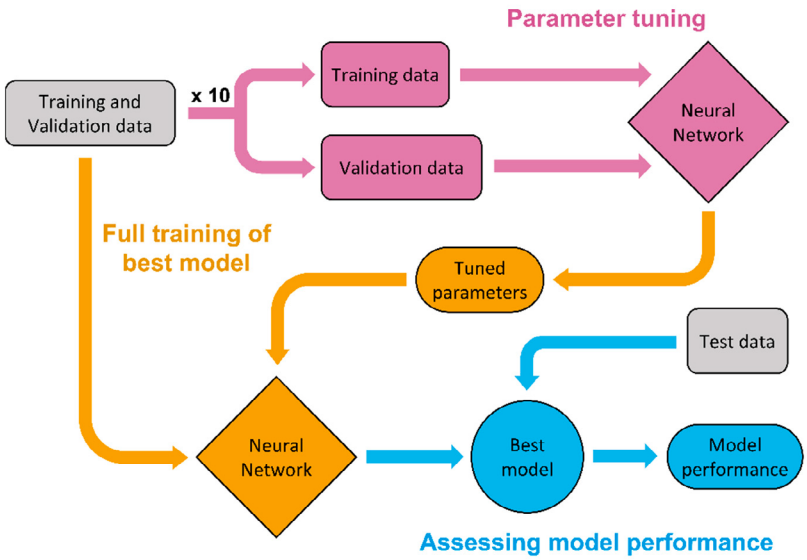

Figure 2. Schematic representation of the machine learning workflow adopted. The data for the parameter tuning were divided into 10 sets of training and validation datasets, allowing cross-validation of the models evaluated and then fed to the neural network algorithm. The algorithm returns the performance of the models on the validation sets, which is the basis for selecting the tuned parameters that allowed best performance for the model. The model is trained on a joint dataset (train + validation) to obtain the best performing model. The performance of the best model is assessed using a test dataset, unseen during the previous phases of the workflow.

Table 3. Crucial parameters of the neural network algorithm, definitions, and values adopted.

Parameter	Value *
Epochs	1000
Stopping metric	Log loss
Loss function	Cross entropy
Distribution	Bernoulli
Learning rate	5×10^{-4}
Momentum start	0.5
Momentum ramp	1×10^{-6}
Momentum stable	0.99
Stopping rounds	20
Stopping tolerance	1×10^{-4}
Input dropout ratio	0
Number of folds	10
Fold assignment	Stratified
Activation function	Rectifier with dropout
L1 regularisation	0
L2 regularisation	0, 1×10^{-4}, 5×10^{-4}, 1×10^{-3}, 5×10^{-3}, 1×10^{-2}, and 5×10^{-2}
Hidden layers	1 and 2
Nodes per layer	3, 7, 11, 15, 19, 23, and 27

* The values used for the parameters refer to the options set in the h2o.deeplearning function in the "h2o" R package [51]. Parameters not shown are left as default as per version 3.36.0.3 of the "h2o" package. When multiple values are shown, the parameter underwent tuning via the brute force approach.

2.4. Parameter Tuning

Machine Learning algorithms operate depending on certain fundamental hyperparameters (henceforth just parameters), whose values govern the way the algorithm performs. To find a suitable model, the initial step is to find the combination of parameter values that provide the best performance for the generated model—an operation referred to as "parameter tuning" [39,51]. Here, parameter tuning was performed using a "brute force" approach (also known as "grid search") by training the algorithm multiple times, each with different combinations of the parameters, and then validating the performance of the models thus generated.

The neural network algorithm depends on several parameters, and the most important ones account for the network's architecture and are the number of hidden layers and the number of nodes per layer; the larger these values, the more complex the output model can be, and this can allow more subtle differences to be identified. Nevertheless, model complexity can lead to overfitting when the model learns to classify the data in the training set but has poor predictive abilities on new data [39]. Overfitting is particularly common in applications using limited amounts of observations, such as this work and several applications in the archaeological and anthropological fields, where data are often scarce. A limited number of features (a characteristic of our dataset) can help lower the chance of overfitting by reducing redundant information [52]—this is the case when using cranial measurements because they are correlated with each other. To further reduce the chance of overfitting, regularisation parameters can be tuned. Regularisation is a set of techniques used to avoid overfitting by reducing complexity through the penalisation of the features' influence [39]. In the case of a Neural Network, regularisation can assign zero to part of the weights (L1-regularisation), or it can make those weights smaller (L2-regularisation).

The training was tuned over two values for the number of hidden layers (1 and 2) and over seven values for the number of nodes (3, 7, 11, 15, 19, 23, and 27—the same number of nodes was used in all hidden layers). Additionally, a sequence of seven values for the L2-regularisation parameter (0, 1×10^{-4}, 5×10^{-4}, 1×10^{-3}, 5×10^{-3}, 1×10^{-2} and 5×10^{-2}) was used in the tuning. The overall number of different models trained during the tuning phase was 98 ($2 \times 7 \times 7$). The values of other parameters (see Table 3) were estimated using a trial-and-error manual tuning, thus reducing the computational time needed for the "brute force" approach.

2.5. Training and Validation

Training and validation were performed for each model for a set number of epochs. Each epoch can be seen as a learning cycle: at each epoch, the training data are fed to the input layer, they get weighed along the path to the hidden layers, and a predictive model is returned through the output layer. A prediction is then performed on the validation data and compared to the observed output (in our case, the observed sex of the individuals in the validation set) to evaluate the performance of the current model. In the next epoch, the weights are modified to improve the model performance according to the result in the previous epoch. The performance can be evaluated based on different metrics [53].

In this work, the training and validation data were obtained from Howell's dataset using 10-fold cross-validation; therefore, each of the 98 models was trained 10 times, with approximately 90% of the data used for training and 10% for validating the model performance. The data were assigned to each fold using a stratified approach [54] to ensure balanced sex classes within the folds.

The model performance is here evaluated on the validation set using the log loss metric (or cross-entropy). Since the model assigns a probability of being female or male to any new observation, we want to obtain a model whose prediction yields the highest possible probability of belonging to a given class. The log loss metric measures how close the predicted probability is to certainty (probability of 1); the smaller the divergence, the lower the log loss [55]. Ideally, we want log loss to approach zero, but for a balanced binary classification task, a realistic and useful upper-threshold value is set at 0.693—this is the

non-informative log loss, or the value of log loss when both classes are predicted with probability equal to 0.5 (same probability of assigning an observation to the female or male class). The training is therefore performed by reducing log loss along the epochs.

Here, training and validation are performed for a maximum of 1000 epochs. To reduce the computational time, we used an early-stopping technique, which stops the training process when the performance does not change over a specified tolerance for a specified number of cycles [56]. In the present case, training is set to stop when log loss stays within a tolerance of 1×10^{-4} for 20 consecutive cycles. Therefore, training does not usually run for the maximum number of epochs allowed. Values of log loss below 0.693 indicate that the fitted model performs better than a random prediction.

2.6. Best Model, Variable Importance, and Testing

All the models generated during tuning (trained and validated) are scouted for the model with the best performance, which is evaluated based on the prediction of each model on the validation set. After the best-performing model is detected, the final model is built, which is the ultimate output of the training procedure. The final training is carried out on a compound dataset including both training and validation data (joined into a single training set), and the parameters are assigned the values that those same parameters have in the best-performing model of the tuning phase. When the final model is obtained, its ability to generalise its predictive power is evaluated on the test set.

Here, the best-performing among the 98 models of the tuning phase was chosen based on multiple factors. First, the best model is the one whose prediction on the validation set returned the lowest log loss; this ensures that the final model is capable of attributing sex with the highest per-class probability. Second, we wanted to maximise the area under the receiver operating characteristic (ROC) curve, a quantity also known as area under curve (AUC). The ROC is a probability curve comparing the false positive rate (FPR or 1-specificity) and true positive rate (TPR or sensitivity) of a binary outcome when the cut-off probability for deciding whether to assign an observation to a certain class is lowered sequentially from one to zero. Therefore, AUC measures how well the model distinguishes both classes of a binary outcome in a way that is independent of the cut-off chosen for the class attribution [53]. Finally, when different models have similar log loss and AUC, the models with lower complexity are chosen; in our case, we gave preference to models with only one layer and a low number of nodes to reduce the chances of overfitting.

When the best-performing model was chosen, the final model was trained on the whole Howell's dataset using the values of the parameters shown in Table 3, as we did during the tuning phase, with the exception of the tuned parameters, whose values were those found via parameter tuning. The relative importance of each feature in the model was computed in the "h2o" R package following the method of Gedeon [57]. The final model was then used to predict the known sex of the observations in the test set, to assess its performance on data not included in the training phase and, therefore, unseen by the model. The model and code to use it are made publicly available on GitHub (github.com/AlessioVeneziano/Papers/tree/main/DelBove_%26_Veneziano_2022, accessed on 9 September 2022).

3. Results

3.1. Best Model Selection

The results of parameter tuning for the 98 models evaluated showed an improvement in performance with an increasing number of nodes and decreasing L2 regularisation (Figure 3). log loss was consistently lower than the non-informative threshold (0.693 for a binary classification), reaching the lowest value of 0.339 at 27 nodes and L2 parameter equal to 5×10^{-3}, when one hidden layer was used, and of 0.346 with 19 nodes, L2 equal to zero and two hidden layers. Log loss was consistently lower for models using one hidden layer rather than two, although the differences were small for models with more than 11 nodes and low L2 parameter. AUC was always higher in models with one hidden

layer and less variable among models (Figure 3), suggesting that two hidden layers may introduce a degree of overfitting in the conditions analysed here. The highest AUC of 0.929 was obtained with one hidden layer, 11 nodes, and L2 equal to 1×10^{-4}.

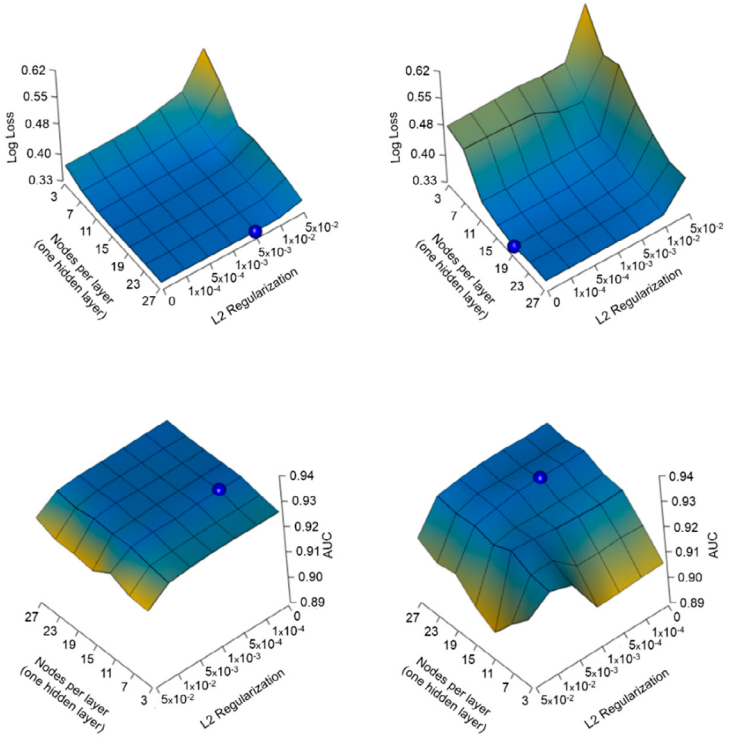

Figure 3. Performance of the sex classification on the validation dataset during parameter tuning. The top graphs show the performance as log loss, while the bottom ones use the area under the receiver operating characteristic (ROC) curve (area under curve or AUC). The performance is compared across different values of the tuned parameters: L2 regularisation, number of nodes per layer, and number of hidden layers (the results for models trained with one hidden layer are shown on the left, with two hidden layers on the right). The performance improves from yellow to blue, specifically with log loss decreasing and AUC increasing. The blue sphere indicates the best performing model: it shows the maximum performance obtained and the relative values of the tuned parameters that produce that performance.

To choose the best model, we accounted for both log loss and AUC, also prioritising the least complex model to avoid overfitting. We picked the best performing model among those trained with one hidden layer because they consistently outperformed models with two hidden layers. Among those models, the lowest log loss and highest AUC were obtained with different parameter values, as reported above: 27 nodes and L2 of 5×10^{-3}, and 11 nodes and L2 of 1×10^{-4}, respectively. The performance of those two models differed negligibly: the difference in AUC and log loss was 5×10^{-4} and 2×10^{-3}, respectively. Based on these results, we can confidently prioritise the least complex model among the ones performing best for AUC and log loss. The selected model had one hidden layer, 11 nodes, and L2 equal to 1×10^{-4}.

The model chosen as the best performing (based on the criteria stated above) was among the models with the lowest log loss and highest AUC among those validated in the present study (Figure 4). The performance on cross-validation returned an accuracy of 0.867 ± 0.022, AUC of 0.929 ± 0.017, and log loss of 0.341 ± 0.033. Furthermore, when

we look at the learning curves for the best model (Figure 5), we can appreciate how the performance (log loss and AUC) of the training and validation sets had a comparable pattern and small difference, reaching a point of stability along the epochs. The pattern shown in Figure 5 suggests that the model selected had not undergone overfitting.

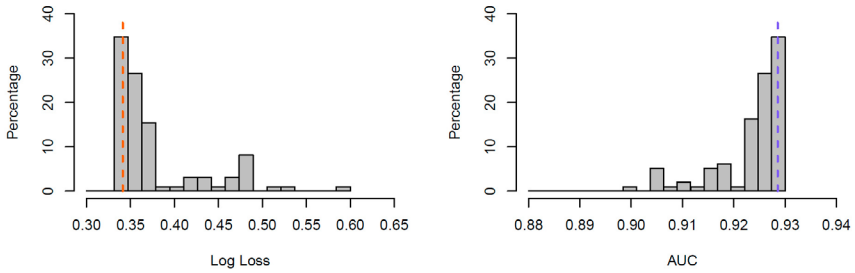

Figure 4. Percentage distribution of the performance metrics—log loss and area under curve (AUC)—across all models trained and validated during parameter tuning. The dashed vertical lines indicate the performance of the best model selected (left: log loss; right: AUC).

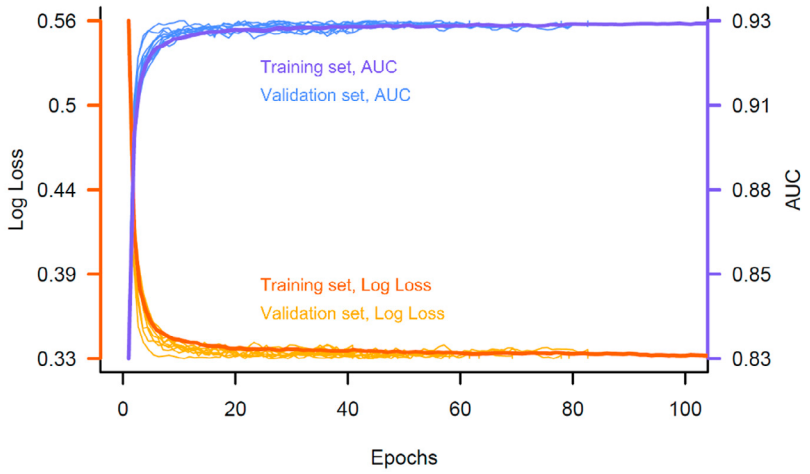

Figure 5. Learning curves showing performance of classification during the epochs. Performance is shown as log loss and area under curve (AUC), measured on the training and validation datasets (in darker and lighter colours, respectively). The similar pattern measured for the two datasets suggests that the performance learned through the training set was generalised to the validation set, thus indicating no overfitting occurred.

3.2. Variable Importance and Model Performance

The estimation of the relative feature importance (Figure 6) shows that the model's prediction was highly influenced by the geometric mean computed on the other measurements (GM: 19.7%), which includes size, followed by the bizygomatic breadth (ZYB: 14.4%) and mastoid height (MDH: 10.2%). The remaining features had smaller contributions (each less than 10%), with the lowest scores shown by basion-bregma height and nasal height (BBH and NLH: 4.7%).

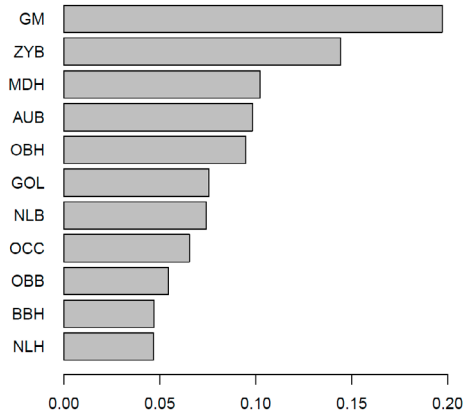

Figure 6. Relative importance of each feature in the best model selected. The importance is shown as a percentage. (GM: geometric mean; ZYB: bizygomatic breadth; MDH: mastoid height; AUB: biauricular breadth; OBH: orbit height; GOL: glabella-occipital length; NLB: nasal breadth; OCC: lambda-opisthion chord; OBB: orbit breadth; BBH: basion-bregma height; NLH: nasal height).

When the performance was assessed on the 606 individuals (303 females, 303 males) of the test dataset, 266 out of 303 females were correctly sexed by the model, and 245 out of 303 for the male group. The model estimated sex with an accuracy of 0.843, and the intra-group accuracy was 0.809 for females and 0.878 for males, thus indicating a better performance for the male group. The log loss estimated on the test set performance was 0.348, much lower than the uninformative threshold of 0.693, suggesting that the observations are estimated with probabilities generally higher than 0.5. Figure 7 shows the histogram of the estimated probabilities of being female/male for the observations whose sex was correctly identified by the model. Ideally, we want the distribution to be negatively skewed (larger frequency of high probabilities); such a pattern was observed for our test sample, with 90% of the correctly sexed observations being estimated with a probability equal or higher than 0.66 (female) and 0.70 (male). The distribution of estimated probabilities for males was particularly skewed, with more than 40% of correctly sexed observations estimated with a probability equal or higher than 0.98.

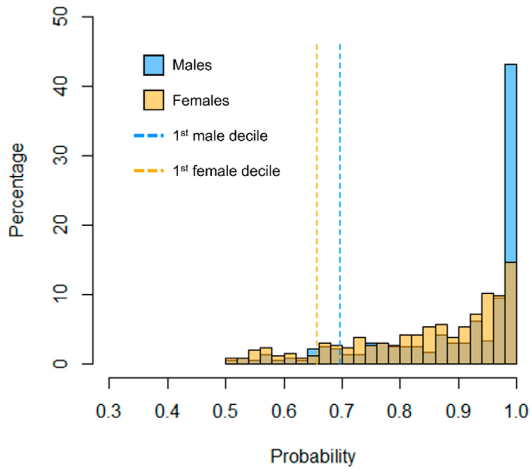

Figure 7. Distribution of the probabilities returned by the best model for correctly estimated females (orange) and males (blue). The dashed vertical lines show the first decile of probability, which indicates the probability above which 90% of observations are estimated.

The AUC of an ROC curve is a better estimator of performance than accuracy when we deal with binary classification. In fact, AUC provides an indication of the performance of both classes through a single metric. The ROC curve of the model prediction is shown in Figure 8. The AUC measured on the test set was 0.923.

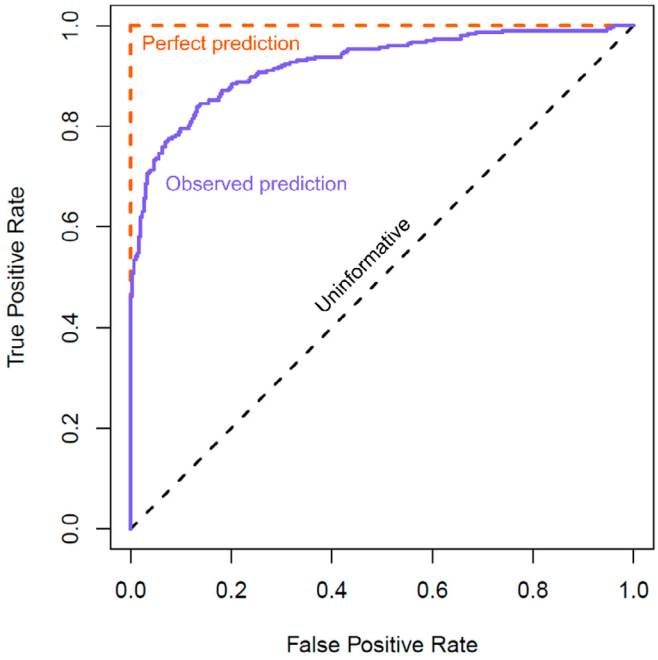

Figure 8. Receiver operating characteristic (ROC) curve showing the observed performance (compared to the uninformative case—random prediction—and a perfect estimation, where all observations were correctly assigned to their true class.

4. Discussion

The literature regarding sex estimation from the human cranium is abundant and has flourished through the use of algorithm-based approaches. Nevertheless, generalising previous findings is tricky because of the focus limited to single populations, but also because the results from such approaches can be misleading if testing is not performed accurately (e.g., using statistically-relevant sample sizes, checking model overfitting, adopting representative performance metrics). Here, we addressed some of those issues by training a neural network on a limited set of cranial measurements from a broad human variability and generating a model independent of ancestry and robust to overfitting. The model was tested on unseen data of known sex, and its performance was evaluated using a probability-based metric (log loss).

4.1. The Model Performance

Our model uses only 10 linear measurements (Table 1) to describe cranial shape, with the addition of the geometric mean computed from those measurements. The best performing model (established based on parameter tuning on cross-validated data) was able to estimate sex with 84% accuracy. This result is virtually free of overfitting (see methods for information about how it was avoided), and the log loss performance shows that 90% of the individuals attributed to the correct sex were estimated with a probability higher than 0.65 (Figure 7). Our findings suggest that the model generated is capable of working efficiently with only a limited number of measurements (a positive characteristic for applications on fragmentary crania). Although this result appears underwhelming if compared to

the higher accuracies reached by other studies [28,58], it must be highlighted that those studies have tested data on only small datasets, which cannot guarantee protection from random sampling effects. In this study, the model was tested on more than 600 individuals, suggesting that the result observed here is more reliable. Furthermore, here we base the evaluation of model performance on log loss, which accounts for the probability of the estimation—this is not common practice in the literature regarding sex estimation from skeletal material, and the absence of such information makes it difficult to assess the performance of previous models.

The model generated here was built on a broad cranial variability of modern *H. sapiens*, which suggests an easier generalisability to applications beyond single populations, although this was not explicitly tested. In addition, the accuracy demonstrated is remarkable if we consider that the training dataset consists of crania whose sex was estimated using a visual approach [41–43]. This finding is relevant because large datasets of known sex are very rare and often difficult to access, and sex estimation through visual inspection approaches can introduce biases, especially with regard to size [14,58]. By monitoring the model performance through metrics such as AUC, it is possible to check for the prevalence of correct estimations for both sexes. In fact, AUC can account simultaneously for the classification of both classes in a binary application [59] (Figure 8). In this study, AUC was taken into account when tuning the parameters to choose the best-performing model among those generated. Thanks to the protocol used and based on the performance observed during testing, we can confidently assume that the model is unbiased toward one or the other sex.

4.2. The Variable Importance

The measurements used to build the neural network model were purposely chosen to represent as much cranial variability as possible by keeping only the essential amount of morphological information. Those choices aim to increase the chances of application (e.g., when crania are only fragmentary) but also to reduce the chances of overfitting. In choosing the measurements to include in the dataset, we also made sure to include traits that were previously recognised as sexually dimorphic in modern humans. How the variables are allowed to interact in the model is hard to pinpoint; in fact, neural networks and other algorithms are referred to as "black boxes" [60]. This means that the way in which the model is classifying the crania (e.g., the nature and degree of interaction across the metric traits used) is not straightforward (especially because we used a non-linear activation function). Nevertheless, we can make assumptions regarding the model based on the measured variable importance, which represents an approximation of the influence of each trait on the estimation.

The variable deemed to be the most relevant in the estimation was the geometric mean (Figure 6). This variable was computed from the 10 metric traits to represent the size of the cranium. Size was virtually erased from the other measurements thanks to the Mosimann transformation [48]; thus, we can expect that the sexual differences in overall dimensions were gathered in this single feature. The observed importance of geometric mean suggests that size is an important aspect of human cranial dimorphism, although it must be highlighted that, in the model, size may have been interacting with other features; thus, it could be important only in association with other sources of morphological variability.

Following size, the second most important feature was the bizygomatic breadth, followed by mastoid height and biauricular height (Figure 6). Bizygomatic breadth was analysed in several studies [17,22,61–64], and in each, bizygomatic breadth measurement positively discriminated sex. Moreover, in other studies using different approaches than the one adopted here, the shape of zygomatic arches resulted in a diagnosis of sex [14,65].

Mastoid height was formerly known to vary between sexes [42,65]. Mastoid bones are more developed in males than in females, and thus, the mastoid influence on our model is not a surprise (see Figure 6). Third in importance in our model was the biauricular breadth,

lesser known than the bizygomatic breadth for its sex-related differences, but previously reported in the literature [17,61,64].

All measurements selected for our model are noted in the literature [17,22,61–64,66], except for the orbital height. This measurement is not considered sexually dimorphic by various authors [17,61,64]; however, it presented a non-negligible influence on our model. This result is in agreement with the use of orbital shapes for sexing individuals through visual inspection [41,59]. Finally, the nasal region seems to contribute to a minor degree to the sexual dimorphism of the human cranium, which could support the idea that the morphology of the nasal area is functionally determined [60].

5. Conclusions

In this work, we attempted to overcome some of the common methodological obstacles encountered when estimating sex from cranial measurements using an algorithm-based approach. Some limitations are still present, such as the model training with crania, whose sex was estimated, a necessary decision (see Section 2.2). Nevertheless, the model generated is a step forward in the establishment of standardised procedures for the semi-automated estimation of individual attributes from skeletal material. The trained neural network model is made publicly available on GitHub with no restrictions (github.com/AlessioVeneziano/Papers/tree/main/DelBove_%26_Veneziano_2022, accessed on 9 September 2022). We also describe the protocol of model training, validating, and testing in detail to allow reproducibility and correct usage of machine learning applications in the field of physical anthropology. The findings presented here provide evidence regarding the extent to which cranial metric traits can be used for attributing sex to skeletal material and highlight the potential that machine learning methods have to automate sex estimation from the crania.

Author Contributions: Conceptualisation, A.D.B. and A.V.; methodology, A.D.B. and A.V.; software, A.V.; validation, A.V.; formal analysis, A.D.B. and A.V.; investigation, A.D.B. and A.V.; resources, A.V.; data curation, A.D.B. and A.V.; writing—original draft preparation, A.D.B.; writing—review and editing, A.D.B. and A.V.; visualisation, A.D.B. and A.V.; supervision, A.V.; project administration, A.V. All authors have read and agreed to the published version of the manuscript.

Funding: A.D.B. is funded by the *Martí i Franquès* fellowship programme (number 2020pmf-pipf-43); A.V. was not supported by external fundings for this work.

Institutional Review Board Statement: The study uses publicly available datasets and did not make physical use of human material. No Ethical Approval was needed or this study.

Informed Consent Statement: The study does not include or disclose personal information that could allow the identification of human individuals, living or dead.

Data Availability Statement: Howell's craniometric dataset is publicly available at https://web.utk.edu/~auerbach/HOWL.htm (accessed on 1 April 2022) by Benjamin M. Auerbach, PhD; the Database for Forensic Anthropology at the University of Tennessee (UT) is distributed by the National Archive of Criminal Justice Data (NACJD) at https://doi.org/10.3886/ICPSR02581.v1. The code to reproduce the analysis, the model generated, and the script to use the model are made publicly available on GitHub at the following link: https://github.com/AlessioVeneziano/Papers/tree/main/DelBove_%26_Veneziano_2022 (accessed on 1 April 2022). The data from the UT Database for Forensic Anthropology cannot be provided by third parties; thus, it is not included in the GitHub source.

Acknowledgments: We want to express our gratitude to Carlos Lorenzo and Antonio Profico for their invaluable insights and inputs provided during the preparation of this work.

Conflicts of Interest: The authors declare no conflict of interest.

References

1. Bass, W.M.; Folkens, P.A. *Human Osteology in a Laboratory and Field Manual of the Human Skeleton*; Gulf Professional Publishing: Houston, TX, USA, 1995.
2. Seidemann, R.M.; Stojanowski, C.M.; Doran, G.H. The use of the supero-inferior femoral neck diameter as a sex assessor. *Am. J. Phys. Anthropol.* **1998**, *107*, 305–313. [CrossRef]
3. López-Lázaro, S.; Pérez-Fernández, A.; Alemán, I.; Viciano, J. Sex estimation of the humerus: A geometric morphometric analysis in an adult sample. *Leg. Med.* **2020**, *47*, 101773. [CrossRef] [PubMed]
4. Phenice, T.W. A newly developed visual method of sexing the os pubis. *Am. J. Phys. Anthropol.* **1969**, *30*, 297–302. [CrossRef] [PubMed]
5. García-Campos, C.; Martinón-Torres, M.; De Pinillos, M.M.; Modesto-Mata, M.; Martín-Francés, L.; Perea-Pérez, B.; Zanolli, C.; De Castro, J.M.B. Modern humans sex estimation through dental tissue patterns of maxillary canines. *Am. J. Phys. Anthropol.* **2018**, *167*, 914–923. [CrossRef]
6. Curate, F.; d'Oliveira Coelho, J.; Silva, A.M. CalcTalus: An online decision support system for the estimation of sex with the calcaneus and talus. *Archaeol. Anthropol. Sci.* **2021**, *13*, 73. [CrossRef]
7. Bidmos, M.A.; Mazengenya, P. Accuracies of discriminant function equations for sex estimation using long bones of upper extremities. *Int. J. Legal. Med.* **2021**, *135*, 1095–1102. [CrossRef]
8. Barrio, P.A.; Trancho, G.J.; Sánchez, J.A. Metacarpal sexual determination in a Spanish population. *J. Forensic Sci.* **2006**, *51*, 990–995. [CrossRef]
9. Spradley, M.K.; Jantz, R.L. Sex estimation in forensic anthropology: Skull versus postcranial elements. *J. Forensic Sci.* **2011**, *56*, 289–296. [CrossRef]
10. Byers, S.N. *Introduction to Forensic Anthropology*; Routledge: Boston, MA, USA, 2002.
11. Acsádi, G.; Nemeskéri, J. History of Human Life Span and Mortality. Available online: https://scholar.google.es/scholar?hl=it&as_sdt=0%2C5&q=acsadi+and+nemeskeri+1970&oq=ascadi+ (accessed on 17 March 2019).
12. Buikstra, J.; Ubelaker, D. Standards for Data Collection from Human Skeletal Remains: Proceedings of a Seminar at the Field Museum of Natural History Arkansas Archaeology, Fayetteville Arkansas Archaeological Survey. Available online: http://scholar.google.com/scholar?hl=en&btnG=Search&q=intitle:Standards+for+Data+Collection+from+Human+Skeletal+Remains+Proceedings+of+a+Seminar+at+the+Field+Museum+of+Natural+History#0 (accessed on 17 March 2019).
13. Walker, P.L. Sexing skulls using discriminant function analysis of visually assessed traits. *Am. J. Phys. Anthropol.* **2008**, *136*, 39–50. [CrossRef]
14. Walrath, D.E.; Turner, P.; Bruzek, J. Reliability test of the visual assessment of cranial traits for sex determination. *Am. J. Phys. Anthropol.* **2004**, *125*, 132–137. [CrossRef]
15. Williams, B.A.; Rogers, T.L. Evaluating the accuracy and precision of cranial morphological traits for sex determination. *J. Forensic Sci.* **2006**, *51*, 729–735. [CrossRef] [PubMed]
16. Klales, A.R. *Sex Estimation of the Human Skeleton*; Academic Press: Cambridge, MA, USA, 2020. [CrossRef]
17. Franklin, D.; Freedman, L.; Milne, N. Sexual dimorphism and discriminant function sexing in indigenous South African crania. *HOMO-J. Comp. Hum. Biol.* **2005**, *55*, 213–228. [CrossRef]
18. Weiss, K.M. On the systematic bias in skeletal sexing. *Am. J. Phys. Anthropol.* **1972**, *37*, 239–249. [CrossRef] [PubMed]
19. Garvin, H.M.; Ruff, C.B. Sexual dimorphism in skeletal browridge and chin morphologies determined using a new quantitative method. *Am. J. Phys. Anthropol.* **2012**, *147*, 661–670. [CrossRef] [PubMed]
20. Franklin, D.; Oxnard, C.E.; O'Higgins, P.; Dadour, I. Sexual dimorphism in the subadult mandible: Quantification using geometric morphometrics. *J. Forensic Sci.* **2007**, *52*, 6–10. [CrossRef]
21. Boucherie, A.; Chapman, T.; García-Martínez, D.; Polet, C.; Vercauteren, M. Exploring sexual dimorphism of human occipital and temporal bones through geometric morphometrics in an identified Western-European sample. *Am. J. Biol. Anthropol.* **2022**, *178*, 54–68. [CrossRef]
22. Dayal, M.R.; Spocter, M.A.; Bidmos, M.A. An assessment of sex using the skull of black South Africans by discriminant function analysis. *HOMO-J. Comp. Hum. Biol.* **2008**, *59*, 209–221. [CrossRef]
23. Green, H.; Curnoe, D. Sexual dimorphism in Southeast Asian crania: A geometric morphometric approach. *HOMO-J. Comp. Hum. Biol.* **2009**, *60*, 517–534. [CrossRef]
24. Milella, M.; Franklin, D.; Belcastro, M.G.; Cardini, A. Sexual differences in human cranial morphology: Is one sex more variable or one region more dimorphic? *Anat. Rec.* **2021**, *304*, 2789–2810. [CrossRef]
25. Attia, M.H.; Kholief, M.A.; Zaghloul, N.M.; Kružić, I.; Anđelinović, Š.; Bašić, Ž.; Jerković, I. Efficiency of the adjusted binary classification (ABC) approach in osteometric sex estimation: A comparative study of different linear machine learning algorithms and training sample sizes. *Biology* **2022**, *11*, 917. [CrossRef]
26. Nikita, E.; Nikitas, P. On the use of machine learning algorithms in forensic anthropology. *Leg. Med.* **2020**, *47*, 101771. [CrossRef] [PubMed]
27. Savall, F.; Faruch-Bilfeld, M.; Dedouit, F.; Sans, N.; Rousseau, H.; Rougé, D.; Telmon, N. Metric sex determination of the human coxal bone on a virtual sample using decision trees. *J. Forensic Sci.* **2015**, *60*, 1395–1400. [CrossRef] [PubMed]

28. Bewes, J.; Low, A.; Morphett, A.; Pate, F.D.; Henneberg, M. Artificial intelligence for sex determination of skeletal remains: Application of a deep learning artificial neural network to human skulls. *J. Forensic Leg. Med.* **2019**, *62*, 40–43. Available online: https://www.sciencedirect.com/science/article/pii/S1752928X18304219 (accessed on 9 April 2021). [CrossRef] [PubMed]
29. Imaizumi, K.; Bermejo, E.; Taniguchi, K.; Ogawa, Y.; Nagata, T.; Kaga, K.; Hayakawa, H.; Shiotani, S. Development of a sex estimation method for skulls using machine learning on three-dimensional shapes of skulls and skull parts. *Forensic Imaging* **2020**, *22*, 200393. [CrossRef]
30. Chovalopoulou, M.-E.; Valakos, E.; Manolis, S.K. Sex determination by three-dimensional geometric morphometrics of craniofacial form. *Anthr. Anz.* **2016**, *73*, 195–206. [CrossRef] [PubMed]
31. Jurda, M.; Urbanová, P. Sex and ancestry assessment of Brazilian crania using semi-automatic mesh processing tools. *Leg. Med.* **2016**, *23*, 34–43. [CrossRef]
32. Kelley, S.R.; Tallman, S.D. Population-Inclusive Assigned-Sex-at-Birth Estimation from Skull Computed Tomography Scans. *Forensic Sci.* **2022**, *2*, 321–348. [CrossRef]
33. Milella, M.; Belcastro, M.G.; Zollikofer, C.P.; Mariotti, V. The effect of age, sex, and physical activity on entheseal morphology in a contemporary Italian skeletal collection. *Am. J. Phys. Anthr.* **2012**, *148*, 379–388. [CrossRef]
34. Ortega, R.F.; Irurita, J.; Campo, E.J.E.; Mesejo, P. Analysis of the performance of machine learning and deep learning methods for sex estimation of infant individuals from the analysis of 2D images of the ilium. *Int. J. Leg. Med.* **2021**, *135*, 2659–2666. [CrossRef]
35. Toneva, D.; Nikolova, S.; Agre, G.; Zlatareva, D.; Hadjidekov, V.; Lazarov, N. Machine learning approaches for sex estimation using cranial measurements. *Int. J. Legal Med.* **2021**, *135*, 951–966. [CrossRef]
36. Navega, D.; Vicente, R.; Vieira, D.N.; Ross, A.H.; Cunha, E. Sex estimation from the tarsal bones in a Portuguese sample: A machine learning approach. *Int. J. Leg. Med.* **2015**, *129*, 651–659. [CrossRef] [PubMed]
37. Ortiz, A.G.; Costa, C.; Silva, R.; Biazevic, M.; Michel-Crosato, E. Sex estimation: Anatomical references on panoramic radiographs using Machine Learning. *Forensic Imaging* **2020**, *20*, 200356. [CrossRef]
38. Curate, F.; Umbelino, C.; Perinha, A.; Nogueira, C.; Silva, A.M.; Cunha, E. Sex determination from the femur in Portuguese populations with classical and machine-learning classifiers. *J. Forensic Leg. Med.* **2017**, *52*, 75–81. [CrossRef]
39. Ying, X. An Overview of Overfitting and its Solutions. *J. Phys. Conf. Ser.* **2019**, *1168*, 022022. [CrossRef]
40. Jerković, I.; Bašić, Ž.; Anđelinović, Š.; Kružić, I. Adjusting posterior probabilities to meet predefined accuracy criteria: A proposal for a novel approach to osteometric sex estimation. *Forensic Sci. Int.* **2020**, *311*, 110273. [CrossRef] [PubMed]
41. Howells, W.W. Who's who in skulls. Ethnic identification of crania from measurements. *Pap. Peabody Mus. Archaeol. Ethnol.* **1995**, *82*, 108.
42. Howells, W.W. Skull shapes and the map. Craniometric analyses in the dispersion of modern homo. *Pap. Peabody Mus. Archaeol. Ethnol.* **1989**, *79*, 189.
43. Howells, W.W. Cranial variation in man. A study by multivariate analysis of patterns of differences among recent human populations. *Pap. Peabody Mus. Archeol. Ethnol.* **1973**, *67*, 259.
44. Jantz, R.L.; Moore-Jansen, P.H. *A Data Base for Forensic Anthropology*; The National Institute of Justice: Washington, DC, USA, 1988.
45. Holland, T.D. Sex determination of fragmentary crania by analysis of the cranial base. *Am. J. Phys. Anthr.* **1986**, *70*, 203–208. [CrossRef]
46. Saini, V.; Srivastava, R.; Rai, R.K.; Shamal, S.N.; Singh, T.B.; Tripathi, S.K. Sex Estimation from the Mastoid Process Among North Indians. *J. Forensic Sci.* **2011**, *57*, 434–439. [CrossRef]
47. Harrell, F.E.; Dupont, C. *Hmisc. Harrell Miscellaneous*; CRAN: Brisbane, Australia, 2022.
48. Mosimann, J.E. Size Allometry: Size and Shape Variables with Characterizations of the Lognormal and Generalized Gamma Distributions. *J. Am. Stat. Assoc.* **1970**, *65*, 930–945. [CrossRef]
49. LeDell, E.; Gill, N.; Aiello, S.; Fu, A.; Candel, A.; Click, C.; Kraljevic, T.; Nykodym, T.; Aboyoun, P.; Kurka, M.; et al. *R Interface for the 'H2O' Scalable Machine Learning Platform*; CRAN: Brisbane, Australia, 2022.
50. Svozil, D.; Kvasnieka, V.; Pospichal, J. Chemometrics and intelligent laboratory systems Introduction to multi-layer feed-forward neural networks. *Chemom. Intell. Lab. Syst.* **1997**, *39*, 43–62. [CrossRef]
51. Lavesson, N.; Davidsson, P. Quantifying the Impact of Learning Algorithm Parameter Tuning. In Proceedings of the National Conference on Artificial Intelligence, Boston, MA, USA, 16–20 July 2006; Volume 1.
52. Venkatesh, B.; Anuradha, J. A Review of Feature Selection and Its Methods. *Cybern. Inf. Technol.* **2019**, *19*, 3–26. [CrossRef]
53. Erickson, B.J.; Kitamura, F. Magician's Corner: 9. Performance Metrics for Machine Learning Models. *Radiol. Artif. Intell.* **2021**, *3*, e200126. [CrossRef] [PubMed]
54. Parsons, V.L. Stratified sampling. In *Wiley StatsRef: Statistics Reference Online*; Wiley: Hoboken, NJ, USA, 2014; pp. 1–11.
55. Cybenko, G.; O'Leary, D.P.; Rissanen, J. *The Mathematics of Information Coding, Extraction and Distribution*; Springer Science & Business Media: Berlin, Germany, 1998; Volume 107.
56. Caruana, R.; Lawrence, S.; Giles, C. Overfitting in neural nets: Backpropagation, conjugate gradient, and early stopping. *Adv. Neural. Inf. Process. Syst.* **2000**, *13*, 381–387.
57. Gedeon, T.D. Data Mining of Inputs: Analysing Magnitude and Functional Measures. *Int. J. Neural Syst.* **1997**, *8*, 209–218. [CrossRef]
58. Gao, H.; Geng, G.; Yang, W. Sex determination of 3D skull based on a novel unsupervised learning method. *Comput. Math. Methods Med.* **2018**, *2018*, 4567267. [CrossRef]

59. Kubat, M.; Matwin, S. Addressing the curse of imbalanced training sets: One-sided selection. *Icml* **1997**, *97*, 179.
60. McClelland, J.L.; Rumelhart, D.E.; PDP Research Group. *Parallel Distributed Processing, Volume 2: Explorations in the Microstructure of Cognition: Psychological and Biological Models*; MIT Press: Cambridge, MA, USA, 1987; Volumes 1 & 2.
61. Ramamoorthy, B.; Pai, M.M.; Prabhu, L.V.; Muralimanju, B.; Rai, R. Assessment of craniometric traits in South Indian dry skulls for sex determination. *J. Forensic Leg. Med.* **2016**, *37*, 8–14. [CrossRef]
62. Saini, V.; Srivastava, R.; Rai, R.K.; Shamal, S.N.; Singh, T.B.; Tripathi, S.K. An Osteometric Study of Northern Indian Populations for Sexual Dimorphism in Craniofacial Region. *J. Forensic Sci.* **2011**, *56*, 700–705. [CrossRef]
63. Kranioti, E.F.; Apostol, M.A. Sexual dimorphism of the tibia in contemporary Greeks, Italians, and Spanish: Forensic implications. *Int. J. Legal. Med.* **2015**, *129*, 357–363. [CrossRef] [PubMed]
64. Cappella, A.; Gibelli, D.; Vitale, A.; Zago, M.; Dolci, C.; Sforza, C.; Cattaneo, C. Preliminary study on sexual dimorphism of metric traits of cranium and mandible in a modern Italian skeletal population and review of population literature. *Leg. Med.* **2020**, *44*, 101695. [CrossRef] [PubMed]
65. Garvin, H.M.; Sholts, S.B.; Mosca, L.A. Sexual dimorphism in human cranial trait scores: Effects of population, age, and body size. *Am. J. Phys. Anthropol.* **2014**, *154*, 259–269. [CrossRef] [PubMed]
66. Ekizoglu, O.; Hocaoglu, E.; Inci, E.; Can, I.O.; Solmaz, D.; Aksoy, S.; Buran, C.F.; Sayin, I. Assessment of sex in a modern Turkish population using cranial anthropometric parameters. *Leg. Med.* **2016**, *21*, 45–52. [CrossRef] [PubMed]

5. Discussion

The main aim of this thesis was to advance the understanding of the sexual dimorphism present in the modern human cranium. As highlighted in the first chapter, the relatively lower level of sexual dimorphism in humans poses a significant challenge in distinguishing between male and female shapes. Our species (*Homo sapiens*) is among the members of the *Hominidae* family characterized by one of the lowest degrees of sexual dimorphism. This phenomenon is likely attributable to evolutionary adaptation strategies that have developed in response to both mate competition and environmental factors (Frayer & Wolpoff, 1985; Plavcan, 2001). Furthermore, the cranium is not the most sexually dimorphic organ in the human skeleton (Byers, 2002).

The necessity to undertake this thesis emerged from the need to address the existing limitations in identifying the sex of the human cranium. Prior to devising a novel methodology for determining the sex of the cranium, it was essential to gain clarity and conduct comprehensive studies on the dimorphic anatomical features. By doing so, the aim was to lay the groundwork for developing an innovative approach to address the issue of sex identification in human remains.

Initially, the research efforts were directed toward examining traits already known to exhibit sexual dimorphism, drawing upon a vast body of previous studies. However, as this investigation progressed, we recognized the importance of minimizing potential biases and the impact of prior knowledge on the findings. It became essential to devise a method that would allow the acquisition of data without being influenced by preconceived notions, thereby obtaining a more genuine and less subjective representation of the phenomenon under consideration. By adopting a more objective approach, we aimed to achieve a clearer and unbiased understanding of sexual dimorphism in the human cranium. This methodological shift allowed us to explore new angles and gain fresh insights into the subject, enhancing the credibility and reliability of our study's outcomes. Ultimately, this endeavor contributed to a more comprehensive and accurate picture of sexual dimorphism in the modern human cranium.

5.1 key findings for the study of cranium dimorphism

In the first part of the doctoral thesis, *trait d'union* is the use of Geometric Morphometrics (GM) as the common thread connecting the analyses of various cranial traits. In the first study on the neurocranium, one of the initial findings was the emergence of a signal indicating sexual dimorphism, primarily centered around the frontal bones. Specifically, observed that the signal of SD of high accuracy was most prominent in the supraorbital torus, followed by the frontal-temporal constriction and parietal eminence. However, it is important to note that in this initial work, the sample size was limited, and one of the open questions did not address the geographical origin of the individuals. In conclusion, the research wrapped up the paper with the intention of considering, in future studies, whether the "population" factor played a role in the observed variations of the neurocranium, potentially more than the sexual variable (Von Cramon-Taubadel, 2014; Von Cramon-Taubadel et al., 2013). This approach represented the first step in visualizing shape variations of modules, considering their association with sexual dimorphism, while also eliminating information not related to sexual dimorphism. The research aimed to move beyond the use of semilandmarks solely based on *a priori* assumptions, meaning without being influenced by prior knowledge about sexual dimorphism in the neurocranium. In that study, the primary signal indicating sexual dimorphism was observed in the frontal bones, particularly in the supraorbital ridges. The signal was less pronounced in the frontal-temporal constriction and parietal eminences. Naturally, as a result of these findings, the research direction shifted towards a more detailed investigation of sexual dimorphism in the frontal bones.

Over the course of several years, research increasingly focused on the most sexually dimorphic trait within the frontal bones: the glabella. This feature played a prominent role in determining the sex of the cranium, as supported by previous studies (Bulut et al., 2016; Kenyhercz et al., 2017; Walker, 2008). To delve deeper into the study of the frontal bone, we made the decision to analyse the entire frontal area. This led to create six different modules: the overall morphology along with five specific modules, each aimed at a particular anatomical trait (glabella, squama, midsagittal profile, supraorbital ridges, temporal lines, and the entire frontal bone). The initial findings from this study reveal that sexual dimorphism significantly influences the morphology of the frontal bone across all the analysed modules. It is important to note that the frontal bone's morphology is influenced not only by sex but also by size, aligning with previous research that highlights the importance of size as a factor in the study of sexual dimorphism and its utility in distinguishing between sexes (Milella et al., 2021). However, the study brings to light that the commonly held perception of anatomical frontal bones being larger in males compared to females is not supported by the results (as indicated by ANOVA and LDA). We did not find a statistically significant relationship between the variables of sex and size in both shape space and form space, suggesting that sex is independent of size. In terms of importance, our results reveal that in shape space, the most sexually dimorphic traits, based on mean accuracy, are as follows: supraorbital ridges (85.5), en-

tire frontal bones (81.7), midsagittal profile (78.9), glabella (78.5), squama (73.3), with the temporal line exhibiting the lowest degree of dimorphism (62.6). In form space, the results are similar, with the following order of importance: supraorbital ridges (84.9), entire frontal bone (79.8), midsagittal profile (76.3), glabella (73.4), squama (72.8), and temporal lines (69.4). These findings indicate a shift in the perceived importance of the glabella, as the module related to supraorbital ridges takes precedence in both form space and shape space, challenging previous conclusions in the literature (Acsádi & Nemeskéri, 1970; Buikstra & Ubelaker, 1994; White & Folkens, 2005; Yas et al.,2001). Another noteworthy aspect of our study is that it doesn't reveal a significant integration between the glabella and supraorbital ridges. Geometric morphometrics has enabled us to uncover shape variations that help us visualize the distinctions between the two sexes (Bigoni et al., 2010; Rosas & Bastir, 2002).

The supraorbital ridges, as well as the glabella area, exhibit a more flattened aspect in females compared to males. In the third paper (study of the entire cranium), it made a significant shift in methodology. I opted for a novel approach using Geometric Morphometrics to address the decision to investigate the same anatomical area not divided into *a priori* patches of semilandmarks. This change in methodology represents an innovative direction in the research.

To accomplish the goal, identified the cranial regions with a higher accuracy related to the SD resulting from the LDA on a small portion of the entire surface of the cranium. In fact, each LDA is independent. Also, in those results in shape space, the medial-inferior portion of the frontal bone (corresponding to the supraorbital ridges) is the area more dimorphic. The results are confirmed in all our studies in that thesis and in some literature (Čechová et al., 2019; Garvin & Ruff, 2012). In females the supraorbital ridge is less developed, the glabella is more expanded and flattened and the superior margin of the orbit is narrower than in males; males have a more robust structure or supraorbital ridges and supratoral sulcus more defined. When including the signal of size (form space) in the LDA analysis there are three different areas of interest with a high level of accuracy: again, the media-inferior portion of the frontal bone, the nasal aperture, and the mastoid process. The divergence of morphology in the medial margin of the orbital and the supraorbital arch between the sexes, in males, is more acute, which probably causes the rounded orbits in females and more squared in males (Bastir et al., 2011; Pretorius et al., 2006).

The nasal aperture, which has received relatively little attention in previous studies on sexual dimorphism (López et al., 2009; Rosas & Bastir, 2002), emerged as an important feature in our results. We found that males tend to have a larger nasal aperture in a central area compared to females. This finding suggests that the nasal aperture could be a promising candidate for inclusion in future protocols aimed at determining an individual's sex. On the other hand, we corroborated existing literature regarding the size of the mastoid process (de Paiva & Segre, 2003; Kemkes & Göbel, 2006). However, our study did not confirm a correlation between the shape of the mastoid process and sexual dimorphism. Interestingly, the occipital protuberances, traditionally considered a dimorphic point and one of the five points used in traditional protocols (Acsádi & Nemeskéri, 1970; Buikstra & Ubelaker, 1994; Walker, 2008), did not exhibit dimorphism in our study. In fact, results showed lower accuracy in this regard. This divergence from traditional findings highlights the importance of continually reassessing and refining the understanding of sexual dimorphism in cranial anatomy with new approaches.

In the last of the three papers involving Geometric Morphometrics analysis, we began to recognize the significance of studying and investigating size-related factors. Consequently, we delved into the concept of allometry. In the results, allometry emerged as the dominant factor influencing the first axis of form variation. Although the allometric trajectories of males and females diverged, it's important to note that the differences were not statistically significant.

Addressing the original question about the impact of population proved to be challenging throughout the thesis. In the last paper, the decision to isolate the Italian sample (see the chapter on Materials and Methods), as it offered the most controlled and homogeneous dataset with a substantial number of individuals. When we applied the analysis specifically to the Italian sample, the results reaffirmed our findings from the broader dataset, albeit with minor, inconsequential differences.

To conclude the thesis, for another different approach, the Neural Network Analysis was adopted to create a new methodology. Over the past five years, AI has made a substantial impact on the study of sexual dimorphism in human cranial anatomy, as evidenced by studies (Imaizumi et al., 2020; Ortega et al., 2021; Toneva et al., 2021). We recognized a common limitation in existing research, which often relied on single, specific populations and sometimes applied testing to the same population used for training and validation, leading to potential overfitting issues (Ying, 2019). To address this limitation, we developed a model that incorporated a broader dataset. Our model utilizes 10 linear measurements and achieves an impressive 84% accuracy in estimating sex. The log loss metric indicates that the model correctly attributes sex in 90% of cases. However, it's important to acknowledge the limitation of this model it requires all 10 measurements, rendering it impractical for use on fragmentary craniums. Nevertheless, our model represents a significant advancement as it overcomes the constraints associated with specific population methods, making it applicable in cases where the origin of the human remains is unknown. In our results, the size, represented by the geometric mean, emerged as the most significant factor, followed by the linear measurements. Notably, the width of the anterior portion of the crania, particularly the bizygomatic breadth, played a crucial role in discriminating between sexes. This finding aligns with previous research (Dayal et al. 2008; Franklin et al. 2005), which has also highlighted the importance of bizygomatic breadth. Additionally, the model placed importance on the mastoid process (de Paiva & Segre, 2003; Kemkes & Göbel, 2006). However, some features such as those related to the nasal regions and orbital height had a comparatively lesser influence on the model's results.

In discussing the accuracy of the study, consistent results are in line with similar investigations (Table 5). For the neurocranium, we achieved an accuracy of 79% in shape space, while for the entire frontal bone, it was 81% in shape space and 80% in form space (with supraorbital ridges being the most dimorphic traits in both spaces at 85%). In the case of the entire cranium, we obtained 66% accuracy in shape space and 73% in form space. Utilizing Artificial Neural Networks, the model performed with an accuracy of 84%. The cranium may not be the most ideal anatomical bone for establishing sex. The accuracy of the results aligns well with previous findings on sexual dimorphism, which have shown accuracy rates ranging from 60% to 90% (see table 5). These accuracy rates can vary based on several factors, including the specific anatomical area of the skull analyzed, the methodology employed, and the population under study.

Table 5:

Summary of previous studies on the sexual dimorphism signal found in the human cranium.

Anatomical region	Repository info	Method	N. of individuals	Accuracy	Reference
Frontal bone	Colombia	Linear discriminant analysis	60	84.31%	Perlaza et al., 2014
Entire cranium	Italia	Cross-validation LOO	92	84%	Milella et al., 2020
Craniofacial traits	Coimbra Collection	Cross-validation LOO	125	62.12-68.90 %	Gonzalez et al., 2011
Facial Traits	Staff of hospital	Logistic regression	131	84.9 %	Hennessy et al., 2002
Brownridge (frontal bone)	Terry Collection	Discriminant analysis	119	91.6%	Garvin & Ruff, 2012
Upper face	Czech population	Cross-validation	154	70.3%-83.3%	Bedjová et al., 2017
Craniofacial form	Greece	Logistic regression	176	74.4 % - 83.3%	Chovalopoulou et al., 2016
Foramen Magnum	Nigerian	Discriminant function	100	62%	Ukoha et al., 2011
Palate and cranial base	Greece	Cross- validation	176	90.4% (Crania) 74.8% (palate)	Chovalopoulou et al., 2013
Mastoid	North Indian	Discriminant analysis	138	87%	Saini et al., 2012
Mastoid	Hammann-Todd Ost. Coll.	Descriptive statistics	100	80-60%	Bernard & Moore-Jansen, 2009

Mastoid triangle	Forensic medicine mainz coll. Germany	Linear discriminant analysis	97	65%	Kemkes, Göbel, 2006
Cranial base	Cretan population	Cross-validation	165	80%-90%	Nikita & Michopoulou, 2017
Crania	Australian	Discriminant analysis	200	87.5 % - 88 %	Franklin et al., 2016
Vault and Midsagittal	Greek population	Logistic regression	176	89.2% 79.4%	Chovalopoulou et al., 2016
Skull based	Thai of Khon Kaen University	Descriptive statistics	91	-	Roopakhun et al., 2010
Occipital condyle	British	Discriminant function	146	69.2% 76.7%	Gapert et al., 2009
Cranial base	Denmark	Discriminant function, cross-validation	102	76.6%	Mana et al., 2016
Cranial base	Terry Collection	Regression model	100	70-85%	Holland, 1986
Occipital and temporal bone s	Western-European	Regression discriminant function	50	82%	Boucherie et al., 2022
Crania	South African	Discriminant function	332	77% - 80%	Franklin et al., 2004
Crania	Raymond Dart collection	Cross-validation (LOO)	120	81% ca	Dayal et al., 2008
Crania	Hamburg University	Descriptive statistics	50	96%	Ramsthaer et al., 2010
Crania	Asian pop.	Discriminant analysis	144	86.8%	Green & Curnoe, 2009
Crania	Bass donated collection	Cross-validation	222	>95%	Abdel Fatah et al., 2014

Skull	Cleveland Hospital collection	Discriminant analysis	85	83.5%	Dereli et al., 2018
Frontal bone	Czech population	Cross-validation	103	98.05% -84.46%	Čechova et al., 2019
Crania facial	Bohemia	Discriminant analysis	139	100%	Bigoni et al., 2010
Supraorbital margin	Germany	Pearson's chi-squared	108	48%	Graw et al., 1999
Crania	Brazilian population	Discriminant analysis	80	82.5%	Jurda et al., 2016
Crania	Turkish population	Logistic regression	400	83%	Ekizoglu et al., 2016
Crania	NMDID	Binary logistic regression and Linear discriminant analysis	431	81%-87%	Kelley & Tallman, 2022
Crania	South India	Discriminant analysis	70	72.9%	Ramamuorthy et al., 2016
Crania	Italian population	Discriminant analysis	80	88.6%	Cappella et al., 2020

One significant advantage of our approach is that it does not rely on specific populations. Furthermore, in the last two studies, we conducted analyses on the entire skull, which contributes to the robustness of the results.

Indeed, achieving higher accuracy in a study is influenced by various factors, including how well the data is balanced (James et al.,2013). As more variables are introduced, it can become more challenging to achieve high accuracy levels. It is true that in situations involving well-controlled populations, controlled age groups, reduced portions of the anatomy, specific anatomical morphologies, and particular methodological choices (e.g., Canonical Variate Analysis or Principal Component Analysis), higher accuracy is more achievable (Cooke &Terhune, 2015).

However, it is important to emphasize that the objective of this thesis was to produce results that closely reflected real-world conditions and criteria. By taking a broader and more inclusive approach, the research aimed to provide insights that could be applied to a wider range of scenarios and populations, thereby contributing to a more comprehensive understanding of sexual dimorphism in cranial anatomy.

In situations such as archaeological remains with no available DNA or proteome analysis when other anatomical parts are absent, that model can provide a reasonable approximation (Welker et al., 2020).

Nevertheless, in forensic cases where legal requirements mandate higher accuracy levels (Christensen et al., 2014; Ubelaker, 2021), the results obtained in the study would preclude the use exclusive of the cranium as a reliable method for determining the sex of individuals. As we continue to delve into this field, we anticipate uncovering further intricacies and nuances that will undoubtedly enhance our knowledge of human cranial variation and its implications in evolutionary and anthropological contexts.

5.2 Methodology: achievements and limitations

The choice of a "modern" (contemporary age) sample for a thesis like this was mainly due to two factors. The first was of a methodological nature; it was necessary to analyse a large number of individuals (crania) whose sex and other information such as age, cause of death, etc. were known. The quantity of individuals included in the application of geometric morphometry is inherently tied to the methodology itself. Given that geometric morphometrics involves multivariate statistical analyses, employing a sample that accurately represents the underlying 'population' is crucial to mitigate potential random bias errors (Fruciano, 2016). This imposed a strong restriction on archaeological or paleoanthropological material. Secondly, we tried to collect as much material as possible from museums and known collections that did not require financial outlay so that we could have a successful response from the Museums and Repositories for access.

The evolution of the thesis is twofold. On one side the increasing sample size of individuals studied. Starting with a smaller number, it culminated in a much larger sample, including 228 individuals for the entire cranium. The methodology employed throughout the thesis has been extensively developed and refined. Initially, the research focused on a limited number of landmarks and semilandmarks, specifically patches of 20 contiguous semilandmarks localized solely within the neurocranium region. However, as the study progressed, the analysis evolved into a more intricate and sophisticated investigation, exemplified by the comprehensive examination of the frontal region and the eventual encompassment of the entire skull (with a big patch of 1000 semilandmarks, (Gunz et al., 2004; Weber, 2001; Weber et al., 2011).

Significantly, as the sequence of papers unfolded, considerable time was devoted not only to investigating sexual dimorphism but also to exploring related aspects such as integration and/or modularity (in the work of frontal bones) and allometry (for the entire cranium) (Adams, 2016; Klingenberg, 2009; Rosas & Bastir, 2002). An advancement in the methodology lies in the separate consideration of Linear Discriminant Analysis (LDA) results within shape space and form space (size shape space). This approach has rendered a clearer interpretation of the obtained outcomes (Klingenberg, 2016; McLachlan, 2004).

This progression in both sample size and analytical methodology showcases the dedication and thoroughness in the research process, leading to a comprehensive and robust investigation of sexual dimorphism in modern human crania. Such advancements are integral to advancing anthropological research and contribute significantly to the knowledge in this field.

Undoubtedly, the limited access to a worldwide sample for the GM (Geometric Morphometrics) part of the thesis represents one of the potential weaknesses. The constraints arose from difficulties in obtaining 3D format samples (external surface models or Ct scan) from various institutions and museums. Many of these organizations declined requests for access, and the ones that responded positively required expensive travel and resources, such as scanners and Ct scans, which were beyond the available funding resources.

This limitation in sample diversity may have implications for the generalizability of the findings. Ideally, a more diverse and extensive sample would have allowed for a broader representation of modern human crania from different populations and regions, enhancing the applicability of the results to a global context. Despite this challenge, the thesis should still be recognized for its valuable contributions, as it managed to achieve significant advancements in understanding sexual dimorphism in modern human crania through the available resources. Nonetheless, it is essential to acknowledge the potential impact of sample limitations on the study's overall scope and draw conclusions with consideration of these constraints in mind.

Indeed, while the sample may not encompass every corner of the world, it is essential to highlight that the study represents a notable advancement in terms of diversity compared to previously published methods (Milella et al., 2020; Gonzalez et al., 2011; Nikita & Michopoulou, 2017; Franklin et al., 2016). The inclusion of the Terry Collection (Copes, 2012), which represents both African and European ancestry, alongside Central American native populations, European populations, and South American (Latin or Spanish) populations, provides a relatively broad and diverse dataset (see Materials & Methods).

While it may not capture the entirety of global variation (Asian ancestry for example is totally absent), the study's sample is certainly quite wide-ranging and covers a range of ancestral backgrounds. This diversity due to mixed geography is significant because it contributes to realizing a study across different populations.

Moreover, the robustness of the method is reinforced by the fact that when you isolated the Italian population for analysis in the last paper, the results remained consistent with those obtained from the entire sample. This consistency suggests that the method is reliable and can be applied effectively across various population groups, further strengthening the validity and applicability of your findings.

The importance of age, as mentioned in the introduction, cannot be underestimated in the study of sexual dimorphism. Age is a critical factor because it can introduce significant morphological changes that could potentially bias the study results. To address this issue, several steps were taken to ensure that the sample primarily consisted of adult individuals (Anzelmo et al., 2015; Jurda & Urbanová, 2016). First, individuals who fell within an adult age range were selected, typically defined as those over 18 years old or those who exhibited the presence of the third molar. These selection criteria helped ensure that the study primarily analysed adult cranial morphology. Additionally, skulls that displayed dental or cranial pathologies capable of altering the cranial structure were excluded. This exclusion was done by information available in the database or by palaeopathological analysis. Lastly, the use of reference points and semilandmarks that covered the entire cranial surface played a crucial role in mitigating the impact of age-related changes. By utilizing these comprehensive reference points, the study aimed to minimize the poten-

tial biases introduced by age-related displacement of certain cranial landmarks (Gunz & Mitteroecker, 2013).

Furthermore, the data from very elderly individuals, typically those over 80 years old, were excluded. This decision was made to minimize the potential influence of age-related changes on the results.

For the last study with the use of Anatomical Network Analysis (Feng & Lu, 2019), we exclusively utilized open repositories as our data source due to the substantial number of individuals involved and the labor-intensive nature of taking each measurement individually. Conducting such measurements personally, especially considering the initial count of 80 measurements which was later reduced to 10, would have required an extensive amount of time and resources, making it impractical for that thesis project. Fortunately, leveraging open repositories allowed us to bypass this time-consuming step and access a large dataset with a sufficient sample size for our study. Moreover, both repositories have been extensively used and referenced by numerous researchers over the years, attesting to their high level of reliability and credibility in the scientific community (Jantz et al., 2005; Uytterschaut, 1986).

By relying on these open repositories, we could focus our efforts on the essential analyses and investigations without compromising the validity and robustness of our research. The availability and reliability of these datasets were instrumental in making our study feasible and ensuring its scientific integrity. As previously mentioned (see Chapter Materials and Methods), Howell's repository provides sex-estimated data, and although this could potentially introduce some margin of error in classification, it did not pose a significant limitation for our survey. The algorithm used in our analysis takes into account the potential uncertainties in sex estimation, ensuring that the results are still reliable and informative. Moreover, while it is true that some measures in the repository were absent for the validation test case, this limitation did not hinder the overall realization of our study. We were able to work with the available data and perform the necessary analyses, demonstrating the robustness and adaptability of the approach.

The *affaire* of open repositories extended beyond the acquisition of data for analysis. In line with evolving open science policies and a commitment to enhancing the reproducibility of scientific findings, this thesis made an effort to generate databases and scripts for open analysis across various facets of the research.

With the exception of the initial article focusing on neurocranial analysis, where data publication did not occur, subsequent articles adhered to a consistent approach. Specifically, the article pertaining to frontal analysis was published on Zenodo, encompassing both data and associated scripts. Similarly, the article encompassing the entire skull analysis followed the same protocol on Zenodo. Lastly, the article concentrating on linear measurements within the NNA's dataset was published on the GitHub platform including data, pre-preparation steps, and the analysis script.

Of course, we acknowledge that future studies with additional databases and more comprehensive data could further enhance and refine the analyses performed in our research. Expanding the scope of data sources would undoubtedly contribute to a broader and more comprehensive understanding of the studied phenomena.

In summary, despite the limitations posed by the sex-estimated data and the absence of

some measures in the validation test case, our study was successfully executed and yielded valuable insights. We remain open to the possibility of future research endeavors that could build upon our findings and advance the field of study even further.

6. Conclusion and future perspectives

The main objective of this Ph.D. dissertation was to contribute novel insights into sexual dimorphism in human cranial anatomy. This thesis aimed to challenge certain assumptions prevalent in the existing literature regarding the anatomical characteristics of crania associated with sexual dimorphism.

Each of the four works comprising this research project made distinct contributions toward the overarching goal of this Ph.D. dissertation. The progression throughout these works is evident, commencing with an initial endeavor to map neurocranial features with minimal influence from prior knowledge, conducted on a limited sample of individuals. Subsequently, the research expanded in terms of sample size, the entire morphology of crania, and, an advance of methodological sophistication. In concluding this sequence of studies, the sample size continued to grow, and a comprehensive approach was devised to supersede prior investigations. Furthermore, the geographical diversity of individuals analyzed was broadened. To ensure transparency and facilitate engagement with the scientific community, we have established a reproducible methodology, with both data and scripts publicly accessible in a dedicated repository.

Despite the exhaustive efforts invested in this Ph.D. thesis, the exploration of sexual dimorphism in human cranial morphology remains an ongoing discourse. This work represents a foundational step, setting the stage for further investigations and contributions to the field. In this regard, the future holds the potential to extend our methodological approaches to larger datasets, thereby advancing our understanding of sexual dimorphism in adult cranial anatomy.

Additionally, we envision different prospective avenues of research. First, Over the course of these years, we have had the opportunity to scan several skulls from two distinct archaeological sites, Mirador (Atapuerca, Burgos, Vergès et al., 2016) and Roc de les

Orenetes (Queralbs, Pyrenees). These two deposits hold the promise of allowing us to conduct future testing of both the GM method and the NNA method. This will provide us with a valuable opportunity to evaluate the differences in accuracy between these two methods when applied to archaeological samples.

By testing these methods on archaeological remains, we can gain insights into their applicability in real-world, protohistoric contexts.

Secondly, the examination of sexual dimorphism in childhood seeks to establish during the growing for the emergence of sexual dimorphic traits during puberty in both girls and boys. This line of inquiry will also explore the various factors influencing the development of physical differences between the sexes during maturation. We also proposed investigating the ontogenesis of sexual dimorphism in infancy (from prenatal to 6 years old). The intent of that would be to create a map of steps of sexual dimorphic traits during different trajectories for boys and girls.

Third, during the Ph.D. in a work presented at the AABA 2022 meeting and during the ESHE meeting in 2022, started an application to study the impact of asymmetry in human crania correlated with sexual dimorphism (in Supplementary the poster communication of ESHE2 2022). Perspectives of the future are to extend the sample and investigate the correlations between the asymmetry of the external cranium and endocranium in both sexes.

For last these methodological approaches are not confined solely to cranial studies; give us the opportunity to use a strong classification method, that may also be applied to other skeletal elements and hold promise for the analysis of human fossils within the paleoanthropological domain.

7. Bibliography

Abdel Fatah, E. E., Shirley, N. R., Jantz, R. L., & Mahfouz, M. R. (2014). Improving sex estimation from crania using a novel three-dimensional quantitative method. *Journal of Forensic Sciences*, *59*(3), 590–600. https://doi.org/10.1111/1556-4029.12379

Ackermann, R. R. (2002). Patterns of covariation in the hominoid craniofacial skeleton: Implications for paleoanthropological models. *Journal of Human Evolution*, *43*(2), 167–187. https://doi.org/10.1006/jhev.2002.0569

Acsádi, G., & Nemeskéri, J. (1970). *History of human life span and mortality*. https://scholar.google.es/scholar?hl=it&as_sdt=0%2C5&q=acsadi+and+nemeskeri+1970&oq=ascadi+

Adams, D. C. (2016). Evaluating modularity in morphometric data: Challenges with the RV coefficient and a new test measure. *Methods in Ecology and Evolution*, *7*(5), 565–572. https://doi.org/10.1111/2041-210X.12511

Adams, D. C., Rohlf, F. J., & Slice, D. E. (2004). Geometric morphometrics: Ten years of progress following the 'revolution.' *Italian Journal of Zoology*, *71*(1), 5–16. https://doi.org/10.1080/11250000409356545

Alpaydin, E. (2020). *introduction to machine learning* (MIT press).

Anzelmo, M., Ventrice, F., Barbeito-Andrés, J., Pucciarelli, H. M., & Sardi, M. L. (2015). Ontogenetic changes in cranial vault thickness in a modern sample of Homo sapiens. *American Journal of Human Biology*, *27*(4), 475–485. https://doi.org/10.1002/ajhb.22673

Ashizawa, K., Kumakura, C., Zhou, X., Jin, F., & Cao, J. (2005). RUS skeletal maturity of children in Beijing. *Annals of Human Biology*, *32*(3), 316–325. https://doi.org/10.1080/03014460500087725

Attia, M. H., Kholief, M. A., Zaghloul, N. M., Kružić, I., Anđelinović, Š., Bašić, Ž., & Jerković, I. (2022). Efficiency of the Adjusted Binary Classification (ABC) Ap-

proach in Osteometric Sex Estimation: A Comparative Study of Different Linear Machine Learning Algorithms and Training Sample Sizes. *Biology*, *11*(6), 917. https://doi.org/10.3390/biology11060917

Bastir, M., Godoy, P., & Rosas, A. (2011). Common features of sexual dimorphism in the cranial airways of different human populations. *American Journal of Physical Anthropology*, *146*(3), 414–422. https://doi.org/10.1002/ajpa.21596

Bejdová, Š., Dupej, J., Krajíček, V., Velemínská, J., & Velemínský, P. (2018). Stability of upper face sexual dimorphism in central European populations (Czech Republic) during the modern age. *International Journal of Legal Medicine*, *132*(1), 321–330. https://doi.org/10.1007/s00414-017-1625-3

Bethard, J. D., & DiGangi, E. A. (2020). Letter to the Editor—Moving Beyond a Lost Cause: Forensic Anthropology and Ancestry Estimates in the United States. In *Journal of Forensic Sciences* (Vol. 65, Issue 5, pp. 1791–1792). Blackwell Publishing Inc. https://doi.org/10.1111/1556-4029.14513

Bhola, S., Chen, J., Fusco, J., Duarte, G. F., Andarawis-Puri, N., Ghillani, R., & Jepsen, K. J. (2011). Variation in childhood skeletal robustness is an important determinant of cortical area in young adults. *Bone*, *49*(4), 799–809. https://doi.org/10.1016/j.bone.2011.07.018

Bigoni, L., Velemínská, J., & Brůžek, J. (2010). Three-dimensional geometric morphometric analysis of cranio-facial sexual dimorphism in a Central European sample of known sex. *HOMO- Journal of Comparative Human Biology*, *61*(1), 16–32. https://doi.org/10.1016/j.jchb.2009.09.004

Birkby, W. H. (n.d.). *An Evaluation of Race and Sex Identification from Cranial Measurements*.

Bishop, C. (2006). *Pattern recognition and machine learning*.

Blackith, R. E., & Reyment, R. A. (1971). *Multivariate morphometrics.*

Bookstein, F. L. (1991). *Morphometric tools for landmark data : geometry and biology*. Cambridge University Press. https://books.google.es/books?hl=it&lr=&id=amwT1ddIDwAC&oi=fnd&pg=PP1&dq=bookstein+1991+morphometric+tools&ots=tKYuJbQzIE&sig=l_dcOCFRZOumMGEEhsn_jitv1vQ#v=onepage&q=bookstein 1991 morphometric tools&f=false

Bookstein, F. L. (1997). Landmark methods for forms without landmarks: morphometrics of group differences in outline shape. *Medical Image Analysis*, *1*(3), 225–243. https://doi.org/10.1016/S1361-8415(97)85012-8

Boucherie, A., Chapman, T., García-Martínez, D., Polet, C., & Vercauteren, M. (2022). Exploring sexual dimorphism of human occipital and temporal bones through geometric morphometrics in an identified Western-European sample . *American Journal of Biological Anthropology*, *178*(1), 54–68. https://doi.org/10.1002/ajpa.24485

Boyden, A. (1943). Homology and analogy: a century after the definitions of" homologue" and" analogue" of Richard Owen. *The Quarterly Review of Biology*, *18*(3), 228–241.

Broca, P. (1875). *Instructions craniologiques et craniométriques de la Société d'Anthropologie de Paris.* (Vol. 2). Masson .

Bruner, E. (2007). Cranial shape and size variation in human evolution: Structural and functional perspectives. *Child's Nervous System*, *23*(12), 1357–1365. https://doi.org/10.1007/s00381-007-0434-2

Bucchi, A., Luengo, J., Fuentes, R., Arellano-Villalón, M., Lorenzo, C., & Bucchi, A. ; (2020). Recommendations for Improving Photo Quality in Close Range Photogrammetry, Exemplified in Hand Bones of Chimpanzees and Gorillas Recomendaciones para Mejorar la Calidad de las Fotos en. In *Int. J. Morphol* (Vol. 38, Issue 2).

Buikstra, J., & Ubelaker, D. (1994). Standards for data collection from human skeletal remains: Proceedings of a seminar at the Field Museum of Natural History (Arkansas Archaeology. In *Fayetteville Arkansas Archaeological Survey*. http://scholar.google.com/scholar?hl=en&btnG=Search&q=intitle:Standards+for+Data+Collection+-from+Human+Skeletal+Remains+Proceedings+of+a+Seminar+at+the+Field+Museum+of+Natural+History#0

Bulut, O., Petaros, A., Hizliol, I., Wärmländer, S. K. T. S., & Hekimoglu, B. (2016). Sexual dimorphism in frontal bone roundness quantified by a novel 3D-based and landmark-free method. *Forensic Science International*, *261*, 162.e1-162.e5. https://doi.org/10.1016/j.forsciint.2016.01.028

Byers, S. N. (2002). *Introduction to Forensic Anthropology*.

Canci, A., & Minozzi, S. (2005). *Archeologia dei resti umani: dallo scavo al laboratorio* (Carocci).

Cao, Y., Ma, Y., Yang, X., Xiong, J., Wang, Y., Zhang, J., Qin, Z., Chen, Y., Vieira, D. N., Chen, F., Zhang, J., & Huang, P. (2022). Use of deep learning in forensic sex estimation of virtual pelvic models from the Han population. *Forensic Sciences Research*, *7*(3), 540–549. https://doi.org/10.1080/20961790.2021.2024369

Caple, J. M., Byrd, J. E., & Stephan, C. N. (2018). The utility of elliptical Fourier analysis for estimating ancestry and sex from lateral skull photographs. *Forensic Science International*, *289*, 352–362.

Castro, J. C., Menéndez, L., Gordón, F., Fuchs, L., Di Bastiano, A., Del Papa, M., Muñe, M. C., & Vázquez, M. C. (2009). Actualizacón del catalogo y de las condiciones de conservación de las coleciones de la división antropología, facultad de ciencias naturales y museo, UNLP.

Catalina-Herrera, C. J. (1987). Study of the anatomic metric values of the foramen magnum and its relation to sex. *Acta Anatomica*, *130*(4), 344–347.

Cattaneo, C., & Grandi, M. (2004). *Antropologia e odontologia forense. Guida allo studio dei resti umani.* (Monduzzi).

Čechová, M., Dupej, J., Brůžek, J., Bejdová, Š., Horák, M., & Velemínská, J. (2019). Sex estimation using external morphology of the frontal bone and frontal sinuses in a contemporary Czech population. *International Journal of Legal Medicine*, 16–19. https://doi.org/10.1007/s00414-019-02063-8

Chatzigianni, A., & Halazonetis, D. J. (2009). Geometric morphometric evaluation of cervical vertebrae shape and its relationship to skeletal maturation. . *American Journal of Orthodontics and Dentofacial Orthopedics,* , *136*(A).

Chovalopoulou, M. E., Valakos, E. D., & Manolis, S. K. (2013). Sex determination by three-dimensional geometric morphometrics of the palate and cranial base. *Anthropologischer Anzeiger*, *70*(4), 407–425. https://doi.org/10.1127/0003-5548/2013/0363

Chovalopoulou, M.-E., Valakos, E. D., & Manolis, S. K. (2016). Sex determination by three-dimensional geometric morphometrics of craniofacial form. *Anthropologischer Anzeiger*, *73*(3), 195–206. https://doi.org/10.1127/anthranz/2016/0470

Christensen, A. M., & Crowder, C. M. (2009). *Ancestry Assessment . Scientific Working Group for Forensic Anthropology (SWGANTH).*

Christensen, A., Passalacqua, N., & Bartelink, E. (2014). *Forensic Anthropology: Current Methods and Practice.* . USA: Academic Press.

Claude, J. (2008). *Morphometrics with R* (1st ed.). Springer New York, NY.

Claudio, I., Galdames, S., Alejandra, D., Matamala, Z., & Smith, R. L. (2008). Sex Determination Using Mastoid Process Measurements in Brazilian Skulls. In *Int. J. Morphol* (Vol. 26, Issue 4).

Cooke, S. B., & Terhune, C. E. (2015). Form, Function, and Geometric Morphometrics. *Anatomical Record*, *298*(1), 5–28. https://doi.org/10.1002/ar.23065

Copes, L. (2012). *Comparative and Experimental Investigations of Cranial Robusticity in Mid-Pleistocene Hominins*. Arizona State University.

Curate, F., Umbelino, C., Perinha, A., Nogueira, C., Silva, A. M., & Cunha, E. (2017). Sex determination from the femur in Portuguese populations with classical and machine-learning classifiers. *Journal of Forensic and Legal Medicine*, *52*, 75–81. https://doi.org/10.1016/j.jflm.2017.08.011

Darmawan, M. F., Yusuf, S. M., Abdul Kadir, M. R., & Haron, H. (2015). Comparison on three classification techniques for sex estimation from the bone length of Asian children below 19 years old: An analysis using different group of ages. *Forensic Science International*, *247*, 130.e1-130.e11. https://doi.org/10.1016/j.forsciint.2014.11.007

Dayal, M. R., Spocter, M. A., & Bidmos, M. A. (2008). An assessment of sex using the skull of black South Africans by discriminant function analysis. *HOMO- Journal of Comparative Human Biology*, *59*(3), 209–221. https://doi.org/10.1016/j.jchb.2007.01.001

de Paiva, L. A. S., & Segre, M. (2003). Sexing the human skull through the mastoid process. *Revista Do Hospital Das Clínicas*, *58*(1), 15–20. https://doi.org/10.1590/s0041-87812003000100004

Dean Holland, T. (1986). Sex Determination of Fragmentary Crania by Analysis of the Cranial Base. In *AMERICAN JOURNAL OF PHYSICAL ANTHROPOLOGY* (Vol. 70).

Del Bove, A., Profico, A., & Lorenzo, C. (2018). Sexual dimorphism in human frontal bone: a landmark-based approach. *ESHE*.

Del Bove, A., Profico, A., Riga, A., Bucchi, A., & Lorenzo, C. (2020). A geometric morphometric approach to the study of sexual dimorphism in the modern human frontal bone. *American Journal of Physical Anthropology*. https://doi.org/10.1002/ajpa.24154

Del Bove, A., & Veneziano, A. (2022). A Generalised Neural Network Model to Estimate Sex from Cranial Metric Traits: A Robust Training and Testing Approach. *Applied Sciences (Switzerland)*, *12*(18). https://doi.org/10.3390/app12189285

Dereli, A. K., Zeybek, V., Sagtas, E., Senol, H., Ozgul, H. A., & Acar, K. (2018). Sex determination with morphological characteristics of the skull by using 3D modeling techniques in computerized tomography. *Forensic Science, Medicine, and Pathology*. https://doi.org/10.1007/s12024-018-0029-0

Digangi, E. A., & Hefner, J. T. (2015). Ancestry Estimation . In *Research Methods in Human Skeletal Biology* (pp. 117–149).

Dirkmaat, D. (2012). *A companion to forensic anthropology* (Vol. 10). John Wiley & Sons .

Dryden, I. L., & Mardia, K. V. (1993). Multivariate shape analysis. *The Indian Journal of Statistics*, *Series A*, 460–480.

du Jardin, P., Ponsaillé, J., Alunni-Perret, V., & Quatrehomme, G. (2009). A comparison between neural network and other metric methods to determine sex from the upper femur in a modern French population. *Forensic Science International*, *192*(1–3), 127.e1-127.e6. https://doi.org/10.1016/j.forsciint.2009.07.014

Dunn, R. R., Spiros, M. C., Kamnikar, K. R., Plemons, A. M., & Hefner, J. T. (2020). Ancestry estimation in forensic anthropology: A review. *WIREs Forensic Science*, *2*(4). https://doi.org/10.1002/wfs2.1369

Edgar, H. J. H., Daneshvari Berry, S., Moes, E., Adolphi, N. L., Bridges, P., & Nolte, K. B. (2020). *New Mexico Decedent Image Database.*

Fairbairn, D. J. (1997). Allometry for sexual size dimorphism: Pattern and process in the coevolution of body size in males and females. In *Annual Review of Ecology and Systematics* (Vol. 28, pp. 659–687). https://doi.org/10.1146/annurev.ecolsys.28.1.659

Feng, J. , & Lu, S. (2019). Performance analysis of various activation functions in artificial neural networks. *Journal of Physics: Conference Series* , *1237*(2), 022–030.

Fischer, B., & Mitteroecker, P. (2017). Allometry and Sexual Dimorphism in the Human Pelvis. *Anatomical Record*, *300*(4), 698–705. https://doi.org/10.1002/ar.23549

Fleagle, J. (2013). *Primate Adaptation and Evolution*. Academic Press.

Franklin, D., Freedman, L., & Milne, N. (2005). Sexual dimorphism and discriminant function sexing in indigenous South African crania. *HOMO- Journal of Comparative Human Biology*, *55*(3). https://doi.org/10.1016/j.jchb.2004.08.001

Franklin, D., Oxnard, C. E., O'Higgins, P., & Dadour, I. (2007). Sexual Dimorphism in the Subadult Mandible: Quantification Using Geometric Morphometrics. *Journal of Forensic Sciences*, *52*(1), 6–10. https://doi.org/10.1111/j.1556-4029.2006.00311.x

Frayer, D. W., & Wolpoff, M. H. (1985). Sexual dimorphism. *Annual Review of Anthropology* , *14*(1), 429–473.

Fruciano, C. (2016). Measurement error in geometric morphometrics. In *Development Genes and Evolution* (Vol. 226, Issue 3, pp. 139–158). Springer Verlag. https://doi.org/10.1007/s00427-016-0537-4

Gapert, R., Black, S., & Last, J. (2009). Sex determination from the foramen magnum: Discriminant function analysis in an eighteenth and nineteenth century British sample. *International Journal of Legal Medicine*, *123*(1), 25–33. https://doi.org/10.1007/s00414-008-0256-0

Gapert, R., & Last, J. (2008). Sex determination from the foramen magnum: Discriminant function analysis in an eighteenth and nineteenth century British sample. *International Journal of Legal Medicine*, *123*, 25–33.

Garvin, H. M., & Ruff, C. B. (2012a). Sexual dimorphism in skeletal browridge and chin morphologies determined using a new quantitative method. *American Journal of Physical Anthropology*, *147*(4), 661–670. https://doi.org/10.1002/ajpa.22036

Garvin, H. M., & Ruff, C. B. (2012b). Sexual dimorphism in skeletal browridge and chin morphologies determined using a new quantitative method. *American Journal of Physical Anthropology*, *147*(4), 661–670. https://doi.org/10.1002/ajpa.22036

Garvin, H. M., Sholts, S. B., & Mosca, L. A. (2014). Sexual dimorphism in human cranial trait scores: Effects of population, age, and body size. *American Journal of Physical Anthropology*, *154*(2), 259–269. https://doi.org/10.1002/ajpa.22502

Gentile, D. A. (1993). Just What Are Sex and Gender, Anyway? A Call for a New Terminological Standard. *Psychological Science*, *4*(2), 120–122.

Giles, E., & Elliot, O. (1963). Sex determination by discriminant function analysis of crania. *American Journal of Physical Anthropology*, *21*(1), 53–68. https://doi.org/10.1002/ajpa.1330210108

Glucksmann, A. (1981). *Sexual Dimorphism in human and Mammalian Biology and Pathology* (Academic Press Inc, Ed.).

Gonzalez, P. N., Bernal, V., & Perez, S. I. (2011). Analysis of Sexual Dimorphism of Craniofacial Traits Using Geometric Morphometric Techniques. *Wiley Online Library*, *21*(1), 82–91. https://doi.org/10.1002/oa.1109

González-José, R., Ramírez-Rozzi, F., Sardi, M., Martínez-Abadías, N., Hernández, M., & Pucciarelli, H. M. (2005). Functional-cranial approach to the influence of economic strategy on skull morphology. *American Journal of Physical Anthropology*, *128*(4), 757–771. https://doi.org/10.1002/ajpa.20161

Gower, J. C. (1975). Generalized procrustes analysis. *Psychometrika*, *40*(1), 33–51.

Graw, M., Czarnetzki, A., & Haffner, H. T. (1999). The form of the supraorbital margin as a criterion in identification of sex from the skull: Investigations based on modern human skulls. *American Journal of Physical Anthropology*, *108*(1), 91–96. https://doi.org/10.1002/(SICI)1096-8644(199901)108:1<91::AID-AJPA5>3.0.CO;2-X

Green, H., & Curnoe, D. (2009). Sexual dimorphism in Southeast Asian crania: A geometric morphometric approach. *HOMO- Journal of Comparative Human Biology*, *60*(6), 517–534. https://doi.org/10.1016/j.jchb.2009.09.001

Guglielmino-Matessi, C. R., Gluckman, P., & Cavalli-Sforza, L. L. (1979). Climate and the Evolution of Skull Metrics in Man. *American Journal of Physical Anthropology* , *50*(4), 549–564.

Guirao Piñeyro, M., & Guirao Pérez, M. (2008). *Biografía íntima del profesor Federico Olóriz Aguilera* (Editorial Comares).

Gülekon, N., & Turgut, H. B. (2003). The External Occipital Protuberance: Can It Be Used as a Criterion in the Determination of Sex? *Journal of Forensic Science* , *48*(5).

Gunz, P., Mitteröcker, P., Seidler, H., Weber, G. W., Prossinger, H., & Schäfer, K. (2004). Virtual Anthropology: The Digital Evolution in Anthropological Sciences. *Journal of PHYSIOLOGICAL ANTHROPOLOGY and Applied Human Science*, *20*(2), 69–80. https://doi.org/10.2114/jpa.20.69

Gunz, P., & Mitteroecker, P. (2013). Semilandmarks: a method for quantifying curves and surfaces. *Hystrix, the Italian Journal of Mammalogy*, 1–7. https://doi.org/doi:10.4404/hystrix-24.1-6292

Gustafsson, A., Werdelin, L., Tullberg, B. S., & Tullberg, B. S. (2007). Stature and sexual stature dimorphism in Sweden, from the 10th to the end of the 20th century. *American Journal Human Biology* , *19*, 861–870.

Harrell, F. E., & Dupont, C. (2022). Hmisc. Harrell Miscellaneous. *CRAN*.

Harrington, T. F. (1911). An appreciation of Dr. Dwight. . *The Sacred Heart Review* , *47*(2), 3–5.

Hefner, J. T. (2009). Cranial nonmetric variation and estimating ancestry. *Journal of Forensic Sciences*, *54*(5), 985–995. https://doi.org/10.1111/j.1556-4029.2009.01118.x

Hefner, J. T., & Ousley, S. D. (2014). Statistical classification methods for estimating ancestry using morphoscopic traits. *Journal of Forensic Sciences*, *59*(4), 883–890. https://doi.org/10.1111/1556-4029.12421

Hennessy, R., Kinsella, A., psychiatry, J. W.-B., & 2002, undefined. (n.d.). 3D laser surface scanning and geometric morphometric analysis of craniofacial shape as an index of cerebro-craniofacial morphogenesis: initial application to sexual. *Elsevier*. Retrieved October 22, 2020, from https://www.sciencedirect.com/science/article/pii/S0006322301013270

Holland, T. D. (1986). Sex determination of fragmentary crania by analysis of the cranial base. *American Journal of Physical Anthropology*, *70*(2), 203–208.

Hoover, K. C., & Thomas, G. P. (2022). Sexual dimorphism and biomechanical loading in occipital bone morphological variation. *American Journal of Human Biology*, *34*(10). https://doi.org/10.1002/ajhb.23792

Hounsfield, G. N. (1973). Computerized transverse axial scanning (tomography). 1. Description of system. . *Br J Radiol.*, *46*(552), 1016--22.

Howells, W. W. (1973). Cranial Variation in Man. A Study by Multivariate Analysis of Patterns of Differences Among Recent Human Populations. . *Papers of the Peabody Museum of Archeology and Ethnology*, *67*, 259.

Howells, W. W. (1989). Skull Shapes and the Map. Craniometric Analyses in the Dispersion of Modern Homo. . *Papers of the Peabody Museum of Archaeology and Ethnology*, *79*, 189.

Howells, W. W. (1995). Who's Who in Skulls. Ethnic Identification of Crania from Measurements. *Papers of the Peabody Museum of Archaeology and Ethnology.*, *82*, 108.

Hrdliča, A. (1919). Anthropometry . *American Journal of Physical Anthropology* , *2*, 43–46.

Hsiao, T. H., Tsai, S. M., Chou, S. T., Pan, J. Y., Tseng, Y. C., Chang, H. P., & Chen, H. Sen. (2010). Sex determination using discriminant function analysis in children and adolescents: A lateral cephalometric study. *International Journal of Legal Medicine*, *124*(2), 155–160. https://doi.org/10.1007/s00414-009-0412-1

Hunt, D. R., & Albanese, J. (2005). History and demographic composition of the Robert J. Terry anatomical collection. In *American Journal of Physical Anthropology* (Vol. 127, Issue 4, pp. 406–417). https://doi.org/10.1002/ajpa.20135

Imaizumi, K., Bermejo, E., Taniguchi, K., Ogawa, Y., Nagata, T., Kaga, K., Hayakawa, H., & Shiotani, S. (2020). Development of a sex estimation method for skulls using machine learning on three-dimensional shapes of skulls and skull parts. *Forensic Imaging*, *22*, 200393. https://doi.org/10.1016/j.fri.2020.200393

Isaza, J., Díaz, C. A., Bedoya, J. F., Monsalve, T., & Botella, M. C. (2014). Assessment of sex from endocranial cavity using volume-rendered CT scans in a sample from medellín, colombia. *Forensic Science International*, *234*, 186.e1-186.e10. https://doi.org/10.1016/j.forsciint.2013.10.023

James, G., Witten, D., Hastie, T., & Tibshiarani, R. (n.d.). *An introduction to statistical learning with applications in R* (Vol. 2013). Springer .

James Rohlf, F., & Marcus, L. F. (1993). A revolution morphometrics. *Trends in Ecology & Evolution*, *8*(4), 129–132. https://doi.org/10.1016/0169-5347(93)90024-J

Jantz, R. L., & Moore-Jansen, P. H. (1988). A data base for forensic anthropology. *Final Report to the National Institute of Justice*.

Jurda, M., & Urbanová, P. (2016). Sex and ancestry assessment of Brazilian crania using semi-automatic mesh processing tools. *Legal Medicine*, *23*, 34–43. https://doi.org/10.1016/j.legalmed.2016.09.004

Kanchan, T., & Krishan, K. (2011). Anthropometry of hand in sex determination of dismembered remains - A review of literature. *Journal of Forensic and Legal Medicine*, *18*(1), 14–17. https://doi.org/10.1016/j.jflm.2010.11.013

Katherine Spradley, M., & Jantz, R. L. (2011). PAPER ANTHROPOLOGY Sex Estimation in Forensic Anthropology: Skull Versus Postcranial Elements. *Wiley Online Library*, *56*(2), 289–296. https://doi.org/10.1111/j.1556-4029.2010.01635.x

Kelley, S. R., & Tallman, S. D. (2022). Population-Inclusive Assigned-Sex-at-Birth Estimation from Skull Computed Tomography Scans. *Forensic Sciences*, *2*(2), 321–348. https://doi.org/10.3390/forensicsci2020024

Kemkes, A., & Göbel, T. (2006). Metric Assessment of the "Mastoid Triangle" for Sex Determination: A Validation Study. *Journal of Forensic Sciences*, *51*(5), 985–989. https://doi.org/10.1111/j.1556-4029.2006.00232.x

Kendall, D. (1977). The diffusion of shape. . *Advances in Applied Probability*, *9*(3), 428–430.

Kendall, D. G. (1984). Shape manifolds, procrustean metrics, and complex projective spaces. *Bulletin of the London Mathematical Society*, *16*(2), 81–121.

Kenyhercz, M. W., Klales, A. R., Stull, K. E., McCormick, K. A., & Cole, S. J. (2017). Worldwide population variation in pelvic sexual dimorphism: A validation and recalibration of the Klales et al. method. *Forensic Science International*, *277*, 259.e1-259.e8. https://doi.org/10.1016/j.forsciint.2017.05.001

Klingenberg, C. P. (2009). Morphometric integration and modularity in configurations of landmarks: Tools for evaluating a priori hypotheses. *Evolution and Development*, *11*(4), 405–421. https://doi.org/10.1111/j.1525-142X.2009.00347.x

Klingenberg, C. P. (2016). Size, shape, and form: concepts of allometry in geometric morphometrics. In *Development Genes and Evolution* (Vol. 226, Issue 3, pp. 113–137). Springer Verlag. https://doi.org/10.1007/s00427-016-0539-2

Kranioti, E. F., Işcan, M. Y., & Michalodimitrakis, M. (2008). Craniometric analysis of the modern Cretan population. *Forensic Science International*, *180*(2–3), 110.e1-110.e5. https://doi.org/10.1016/j.forsciint.2008.06.018

Krüger, G. C., L'Abbé, E. N., Stull, K. E., & Kenyhercz, M. W. (2015). Sexual dimorphism in cranial morphology among modern South Africans. *International Journal of Legal Medicine*, *129*(4), 869–875. https://doi.org/10.1007/s00414-014-1111-0

Kunar, A., & Nagar, M. (2014). Human adult occipital condyles: A morphometric analysis. *Research & Reviews: Journal of Medical and Health Sciences*, *3*(4), 112–116.

LeDell, E., Gill, N., Aiello, S., Fu, A., Candel, A., Click, C., Kraljevic, T., Nykodym, T., Aboyoun, P., Kurka, M., Malohlava, M., Rehak, L., Eckstrand, E., Hill, B., Vidrio, S., Jadhawani, S., Wang, A., Peck, R., Wong, W., … Maurerova, V. (2022). *R Interface for the "H2O" Scalable Machine Learning Platform* (3.36.1.2). CRAN .

Lestrel, P. E., Cesar, R. M., Takahashi, O., & Kanazawa, E. (2005). Sexual dimorphism in the Japanese cranial base: A fourier-wavelet representation. *American Journal of Physical Anthropology*, *128*(3), 608–622. https://doi.org/10.1002/ajpa.20209

Lewis, J. E., Degusta, D., Meyer, M. R., Monge, J. M., Mann, A. E., Holloway, R. L., & Gould, S. J. (n.d.). *Historical and Philosophical Perspective The Mismeasure of Science: Stephen Jay Gould versus Samuel George Morton on Skulls and Bias*. https://doi.org/10.1371/journal.pbio.1001071.g001

Lieberman, D. (2011). *The evolution of the human head*. Belknap Press of Harvard University Press. http://www.hup.harvard.edu/catalog.php?isbn=9780674046368

Lillie, E. M., Urban, J. E., Lynch, S. K., Weaver, A. A., & Stitzel, J. D. (2016). Evaluation of Skull Cortical Thickness Changes with Age and Sex from Computed Tomography Scans. *Journal of Bone and Mineral Research*, *31*(2), 299–307. https://doi.org/10.1002/jbmr.2613

Lo, M., Mariconti, E., Nakhaeizadeh, S., & Morgan, R. M. (2023). Preparing computed tomography images for machine learning in forensic and virtual anthropology. *Forensic Science International: Synergy*, *6*, 100319. https://doi.org/10.1016/j.fsisyn.2023.100319

López, M. C., Suazo Galdames, I. C., Zavando Matamala, D. A., & Smith, R. L. (2009). Sexual Dimorphism Determination by Piriform Aperture Morphometric Analysis in Brazilian Human Skulls. *Int. J. Morphol.* , *27*(2), 327–331.

Lozano, M., Jiménez-Brobeil, S., … J. W.-J. of, & 2020, undefined. (n.d.). Argaric craftswomen: Sex-based division of labor in the Bronze Age southeastern Iberia. *Elsevier*. Retrieved October 22, 2020, from https://www.sciencedirect.com/science/article/pii/S0305440320301606

Lugli, F., Figus, C., Silvestrini, S., Costa, V., Bortolini, E., Conti, S., Peripoli, B., Nava, A., Sperduti, A., Lamanna, L., Bondioli, L., & Benazzi, S. (2020). Sex-related morbidity and mortality in non-adult individuals from the Early Medieval site of Valdaro (Italy): the contribution of dental enamel peptide analysis. *Journal of Archaeological Science: Reports*, *34*. https://doi.org/10.1016/j.jasrep.2020.102625

Macaluso, P. J. (2011). Détermination biométrique du sexe dans une population française à partir de mesures de la région basale de l'os occipital. *Bulletins et Mémoires de La Société d'anthropologie de Paris*, *23*(1), 19–26.

Mahfouz, M., Badawi, A., Merkl, B., Fatah, E. E. A., Pritchard, E., Kesler, K., Moore, M., Jantz, R., & Jantz, L. (2007). Patella sex determination by 3D statistical shape models and nonlinear classifiers. *Forensic Science International*, *173*(2–3), 161–170. https://doi.org/10.1016/j.forsciint.2007.02.024

Mardia, K. V., Kent, J. T., & Bibby, J. M. (1979). Multivariate Analysis. *Academic Press*.

Marino, E. A. (1995). Sex estimation using the first cervical vertebra. *American Journal of Physical Anthropology*, *97*(2), 127–133.

McLachlan, G. J. (2004). *Discriminant Analysis and Statistical Pattern Recognition.* (Wiley Interscience).

Milella, M., Franklin, D., Belcastro, M. G., & Cardini, A. (2021). Sexual differences in human cranial morphology: Is one sex more variable or one region more dimorphic? *Anatomical Record*, *304*(12). https://doi.org/10.1002/ar.24626

Mitteroecker, P., Gunz, P., Bernhard, M., Schaefer, K., & Bookstein, F. L. (2004). Comparison of cranial ontogenetic trajectories among great apes and humans. *Journal of Human Evolution*, *46*(6), 679–698.

Mitteroecker, P., Gunz, P., Windhager, S., & Schaefer, K. (2013). A brief review of shape, form, and allometry in geometric morphometrics, with applications to human facial morphology. *Hystrix*, *24*(1). https://doi.org/10.4404/hystrix-24.1-6369

Mitteroecker, P., & Philipp Gunz, A. E. (2009). Advances in Geometric Morphometrics. *Evolutionary Biology*, *36*, 235–247. https://doi.org/10.1007/s11692-009-9055-x

Moggi Cecchi, J., & Stanyon, R. (2014). *The Anthropological and Ethnological Collections Il Museo di Storia Naturale*. *V*(December).

Monson, T. A., Armitage, D. W., Monson, T. A., Armitage, D. W., & Hlusko, L. J. (2018). *Using Machine Learning to Classify Extant Apes and Interpret the Dental Morphology of the Chimpanzee-human Last Common Ancestor Recommended Citation*. https://escholarship.org/uc/item/84d1304f#supplemental

Moore, M. K. (2013). Sex estimation and assessment. *Research Methods in Human Skeletal Biology*, 91–116.

Mosimann, J. E. (1970). Size allometry: Size and shape variables with characterizations of the lognormal and generalized gamma distributions. *Journal of the American Statistical Association*, *65*(330). https://doi.org/10.1080/01621459.1970.10481136

Navega, D., Vicente, R., Vieira, D. N., Ross, A. H., & Cunha, E. (2015). Sex estimation from the tarsal bones in a Portuguese sample: a machine learning approach. *International Journal of Legal Medicine*, *129*(3), 651–659. https://doi.org/10.1007/s00414-014-1070-5

Nikita, E., & Michopoulou, E. (2018). A quantitative approach for sex estimation based on cranial morphology. *American Journal of Physical Anthropology*, *165*(3), 507–517. https://doi.org/10.1002/ajpa.23376

Nikita, E., & Nikitas, P. (2020). On the use of machine learning algorithms in forensic anthropology. *Legal Medicine*, *47*. https://doi.org/10.1016/j.legalmed.2020.101771

Olivier, G. (1975). Biometry of the human occipital bone. *Journal of Anatomy*, *120*(3), 507–518.

Ortega, R. F., Irurita, J., Campo, E. J. E., & Mesejo, P. (2021). Analysis of the performance of machine learning and deep learning methods for sex estimation of infant individuals from the analysis of 2D images of the ilium. *International Journal of Legal Medicine*, *135*(6), 2659–2666. https://doi.org/10.1007/s00414-021-02660-6

Paknahad, M., Shahidi, S., & Zarei, Z. (2017). Sexual Dimorphism of Maxillary Sinus Dimensions Using Cone-Beam Computed Tomography. *Journal of Forensic Science* , *62*(2), 395–398.

Patterson, J., & Gibson, A. (2017). *Deep Learning: A Practitioner's Approach*. O'Reilly Media.

Perlaza, N. A. (2014). Sex Determination from the Frontal Bone: A Geometric Morphometric Study. *Journal of Forensic Sciences*, *59*(5), 1330–1332. https://doi.org/10.1111/1556-4029.12467

Petaros, A., Sholts, S. B., Slaus, M., Bosnar, A., & Wärmländer, S. K. T. S. (2015). Evaluating sexual dimorphism in the human mastoid process: A viewpoint on the methodology. *Clinical Anatomy*, *28*(5), 593–601. https://doi.org/10.1002/ca.22545

Pinto, S. C. D., Urbanova, P., & Cesar, R. M. (2016). Two-Dimensional Wavelet Analy-

sis of Supraorbital Margins of the Human Skull for Characterizing Sexual Dimorphism. *IEEE Transactions on Information Forensics and Security*, *11*(7), 1542–1548. https://doi.org/10.1109/TIFS.2016.2541611

Plavcan, J. M. (2001). Sexual dimorphism in primate evolution. *American Journal of Physical Anthropology*, *Suppl 33*, 25–53. https://doi.org/10.1002/ajpa.10011

Pretorius, E., Steyn, M., & Scholtz, Y. (2006). Investigation into the usability of geometric morphometric analysis in assessment of sexual dimorphism. *American Journal of Physical Anthropology*, *129*(1), 64–70. https://doi.org/10.1002/ajpa.20251

Profico, A., Bellucci, L., Buzi, C., Di Vincenzo, F., Micarelli, I., Strani, F., Tafuri, M. A., & Manzi, G. (2019). Virtual Anthropology and its Application in Cultural Heritage Studies. *Studies in Conservation*, *64*(6), 323–336. https://doi.org/10.1080/00393630.2018.1507705

Profico, A., Buzi, C., Castiglione, S., Melchionna, M., Piras, P., Veneziano, A., & Raia, P. (2021). Arothron: An R package for geometric morphometric methods and virtual anthropology applications. *American Journal of Physical Anthropology*, *176*(1), 144–151. https://doi.org/10.1002/ajpa.24340

Pujol, A., Rissech, C., Ventura, J., & Turbón, D. (2016). Ontogeny of the male femur: Geometric morphometric analysis applied to a contemporary Spanish population. . *American Journal of Physical Anthropology*, *159*(1), 146-163.

Relethford, J. H. (1994). Craniometric Variation Among Modern Human Populations. In *AMERICAN JOURNAL, OF PHYSICAL ANTHROPOLOGY* (Vol. 95).

Richtsmeier, J. T., Cheverud, J. M., & Lele, S. (1992). ADVANCES IN ANTHROPOLOGICAL MORPHOMETRIeS. In *Annu. Rev. Anthropol* (Vol. 21). www.annualreviews.org

Rohlf, F. J., & Leslie, F. M. (1993). A revolution morphometrics. *Trends in Ecology & Evolution*, *8*(4), 129–132.

Rohlf, F. J., & Marcus, L. F. (1993). A revolution in Morphometrics. *Trends in Ecology and Evolution* , *8*(4).

Rohlf, F. J., & Slice, D. (1990). EXTENSIONS OF THE PROCRUSTES METHOD FOR THE OPTIMAL SUPERIMPOSITION OF LANDMARKS. In *Syst. Zool* (Vol. 39, Issue 1).

Rooppakhun MEng, S., Piyasin, S., Vatanapatimakul, N., Kaewprom BNS, Y., & Sitthiseripratip DEng, K. (2010). Craniometric Study of Thai Skull Based on Three-Dimensional Computed Tomography (CT) Data. In *J Med Assoc Thai* (Vol. 93, Issue 1). http://www.mat.or.th/journal

Rosas, A., & Bastir, M. (2002). Thin-plate spline analysis of allometry and sexual dimorphism in the human craniofacial complex. *American Journal of Physical Anthropology*, *117*(3), 236–245. https://doi.org/10.1002/ajpa.10023

Rubini, M., & Scarani, P. (1989). Studio antropologico e patologico su 38 crani di individui deceduti durante la prima metà del XIX secolo presso il manicomio dell'Ospedale di S. Orsola in Bologna. Patologie associate e variabilità dei caratteri metrici e disconti-

nuf. *Riv. Di Antropol.*, *LXVII*, 237–298.

Safont, S., Malgosa, A., & Subira, M. E. (2000). Sex assessment on the basis of long bone circumference. . *American Journal of Physical Anthropology* , *113*, 317–328.

Saini, V., Srivastava, R., Rai, R. K., Shamal, S. N., Singh, T. B., & Tripathi, S. K. (2012). Sex Estimation from the Mastoid Process Among North Indians. *Journal of Forensic Sciences*, *57*(2), 434–439. https://doi.org/10.1111/j.1556-4029.2011.01966.x

Sampson, P. D., Bookstein, F. L., Sheehan, F. H., & Bolson, E. L. (1996). Eigenshape Analysis of Left Ventricular Outlines from Contrast Ventriculograms. In *Advances in Morphomterics* (Springer, Vol. 284).

Scheuer, L., & Black, S. (2000). Development and ageing of the juvenile skeleton. *Human Osteology in Archaeology and Forensic Science*, 9–22.

Schiebinger, L. (2015). *Skeletons in the Closet: The First Illustrations of the Female Skeleton in Eighteenth-Century Anatomy* (Issue 14).

Schlager, S. (2017). *Chapter 9 - Morpho and Rvcg – Shape Analysis in R: R-Packages for Geometric Morphometrics, Shape Analysis and Surface Manipulations* (G. Zheng, S. Li, & G. B. T.-S. S. and D. A. Székely, Eds.; pp. 217–256). Academic Press. https://doi.org/https://doi.org/10.1016/B978-0-12-810493-4.00011-0

Schlager, S., & Rüdell, A. (2017). Sexual Dimorphism and Population Affinity in the Human Zygomatic Structure—Comparing Surface to Outline Data. *Anatomical Record*, *300*(1), 226–237. https://doi.org/10.1002/ar.23450

Scott, G. R., & Turner II, C. G. (1997). *The Anthropology of Modern Human Teeth: Dental Morphology and Its Variation in Recent Human Populations*. Cambridge University Press.

Sholapurkar, V. T., Virupaxi, R. D., & Desai, S. P. (2017). Morphometric analysis of human occipital condyles for sex determination in dry adult skulls. *International Journal of Anatomy and Research*, *5*(1), 3318–3323.

Smith, O. A. M., Nashed, Y. S. G., Duncan, C., Pears, N., Profico, A., & O'Higgins, P. (2021). 3D Modeling of craniofacial ontogeny and sexual dimorphism in children. *Anatomical Record*, *304*(9), 1918–1926. https://doi.org/10.1002/ar.24582

Stewart, T. D. (1979). *Essentials of forensic anthropology: especially as developed in the United States* (C. T. Charles, Ed.).

Stolberg, M. (2003). A woman down to her bones: The anatomy of sexual difference in the sixteenth and early seventeenth centuries. *Isis*, *94*(2), 274–299.

Svozil, D., Kvasnieka, V., & Pospichal, J. (1997). Introduction to multi-layer feed-forward neural networks. *Chemometrics and Intelligent Laboratory Systems*, *39*.

Swindler, D. R., & Wood, C. D. (1973). *An atlas of primate gross anatomy*. University of Washington Press.

Thi Porter, S., Roussel, M., & Soressi, M. (2016). A simple photogrammetry Rig for the reliable creation of 3D artifact models in the field. Lithic Examples from the early upper paleolithic sequence of Les Cottés (France). *Advances in Archaeological Practice* , *4*(1).

https://doi.org/DOI: 10.7183/2326-3768.4.1.11

Toneva, D., Nikolova, S., Agre, G., Zlatareva, D., Hadjidekov, V., & Lazarov, N. (2021). Machine learning approaches for sex estimation using cranial measurements. *International Journal of Legal Medicine* , *135*, 951–966. https://doi.org/10.1007/s00414-020-02460-4/Published

Ubelaker, D. H. (2021). Research integrity in forensic anthropology. In *Forensic Sciences Research* (Vol. 6, Issue 4, pp. 285–291). Taylor and Francis Ltd. https://doi.org/10.1080/20961790.2021.1963515

Ubelaker, D. H., & DeGaglia, C. M. (2017). Population variation in skeletal sexual dimorphism. *Forensic Science International*, *278*, 407.e1-407.e7. https://doi.org/10.1016/j.forsciint.2017.06.012

Uldin, T. (2017). Virtual anthropology – a brief review of the literature and history of computed tomography. In *Forensic Sciences Research* (Vol. 2, Issue 4, pp. 165–173). Taylor and Francis Ltd. https://doi.org/10.1080/20961790.2017.1369621

Uysal, S., Gokharman, D., Kacar, M., Tuncbilek, I., & Kosa, U. (2005). Estimation of sex by 3D CT measurements of the foramen magnum. *Journal of Forensic Sciences*, *50*(6), 1310–1314.

Uytterschaut, T. (1986). Sexual Dimorphism in Human Skulls. A Comparison of Sexual Dimorphism in Different Populations. In *HUMAN EVOLUTION* (Vol. 1, Issue 3).

Velemínská, J., Fleischmannová, N., Suchá, B., Dupej, J., Bejdová, Š., Kotěrová, A., & Brůžek, J. (2021). Age-related differences in cranial sexual dimorphism in contemporary Europe. *International Journal of Legal Medicine*, *135*(5), 2033–2044. https://doi.org/10.1007/s00414-021-02547-6

Vesalius, A., Saunders, J. B. D. C. M., & O'Malley, C. D. (1973). *The illustrations from the works of Andreas Vesalius of Brussels: with annotations and translations, a discussion of the plates and their background, authorship and influence, and a biographical sketch of Vesalius (Vol. 56).* (Courier Corporation, Vol. 56).

Von Cramon-Taubadel, N. (2014). *Evolutionary insights into global patterns of human cranial diversity: population history, climatic and dietary effects*. *92*, 43–77. https://doi.org/10.4436/JASS.91010

von Cramon-Taubadel, N., Stock, J. T., & Pinhasi, R. (2013). Skull and limb morphology differentially track population history and environmental factors in the transition to agriculture in Europe. *Proceedings of the Royal Society B: Biological Sciences*, *280*(1767), 12. https://doi.org/10.1098/rspb.2013.1337

Wahl, J., & Graw, M. (2001). Metric sex differentiation of the pars petrosa ossis temporalis. *Int J Legal Med*, *114*, 215–223.

Walker, P. L. (2008). Sexing skulls using discriminant function analysis of visually assessed traits. *American Journal of Physical Anthropology*, *136*(1), 39–50. https://doi.org/10.1002/ajpa.20776

Walrath, D. E., Turner, P., & Bruzek, J. (2004). Reliability test of the visual assessment of cranial traits for sex determination. *American Journal of Physical Anthropology*,

125(2), 132–137. https://doi.org/10.1002/ajpa.10373

Weber, G. W. (2001). Virtual anthropology (VA): A call forGlasnost in paleoanthropology. *The Anatomical Record*, *265*(4), 193–201. https://doi.org/10.1002/ar.1153

Weber, G. W. (2015). Virtual anthropology. *American Journal of Physical Anthropology*, *156*(S59), 22–42. https://doi.org/10.1002/ajpa.22658

Weber, G. W., Bookstein, F. L., & Strait, D. S. (2011). Virtual anthropology meets biomechanics. In *Journal of Biomechanics*. https://doi.org/10.1016/j.jbiomech.2011.02.079

Welker, F., Ramos-Madrigal, J., Gutenbrunner, P., Mackie, M., Tiwary, S., Rakownikow Jersie-Christensen, R., Chiva, C., Dickinson, M. R., Kuhlwilm, M., de Manuel, M., Gelabert, P., Martinón-Torres, M., Margvelashvili, A., Arsuaga, J. L., Carbonell, E., Marques-Bonet, T., Penkman, K., Sabidó, E., Cox, J., … Cappellini, E. (2020). The dental proteome of Homo antecessor. *Nature*, *580*(7802), 235–238. https://doi.org/10.1038/s41586-020-2153-8

Werner Platzer. (2014). *Color Atlas of Human Anatomy: Vol 1. Locomotor System* (7 ed, Vol. 1).

Wescott, D. J., & Moore-Jansen, P. H. (2001). Metric variation in the human occipital bone: Forensic anthropological applications. *Journal of Forensic Sciences*, *46*(5), 1159–1163.

White, T. D., & Folkens, P. Arend. (2005). *The Human Bone Manual.* Elsevier. https://books.google.it/books?id=ctMRLv6oA8wC&dq=william bass&hl=it&source=gbs_similarbooks

White, T. D. (Timothy D.), & Folkens, P. A. (2000). *Human osteology*. Academic Press. https://books.google.it/books?id=lrLL-X5bg_0C&dq=william bass&hl=it&source=gbs_similarbooks

Wilkinson C. (2004). *Forensic Facial Reconstruction.* Cambridge: University Press.

Wood S.W. (1995). The first use of the terms “homology “ and “analogy” in the writings of Richard Owen. *Archives of Natural History*, *22*, 255–259.

Worthman, C. M. (1995). Hormones, sex, and gender. *Annual Review of Anthropology*, *24*(1), 593–617.

Wu, X., & Schepartz, L. (2009). Application of computed tomography in paleoanthropological research. *Progress in Natural Science*, *19*, 913–921.

Yas, M., Ç, ar I., Soysal, Z., & Ïdir Adli Tõp Kurumu, ag. (2001). *Sexual diagnosis of the glabellar region*. www.elsevier.com/locate/legalmed

Ying, X. (2019). An Overview of Overfitting and its Solutions. *Journal of Physics: Conference Series*, *1168*(2). https://doi.org/10.1088/1742-6596/1168/2/022022

Zdilla, M. J., Russell, M. L., Bliss, K. N., Mangus, K. R., & Koons, A. W. (2017). The size and shape of the foramen magnum in man. *Journal of Craniovertebral Junction & Spine*, *8*(3), 205–221.

UNIVERSITAT ROVIRA I VIRGILI
A COMPUTATIONAL RE-ASSESSMENT OF SEXUAL DIMORPHISM IN THE HUMAN CRANIUM BEYOND TRADITIONAL MORPHOMETRICS: GEOMETRIC MORPHOMETRIC METHODS AND NEURAL NETWORK ANALYSIS
Antonietta Del Bove

8. Supplementary materials

8.1 Scripts in open repositories

To accomplish this thesis, the analyses were conducted using R Studio as the programming language. In four instances (on work packages 2, 3, 4, and 5), the analyses and data were made available in open repositories. This was done to facilitate replication and provide future access to interested third parties. For each work package, we have provided the link where you can download the script and the accompanying data.

II. script analysis" Sexual Dimorphism in the Frontal Bone"

Published in Zenodo link: https://zenodo.org/record/3940597

doi: 10.5281/zenodo.3940597

fffffffffffload("data.rda")

```
#Load function for visualizing shape variations
localmeshdiff<-function(mesh1,mesh2,ploton,
                        paltot=rainbow(200),from=0,to=0.4,
                        n.int=200,out.rem=FALSE,fact=1.5,
                        visual=c(1,2),scale01=TRUE,colwire="pink"){

 range01<-function(x){
  (x-min(x))/(max(x)-min(x))
 }

 area_shape1<-vcgArea(mesh1,perface=T)$pertriangle
 area_shape2<-vcgArea(mesh2,perface=T)$pertriangle
 diff_areas<-(area_shape1-area_shape2)/area_shape1
 sel<-which(is.na(diff_areas))

 if(length(sel)>0){
  mesh1$it<-mesh1$it[,-sel]
  mesh2$it<-mesh2$it[,-sel]
  mesh1<-rmUnrefVertex(mesh1)
```

```
  mesh2<-rmUnrefVertex(mesh2)
  area_shape1<-vcgArea(mesh1,perface=T)$pertriangle
  area_shape2<-vcgArea(mesh2,perface=T)$pertriangle
  diff_areas<-(area_shape1-area_shape2)/area_shape1
 }

 if(out.rem==TRUE){
  x=diff_areas
  qq <- quantile(x, c(1,3)/4, names=FALSE)
  r <- diff(qq) * fact
  tst <- x < qq[1] - r | x > qq[2] + r
  tstp<-qq[2] + r
  tstn<-qq[1] - r
  diff_areas[x>tstp]<-tstp
  diff_areas[x<tstn]<-tstn
 }else{
  diff_areas=diff_areas}

 if(scale01==TRUE){
  diff_areas<-range01(diff_areas)
 }
 cat("the range of diff_areas is ",range(diff_areas),sep="\n"
 if(is.null(to)==TRUE){
  to<-max(diff_areas)*1.01
 }
 if(is.null(from)==TRUE){
  from<-min(diff_areas)*1.01
 }
 selfromto<-which(diff_areas<to & diff_areas>=from)
 diff_areas_fromto<-diff_areas[selfromto]
 if(ploton==1){
  meshfromto<-mesh1
  meshwhite<-mesh1
 }
 if(ploton==2){
```

```
    meshfromto<-mesh2
    meshwhite<-mesh2
  }
  meshfromto$it<-meshfromto$it[,selfromto]
  meshwhite$it<-meshwhite$it[,-selfromto]
  colmap_tot<-colorRampPalette(paltot)   #negative=expansion=red/orange
  breaks_tot<-cut(c(from,diff_areas_fromto,to),n.int)
  cols_tot<-colmap_tot(n.int)[breaks_tot]
  cols_tot<-cols_tot[-c(1,length(cols_tot))]
  plot(density(c(from,diff_areas,to)),main="",xlab="",ylab="")
  abline(v=seq(from,to,length.out = n.int),col=colmap_tot(n.int),lwd=5)
  points(density(diff_areas),type="l",lwd=2)

  if(visual==1){
   triangles3d(t(meshfromto$vb[,meshfromto$it]),
          col=rep(cols_tot,each=3),alpha=1,lit=T,specular="black")
   triangles3d(t(meshwhite$vb[,meshwhite$it]),
          col="grey",alpha=1,lit=T,specular="black")
  }
  if(visual==2){
   triangles3d(t(meshfromto$vb[,meshfromto$it]),
          col=rep(cols_tot,each=3),alpha=1,lit=F,specular="black")
   triangles3d(t(meshwhite$vb[,meshwhite$it]),
          col="grey",alpha=1,lit=F,specular="black")
   wire3d(meshfromto,col=colwire,lit=F,lwd=2)
  }
}
#Define modules
list.order<-list("Entire"=data$Entire,"Glabella"=data$Glabella,
          "Squama"=data$Squama,"Midsagittal"=data$Midsagittal_profile,
          "Torus"=data$`Supraorbital ridges`,"TempLines"=data$`Temporal lines`)
slsets<-data$slsets
sex<-data$sex
{
mshape<-procSym(slsets,CSinit = FALSE,scale=FALSE)$mshape
```

```
means<-NULL
neigh<-10
for(i in 1:dim(mshape)[1]){
dists<-aro.clo.points(t(mshape[i,]),mshape[-i,])$distances
meani<-mean(dists[order(dists)[1:neigh]])
means[i]<-meani
}
mean(means)
sd(means)
} #Density semi-landmarks
{
 combs<-combn(2:6,2)
 fem_int_mod_matrix<-matrix(NA,ncol=5,nrow=ncol(combs))
 colnames(fem_int_mod_matrix)<-c("PLS-corr","PLS-pvalue","CR-corr","CR-pvalue",
                  "Effect size")
 rownames<-NULL
 for(i in 1:ncol(combs)){
 mod1<-procSym(slsets[list.order[[combs[1,i]]],,sex=="F"])
 mod2<-procSym(slsets[list.order[[combs[2,i]]],,sex=="F"])
 PLS<-pls2B(mod1$rotated,mod2$rotated,rounds = 1000)
 fem_int_mod_matrix[i,1]<-PLS$CoVar[1,3]
 fem_int_mod_matrix[i,2]<-PLS$CoVar[1,4]
 modl<-c(rep("A",dim(mod1$rotated)[1]),rep("B",dim(mod2$rotated)[1]))
 set<-procSym(bindArr(slsets[list.order[[combs[1,i]]],,sex=="F"],
                  slsets[list.order[[combs[2,i]]],,sex=="F"],along=1))$rotated
 CR<-modularity.test(set,modl)
 rownames[i]<-paste(names(list.order)[combs[1,i]],names(list.order)[combs[2,i]],sep="_")
 fem_int_mod_matrix[i,3]<-CR$CR
 fem_int_mod_matrix[i,4]<-CR$P.value
 fem_int_mod_matrix[i,5]<-CR$Z
 }
 rownames(fem_int_mod_matrix)<-rownames
 write.table(round(fem_int_mod_matrix,2),"Integr_Modul_Fem.csv",
          dec=".",sep=";",col.names = NA)
} #Integration and modularity (females)
```

```
{
 combs<-combn(2:6,2)
 mal_int_mod_matrix<-matrix(NA,ncol=5,nrow=ncol(combs))
 colnames(mal_int_mod_matrix)<-c("PLS-corr","PLS-pvalue","CR-corr","CR-pvalue",
                    "Effect size")
 rownames<-NULL
 for(i in 1:ncol(combs)){
  mod1<-procSym(slsets[list.order[[combs[1,i]]],,sex=="M"])
  mod2<-procSym(slsets[list.order[[combs[2,i]]],,sex=="M"])
  PLS<-pls2B(mod1$rotated,mod2$rotated,rounds = 1000)
  mal_int_mod_matrix[i,1]<-PLS$CoVar[1,3]
  mal_int_mod_matrix[i,2]<-PLS$CoVar[1,4]
  modl<-c(rep("A",dim(mod1$rotated)[1]),rep("B",dim(mod2$rotated)[1]))
  set<-procSym(bindArr(slsets[list.order[[combs[1,i]]],,sex=="M"],
              slsets[list.order[[combs[2,i]]],,sex=="M"],along=1))$rotated
  CR<-modularity.test(set,modl)
  rownames[i]<-paste(names(list.order)[combs[1,i]],names(list.order)[combs[2,i]],sep="_")
  mal_int_mod_matrix[i,3]<-CR$CR
  mal_int_mod_matrix[i,4]<-CR$P.value
  mal_int_mod_matrix[i,5]<-CR$Z
 }
 rownames(mal_int_mod_matrix)<-rownames
 write.table(round(mal_int_mod_matrix,2),"Integr_Modul_Mal.csv",
        dec=".",sep=";",col.names = NA)
} #Integration and modularity (males
{
res_aovs<-matrix(NA,ncol=6,nrow=length(list.order))
colnames(res_aovs)<-c("RsqSex","pSex","RsqSiz","pSiz",
                "RsqSexSiz","pSexSiz")
rownames(res_aovs)<-names(list.order)
for(i in 1:6){
 gpa<-procSym(slsets[list.order[[i]],,])
 gpa_df<-list("shape"=gpa$PCscores,"Csize"=log(gpa$size),"Sex"=sex)
 praov_res<-procD.lm(shape~Sex*Csize,data=gpa_df)
 R2_sex<-unlist(summary(praov_res))$table.Rsq1
```

```
  R2_siz<-unlist(summary(praov_res))$table.Rsq2
  R2_sexsiz<-unlist(summary(praov_res))$table.Rsq3
  P_sex<-unlist(summary(praov_res))$'table.Pr(>F)1'
  P_siz<-unlist(summary(praov_res))$'table.Pr(>F)2'
  P_sexsiz<-unlist(summary(praov_res))$'table.Pr(>F)3'
  res_aovs[i,1]<-R2_sex
  res_aovs[i,2]<-P_sex
  res_aovs[i,3]<-R2_siz
  res_aovs[i,4]<-P_siz
  res_aovs[i,5]<-R2_sexsiz
  res_aovs[i,6]<-P_sexsiz
 }
 write.table(res_aovs,"ProAov_ShapeSpace.csv",
          dec=".",sep=";",col.names = NA)
 } #Procrustes Anova (Shape Space)
 {
 res_aovs<-matrix(NA,ncol=6,nrow=length(list.order))
 colnames(res_aovs)<-c("RsqSex","pSex","RsqSiz","pSiz",
                "RsqSexSiz","pSexSiz")
 rownames(res_aovs)<-names(list.order)
 for(i in 1:6){
  gpa<-procSym(slsets[list.order[[i]],,],sizeshape = TRUE)
  gpa_df<-list("shape"=gpa$PCscores,"Csize"=log(gpa$size),"Sex"=sex)
  praov_res<-procD.lm(shape~Sex*Csize,data=gpa_df)
  R2_sex<-unlist(summary(praov_res))$table.Rsq1
  R2_siz<-unlist(summary(praov_res))$table.Rsq2
  R2_sexsiz<-unlist(summary(praov_res))$table.Rsq3
  P_sex<-unlist(summary(praov_res))$'table.Pr(>F)1'
  P_siz<-unlist(summary(praov_res))$'table.Pr(>F)2'
  P_sexsiz<-unlist(summary(praov_res))$'table.Pr(>F)3'
  res_aovs[i,1]<-R2_sex
  res_aovs[i,2]<-P_sex
  res_aovs[i,3]<-R2_siz
  res_aovs[i,4]<-P_siz
  res_aovs[i,5]<-R2_sexsiz
```

```
res_aovs[i,6]<-P_sexsiz

}

write.table(res_aovs,"ProAov_FormSpace.csv",

        dec=".",sep=";",col.names = NA)

} #Procrustes Anova (Form Space)

{

 res_LDA_boo<-matrix(NA,ncol=9,nrow=length(list.order))

 colnames(res_LDA_boo)<-c("Accuracy upper","Accuracy mean","Accuracy lower",

                "Precision Female upper","Precision Female mean","Precision Female lower",

                "Precision Male upper","Precision Male mean","Precision Male lower")

 rownames(res_LDA_boo)<-names(list.order)

 iter<-1000 #number of iterations

 n<-100 #number of specimen sampled at each iteration

 alpha<-0.95 #interval of confidence

 for(i in 1:6){

 accur_r<-NULL

 preci_f<-NULL

 preci_m<-NULL

  for(j in 1:iter){

  specs<-sample(1:dim(slsets)[3],n)

  sexr<-sex[specs]

  gpa<-procSym(slsets[list.order[[i]],,specs])

  train<-data.frame(sexr,gpa$PCscores[,which(gpa$Variance[,3]<95)])

  form<- as.formula(c("sexr~",c(paste(paste("PC",(which(gpa$Variance[,3]<95)[1:(length(whi-
ch(gpa$Variance[,3]<95))-1)]),sep=""),"+",sep=""),

                paste("PC",length(which(gpa$Variance[,3]<95)),sep=""))))


  da<-train(form,data=train,method="lda")

  DApred<-predict(da)

  res<-table(sexr,DApred)

  accuracy<-round(sum(diag(res))/sum(res),2)

  precision<-round(diag(res)/apply(res,2,sum),2)

  if(is.na(precision[1])) precision[1]<-0

  if(is.na(precision[2])) precision[2]<-0

  accur_r[j]<-accuracy
```

```
    preci_f[j]<-precision[1]
    preci_m[j]<-precision[2]
    }
  res_LDA_boo[i,1:3]<- unlist(CI(accur_r,alpha))
  res_LDA_boo[i,4:6]<- unlist(CI(preci_f,alpha))
  res_LDA_boo[i,7:9]<- unlist(CI(preci_m,alpha))
  }
  write.table(res_LDA_boo,"LDA_Bootstrap_ShapeSpace.csv",dec=".",sep=";",col.names =
NA)

} #LDA with bootstrapping in the Shape Space (iter=1000, n=100)
{
  res_LDA_boo<-matrix(NA,ncol=9,nrow=length(list.order))
  colnames(res_LDA_boo)<-c("Accuracy upper","Accuracy mean","Accuracy lower",
                           "Precision Female upper","Precision Female mean","Precision Female lower",
                           "Precision Male upper","Precision Male mean","Precision Male lower")
  rownames(res_LDA_boo)<-names(list.order)
  iter=1000 #number of resamples
  n=100 #number of specimen resampled at each iteration
  alpha=0.95 #interval of confidence
  for(i in 1:6){
    accur_r<-NULL
    preci_f<-NULL
    preci_m<-NULL
    for(j in 1:iter){
      specs<-sort(sample(1:dim(slsets)[3],n))
      sexr<-sex[specs]
      gpa<-procSym(slsets[list.order[[i]],,specs],sizeshape = TRUE)
      train<-data.frame(sexr,gpa$PCscores[,which(gpa$Variance[,3]<95)])
      form<- as.formula(c("sexr~",c(paste(paste("PC",(which(gpa$Variance[,3]<95)
[1:(length(which(gpa$Variance[,3]<95))-1)]),sep=""),"+",sep=""),
                                    paste("PC",length(which(gpa$Variance[,3]<95)),sep=""))))

      da<-train(form,data=train,method="lda")
      DApred<-predict(da)
```

```
    res<-table(sexr,DApred)
     accuracy<-round(sum(diag(res))/sum(res),2)
     precision<-round(diag(res)/apply(res,2,sum),2)
     if(is.na(precision[1])) break
     if(is.na(precision[2])) break
     accur_r[j]<-accuracy
     preci_f[j]<-precision[1]
     preci_m[j]<-precision[2]
    }
   res_LDA_boo[i,1:3]<- unlist(CI(accur_r,alpha))
   res_LDA_boo[i,4:6]<- unlist(CI(preci_f,alpha))
   res_LDA_boo[i,7:9]<- unlist(CI(preci_m,alpha))
   }
  write.table(res_LDA_boo,"LDA_Bootstrap_FormSpace.csv",dec=".",sep=";",col.names =
NA)
} #LDA with bootstrapping in the Form space (iter=1000, n=100)
{
 magnf<-2
 Fshapevar<-list()
 Mshapevar<-list()
 for(i in 1:6){
  gpa<-procSym(slsets[list.order[[i]],,])
  sel<-which(gpa$Variance[,3]<95)
  pvalj<-NULL
  meanF<-NULL
  meanM<-NULL
  for(j in 1:length(sel)){
   pvalj[j]<-t.test(gpa$PCscores[,sel[j]]~sex)$p.value
   meanF[j]<-mean(gpa$PCscores[sex=="F",sel[j]])
   meanM[j]<-mean(gpa$PCscores[sex=="M",sel[j]])
  }
  selPCs<-which(pvalj<0.05)
  PCf<-showPC(meanF[selPCs],
          gpa$PCs[,selPCs],gpa$mshape)
  PCm<-showPC(meanM[selPCs],
```

```
                gpa$PCs[,selPCs],gpa$mshape)
  PCfmagn<-(PCf-gpa$mshape)*magnf+gpa$mshape
  PCmmagn<-(PCm-gpa$mshape)*magnf+gpa$mshape
  Fshapevar[[i]]<-PCfmagn
  Mshapevar[[i]]<-PCmmagn
 }
 names(Fshapevar)<-names(list.order)
 names(Mshapevar)<-names(list.order)
} #Calculation of the magnified Shape Variations
{
 {
 refsur<-data$Entire_tri
 Ftri<-refsur
 Mtri<-refsur
 Ftri$vb[1:3,]<-t(Fshapevar[[1]])
 Mtri$vb[1:3,]<-t(Mshapevar[[1]])
 open3d()
 layout3d(t(c(1,2)),sharedMouse = TRUE)
 localmeshdiff(Ftri,Mtri,ploton = 1,from = -0.13,to=0.13,
          paltot=c("red","orange","white","lightblue","blue"),
          out.rem = TRUE,scale01 = FALSE,visual = 2,colwire="darkgreen")
 next3d()
 localmeshdiff(Mtri,Ftri,ploton = 1,from = -0.13,to=0.13,
          paltot=c("red","orange","white","lightblue","blue"),
          out.rem = TRUE,scale01 = FALSE,visual = 2,colwire = "darkorchid4")
 }#Entire module
 {
  refsur<-data$Glabella_tri
  Ftri<-refsur
  Mtri<-refsur
  Ftri$vb[1:3,]<-t(Fshapevar[[2]])
  Mtri$vb[1:3,]<-t(Mshapevar[[2]])
  open3d()
  layout3d(t(c(1,2)),sharedMouse = TRUE)
  localmeshdiff(Ftri,Mtri,ploton = 1,from = 0,to=0.07,
```

```
                paltot=c("red","orange","white","lightblue","blue"),
                out.rem = TRUE,scale01 = FALSE,visual = 2,colwire="darkgreen")
  wire3d(tps3d(data$Entire_tri,vert2points(refsur),vert2points(Ftri)),lwd=1,add=TRUE)
  next3d()
  localmeshdiff(Mtri,Ftri,ploton = 1,from = -0.07,to=0,
                paltot=c("red","orange","white","lightblue","blue"),
                out.rem = TRUE,scale01 = FALSE,visual = 2,colwire = "darkorchid4")
  wire3d(tps3d(data$Entire_tri,vert2points(refsur),vert2points(Mtri)),lwd=1,add=TRUE
  }#Glabella module
 {
  refsur<-data$Squama_tri
  Ftri<-refsur
  Mtri<-refsur
  Ftri$vb[1:3,]<-t(Fshapevar[[3]])
  Mtri$vb[1:3,]<-t(Mshapevar[[3]])

  open3d()
  layout3d(t(c(1,2)),sharedMouse = TRUE)
  localmeshdiff(Ftri,Mtri,ploton = 1,from = -0.06,to=0.06,
                paltot=c("red","orange","white","lightblue","blue"),
                out.rem = TRUE,scale01 = FALSE,visual = 2,colwire="darkgreen")
  wire3d(tps3d(data$Entire_tri,vert2points(refsur),vert2points(Ftri)),lwd=1,add=TRUE)
  next3d()
  localmeshdiff(Mtri,Ftri,ploton = 1,from = -0.06,to=0.06,
                paltot=c("red","orange","white","lightblue","blue"),
                out.rem = TRUE,scale01 = FALSE,visual = 2,colwire = "darkorchid4")
  wire3d(tps3d(data$Entire_tri,vert2points(refsur),vert2points(Mtri)),lwd=1,add=TRUE)
 }#Squama module
 {
  open3d()
  deformGrid3d(Fshapevar[[4]],Mshapevar[[4]],type="s",size=0.0075,col1="dark-
green",col2="darkorchid4")
 }#Midsagittal profile
 {
  refsur<-data$Torus_tri
```

```
Ftri<-refsur
Mtri<-refsur
Ftri$vb[1:3,]<-t(Fshapevar[[5]])
Mtri$vb[1:3,]<-t(Mshapevar[[5]])
open3d()
layout3d(t(c(1,2)),sharedMouse = TRUE)
localmeshdiff(Ftri,Mtri,ploton = 1,from = -0.13,to=0.13,
              paltot=c("red","orange","white","lightblue","blue"),
             out.rem = TRUE,scale01 = FALSE,visual = 2,colwire="darkgreen")
wire3d(tps3d(data$Entire_tri,vert2points(refsur),vert2points(Ftri)),lwd=1,add=TRUE)
next3d()
localmeshdiff(Mtri,Ftri,ploton = 1,from = -0.13,to=0.13,
              paltot=c("red","orange","white","lightblue","blue"),
              out.rem = TRUE,scale01 = FALSE,visual = 2,colwire = "darkorchid4")
wire3d(tps3d(data$Entire_tri,vert2points(refsur),vert2points(Mtri)),lwd=1,add=TRUE)


 }#Supraorbital ridges module
 {
  deformGrid3d(Fshapevar[[6]],Mshapevar[[6]],type="s",size=0.0075,col1="darkgreen",col2="darkorchid4")
 }#Temporal lines
} #Local variations on Shape Variations
{
 comm<-NA
 for(i in 1:6){
  gpa<-procSym(slsets[list.order[[i]],,])
  train<-data.frame(sex,"Csize"=log(gpa$size))
  train2<-data.frame(sex,gpa$PCscores[,which(gpa$Variance[,3]<95)])
  form<- as.formula(c("sex~Csize"))
  form2<- as.formula(c("sex~",c(paste(paste("PC",(which(gpa$Variance[,3]<95)[1:(length(which(gpa$Variance[,3]<95))-1)]),sep=""),"+",sep=""),
                                paste("PC",length(which(gpa$Variance[,3]<95)),sep=""))))
  da=train(form,data=train,method="lda")
  DApred=predict(da)
  da2=train(form2,data=train2,method="lda")
```

```
    DApred2<-predict(da2
    pred1ok<-as.numeric(DApred)
    pred1ok[which(pred1ok==as.numeric(as.factor(sex)))]<-10
    pred1ok[which(pred1ok!=10)]<-5
    pred2ok<-as.numeric(DApred2)
    pred2ok[which(pred2ok==as.numeric(as.factor(sex)))]<-10
    pred2ok[which(pred2ok!=10)]<-5
    comm[i]<-(length(which(rowSums(cbind(pred1ok,pred2ok))==20))/length(DApred))*100
  }
  names(comm)<-names(list.order)

} #Comparison accuracy using shape and size separately as predictors
```

III script: Sexual dimorphism in the entire crania and creation of a new map

Published in Zenodo link: https://zenodo.org/record/8304736

doi: 10.5281/zenodo.8304736

```
#####################################################################
##### Mapping sexual dimorphism signal in the human cranium #####
#######################    R code     ##########################
#####################################################################


#load libraries
{
  library(Morpho)
  library(Arothron)
  library(Rvcg)
  library(rgl)
  library(stringr)
  library(doParallel)
  library(geomorph)
  library(MASS)
  library(vegan)
  library(vioplot)
  library(phangorn)
  library(plotrix)


}


#load functions
{
  restoreShapes <- function(scores,PC,mshape,sizeshape=FALSE,origsize=FALSE,meanlogCS)
  {
    dims <- dim(mshape)
    PC <- as.matrix(PC)

    if (!is.matrix(scores) && ncol(PC) == 1)
      if (length(scores) > 1)
```

```
    scores <- as.matrix(scores)
  if (!is.matrix(scores)){
   if (length(scores) != ncol(PC))
    stop("scores must be of the same length as ncol(PC)")
   predPC <- PC%*%scores
   if (!sizeshape)
    modell <- mshape+matrix(predPC,dims[1],dims[2])
   else {
    modell <- mshape+matrix(predPC[-1],dims[1],dims[2])
    if (origsize) {

     if (missing(meanlogCS))
      stop("please provide mean log centroid size")

     modell <- modell*(exp(predPC[1]+meanlogCS))
    }
   }
   return(modell)
  } else {
   n <- nrow(scores)
   outarr <- array(0,dim=c(dims,n))
   for (i in 1:n) {
    outarr[,,i] <- restoreShapes(scores[i,],PC,mshape,sizeshape=sizeshape,origsize=origsize,-
meanlogCS=meanlogCS)
   }
   if (!is.null(rownames(scores)))
    dimnames(outarr)[[3]] <- rownames(scores)
   return(outarr)
  }
 }


 localmeshdiff<-function (mesh1, mesh2, ploton = 1, diffarea = ((area_shape1 -
                                                area_shape2)/area_shape2) * 100, paltot = rain-
bow(200), from = NULL,
                    to = NULL, n.int = 200, out.rem = TRUE, fact = 1.5, visual = 1,
```

```
                    scale01 = TRUE, colwire = "pink")
{
 range01 <- function(x) {
  (x - min(x))/(max(x) - min(x))
 }
 area_shape1 <- vcgArea(mesh1, perface = T)$pertriangle
 area_shape2 <- vcgArea(mesh2, perface = T)$pertriangle
 diff_areas <- diffarea
 sel <- which(is.na(diff_areas))
 if (length(sel) > 0) {
  mesh1$it <- mesh1$it[, -sel]
  mesh2$it <- mesh2$it[, -sel]
  mesh1 <- rmUnrefVertex(mesh1)
  mesh2 <- rmUnrefVertex(mesh2)
  area_shape1 <- vcgArea(mesh1, perface = T)$pertriangle
  area_shape2 <- vcgArea(mesh2, perface = T)$pertriangle
  diff_areas <- (area_shape1 - area_shape2)/area_shape1
 }
 if (out.rem == TRUE) {
  x = diff_areas
  qq <- quantile(x, c(1, 3)/4, names = FALSE)
  r <- diff(qq) * fact
  tst <- x < qq[1] - r | x > qq[2] + r
  tstp <- qq[2] + r
  tstn <- qq[1] - r
  diff_areas[x > tstp] <- tstp
  diff_areas[x < tstn] <- tstn
 }
 else {
  diff_areas = diff_areas
 }
 if (scale01 == TRUE) {
  diff_areas <- range01(diff_areas)
 }
 cat("the range of diff_areas is ", range(diff_areas), sep = "\n")
```

```
if (is.null(to) == TRUE) {
 to <- max(diff_areas) * 1.01
}
if (is.null(from) == TRUE) {
 from <- min(diff_areas) * 1.01
}
selfromto <- which(diff_areas < to & diff_areas >= from)
diff_areas_fromto <- diff_areas[selfromto]
if (ploton == 1) {
 meshfromto <- mesh1
 meshwhite <- mesh1
}
if (ploton == 2) {
 meshfromto <- mesh2
 meshwhite <- mesh2
}
meshfromto$it <- meshfromto$it[, selfromto]
meshwhite$it <- meshwhite$it[, -selfromto]
colmap_tot <- colorRampPalette(paltot)
breaks_tot <- cut(c(from, diff_areas_fromto, to), n.int)
cols_tot <- colmap_tot(n.int)[breaks_tot]
cols_tot <- cols_tot[-c(1, length(cols_tot))]
plot(density(c(from, diff_areas, to)), main = "", xlab = "",
    ylab = "")
abline(v = seq(from, to, length.out = n.int), col = colmap_tot(n.int),
      lwd = 5)
points(density(diff_areas), type = "l", lwd = 2)
if (visual == 1) {
 triangles3d(t(meshfromto$vb[, meshfromto$it]), col = rep(cols_tot,
                                        each = 3), alpha = 1, lit = T, specular = "black")
 triangles3d(t(meshwhite$vb[, meshwhite$it]), col = "grey",
           alpha = 1, lit = T, specular = "black")
}
if (visual == 2) {
```

```
    triangles3d(t(meshfromto$vb[, meshfromto$it]), col = rep(cols_tot,
                                                each = 3), alpha = 1, lit = F, specular = "black")
    triangles3d(t(meshwhite$vb[, meshwhite$it]), col = "grey",
            alpha = 1, lit = F, specular = "black")
    wire3d(meshfromto, col = colwire, lit = F, lwd = 2)
  }
  out <- list(vect = diff_areas)
  return(out)
}

colmat2mesh<-function(sur,mat,vector, k, from=0.50,to=0.75,cols=colorRampPalette(c("white","dodgerblue4","magenta3"))(100),nacolor="darkgray"){
  pmeshdist <- vcgClostKD(mat, sur)
  pmeshdist$quality
  thick_values<-vector
  mean(c(1,2,3))
  intervals <- seq(from, to, length = length(cols))
  pos_cols <- NULL
  for (i in which(is.na(thick_values)==FALSE)) {
    pos_cols[i] <- which.min(abs(thick_values[i] - intervals))
  }
  clostInd <- mcNNindex(mat, t(sur$vb)[, 1:3], k = k)
  distInd <- clostInd
  for (i in 1:ncol(clostInd)) {
    distInd[, i] <- sqrt(rowSums((t(sur$vb)[, 1:3] -
                                  mat[clostInd[, k], ])^2))
  }
  colsInd <- NULL
  for (i in 1:dim(clostInd)[1]) {
    colsInd[i] <- round(weighted.mean(pos_cols[clostInd[i,]], distInd[i, ]/sum(distInd[i, ])))
  }
  nasel<-which(is.na(colsInd)==TRUE)
  meshcols<-cols[colsInd]
  meshcols[nasel]<-nacolor
  shade3d(sur,col=meshcols,specular="black")
```

```
 out<-list(sur,meshcols)
 return(out)
}

plotSD_map<-function(SD_map_object,matrix,pal,from,to,radius=3){
 plscorrs<-NULL
 for(i in 1:dim(matrix)[1]){
  plscorrs[i]<- SD_map_object[[2]][i]
 }

 index<-list()
 for(i in 1:dim(matrix)[1]){
  index[[i]]<- SD_map_object[[1]][i]
 }

 corr_scores<-matrix(NA,nrow=dim(matrix)[1],ncol=dim(matrix)[1])
 # dim(corr_scores)
 for(i in 1:length(index)){
  corr_scores[index[[i]][[1]],i]<-plscorrs[[i]]
 }

 corr_values<-NULL
 for(i in 1:nrow(corr_scores)){
  selv<-which(is.na(corr_scores[i,])==FALSE)
  corr_values[i]<-mean(corr_scores[i,selv])
 }

 print(range(corr_values,na.rm = TRUE))

 corr_values[which(is.na(corr_values))]<-mean(corr_values)
 boxplot(corr_values)
 # corr_values[corr_values>0.03]<-min(corr_values)
 if(is.null(from)) from<-min(corr_values)
 if(is.null(to)) to<-max(corr_values)
```

```
  sel<-which(corr_values< from | corr_values> to)
  corr_values[sel]<-NA
  colseq <- seq(from=min(corr_values,na.rm = TRUE),to=max(corr_values,na.rm = T),length.
out=100)
  breaks_tot <- cut(c(from, corr_values, to), 100)
  colmap_tot <- colorRampPalette(pal)
  cols_tot <- colmap_tot(100)[breaks_tot]
  cols_tot <- cols_tot[-c(1, length(cols_tot))]
  spheres3d(matrix,col=cols_tot,radius=radius)
  return(corr_values)
 }

 range01 <- function(x) {
  (x - min(x))/(max(x) - min(x))
 }

 predict.var <- function(mat, var, value) {
  mylm <- lm(mat ~ var)
  new <- data.frame(var = value)
  pred <- predict(mylm, new)
  return(pred)
 }

 lda_bootstrap<-function(set,group,wMal,wFem,n=100,perm=100,PCs=3,var=NULL,cores=4,
                         shapespace=FALSE,shapesize=FALSE,onlysize=FALSE){


  multiResultClass <- function(result1 = NULL, result2=NULL,result3 =NULL) {
   me <- list(result1 = result1, result2=result2, result3=result3)
   class(me) <- append(class(me), "multiResultClass")
   return(me)
  }

  registerDoParallel(cores = cores)
```

```
    res <- foreach(j = 1:perm, .combine  = 'c',.packages = c("Arothron","Morpho","MASS"))
%dopar%{
  result <- multiResultClass()

  sel<-c(sample(wFem,n/2),sample(wMal,n/2))
  ref_set<-set[,,sel]
  var_ref<-group[sel]
  if(shapespace==TRUE){
   block_ref<-suppressMessages(procSym(ref_set))
   coo_ref<-vecx(block_ref$rotated)
   PCA_ref<-prcomp(coo_ref,scale=FALSE,center = TRUE)
   PCscores<-PCA_ref$x
   colnames(PCscores)<-paste("PC",1:dim(PCscores)[2],sep="")
   eigv<-PCA_ref$sdev^2
   Variance <- cbind(sqrt(eigv), eigv/sum(eigv), cumsum(eigv)/sum(eigv)) * 100
  }
  if(shapesize==TRUE){
   block_ref<-suppressMessages(procSym(ref_set,scale = FALSE,CSinit = FALSE))
   coo_ref<-vecx(block_ref$rotated)
   PCA_ref<-prcomp(coo_ref,scale=FALSE,center = TRUE)
   PCscores<-PCA_ref$x
   colnames(PCscores)<-paste("PC",1:dim(PCscores)[2],sep="")
   eigv<-PCA_ref$sdev^2
   Variance <- cbind(sqrt(eigv), eigv/sum(eigv), cumsum(eigv)/sum(eigv)) * 100
  }
  if(onlysize==TRUE){
   PCscores<-apply(ref_set,3,cSize)
  }

  # plot(PCscores,col=as.factor(var_ref),pch=19)

  if(onlysize==TRUE){
   PCs<-1
```

```
var<-NULL
trains<-data.frame(var_ref,PCscores)
colnames(trains)[1]<-"group"
colnames(trains)[2]<-"PC1"
form=suppressWarnings(as.formula(c(paste("group~PC1"))))
}

if(onlysize!=TRUE){
trains<-data.frame(var_ref,PCscores)
colnames(trains)[1]<-"group"
if(!is.null(var)){
form= suppressWarnings(as.formula(c("group~",c(paste(paste("PC",(which(Variance[,3]<var)[1:(length(which(Variance[,3]<var))-1)]),sep=""),"+",sep=""),
paste("PC",length(which(Variance[,3]<var)),sep=""))))))}
if(!is.null(PCs)){
if(PCs==1){
form<-suppressWarnings(as.formula(c(paste("group~PC1")))))}else{
form=suppressWarnings(as.formula(c(paste("group~"),paste("PC",1:(PCs-1),"+",sep=""),paste("PC",PCs,sep=""))))
}
}
}
da<-lda(form,data=trains,prior=c(0.5,0.5),tol = 1.0e-7)
pred<-predict(da)
res<-table(var_ref,pred$class)
accuracy_ref<-round(sum(diag(res))/sum(res),2)
res_ref<-accuracy_ref
block_tar<-set[,,-sel]

if(onlysize!=TRUE){
if(shapespace==TRUE){
coo_tar<-t(apply(block_tar,3,function(x) rotonmat(x,x,block_ref$mshape,scale=TRUE)))}
if(shapesize==TRUE){
coo_tar<-t(apply(block_tar,3,function(x) rotonmat(x,x,block_ref$mshape,scale=FALSE)))}
```

```
    var_tar<-group[-sel]
    PCscores_tar<-pred <- predict(PCA_ref, newdata=coo_tar)
    colnames(PCscores_tar)<-paste("PC",1:dim(PCscores_tar)[2],sep="")

  }
  if(onlysize==TRUE){
   coo_tar<-apply(block_tar,3,cSize)
   PCscores_tar<-t(t(coo_tar))
   var_tar<-group[-sel]
   colnames(PCscores_tar)<-"PC1"
  }
  # plot(PCscores_tar,pch=19,col=as.factor(var_tar))
  trains_tar<-data.frame(var_tar,PCscores_tar)
  colnames(trains_tar)[1]<-"var"
  pred_tar<-predict(da,newdata=trains_tar)
  res_tar<-table(var_tar,pred_tar$class)
  accuracy_tar<-round(sum(diag(res_tar))/sum(res_tar),2)
  result$result1<-accuracy_tar
  result$result2<-res_tar[1,1]/sum(res_tar[,1])
  result$result3<-res_tar[2,2]/sum(res_tar[,2])
  # result$result1<-accuracy_tar
  return(result)
 }
}


 SD_map_boot<-function(set,group,wMal,wFem,n=100,perm=100,PCs=3,var=NULL,core=40,
cores=3,iter=dim(lset)[1],
                shapespace=TRUE,shapesize=FALSE,onlysize=FALSE){


  Core_i <- list()
  BooAcc<-list()
  for(i in 1:iter){
   print(i)
   land_i<-set[i,,1]
```

```
core_i<-as.vector(mcNNindex(set[,,1],t(land_i),k = core))
    seti<-set[core_i,,]
    bootacc<-lda_bootstrap(seti,group,wMal,wFem,n=n,perm=perm,PCs=PCs,var=var,cores=cores,shapespace=shapespace,shapesize=shapesize,onlysize=onlysize)
    Core_i[[i]]<-core_i
    # BooAcc[[i]]<-mean(bootacc)
    BooAcc[[i]]<-mean(unlist(bootacc)[which(names(unlist(bootacc))=="result1")])
    closeAllConnections()
  }
  out<-list(Core_i,BooAcc)
 }


}

#load data
{
load("data.rda")
group<-substr(dimnames(data$set)[[3]],1,1)
pair<-cbind(L=c(seq(12,50,2),c(51:550)),R=c(seq(11,50,2),(551:1050)))
lset<-symmetrize(data$set,pairedLM = pair)
wMal<-which(group=="M")
wFem<-which(group=="F")
sur<-data$sur
}

#Figure 1 - R code
{
PCA<-procSym(lset,sizeshape = TRUE)
PCscores<-PCA$PCscores
Variance<-PCA$Variance
PCx<-1
PCy<-2
xlim<-c(-1*max(abs(PCscores[,PCx])),max(abs(PCscores[,PCx])))
ylim<-c(-1*max(abs(PCscores[,PCy])),max(abs(PCscores[,PCy])))
```

```
Xlab<-paste("PC",PCx," ",round(Variance[PCx,2],2),"%",sep="")
Ylab<-paste("PC",PCy," ",round(Variance[PCy,2],2),"%",sep="")
dir.create("Figure_1")
t.test(PCscores[,1]~group)
t.test(PCscores[,2]~group)
summary(procD.lm(PCscores~group))
summary(procD.lm(PCscores~PCA$size))
summary(procD.lm(PCscores~PCA$size*group))
summary(procD.lm(PCscores[,1]~group))
summary(procD.lm(PCscores[,1]~PCA$size))
summary(procD.lm(PCscores[,2]~group))
summary(procD.lm(PCscores[,2]~PCA$size))



tiff("Figure_1/Fig. 1 - PCA_formspace.tiff",width = 1500,height = 1500,pointsize = 6,res = 300)
par(mar = c(5, 5, 5, 5))
plot(NA,xlim=extendrange(xlim),ylim=extendrange(ylim),xlab=Xlab,ylab=Ylab,asp=1,
    main="",cex.axis=1.5,cex.main=2.5,cex.lab=2,
    cex=2)
abline(v=0,lty=2,lwd=0.7)
abline(h=0,lty=2,lwd=0.7)

cols<-c("deepskyblue3","khaki2")
sex<-group
for(i in 1:2){
 sel<-which(sex==levels(as.factor(sex))[[i]])
 pchi<-sex[sel]
 pchi[pchi=="M"]<-19
 pchi[pchi=="F"]<-19
 mat<-PCscores[sel,c(PCx,PCy)]
 conv<-chull(mat)
 polygon(mat[c(conv,conv[1]),],col=adjustcolor(cols[i],alpha.f=0.3))
 points(mat,col=cols[i],pch=as.numeric(pchi),cex=1.5)
}
dev.off()
```

```
tiff("Figure_1/Fig. 1 - PCA_formspace_VP_PC1.tiff",width = 1500,height = 1500,pointsize = 6,res = 300)

vioplot(PCscores[group=="F",1],PCscores[group=="M",1],side="right",ylim=extendrange(x-lim),xaxt='n' ,bty="n",at=c(1,1),horizontal=TRUE,drawRect=FALSE,border=NA,col=c(adjust-color( "deepskyblue3", alpha.f = 0.4),adjustcolor( "khaki1", alpha.f = 0.4)))

dev.off()

tiff("Figure_1/Fig. 1 - PCA_formspace_VP_PC2.tiff",width = 1500,height = 1500,pointsize = 6,res = 300)

vioplot(PCscores[group=="F",2],PCscores[group=="M",2],side="right",ylim=exten-drange(ylim),xaxt='n' ,bty="n",at=c(1,1),horizontal=TRUE,drawRect=FALSE,bor-der=NA,col=c(adjustcolor( "deepskyblue3", alpha.f = 0.4),adjustcolor( "khaki1", alpha.f = 0.4)))

dev.off()

}


#Figure 2 - R code

{

PC1sv<-restoreShapes(range(PCA$PCscores[,1]),PCA$PCs[,1],PCA$mshape,sizeshape = TRUE,origsize = TRUE,meanlogCS=mean(log(PCA$size)))

PC2sv<-restoreShapes(range(PCA$PCscores[,2]),PCA$PCs[,2],PCA$mshape,sizeshape = TRUE,origsize = TRUE,meanlogCS=mean(log(PCA$size)))

mssv<-restoreShapes(0,PCA$PCs[,1],PCA$mshape,sizeshape = TRUE,origsize = TRUE,mean-logCS=mean(log(PCA$size)))


PC1minSW<-tps3d(sur,data$set[,,104],PC1sv[,,1])

PC1maxSW<-tps3d(sur,data$set[,,104],PC1sv[,,2])

PC2minSW<-tps3d(sur,data$set[,,104],PC2sv[,,1])

PC2maxSW<-tps3d(sur,data$set[,,104],PC2sv[,,2])

meanshape<-tps3d(sur,data$set[,,104],mssv)


selMaxCS<-which.max(apply(bindArr(PC1sv,PC2sv,along=3),3,cSize))

SVmeshes<-list(PC1minSW,PC1maxSW,PC2minSW,PC2maxSW)

hidmat<-as.matrix(meshcube(SVmeshes[[selMaxCS]]))


layout3d(matrix(1:4,ncol=2,byrow = TRUE),sharedMouse = TRUE)

spheres3d(hidmat,radius=0)

localmeshdiff(PC1minSW,meanshape,ploton = 1,out.rem = TRUE,fact = 2.5,scale01 = FALSE,-from=NULL,to=NULL,paltot = c("dodgerblue4","magenta3","tomato2","khaki1"))  #change
```

```
here palette

next3d()

spheres3d(hidmat,radius=0)

localmeshdiff(PC1maxSW,meanshape,ploton = 1,out.rem = TRUE,fact = 2.5,scale01 = FALSE,-
from=NULL,to=NULL,paltot = c("dodgerblue4","magenta3","tomato2","khaki1"))  #change
here palette

next3d()

spheres3d(hidmat,radius=0)

localmeshdiff(PC2minSW,meanshape,ploton = 1,out.rem = TRUE,fact = 2.5,scale01 = FALSE,-
from=NULL,to=NULL,paltot = c("dodgerblue4","magenta3","tomato2","khaki1"))  #change
here palette

next3d()

spheres3d(hidmat,radius=0)

localmeshdiff(PC2maxSW,meanshape,ploton = 1,out.rem = TRUE,fact = 2.5,scale01 = FALSE,-
from=NULL,to=NULL,paltot = c("dodgerblue4","magenta3","tomato2","khaki1"))  #change
here palette

}


#Figure 4 - R code

{

CR_Sh<-data$LDA_Sh

CR_Fo<-data$LDA_Fo

CR_Sz<-data$LDA_Sz


layout3d(t(c(1:3)),sharedMouse = TRUE)

SH<-plotSD_map(CR_Sh,procSym(data$set,scale=F,CSinit = F)$mshape,c("gray","light-
blue","blue","yellow","orange","darkred"),

        0.40,0.80,radius=5)

next3d()

FS<-plotSD_map(CR_Fo,procSym(data$set,scale=F,CSinit = F)$mshape,c("gray","li-
ghtblue","blue","yellow","orange","darkred"),

        0.42,0.80,radius=5)

next3d()

OS<-plotSD_map(CR_Sz,procSym(data$set,scale=F,CSinit = F)$mshape,c("gray","li-
ghtblue","blue","yellow","orange","darkred"),

        0.42,0.80,radius=5)

closeAllConnections()

range(SH)
```

```
range(FS)

range(OS)


mshape<-procSym(data$set,scale=F,CSinit = F)$mshape

sur<-tps3d(data$sur,data$set[,,104],mshape)


layout3d(t(c(1:3)),sharedMouse = TRUE)

colmat2mesh(sur,mshape,SH,k=2,from=0.50,to=0.77,cols=colorRampPalette(c("dodger-
blue4","magenta3","tomato2","khaki1"))(100),nacolor="darkgray")

next3d()

colmat2mesh(sur,mshape,FS,k=2,from=0.50,to=0.77,cols=colorRampPalette(c("dodger-
blue4","magenta3","tomato2","khaki1"))(100),nacolor="darkgray")

next3d()

colmat2mesh(sur,mshape,OS,k=2,from=0.50,to=0.77,cols=colorRampPalette(c("dodger-
blue4","magenta3","tomato2","khaki1"))(100),nacolor="darkgray")


vioplot(SH,FS,OS,names = c("shape space","form space","centroid size"),col="gray")

}


#Figure 5 - R code - frontal region

{

group<-substr(dimnames(data$set)[[3]],1,1)

pair<-cbind(L=c(seq(12,50,2),c(51:550)),R=c(seq(11,50,2),(551:1050)))

lset<-symmetrize(data$set,pairedLM = pair)

wMal<-which(group=="M")

wFem<-which(group=="F")

sur<-data$sur


CR_Sh<-data$LDA_Sh

AccShape<-plotSD_map(CR_Sh,procSym(lset,CSinit = FALSE,scale=FALSE)$mshape,rain-
bow(10),from=NULL,to=NULL,radius=4)

sel_BR<-which(AccShape>0.72)

range(AccShape[sel_BR])

pca<-procSym(lset,scale=F,CSinit = F)

testset<-pca$rotated[sel_BR,,]

frontal<-pca$rotated[sel_BR,,]
```

```
#Figure 5 - frontal module
comPCA<-procSym(frontal)
PCscores<-comPCA$PCscores
Variance<-comPCA$Variance
round(Variance[1:2,2],2)

t.test(comPCA$PCscores[,1]~group)
t.test(comPCA$PCscores[,2]~group)
summary(procD.lm(comPCA$PCscores~group))
summary(procD.lm(comPCA$PCscores~comPCA$size))
summary(procD.lm(comPCA$PCscores~comPCA$size*group))
summary(procD.lm(comPCA$PCscores[,1]~group))
summary(procD.lm(comPCA$PCscores[,1]~comPCA$size))
summary(procD.lm(comPCA$PCscores[,2]~group))
summary(procD.lm(comPCA$PCscores[,2]~comPCA$size))

PCx<-1
PCy<-2
xlim<-c(-1*max(abs(PCscores[,PCx])),max(abs(PCscores[,PCx])))
ylim<-c(-1*max(abs(PCscores[,PCy])),max(abs(PCscores[,PCy])))
Xlab<-paste("PC",PCx," ",round(Variance[PCx,2],2),"%",sep="")
Ylab<-paste("PC",PCy," ",round(Variance[PCy,2],2),"%",sep="")


dir.create("Figure_5")
tiff("Figure_5/Fig. 5 - PCA_shapepace_Frontal.tiff",width = 1500,height = 1500,pointsize =
6,res = 300)
par(mar = c(5, 5, 5, 5))
plot(NA,xlim=extendrange(xlim),ylim=extendrange(ylim),xlab=Xlab,ylab=Ylab,asp=1,
    main="Frontal region",cex.axis=2,cex.main=2.5,cex.lab=2,cex=2)
abline(v=0,lty=2,lwd=0.7)
abline(h=0,lty=2,lwd=0.7)
cols<-c("deepskyblue3","khaki2")
sex=group
```

```
for(i in 1:2){
  sel<-which(sex==levels(as.factor(sex))[[i]])
  mat<-PCscores[sel,c(PCx,PCy)]
  conv<-chull(mat)
  polygon(mat[c(conv,conv[1]),],col=adjustcolor(cols[i],alpha.f=0.3))
  points(mat,col=cols[i],pch=19,cex=1.5)
  points(mat,col=1,pch=1,cex=1.51)

}
dev.off()

tiff("Figure_5/Fig. 5 - PCA_shapespace_Frontal_VP_PC1.tiff",width = 1500,height = 1500,pointsize = 6,res = 300)
vioplot(PCscores[group==”F”,1],PCscores[group==”M”,1],side=”right”,ylim=extendrange(x-lim),xaxt='n' ,bty=”n”,at=c(1,1),horizontal=TRUE,drawRect=FALSE,border=NA,col=c(adjust-color( “deepskyblue3”, alpha.f = 0.4),adjustcolor( “khaki1”, alpha.f = 0.4)))
dev.off()
tiff("Figure_5/Fig. 5 - PCA_shapespace_Frontal_VP.tiff",width = 1500,height = 1500,pointsize = 6,res = 300)
vioplot(PCscores[group==”F”,2],PCscores[group==”M”,2],side=”right”,ylim=exten-drange(ylim),xaxt='n' ,bty=”n”,at=c(1,1),horizontal=TRUE,drawRect=FALSE,bor-der=NA,col=c(adjustcolor( “deepskyblue3”, alpha.f = 0.4),adjustcolor( “khaki1”, alpha.f = 0.4)))
dev.off()

out.sur<-data$sur
mat<-data$set[sel_BR,,104]
pmeshdist <- mcNNindex(mat,out.sur,k=1)
quality<-sqrt((rowSums((vert2points(out.sur)-mat[pmeshdist[,1],])^2)))
selV<-which(quality<=10)
refsurSV<-rmVertex(out.sur,index = selV,keep = TRUE)

refsur<-rmVertex(out.sur,index = sel,keep = T)
cols <- (colorRampPalette(c(“dodgerblue4”,”magenta3”,”white”,”khaki1”,”tomato2”))(100))
PC1min<-restoreShapes(min(comPCA$PCscores[,1]),comPCA$PCs[,1],comPCA$mshape)
PC1max<-restoreShapes(max(comPCA$PCscores[,1]),comPCA$PCs[,1],comPCA$mshape)
PC2min<-restoreShapes(min(comPCA$PCscores[,2]),comPCA$PCs[,2],comPCA$mshape)
```

```
PC2max<-restoreShapes(max(comPCA$PCscores[,2]),comPCA$PCs[,2],comPCA$mshape)

meanshape<-restoreShapes(0,comPCA$PCs[,1],comPCA$mshape)

PC1minSW<-tps3d(refsurSV,mat,PC1min)

PC1maxSW<-tps3d(refsurSV,mat,PC1max)

PC2minSW<-tps3d(refsurSV,mat,PC2min)

PC2maxSW<-tps3d(refsurSV,mat,PC2max)

meanshapeSW<-tps3d(refsurSV,mat,meanshape)


selMaxCS<-which.max(apply(bindArr(PC1min,PC1max,PC2min,PC2max,along=3),3,cSize))

SVmeshes<-list(PC1minSW,PC1maxSW,PC2minSW,PC2maxSW)

hidmat<-as.matrix(meshcube(SVmeshes[[selMaxCS]]))


layout3d(matrix(1:4,ncol=2,byrow = TRUE),sharedMouse = TRUE)

spheres3d(hidmat,radius=0)

localmeshdiff(PC1minSW,meanshapeSW,ploton = 1,out.rem = TRUE,fact = 2.5,scale01 =
FALSE,from=NULL,to=NULL,paltot = c("dodgerblue4","magenta3","tomato2","khaki1"))
#change here palette

next3d()

spheres3d(hidmat,radius=0)

localmeshdiff(PC1maxSW,meanshapeSW,ploton = 1,out.rem = TRUE,fact = 2.5,scale01 =
FALSE,from=NULL,to=NULL,paltot = c("dodgerblue4","magenta3","tomato2","khaki1"))
#change here palette

next3d()

spheres3d(hidmat,radius=0)

localmeshdiff(PC2minSW,meanshapeSW,ploton = 1,out.rem = TRUE,fact = 2.5,scale01 =
FALSE,from=NULL,to=NULL,paltot = c("dodgerblue4","magenta3","tomato2","khaki1"))
#change here palette

next3d()

spheres3d(hidmat,radius=0)

localmeshdiff(PC2maxSW,meanshapeSW,ploton = 1,out.rem = TRUE,fact = 2.5,scale01 =
FALSE,from=NULL,to=NULL,paltot = c("dodgerblue4","magenta3","tomato2","khaki1"))
#change here palette

}


#Figure 6 - R code - module definition

{

load("data.rda")
```

```
CR_Fo<-data$LDA_Fo

lset<-data$set

AccForm<-plotSD_map(CR_Fo,procSym(lset,CSinit = FALSE,scale=FALSE)$mshape,rainbow(10),from=NULL,to=NULL,radius=4)

sel_BR<-which(AccForm>0.681)

pca<-procSym(lset,scale=F,CSinit = F)


set.seed(300)

allmods<-kmeans(as.matrix(dist(pca$mshape[sel_BR,])),iter.max = 30000,centers = 4)

spheres3d(pca$mshape[sel_BR,],radius=2,col=as.factor(allmods$cluster))


frontal<-pca$rotated[sel_BR,,][allmods$cluster==1,,]

mastoid<-pca$rotated[sel_BR,,][allmods$cluster==2,,]

nasal<-pca$rotated[sel_BR,,][allmods$cluster==3,,]

spheres3d(frontal[,,1],radius=2,col=1)

spheres3d(mastoid[,,1],radius=2,col=2)

spheres3d(nasal[,,1],radius=2,col=3)


range(AccForm[allmods$cluster==1])

range(AccForm[allmods$cluster==2])

range(AccForm[allmods$cluster==3])

}

#Figure 6 - nasal region module

{

comPCA<-procSym(nasal,sizeshape = TRUE)

PCscores<-comPCA$PCscores

Variance<-comPCA$Variance


PCx<-1

PCy<-2

xlim<-c(-1*max(abs(PCscores[,PCx])),max(abs(PCscores[,PCx])))

ylim<-c(-1*max(abs(PCscores[,PCy])),max(abs(PCscores[,PCy])))

Xlab<-paste("PC",PCx," ",round(Variance[PCx,2],2),"%",sep="")

Ylab<-paste("PC",PCy," ",round(Variance[PCy,2],2),"%",sep="")
```

```
t.test(comPCA$PCscores[,1]~group)

t.test(comPCA$PCscores[,2]~group)

summary(procD.lm(comPCA$PCscores~group))

summary(procD.lm(comPCA$PCscores~comPCA$size))

summary(procD.lm(comPCA$PCscores~comPCA$size*group))

summary(procD.lm(comPCA$PCscores[,1]~group))

summary(procD.lm(comPCA$PCscores[,1]~comPCA$size))

summary(procD.lm(comPCA$PCscores[,2]~group))

summary(procD.lm(comPCA$PCscores[,2]~comPCA$size))


dir.create("Figure_6")

tiff("Figure_6/Fig. 6 - PCA_formspace_nasalregion.tiff",width = 1500,height = 1500,pointsize =
6,res = 300)

par(mar = c(5, 5, 5, 5))

plot(NA,xlim=extendrange(xlim),ylim=extendrange(ylim),xlab=Xlab,ylab=Ylab,asp=1,

    main="Nasal region",cex.axis=2,cex.main=2.5,cex.lab=2,cex=2)

abline(v=0,lty=2,lwd=0.7)

abline(h=0,lty=2,lwd=0.7)

cols<-c("deepskyblue3","khaki2")

sex=group

for(i in 1:2){

 sel<-which(sex==levels(as.factor(sex))[[i]])

 mat<-PCscores[sel,c(PCx,PCy)]

 conv<-chull(mat)

 polygon(mat[c(conv,conv[1]),],col=adjustcolor(cols[i],alpha.f=0.3))

 points(mat,col=cols[i],pch=19,cex=1.5)

 points(mat,col=1,pch=1,cex=1.51)


}

dev.off()


group<-sex

tiff("Figure_6/Fig. 6 - PCA_formspace_Nasalregion_VP_PC1.tiff",width = 1500,height =
1500,pointsize = 6,res = 300)

vioplot(PCscores[group=="F",1],PCscores[group=="M",1],side="right",ylim=extendrange(x-
lim),xaxt='n' ,bty="n",at=c(1,1),horizontal=TRUE,drawRect=FALSE,border=NA,col=c(adjust-
```

```
color( “deepskyblue3”, alpha.f = 0.4),adjustcolor( “khaki1”, alpha.f = 0.4)))

dev.off()

tiff(“Figure_6/Fig. 6 - PCA_formspace_Nasalregion_VP.tiff”,width = 1500,height = 1500,pointsize = 6,res = 300)

vioplot(PCscores[group==”F”,2],PCscores[group==”M”,2],side=”right”,ylim=extendrange(ylim),xaxt=’n’ ,bty=”n”,at=c(1,1),horizontal=TRUE,drawRect=FALSE,border=NA,col=c(adjustcolor( “deepskyblue3”, alpha.f = 0.4),adjustcolor( “khaki1”, alpha.f = 0.4)))

dev.off()


out.sur<-data$sur

mat<-data$set[sel_BR,,104][allmods$cluster==3,]

pmeshdist <- mcNNindex(mat,out.sur,k=1)

quality<-sqrt((rowSums((vert2points(out.sur)-mat[pmeshdist[,1],])^2)))

sel<-which(quality<=10)


refsurSV<-rmVertex(out.sur,index = sel,keep = T)

cols <- (colorRampPalette(c(“dodgerblue4”,”magenta3”,”tomato2”,”khaki1”))(100))

PC1min<-restoreShapes(min(comPCA$PCscores[,1]),comPCA$PCs[,1],comPCA$mshape,sizeshape=TRUE,origsize = TRUE,meanlogCS = log(mean(comPCA$size)))

PC1max<-restoreShapes(max(comPCA$PCscores[,1]),comPCA$PCs[,1],comPCA$mshape,sizeshape=TRUE,origsize = TRUE,meanlogCS = log(mean(comPCA$size)))

PC2min<-restoreShapes(min(comPCA$PCscores[,2]),comPCA$PCs[,2],comPCA$mshape,sizeshape=TRUE,origsize = TRUE,meanlogCS = log(mean(comPCA$size)))

PC2max<-restoreShapes(max(comPCA$PCscores[,2]),comPCA$PCs[,2],comPCA$mshape,sizeshape=TRUE,origsize = TRUE,meanlogCS = log(mean(comPCA$size)))

mssv<-restoreShapes(0,comPCA$PCs[,1],comPCA$mshape,sizeshape = TRUE,origsize = TRUE,meanlogCS=mean(log(comPCA$size)))

selMaxCS<-which.max(apply(bindArr(PC1min,PC1max,PC2min,PC2max,along=3),3,cSize))


PC1minSW<-tps3d(refsurSV,mat,PC1min)

PC1maxSW<-tps3d(refsurSV,mat,PC1max)

PC2minSW<-tps3d(refsurSV,mat,PC2min)

PC2maxSW<-tps3d(refsurSV,mat,PC2max)

meanshape<-tps3d(refsurSV,data$set[sel_BR,,104][allmods$cluster==3,],mssv)


SVmeshes<-list(PC1minSW,PC1maxSW,PC2minSW,PC2maxSW)

hidmat<-as.matrix(meshcube(SVmeshes[[selMaxCS]]))
```

```
layout3d(matrix(1:4,ncol=2,byrow = TRUE),sharedMouse = TRUE)

spheres3d(hidmat,radius=0)

localmeshdiff(PC1minSW,meanshape,ploton = 1,out.rem = TRUE,fact = 2.5,scale01 = FALSE,-
from=NULL,to=NULL,paltot = c("dodgerblue4","magenta3","tomato2","khaki1"))  #change
here palette

next3d()

spheres3d(hidmat,radius=0)

localmeshdiff(PC1maxSW,meanshape,ploton = 1,out.rem = TRUE,fact = 2.5,scale01 = FALSE,-
from=NULL,to=NULL,paltot = c("dodgerblue4","magenta3","tomato2","khaki1"))  #change
here palette

next3d()

spheres3d(hidmat,radius=0)

localmeshdiff(PC2minSW,meanshape,ploton = 1,out.rem = TRUE,fact = 2.5,scale01 = FALSE,-
from=NULL,to=NULL,paltot = c("dodgerblue4","magenta3","tomato2","khaki1"))  #change
here palette

next3d()

spheres3d(hidmat,radius=0)

localmeshdiff(PC2maxSW,meanshape,ploton = 1,out.rem = TRUE,fact = 2.5,scale01 = FALSE,-
from=NULL,to=NULL,paltot = c("dodgerblue4","magenta3","tomato2","khaki1"))  #change
here palette

# rgl.snapshot("Shape Variations_Nasal_formSpace_1.png ")

}


#Figure 6 - frontal region module

{

comPCA<-procSym(frontal,sizeshape = TRUE)

PCscores<-comPCA$PCscores

Variance<-comPCA$Variance

round(Variance[1:2,2],2)


t.test(comPCA$PCscores[,1]~group)

t.test(comPCA$PCscores[,2]~group)

summary(procD.lm(comPCA$PCscores~group))

summary(procD.lm(comPCA$PCscores~comPCA$size))

summary(procD.lm(comPCA$PCscores~comPCA$size*group))

summary(procD.lm(comPCA$PCscores[,1]~group))
```

```
summary(procD.lm(comPCA$PCscores[,1]~comPCA$size))

summary(procD.lm(comPCA$PCscores[,2]~group))

summary(procD.lm(comPCA$PCscores[,2]~comPCA$size))


PCx<-1

PCy<-2

xlim<-c(-1*max(abs(PCscores[,PCx])),max(abs(PCscores[,PCx])))

ylim<-c(-1*max(abs(PCscores[,PCy])),max(abs(PCscores[,PCy])))

Xlab<-paste("PC",PCx," ",round(Variance[PCx,2],2),"%",sep="")

Ylab<-paste("PC",PCy," ",round(Variance[PCy,2],2),"%",sep="")


tiff("Figure_6/Fig. 6 - PCA_formspace_frontalregion.tiff",width = 1500,height = 1500,pointsize = 6,res = 300)

plot(NA,xlim=extendrange(xlim),ylim=extendrange(ylim),xlab=Xlab,ylab=Ylab,asp=1,

    main="Medio-Inferior frontal bone",cex.axis=2,cex.main=2.5,cex.lab=2,cex=2)

abline(v=0,lty=2,lwd=0.7)

abline(h=0,lty=2,lwd=0.7)

cols<-c("deepskyblue3","khaki2")

sex=group

for(i in 1:2){

  sel<-which(sex==levels(as.factor(sex))[[i]])

  mat<-PCscores[sel,c(PCx,PCy)]

  conv<-chull(mat)

  polygon(mat[c(conv,conv[1]),],col=adjustcolor(cols[i],alpha.f=0.3))

  points(mat,col=cols[i],pch=19,cex=1.5)

  points(mat,col=1,pch=1,cex=1.51)


}

dev.off()


group<-sex

tiff("Figure_6/Fig. 6 - PCA_formspace_Frontalregion_VP_PC1.tiff",width = 1500,height = 1500,pointsize = 6,res = 300)

vioplot(PCscores[group=="F",1],PCscores[group=="M",1],side="right",ylim=extendrange(x-lim),xaxt='n' ,bty="n",at=c(1,1),horizontal=TRUE,drawRect=FALSE,border=NA,col=c(adjust-color( "deepskyblue3", alpha.f = 0.4),adjustcolor( "khaki1", alpha.f = 0.4)))
```

```
dev.off()

tiff("Figure_6/Fig. 6 - PCA_formspace_Frontalregion_VP.tiff",width = 1500,height =
1500,pointsize = 6,res = 300)

vioplot(PCscores[group==”F”,2],PCscores[group==”M”,2],side=”right”,ylim=exten-
drange(ylim),xaxt='n' ,bty=”n”,at=c(1,1),horizontal=TRUE,drawRect=FALSE,bor-
der=NA,col=c(adjustcolor( “deepskyblue3”, alpha.f = 0.4),adjustcolor( “khaki1”, alpha.f =
0.4)))

dev.off()


out.sur<-data$sur

mat<-data$set[sel_BR,,104][allmods$cluster==1,]

pmeshdist <- mcNNindex(mat,out.sur,k=1)

quality<-sqrt((rowSums((vert2points(out.sur)-mat[pmeshdist[,1],])^2)))

sel<-which(quality<=10)


refsurSV<-rmVertex(out.sur,index = sel,keep = T)

PC1min<-restoreShapes(min(comPCA$PCscores[,1]),comPCA$PCs[,1],comPCA$mshape,size-
shape=TRUE,origsize = TRUE,meanlogCS = log(mean(comPCA$size)))

PC1max<-restoreShapes(max(comPCA$PCscores[,1]),comPCA$PCs[,1],comPCA$mshape,-
sizeshape=TRUE,origsize = TRUE,meanlogCS = log(mean(comPCA$size)))

PC2min<-restoreShapes(min(comPCA$PCscores[,2]),comPCA$PCs[,2],comPCA$mshape,size-
shape=TRUE,origsize = TRUE,meanlogCS = log(mean(comPCA$size)))

PC2max<-restoreShapes(max(comPCA$PCscores[,2]),comPCA$PCs[,2],comPCA$mshape,-
sizeshape=TRUE,origsize = TRUE,meanlogCS = log(mean(comPCA$size)))

mssv<-restoreShapes(0,comPCA$PCs[,1],comPCA$mshape,sizeshape = TRUE,origsize =
TRUE,meanlogCS=mean(log(comPCA$size)))

selMaxCS<-which.max(apply(bindArr(PC1min,PC1max,PC2min,PC2max,along=3),3,cSize))


PC1minSW<-tps3d(refsurSV,mat,PC1min)

PC1maxSW<-tps3d(refsurSV,mat,PC1max)

PC2minSW<-tps3d(refsurSV,mat,PC2min)

PC2maxSW<-tps3d(refsurSV,mat,PC2max)

meanshape<-tps3d(refsurSV,data$set[sel_BR,,104][allmods$cluster==1,],mssv)


SVmeshes<-list(PC1minSW,PC1maxSW,PC2minSW,PC2maxSW)

hidmat<-as.matrix(meshcube(SVmeshes[[selMaxCS]]))


layout3d(matrix(1:4,ncol=2,byrow = TRUE),sharedMouse = TRUE)
```

```
spheres3d(hidmat,radius=0)

localmeshdiff(PC1minSW,meanshape,ploton = 1,out.rem = TRUE,fact = 2.5,scale01 = FALSE,-
from=NULL,to=NULL,paltot = c("dodgerblue4","magenta3","tomato2","khaki1"))  #change
here palette

next3d()

spheres3d(hidmat,radius=0)

localmeshdiff(PC1maxSW,meanshape,ploton = 1,out.rem = TRUE,fact = 2.5,scale01 = FALSE,-
from=NULL,to=NULL,paltot = c("dodgerblue4","magenta3","tomato2","khaki1"))  #change
here palette

next3d()

spheres3d(hidmat,radius=0)

localmeshdiff(PC2minSW,meanshape,ploton = 1,out.rem = TRUE,fact = 2.5,scale01 = FALSE,-
from=NULL,to=NULL,paltot = c("dodgerblue4","magenta3","tomato2","khaki1"))  #change
here palette

next3d()

spheres3d(hidmat,radius=0)

localmeshdiff(PC2maxSW,meanshape,ploton = 1,out.rem = TRUE,fact = 2.5,scale01 = FALSE,-
from=NULL,to=NULL,paltot = c("dodgerblue4","magenta3","tomato2","khaki1"))  #change
here palette

# rgl.snapshot("Form Variations_Frontal_1.png ")

}


#Figure 6 - mastoid process module

{

comPCA<-procSym(mastoid,sizeshape = TRUE)

PCscores<-comPCA$PCscores

Variance<-comPCA$Variance

round(Variance[1:2,2],2)


t.test(comPCA$PCscores[,1]~group)

t.test(comPCA$PCscores[,2]~group)

summary(procD.lm(comPCA$PCscores~group))

summary(procD.lm(comPCA$PCscores~comPCA$size))

summary(procD.lm(comPCA$PCscores~comPCA$size*group))

summary(procD.lm(comPCA$PCscores[,1]~group))

summary(procD.lm(comPCA$PCscores[,1]~comPCA$size))

summary(procD.lm(comPCA$PCscores[,2]~group))
```

```
summary(procD.lm(comPCA$PCscores[,2]~comPCA$size))

PCx<-1

PCy<-2

xlim<-c(-1*max(abs(PCscores[,PCx])),max(abs(PCscores[,PCx])))

ylim<-c(-1*max(abs(PCscores[,PCy])),max(abs(PCscores[,PCy])))

Xlab<-paste("PC",PCx," ",round(Variance[PCx,2],2),"%",sep="")

Ylab<-paste("PC",PCy," ",round(Variance[PCy,2],2),"%",sep="")




tiff("Figure_6/Fig. 6 - PCA_formspace_Mastoid.tiff",width = 1500,height = 1500,pointsize =
6,res = 300)

par(mar = c(5, 5, 5, 5))

plot(NA,xlim=extendrange(xlim),ylim=extendrange(ylim),xlab=Xlab,ylab=Ylab,asp=1,

    main="Mastoid process",cex.axis=2,cex.main=2.5,cex.lab=2,cex=2)

abline(v=0,lty=2,lwd=0.7)

abline(h=0,lty=2,lwd=0.7)

cols<-c("deepskyblue3","khaki2")

sex=group

for(i in 1:2){

 sel<-which(sex==levels(as.factor(sex))[[i]])

 mat<-PCscores[sel,c(PCx,PCy)]

 conv<-chull(mat)

 polygon(mat[c(conv,conv[1]),],col=adjustcolor(cols[i],alpha.f=0.3))

 points(mat,col=cols[i],pch=19,cex=1.5)

 points(mat,col=1,pch=1,cex=1.51)


}

dev.off()


group<-sex

tiff("Figure_6/Fig. 6 - PCA_formspace_Mastoid_VP_PC1.tiff",width = 1500,height =
1500,pointsize = 6,res = 300)

vioplot(PCscores[group=="F",1],PCscores[group=="M",1],side="right",ylim=extendrange(x-
lim),xaxt='n' ,bty="n",at=c(1,1),horizontal=TRUE,drawRect=FALSE,border=NA,col=c(adjust-
color( "deepskyblue3", alpha.f = 0.4),adjustcolor( "khaki1", alpha.f = 0.4)))
```

```
dev.off()

tiff("Figure_6/Fig. 6 - PCA_formspace_Mastoidregion_VP.tiff",width = 1500,height =
1500,pointsize = 6,res = 300)

vioplot(PCscores[group==”F”,2],PCscores[group==”M”,2],side=”right”,ylim=exten-
drange(ylim),xaxt='n' ,bty=”n”,at=c(1,1),horizontal=TRUE,drawRect=FALSE,bor-
der=NA,col=c(adjustcolor( “deepskyblue3”, alpha.f = 0.4),adjustcolor( “khaki1”, alpha.f =
0.4)))

dev.off()


out.sur<-data$sur

mat<-data$set[sel_BR,,104][allmods$cluster==2,]

pmeshdist <- mcNNindex(mat,out.sur,k=1)

quality<-sqrt((rowSums((vert2points(out.sur)-mat[pmeshdist[,1],])^2)))

sel<-which(quality<=10)


refsurSV<-rmVertex(out.sur,index = sel,keep = T)

PC1min<-restoreShapes(min(comPCA$PCscores[,1]),comPCA$PCs[,1],comPCA$mshape,size-
shape=TRUE,origsize = TRUE,meanlogCS = log(mean(comPCA$size)))

PC1max<-restoreShapes(max(comPCA$PCscores[,1]),comPCA$PCs[,1],comPCA$mshape,-
sizeshape=TRUE,origsize = TRUE,meanlogCS = log(mean(comPCA$size)))

PC2min<-restoreShapes(min(comPCA$PCscores[,2]),comPCA$PCs[,2],comPCA$mshape,size-
shape=TRUE,origsize = TRUE,meanlogCS = log(mean(comPCA$size)))

PC2max<-restoreShapes(max(comPCA$PCscores[,2]),comPCA$PCs[,2],comPCA$mshape,-
sizeshape=TRUE,origsize = TRUE,meanlogCS = log(mean(comPCA$size)))

mssv<-restoreShapes(0,comPCA$PCs[,1],comPCA$mshape,sizeshape = TRUE,origsize =
TRUE,meanlogCS=mean(log(comPCA$size)))

selMaxCS<-which.max(apply(bindArr(PC1min,PC1max,PC2min,PC2max,along=3),3,cSize))


PC1minSW<-tps3d(refsurSV,mat,PC1min)

PC1maxSW<-tps3d(refsurSV,mat,PC1max)

PC2minSW<-tps3d(refsurSV,mat,PC2min)

PC2maxSW<-tps3d(refsurSV,mat,PC2max)

meanshape<-tps3d(refsurSV,data$set[sel_BR,,104][allmods$cluster==2,],mssv)


SVmeshes<-list(PC1minSW,PC1maxSW,PC2minSW,PC2maxSW)

hidmat<-as.matrix(meshcube(SVmeshes[[selMaxCS]]))


layout3d(matrix(1:4,ncol=2,byrow = TRUE),sharedMouse = TRUE)
```

```
spheres3d(hidmat,radius=0)

localmeshdiff(PC1minSW,meanshape,ploton = 1,out.rem = TRUE,fact = 2.5,scale01 = FALSE,-
from=NULL,to=NULL,paltot = c("dodgerblue4","magenta3","tomato2","khaki1"))  #change
here palette

next3d()

spheres3d(hidmat,radius=0)

localmeshdiff(PC1maxSW,meanshape,ploton = 1,out.rem = TRUE,fact = 2.5,scale01 = FALSE,-
from=NULL,to=NULL,paltot = c("dodgerblue4","magenta3","tomato2","khaki1"))  #change
here palette

next3d()

spheres3d(hidmat,radius=0)

localmeshdiff(PC2minSW,meanshape,ploton = 1,out.rem = TRUE,fact = 2.5,scale01 = FALSE,-
from=NULL,to=NULL,paltot = c("dodgerblue4","magenta3","tomato2","khaki1"))  #change
here palette

next3d()

spheres3d(hidmat,radius=0)

localmeshdiff(PC2maxSW,meanshape,ploton = 1,out.rem = TRUE,fact = 2.5,scale01 = FALSE,-
from=NULL,to=NULL,paltot = c("dodgerblue4","magenta3","tomato2","khaki1"))  #change
here palette

# rgl.snapshot("Form Variations_Mastoid_1.png ")

}


#Figure 7 - R code

{

group<-substr(dimnames(data$set)[[3]],1,1)

pair<-cbind(L=c(seq(12,50,2),c(51:550)),R=c(seq(11,50,2),(551:1050)))

lset<-symmetrize(data$set,pairedLM = pair)

wMal<-which(group=="M")

wFem<-which(group=="F")

sur<-data$sur


wFem_set<-lset[,,wFem]

wMal_set<-lset[,,wMal]

Array<-bindArr(wFem_set,wMal_set,along=3)

CS<-apply(Array,3,cSize)

Sex<-c(rep("F",dim(wFem_set)[3]),rep("M",dim(wMal_set)[3]))
```

```
AllTrajFB<-permutangle(procSym(Array,scale=FALSE,CSinit = FALSE)$PCscores,
                       var=CS,group1=wFem,
                       group2=wMal,col1 = “deepskyblue3”,
                       col2=”khaki1”,
                       labels = c(“Fem-”,”Mal-”,”Fem+”,”Mal+”),
                       scale=FALSE,iter=1000,
                       cex1 = range01(CS[wFem])+0.5, cex2 = range01(CS[wMal])+0.5)

hist(AllTrajFB$iterangles,breaks = 100,xlim=c(0,90),xlab=”angle”,main=””)
box()
abline(v=AllTrajFB$angle,lwd=2,col=”red”)

hist(AllTrajFB$PCA_iterangles,breaks = 100,xlim=c(0,90))
abline(v=AllTrajFB$PCA_angle,lwd=2,col=”red”)



predict.var <- function(mat, var, value) {
  mat<-vecx(mat)
  mylm <- lm(mat ~ var)
  new <- data.frame(var = value)
  pred <- predict(mylm, new)
  pred<-vecx(pred,revert = T,lmdim = 3)
  return(pred)
}
predArrayF<-array(NA,dim=c(dim(Array)[1],dim(Array)[2],2))
predArrayF[,,1]<-predict.var(procSym(wFem_set,scale=F,CSinit = F)$rotated,
                       apply(wFem_set,3,cSize),min(apply(wFem_set,3,cSize)))[,,1]
predArrayF[,,2]<-predict.var(procSym(wFem_set,scale=F,CSinit = F)$rotated,
                       apply(wFem_set,3,cSize),max(apply(wFem_set,3,cSize)))[,,1]

predArrayM<-array(NA,dim=c(dim(Array)[1],dim(Array)[2],2))
predArrayM[,,1]<-predict.var(procSym(wMal_set,scale=F,CSinit = F)$rotated,
                       apply(wMal_set,3,cSize),min(apply(wMal_set,3,cSize)))[,,1]
predArrayM[,,2]<-predict.var(procSym(wMal_set,scale=F,CSinit = F)$rotated,
                       apply(wMal_set,3,cSize),max(apply(wMal_set,3,cSize)))[,,1]
```

```
out.sur<-vcgIsolated(data$sur)

mat<-data$set[,,104]

AllPred<-bindArr(predArrayF,predArrayM,along=3)

AllPred<-procSym(AllPred,CSinit = F,scale=F)$rotated


minsurF<-tps3d(out.sur,mat,AllPred[,,1])

maxsurF<-tps3d(out.sur,mat,AllPred[,,2])

minsurM<-tps3d(out.sur,mat,AllPred[,,3])

maxsurM<-tps3d(out.sur,mat,AllPred[,,4])

meanshapeSW<-tps3d(out.sur,mat,procSym(AllPred,CSinit = F,scale=F)$mshape)

hidmat<-as.matrix(meshcube(maxsurM))


layout3d(matrix(1:4,ncol=2,byrow = TRUE),sharedMouse = TRUE)

spheres3d(hidmat,radius=0)

localmeshdiff(minsurF,maxsurF,ploton = 1,out.rem = TRUE,fact = 2,scale01 = FALSE,-
from=NULL,to=NULL,paltot = c("dodgerblue4","magenta3","tomato2","khaki1"))  #change
here palette

next3d()

spheres3d(hidmat,radius=0)

localmeshdiff(maxsurF,minsurF,ploton = 1,out.rem = TRUE,fact = 2,scale01 = FALSE,from=-
NULL,to=NULL,paltot = c("dodgerblue4","magenta3","tomato2","khaki1"))  #change here
palette

next3d()

spheres3d(hidmat,radius=0)

localmeshdiff(minsurM,maxsurM,ploton = 1,out.rem = TRUE,fact = 2,scale01 = FALSE,from=-
NULL,to=NULL,paltot = c("dodgerblue4","magenta3","tomato2","khaki1"))  #change here
palette

next3d()

spheres3d(hidmat,radius=0)

localmeshdiff(maxsurM,minsurM,ploton = 1,out.rem = TRUE,fact = 2,scale01 = FALSE,from=-
NULL,to=NULL,paltot = c("dodgerblue4","magenta3","tomato2","khaki1"))  #change here
palette

}


#Table 1 - R code

{
```

```
group<-substr(dimnames(data$set)[[3]],1,1)

pair<-cbind(L=c(seq(12,50,2),c(51:550)),R=c(seq(11,50,2),(551:1050)))

lset<-symmetrize(data$set,pairedLM = pair)

wMal<-which(group==”M”)

wFem<-which(group==”F”)

sur<-data$sur

array<-procSym(lset)$rotated


Table1<-matrix(NA,ncol=9,nrow=6)

entireShape<-lda_bootstrap(lset,group,wMal,wFem,PCs=NULL,var=90,perm=1000,-
shapespace=TRUE)

entireShapeRes<-unlist(entireShape)

Table1[1,1]<-mean(entireShapeRes[which(names(entireShapeRes)==”result1”)])

Table1[1,2]<-mean(entireShapeRes[which(names(entireShapeRes)==”result2”)])

Table1[1,3]<-mean(entireShapeRes[which(names(entireShapeRes)==”result3”)])


entireShSize<-lda_bootstrap(lset,group,wMal,wFem,PCs=NULL,var=90,perm=1000,-
shapesize=TRUE)

entireShSizeRes<-unlist(entireShSize)

Table1[1,4]<-mean(entireShSizeRes[which(names(entireShSizeRes)==”result1”)])

Table1[1,5]<-mean(entireShSizeRes[which(names(entireShSizeRes)==”result2”)])

Table1[1,6]<-mean(entireShSizeRes[which(names(entireShSizeRes)==”result3”)])


entireSize<-lda_bootstrap(lset,group,wMal,wFem,PCs=NULL,var=90,perm=1000,only-
size=TRUE)

entireSizeRes<-unlist(entireSize)

Table1[1,7]<-mean(entireSizeRes[which(names(entireSizeRes)==”result1”)])

Table1[1,8]<-mean(entireSizeRes[which(names(entireSizeRes)==”result2”)])

Table1[1,9]<-mean(entireSizeRes[which(names(entireSizeRes)==”result3”)])


CR_Sh<-data$LDA_Sh

AccShape<-plotSD_map(CR_Sh,procSym(lset,CSinit = FALSE,scale=FALSE)$mshape,rain-
bow(10),from=NULL,to=NULL,radius=4)

sel_BR<-which(AccShape>0.72)

pca<-procSym(lset,scale=F,CSinit = F)

frontal<-pca$rotated[sel_BR,,]
```

```
frontalShape<-lda_bootstrap(frontal,group,wMal,wFem,PCs=NULL,var=90,perm=1000,shapespace=TRUE)

frontalShapeRes<-unlist(frontalShape)

Table1[2,1]<-mean(frontalShapeRes[which(names(frontalShapeRes)==”result1”)])

Table1[2,2]<-mean(frontalShapeRes[which(names(frontalShapeRes)==”result2”)])

Table1[2,3]<-mean(frontalShapeRes[which(names(frontalShapeRes)==”result3”)])


frontalShSize<-lda_bootstrap(frontal,group,wMal,wFem,PCs=NULL,var=90,perm=1000,shapesize=TRUE)

frontalShSizeRes<-unlist(frontalShSize)

Table1[2,4]<-mean(frontalShSizeRes[which(names(frontalShSizeRes)==”result1”)])

Table1[2,5]<-mean(frontalShSizeRes[which(names(frontalShSizeRes)==”result2”)])

Table1[2,6]<-mean(frontalShSizeRes[which(names(frontalShSizeRes)==”result3”)])


frontalSize<-lda_bootstrap(frontal,group,wMal,wFem,PCs=NULL,var=90,perm=1000,onlysize=TRUE)

frontalSizeRes<-unlist(frontalSize)

Table1[2,7]<-mean(frontalSizeRes[which(names(frontalSizeRes)==”result1”)])

Table1[2,8]<-mean(frontalSizeRes[which(names(frontalSizeRes)==”result2”)])

Table1[2,9]<-mean(frontalSizeRes[which(names(frontalSizeRes)==”result3”)])


CR_Fo<-data$LDA_Fo

AccForm<-plotSD_map(CR_Fo,procSym(lset,CSinit = FALSE,scale=FALSE)$mshape,rainbow(10),from=NULL,to=NULL,radius=4)

sel_BR<-which(AccForm>0.681)

pca<-procSym(lset,scale=F,CSinit = F)

set.seed(300)

allmods<-kmeans(as.matrix(dist(pca$mshape[sel_BR,])),iter.max = 30000,centers = 4)

frontal<-pca$rotated[sel_BR,,][allmods$cluster==1,,]

mastoid<-pca$rotated[sel_BR,,][allmods$cluster==2,,]

nasal<-pca$rotated[sel_BR,,][allmods$cluster==3,,]


frontal2Shape<-lda_bootstrap(frontal,group,wMal,wFem,PCs=NULL,var=90,perm=1000,shapespace=TRUE)

frontal2ShapeRes<-unlist(frontal2Shape)
```

```
Table1[3,1]<-mean(frontal2ShapeRes[which(names(frontal2ShapeRes)==”result1”)])

Table1[3,2]<-mean(frontal2ShapeRes[which(names(frontal2ShapeRes)==”result2”)])

Table1[3,3]<-mean(frontal2ShapeRes[which(names(frontal2ShapeRes)==”result3”)])


frontal2ShSize<-lda_bootstrap(frontal,group,wMal,wFem,PCs=NULL,var=90,perm=1000,sha-
pesize=TRUE)

frontal2ShSizeRes<-unlist(frontal2ShSize)

Table1[3,4]<-mean(frontal2ShSizeRes[which(names(frontal2ShSizeRes)==”result1”)])

Table1[3,5]<-mean(frontal2ShSizeRes[which(names(frontal2ShSizeRes)==”result2”)])

Table1[3,6]<-mean(frontal2ShSizeRes[which(names(frontal2ShSizeRes)==”result3”)])


frontal2Size<-lda_bootstrap(frontal,group,wMal,wFem,PCs=NULL,var=90,perm=1000,only-
size=TRUE)

frontal2SizeRes<-unlist(frontal2Size)

Table1[3,7]<-mean(frontal2SizeRes[which(names(frontal2SizeRes)==”result1”)])

Table1[3,8]<-mean(frontal2SizeRes[which(names(frontal2SizeRes)==”result2”)])

Table1[3,9]<-mean(frontal2SizeRes[which(names(frontal2SizeRes)==”result3”)])


mastoidShape<-lda_bootstrap(mastoid,group,wMal,wFem,PCs=NULL,var=90,per-
m=1000,shapespace=TRUE)

mastoidShapeRes<-unlist(mastoidShape)

Table1[4,1]<-mean(mastoidShapeRes[which(names(mastoidShapeRes)==”result1”)])

Table1[4,2]<-mean(mastoidShapeRes[which(names(mastoidShapeRes)==”result2”)])

Table1[4,3]<-mean(mastoidShapeRes[which(names(mastoidShapeRes)==”result3”)])


mastoidShSize<-lda_bootstrap(mastoid,group,wMal,wFem,PCs=NULL,var=90,perm=1000,-
shapesize=TRUE)

mastoidShSizeRes<-unlist(mastoidShSize)

Table1[4,4]<-mean(mastoidShSizeRes[which(names(mastoidShSizeRes)==”result1”)])

Table1[4,5]<-mean(mastoidShSizeRes[which(names(mastoidShSizeRes)==”result2”)])

Table1[4,6]<-mean(mastoidShSizeRes[which(names(mastoidShSizeRes)==”result3”)])


mastoidSize<-lda_bootstrap(mastoid,group,wMal,wFem,PCs=NULL,var=90,perm=1000,only-
size=TRUE)

mastoidSizeRes<-unlist(mastoidSize)

Table1[4,7]<-mean(mastoidSizeRes[which(names(mastoidSizeRes)==”result1”)])
```

```
Table1[4,8]<-mean(mastoidSizeRes[which(names(mastoidSizeRes)==”result2”)])

Table1[4,9]<-mean(mastoidSizeRes[which(names(mastoidSizeRes)==”result3”)])


nasalShape<-lda_bootstrap(nasal,group,wMal,wFem,PCs=NULL,var=90,perm=1000,shapespace=TRUE)

nasalShapeRes<-unlist(nasalShape)

Table1[5,1]<-mean(nasalShapeRes[which(names(nasalShapeRes)==”result1”)])

Table1[5,2]<-mean(nasalShapeRes[which(names(nasalShapeRes)==”result2”)])

Table1[5,3]<-mean(nasalShapeRes[which(names(nasalShapeRes)==”result3”)])


nasalShSize<-lda_bootstrap(nasal,group,wMal,wFem,PCs=NULL,var=90,perm=1000,shapesize=TRUE)

nasalShSizeRes<-unlist(nasalShSize)

Table1[5,4]<-mean(nasalShSizeRes[which(names(nasalShSizeRes)==”result1”)])

Table1[5,5]<-mean(nasalShSizeRes[which(names(nasalShSizeRes)==”result2”)])

Table1[5,6]<-mean(nasalShSizeRes[which(names(nasalShSizeRes)==”result3”)])


nasalSize<-lda_bootstrap(nasal,group,wMal,wFem,PCs=NULL,var=90,perm=1000,onlysize=TRUE)

nasalSizeRes<-unlist(nasalSize)

Table1[5,7]<-mean(nasalSizeRes[which(names(nasalSizeRes)==”result1”)])

Table1[5,8]<-mean(nasalSizeRes[which(names(nasalSizeRes)==”result2”)])

Table1[5,9]<-mean(nasalSizeRes[which(names(nasalSizeRes)==”result3”)])


LIST<-list(“frontal”=arraytolist(frontal),”mastoid”=arraytolist(mastoid),”nasal”=arraytolist(nasal))

combin2D<-twodviews(LIST,scale=TRUE,vector=c(1:3))

accs<-NULL

macc<-NULL

facc<-NULL

var<-90

n<-100

for(i in 1:100){

 print(i)

 sel<-c(sample(wFem,n/2),sample(wMal,n/2))

 # ref_set<-set[,,sel]
```

```
var_ref<-group[sel]

LIST<-list("frontal"=arraytolist(frontal[,,sel]),"mastoid"=arraytolist(mastoid[,,sel]),"nasal"=arraytolist(nasal[,,sel]))


Frontal<-suppressMessages(procSym(frontal[,,sel])$rotated)

FrontalMat<-vecx(Frontal)*sqrt(dim(Frontal)[1])

Mastoid<-suppressMessages(procSym(mastoid[,,sel])$rotated)

MastoidMat<-vecx(Mastoid)*sqrt(dim(Mastoid)[1])

Nasal<-suppressMessages(procSym(nasal[,,sel])$rotated)

NasalMat<-vecx(Nasal)*sqrt(dim(Nasal)[1])


coo_tar1<-t(apply(frontal[,,-sel],3,function(x) rotonmat(x,x,mshape(Frontal),scale=T)))*sqrt(dim(Frontal)[1])

coo_tar2<-t(apply(mastoid[,,-sel],3,function(x) rotonmat(x,x,mshape(Mastoid),scale=T)))*sqrt(dim(Mastoid)[1])

coo_tar3<-t(apply(nasal[,,-sel],3,function(x) rotonmat(x,x,mshape(Nasal),scale=T)))*sqrt(dim(Nasal)[1])


Rots_pca<-prcomp(cbind(FrontalMat,MastoidMat,NasalMat), scale. = FALSE)

PCscores<-Rots_pca$x

eigv<-Rots_pca$sdev^2

Variance <- cbind(sqrt(eigv), eigv/sum(eigv), cumsum(eigv)/sum(eigv)) * 100

trains<-data.frame(var_ref,PCscores)

colnames(trains)[1]<-"group"

form= suppressWarnings(as.formula(c("group~",c(paste(paste("PC",(which(Variance[,3]<var)[1:(length(which(Variance[,3]<var))-1)]),sep=""),"+",sep=""),
                                    paste("PC",length(which(Variance[,3]<var)),sep="")))))


da<-lda(form,data=trains,prior=c(0.5,0.5),tol = 1.0e-7)

pred<-predict(da)

res<-table(var_ref,pred$class)

accuracy_ref<-round(sum(diag(res))/sum(res),2)

res_ref<-accuracy_ref


var_tar<-group[-sel]

PCscores_tar<- predict(Rots_pca, newdata=cbind(coo_tar1,coo_tar2,coo_tar3))
```

```
  colnames(PCscores_tar)<-paste("PC",1:dim(PCscores_tar)[2],sep="")
  trains_tar<-data.frame(var_tar,PCscores_tar)
  colnames(trains_tar)[1]<-"var"
  pred_tar<-predict(da,newdata=trains_tar)
  res_tar<-table(var_tar,pred_tar$class)
  accuracy_tar<-round(sum(diag(res_tar))/sum(res_tar),2)
  accs[i]<-accuracy_tar
  macc[i]<-res_tar[1,1]/sum(res_tar[,1])
  facc[i]<-res_tar[2,2]/sum(res_tar[,2])
}
Table1[6,1]<-mean(accs)
Table1[6,2]<-mean(facc)
Table1[6,3]<-mean(macc)



LIST<-list("frontal"=arraytolist(frontal),"mastoid"=arraytolist(mastoid),"nasal"=arraytolist(nasal))
combin2D<-twodviews(LIST,scale=FALSE,vector=c(1:3))
plot(combin2D$PCscores[,c(2,4)],pch=19,col=as.factor(group))
accs<-NULL
macc<-NULL
facc<-NULL
var<-90
n<-100
for(i in 1:100){
  print(i)
  sel<-c(sample(wFem,n/2),sample(wMal,n/2))
  # ref_set<-set[,,sel]
  var_ref<-group[sel]
  LIST<-list("frontal"=arraytolist(frontal[,,sel]),"mastoid"=arraytolist(mastoid[,,sel]),"nasal"=arraytolist(nasal[,,sel]))
  Frontal<-suppressMessages(procSym(frontal[,,sel],scale=FALSE,CSinit = FALSE)$rotated)
  FrontalMat<-vecx(Frontal)*sqrt(dim(Frontal)[1])
  Mastoid<-suppressMessages(procSym(mastoid[,,sel],scale=FALSE,CSinit = FALSE)$rotated)
  MastoidMat<-vecx(Mastoid)*sqrt(dim(Mastoid)[1])
```

```
Nasal<-suppressMessages(procSym(nasal[,,sel],scale=FALSE,CSinit = FALSE)$rotated)

NasalMat<-vecx(Nasal)*sqrt(dim(Nasal)[1])


coo_tar1<-t(apply(frontal[,,-sel],3,function(x) rotonmat(x,x,mshape(Frontal),scale=-
FALSE)))*sqrt(dim(Frontal)[1])

coo_tar2<-t(apply(mastoid[,,-sel],3,function(x) rotonmat(x,x,mshape(Mastoid),scale=-
FALSE)))*sqrt(dim(Mastoid)[1])

coo_tar3<-t(apply(nasal[,,-sel],3,function(x) rotonmat(x,x,mshape(Nasal),scale=FALSE)))*-
sqrt(dim(Nasal)[1])


Rots_pca<-prcomp(cbind(FrontalMat,MastoidMat,NasalMat), scale. = FALSE)

PCscores<-Rots_pca$x

eigv<-Rots_pca$sdev^2

Variance <- cbind(sqrt(eigv), eigv/sum(eigv), cumsum(eigv)/sum(eigv)) * 100

trains<-data.frame(var_ref,PCscores)

colnames(trains)[1]<-"group"

form= suppressWarnings(as.formula(c("group~",c(paste(paste("PC",(which(Variance[,3]<var)
[1:(length(which(Variance[,3]<var))-1)]),sep=""),"+",sep=""),
                                    paste("PC",length(which(Variance[,3]<var)),sep=""))))


da<-lda(form,data=trains,prior=c(0.5,0.5),tol = 1.0e-7)

pred<-predict(da)

res<-table(var_ref,pred$class)

accuracy_ref<-round(sum(diag(res))/sum(res),2)

res_ref<-accuracy_ref


var_tar<-group[-sel]

PCscores_tar<- predict(Rots_pca, newdata=cbind(coo_tar1,coo_tar2,coo_tar3))

colnames(PCscores_tar)<-paste("PC",1:dim(PCscores_tar)[2],sep="")

trains_tar<-data.frame(var_tar,PCscores_tar)

colnames(trains_tar)[1]<-"var"

pred_tar<-predict(da,newdata=trains_tar)

res_tar<-table(var_tar,pred_tar$class)

accuracy_tar<-round(sum(diag(res_tar))/sum(res_tar),2)

accs[i]<-accuracy_tar

macc[i]<-res_tar[1,1]/sum(res_tar[,1])
```

```
facc[i]<-res_tar[2,2]/sum(res_tar[,2])
}
Table1[6,4]<-mean(accs)
Table1[6,5]<-mean(facc)
Table1[6,6]<-mean(macc)

accs<-NULL
macc<-NULL
facc<-NULL
var<-90
for(i in 1:1000){
 print(i)
 sel<-c(sample(wFem,n/2),sample(wMal,n/2))
 var_ref<-group[sel]

 PCscores1<-apply(frontal[,,sel],3,cSize)/sqrt(dim(frontal[,,sel])[1])
 PCscores2<-apply(mastoid[,,sel],3,cSize)/sqrt(dim(mastoid[,,sel])[1])
 PCscores3<-apply(nasal[,,sel],3,cSize)/sqrt(dim(nasal[,sel])[1])
 PCscores<-PCscores1+PCscores2+PCscores3
 PCs<-1
 var<-NULL
 trains<-data.frame(var_ref,PCscores)
 colnames(trains)[1]<-"group"
 colnames(trains)[2]<-"PC1"
 form=suppressWarnings(as.formula(c(paste("group~PC1"))))
 da<-lda(form,data=trains,prior=c(0.5,0.5),tol = 1.0e-7)
 pred<-predict(da)
 res<-table(var_ref,pred$class)
 accuracy_ref<-round(sum(diag(res))/sum(res),2)
 res_ref<-accuracy_ref

 PCscores1t<-apply(frontal[,,-sel],3,cSize)/sqrt(dim(frontal[,,-sel])[1])
```

```
  PCscores2t<-apply(mastoid[,,-sel],3,cSize)/sqrt(dim(mastoid[,,-sel])[1])
  PCscores3t<-apply(nasal[,,-sel],3,cSize)/sqrt(dim(nasal[,,-sel])[1])

  PCscores_tar<-t(t(PCscores1t+PCscores2t+PCscores3t))
  var_tar<-group[-sel]
  colnames(PCscores_tar)<-"PC1"
  trains_tar<-data.frame(var_tar,PCscores_tar)
  colnames(trains_tar)[1]<-"var"
  pred_tar<-predict(da,newdata=trains_tar)
  res_tar<-table(var_tar,pred_tar$class)
  accuracy_tar<-round(sum(diag(res_tar))/sum(res_tar),2)
  accs[i]<-accuracy_tar
  macc[i]<-res_tar[1,1]/sum(res_tar[,1])
  facc[i]<-res_tar[2,2]/sum(res_tar[,2])
}
Table1[6,7]<-mean(accs)
Table1[6,8]<-mean(facc)
Table1[6,9]<-mean(macc)

round(Table1,2)
}

#Supplementary Fig. S1 and S2
{
load("data2.rda")
load("data.rda")

matrix<-procSym(data$set,CSinit = F,scale=F)$mshape
mesh<-data$sur
{
 plscorrs<-NULL
 for(i in 1:dim(matrix)[1]){
   plscorrs[i]<- unlist(data2[[1]]$ItaShape[[2]][i])
 }
```

```
  index<-list()
  for(i in 1:dim(matrix)[1]){
   index[[i]]<- unlist(data2[[1]]$ItaShape[[1]][i])
  }

  corr_scores<-matrix(NA,nrow=dim(matrix)[1],ncol=dim(matrix)[1])
  # dim(corr_scores)
  for(i in 1:length(index)){
   corr_scores[index[[i]][[1]],i]<-plscorrs[[i]]
  }

  corr_values<-NULL
  for(i in 1:nrow(corr_scores)){
   selv<-which(is.na(corr_scores[i,])==FALSE)
   corr_values[i]<-mean(corr_scores[i,selv])
  }
  ITA_Shape<-corr_values
 } #Itashape
 {
  plscorrs<-NULL
  for(i in 1:dim(matrix)[1]){
   plscorrs[i]<- unlist(data2[[1]]$ItaForm[[2]][i])
  }

  index<-list()
  for(i in 1:dim(matrix)[1]){
   index[[i]]<- unlist(data2[[1]]$ItaForm[[1]][i])
  }

  corr_scores<-matrix(NA,nrow=dim(matrix)[1],ncol=dim(matrix)[1])
  # dim(corr_scores)
  for(i in 1:length(index)){
   corr_scores[index[[i]][[1]],i]<-plscorrs[[i]]
  }
```

```
 corr_values<-NULL
 for(i in 1:nrow(corr_scores)){
  selv<-which(is.na(corr_scores[i,])==FALSE)
  corr_values[i]<-mean(corr_scores[i,selv])
 }
 ITA_Form<-corr_values
} #ItaForm
{
 plscorrs<-NULL
 for(i in 1:dim(matrix)[1]){
  plscorrs[i]<- unlist(data2[[1]]$ItaSize[[2]][i])
 }

 index<-list()
 for(i in 1:dim(matrix)[1]){
  index[[i]]<- unlist(data2[[1]]$ItaSize[[1]][i])
 }

 corr_scores<-matrix(NA,nrow=dim(matrix)[1],ncol=dim(matrix)[1])
 # dim(corr_scores)
 for(i in 1:length(index)){
  corr_scores[index[[i]][[1]],i]<-plscorrs[[i]]
 }

 corr_values<-NULL
 for(i in 1:nrow(corr_scores)){
  selv<-which(is.na(corr_scores[i,])==FALSE)
  corr_values[i]<-mean(corr_scores[i,selv])
 }
 ITA_Size<-corr_values
} #ItaSize

{
```

```
plscorrs<-NULL
for(i in 1:dim(matrix)[1]){
 plscorrs[i]<- data$LDA_Sh[[2]][i]
}

index<-list()
for(i in 1:dim(matrix)[1]){
 index[[i]]<- data$LDA_Sh[[1]][i]
}

corr_scores<-matrix(NA,nrow=dim(matrix)[1],ncol=dim(matrix)[1])
# dim(corr_scores)
for(i in 1:length(index)){
 corr_scores[index[[i]][[1]],i]<-plscorrs[[i]]
}

corr_values<-NULL
for(i in 1:nrow(corr_scores)){
 selv<-which(is.na(corr_scores[i,])==FALSE)
 corr_values[i]<-mean(corr_scores[i,selv])
}
FULL_Shape<-corr_values
} #Fullshape
{
plscorrs<-NULL
for(i in 1:dim(matrix)[1]){
 plscorrs[i]<- data$LDA_Fo[[2]][i]
}

index<-list()
for(i in 1:dim(matrix)[1]){
 index[[i]]<- data$LDA_Fo[[1]][i]
}

corr_scores<-matrix(NA,nrow=dim(matrix)[1],ncol=dim(matrix)[1])
```

```
  # dim(corr_scores)
  for(i in 1:length(index)){
   corr_scores[index[[i]][[1]],i]<-plscorrs[[i]]
  }

  corr_values<-NULL
  for(i in 1:nrow(corr_scores)){
   selv<-which(is.na(corr_scores[i,])==FALSE)
   corr_values[i]<-mean(corr_scores[i,selv])
  }
  FULL_Form<-corr_values
 } #FullForm
 {
  plscorrs<-NULL
  for(i in 1:dim(matrix)[1]){
   plscorrs[i]<- data$LDA_Sz[[2]][i]
  }

  index<-list()
  for(i in 1:dim(matrix)[1]){
   index[[i]]<- data$LDA_Sz[[1]][i]
  }

  corr_scores<-matrix(NA,nrow=dim(matrix)[1],ncol=dim(matrix)[1])
  # dim(corr_scores)
  for(i in 1:length(index)){
   corr_scores[index[[i]][[1]],i]<-plscorrs[[i]]
  }

  corr_values<-NULL
  for(i in 1:nrow(corr_scores)){
   selv<-which(is.na(corr_scores[i,])==FALSE)
   corr_values[i]<-mean(corr_scores[i,selv])
  }
  FULL_Size<-corr_values
```

```
} #FullSize


{
 plscorrs<-NULL
 for(i in 1:dim(matrix)[1]){
  plscorrs[i]<- unlist(data2[[2]]$NoItaShape[[2]][i])
 }

 index<-list()
 for(i in 1:dim(matrix)[1]){
  index[[i]]<- unlist(data2[[2]]$NoItaShape[[1]][i])
 }

 corr_scores<-matrix(NA,nrow=dim(matrix)[1],ncol=dim(matrix)[1])
 # dim(corr_scores)
 for(i in 1:length(index)){
  corr_scores[index[[i]][[1]],i]<-plscorrs[[i]]
 }

 corr_values<-NULL
 for(i in 1:nrow(corr_scores)){
  selv<-which(is.na(corr_scores[i,])==FALSE)
  corr_values[i]<-mean(corr_scores[i,selv])
 }
 PART_Shape<-corr_values
} #Partshape
{
 plscorrs<-NULL
 for(i in 1:dim(matrix)[1]){
  plscorrs[i]<- unlist(data2[[2]]$NoItaForm[[2]][i])
 }

 index<-list()
 for(i in 1:dim(matrix)[1]){
  index[[i]]<- unlist(data2[[2]]$NoItaForm[[1]][i])
```

```
  }

  corr_scores<-matrix(NA,nrow=dim(matrix)[1],ncol=dim(matrix)[1])
  # dim(corr_scores)
  for(i in 1:length(index)){
   corr_scores[index[[i]][[1]],i]<-plscorrs[[i]]
  }

  corr_values<-NULL
  for(i in 1:nrow(corr_scores)){
   selv<-which(is.na(corr_scores[i,])==FALSE)
   corr_values[i]<-mean(corr_scores[i,selv])
  }
  PART_Form<-corr_values
 } #PartForm
 {
  plscorrs<-NULL
  for(i in 1:dim(matrix)[1]){
   plscorrs[i]<- unlist(data2[[2]]$NoItaSize[[2]][i])
  }

  index<-list()
  for(i in 1:dim(matrix)[1]){
   index[[i]]<- unlist(data2[[2]]$NoItaSize[[1]][i])
  }

  corr_scores<-matrix(NA,nrow=dim(matrix)[1],ncol=dim(matrix)[1])
  # dim(corr_scores)
  for(i in 1:length(index)){
   corr_scores[index[[i]][[1]],i]<-plscorrs[[i]]
  }

  corr_values<-NULL
  for(i in 1:nrow(corr_scores)){
   selv<-which(is.na(corr_scores[i,])==FALSE)
```

```
corr_values[i]<-mean(corr_scores[i,selv])

 }

 PART_Size<-corr_values

} #PartSize


sur<-tps3d(mesh,data$set[,,104],matrix)

layout3d((t(c(1:3))),sharedMouse = TRUE)

colmat2mesh(sur,matrix,ITA_Shape,k=5,from=0.45,to=0.77,cols=colorRampPalette(c("dodg-
erblue4","magenta3","tomato2","khaki1"))(100),nacolor="darkgray")

next3d()

colmat2mesh(sur,matrix,ITA_Form,k=5,from=0.45,to=0.77,cols=colorRampPalette(c("dodger-
blue4","magenta3","tomato2","khaki1"))(100),nacolor="darkgray")

next3d()

colmat2mesh(sur,matrix,ITA_Size,k=5,from=0.45,to=0.77,cols=colorRampPalette(c("dodger-
blue4","magenta3","tomato2","khaki1"))(100),nacolor="darkgray")


cor.test(ITA_Shape,FULL_Shape)

cor.test(ITA_Form,FULL_Form)

cor.test(ITA_Size,FULL_Size)


cor.test(ITA_Shape,PART_Shape)

cor.test(ITA_Form,PART_Form)

cor.test(ITA_Size,PART_Size)


par(mfrow=c(2,3))

CorSh<-cor.test(ITA_Shape,FULL_Shape)

plot(ITA_Shape,FULL_Shape,pch=19,main=paste("Shape space: ","cor = ",round(CorSh$esti-
mate,2),sep=""),

    xlab="3D map (Ita) - accuracy",ylab="3D map (All) - accuracy",xlim=c(0.4,0.75),ylim=c(0.
4,0.75),asp=1)

lmshape<-lm(FULL_Shape~ITA_Shape)

lmshapesel<-lm(FULL_Shape[which(ITA_Shape>=quantile(FULL_Shape)[4])]~ITA_
Shape[which(ITA_Shape>=quantile(FULL_Shape)[4])])

abline(lmshape,lwd=2,lty=2,col="blue")

ablineclip(lmshapesel,x1=quantile(ITA_Shape)[4],x2=quantile(ITA_Shape)
[5],lwd=2,lty=2,col="gold2")
```

```
CorFo<-cor.test(ITA_Form,FULL_Form)

plot(ITA_Form,FULL_Form,pch=19,main=paste("Shape & size space: ","cor = ",round(Cor-
Fo$estimate,2),sep=""),

    xlab="3D map (Ita) - accuracy",ylab="3D map (All) - accuracy",xlim=c(0.4,0.75),ylim=c(0.
4,0.75),asp=1)

lmform<-lm(FULL_Form~ITA_Form)

abline(lmform,lwd=2,lty=2,col="blue")


CorSz<-cor.test(ITA_Size,FULL_Size)

plot(ITA_Size,FULL_Size,pch=19,main=paste("Centroid size: ","cor = ",round(CorSz$esti-
mate,2),sep=""),

    xlab="3D map (Ita) - accuracy",ylab="3D map (All) - accuracy",xlim=c(0.4,0.75),ylim=c(0.
4,0.75),asp=1)

lmsize<-lm(FULL_Size~ITA_Size)

abline(lmsize,lwd=2,lty=2,col="blue")


CorSh<-cor.test(ITA_Shape,PART_Shape)

plot(ITA_Shape,PART_Shape,pch=19,main=paste("Shape space: ","cor = ",round(CorSh$esti-
mate,2),sep=""),

    xlab="3D map (Ita) - accuracy",ylab="3D map (All no Ita) - accuracy",xlim=c(0.4,0.75),yli
m=c(0.4,0.75),asp=1)


lmshape<-lm(PART_Shape~ITA_Shape)

lmshapesel<-lm(PART_Shape[which(ITA_Shape>=quantile(FULL_Shape)[4])]~ITA_
Shape[which(ITA_Shape>=quantile(FULL_Shape)[4])])


abline(lmshape,lwd=2,lty=2,col="blue")

ablineclip(lmshapesel,x1=quantile(ITA_Shape)[4],x2=quantile(ITA_Shape)
[5],lwd=2,lty=2,col="gold2")


CorFo<-cor.test(ITA_Form,PART_Form)

plot(ITA_Form,PART_Form,pch=19,main=paste("Shape & size space: ","cor = ",round(Cor-
Fo$estimate,2),sep=""),

    xlab="3D map (Ita) - accuracy",ylab="3D map (All no Ita) - accuracy",xlim=c(0.4,0.75),yli
m=c(0.4,0.75),asp=1)

lmform<-lm(PART_Form~ITA_Form)

abline(lmform,lwd=2,lty=2,col="blue")
```

```
CorSz<-cor.test(ITA_Size,PART_Size)

plot(ITA_Size,PART_Size,pch=19,main=paste("Centroid size: ","cor = ",round(CorSz$esti-
mate,2),sep=""),

    xlab="3D map (Ita) - accuracy",ylab="3D map (All no Ita) - accuracy",xlim=c(0.4,0.75),yli
m=c(0.4,0.75),asp=1)

lmsize<-lm(PART_Size~ITA_Size)

abline(lmsize,lwd=2,lty=2,col="blue")


cor.test(ITA_Shape[which(ITA_Shape>=quantile(FULL_Shape)[4])],FULL_Shape[which(I-
TA_Shape>=quantile(FULL_Shape)[4])])

cor.test(ITA_Shape[which(ITA_Shape>=quantile(FULL_Shape)[4])],PART_Shape[which(I-
TA_Shape>=quantile(FULL_Shape)[4])])

}


#Intraobserver error

{

load("data3.rda")

cols_rip<-as.factor(str_sub(dimnames(data3)[[3]],-1))

levels(cols_rip)<-c("red","orange","pink","lightblue")

cols_ids<-as.factor(str_sub(dimnames(data3)[[3]],3,3))

levels(cols_ids)<-rainbow(8)


gpa_rep<-procSym(data3,scale=FALSE,CSinit = FALSE)

plot(gpa_rep$PCscores,col=cols_ids,pch=19)

rownames(gpa_rep$PCscores)<-NULL

procD.lm(gpa_rep$PCscores~cols_rip,iter = 1000)$aov.table

AOV<-procD.lm(gpa_rep$PCscores~cols_ids+cols_rip,iter = 1000)$aov.table

Rf<-AOV[1,2]/(AOV[1,2]+AOV[2,2])

Rf*4/(1+(4-1)*Rf)

}
```

IV. script : The realize a Neural network analysis with the use of linear measurements to elaborate a new method to establish the sex in human modern crania.
Published in Github.com link: https://github.com/AlessioVeneziano/Papers/tree/main/DelBove_%26_Veneziano_2022

INFORMATION - Del Bove & Veneziano, 2022

This folder contains functions and scripts to reproduce the paper *A generalised neural network model to estimate sex from cra-nial metric traits: a robust training and testing approach about sex estimation from human cranial metric measurements*. In addition, the Neural Network model generated in the paper is provided and its usage for prediction is shown in script number 3.

##

########################## Del Bove & Veneziano 2022: SCRIPT 1

```
# Load functions
source("Functions.R")


# Read Howell dataset (you need an internet connection to read the data)
how<-read.csv("https://web.utk.edu/~auerbach/Howell.csv")


# Compute table showing sex by population and remove populations represented
# by only one sex
tab<-as.matrix(table(how$Population,how$Sex))
del<-rownames(which(tab==0,T))
  how<-how[!how$Population%in%del,]

# Keep a subset of measurements (refer to the main text for definitions)
meas<-c("GOL","BBH","ZYB","AUB","NLH","OBH","OBB","NLB","MDH","OCC")
vars<-c("Sex","Population",meas)
  how<-how[,vars]


# Z-score transformation to remove observations exhibiting 3 or more standard
# deviations from the mean for at least one measurement
```

```
rm(del)
scaled<-scale(how[,-c(1,2)])
del<-unique(which(abs(scaled)>3,T)[,1])
 how<-how[-del,]

# Homogenise sex proportion (collecting equal numbers of males and females)
dif<-diff(table(how$Sex))
set.seed(42)
subm<-sample(which(how$Sex=="M"),dif,F)
 how<-how[-subm,]


# Compute Geometric Mean and add to training dataset
how$GM<-apply(how[,3:12],1,gmean)


# Compute Mosimann transformation
how[,3:12]<-t(apply(how[,3:12],1,mosimann))
how[,3:13]<-round(how[,3:13],3)


# Save transformed data
write.csv(how,"how_transformed.csv",quote=F,row.names=F)


############################################## END OF SCRIPT
#############################################################
#
```

```
############################################################
#
###################### Del Bove & Veneziano 2022: SCRIPT 2


# Load packages
library(h2o)



# Set memory and h2o environment (the memory allocated and the specifics of
# 'h2o.init' can be changed depending on the specifics of your system); the
# function 'h2o.shutdown' removes any h2o environment previously initialised;
# the launch of a new h2o environment can take a few seconds
memory.limit(1e+09)

h2o.shutdown()
h2o.init(nthreads=-1, max_mem_size="4g")



# Read dataset (this is the dataset prepared in the Script 1)
how<-read.csv("how_transformed.csv")



# Prepare training and validation sets from the whole training dataset (for
# consistency with the h2o package, the data is transformed into an object of
# class'H2OFrame')
dtv<-how[,-2]
dtv$Sex<-as.factor(dtv$Sex)
  dtv<-as.h2o(dtv)

# Define outcome (sex) and variables
xs<-colnames(dtv)[-1]
ys<-colnames(dtv)[1]
```

```
# Prepare parameters for model tuning using a 'brute force' approach: generate
# a dataframe with all the combinations of the values to test for each parameter
# to tune
hlist<-list(3,7,11,15,19,23,27,c(3,3),c(7,7),c(11,11),c(15,15),c(19,19),c(23,23),c(27,27))
l2list<-list(0,1e-4,5e-4,1e-3,5e-3,1e-2,5e-2)
 pars<-expand.grid(hlist,l2list)

# Model tuning: models with different combinations of parameters are fitted on
# the training set and their performance is assessed on the validation set
# (a more computationally efficient tuning can be attained using the function
# 'h2o.grid', but due to system limitations we preferred a for loop - it can
# take up to a few hours)
stats<-matrix(NA,nrow(pars),40)
for(i in 1:nrow(pars)){
 print(i)

mod<-h2o.deeplearning(x=xs,y=ys,training_frame=dtv,epochs=1000,stopping_metric="logloss",
                      loss="CrossEntropy",distribution="bernoulli",standardize=T,
                      adaptive_rate=F,rate=0.0005,momentum_start=0.5,momentum_ramp=1e6,
                      momentum_stable=0.99,stopping_rounds=20,stopping_tolerance=0.0001,
                      input_dropout_ratio=0,reproducible=T,seed=42,nfolds=10,
                      fold_assignment="Stratified",activation="RectifierWithDropout",
                      fast_mode=F,hidden=pars[i,1][[1]],l2=pars[i,2][[1]])

 statcv<-mod@model$cross_validation_metrics_summary[,1:2]
 stats[i,]<-c(t(statcv))

 rm("mod")
 if(i%%10==0){print("Cleaning in progress...") ; gc()}
}

# Put together the results obtained from the tuning ('mean' and 'sd' refer to the
# statistics calculated for each model tuned and computed over the cross-validated
# results) and save the table
```

```
stats<-cbind.data.frame(pars,stats)
  colnam<-c(t(cbind(rownames(statcv),rownames(statcv))))
  colnam<-paste(colnam,c("mean","sd"),sep="_")
   colnames(stats)<-c("hlayer","l2reg",colnam)

saveRDS(stats,"tunedModel_stats.RData")



# Choosing best model: the choice can be based on multiple considerations (refer
# to the main text of the paper for the criteria used); here, for example, we
# choose the model maximising the Area Under Curve (AUC) of a Receiver Operating
# Characteristic curve (ROC); the parameters of the best model are extracted
bmPars<-stats[which.max(stats$auc_mean),1:2]
 par1<-unlist(bmPars[1])
  names(par1)<-NULL
 par2<-unlist(bmPars[2])
  names(par2)<-NULL



# Train best model using the whole training data (no validation set provided -
# this is the final model that can be used to estimate sex to new observations)
mod<-h2o.deeplearning(x=xs,y=ys,training_frame=dtv,epochs=1000,stopping_metric="log-
gloss",
                      loss="CrossEntropy",distribution="bernoulli",standardize=T,
                      adaptive_rate=F,rate=0.0005,momentum_start=0.5,momentum_ramp=1e6,
                      momentum_stable=0.99,stopping_rounds=20,stopping_tolerance=0.00001,
                      input_dropout_ratio=0,reproducible=T,seed=42,activation="RectifierWithDro-
pout",
                      variable_importances=T,fast_mode=F,export_weights_and_biases=T,
                      hidden=par1,l2=par2)



# Save best model for later use
h2o.saveModel(mod,getwd(),filename="BestModel_hidden11_l2reg1e-04")
```

END OF SCRIPT

##

#

###################### Del Bove & Veneziano 2022: SCRIPT 3

This script shows how to use the best model to estimate sex on the data

measured on new crania.

Load packages and functions

source("Functions.R")

library(h2o)

Set memory and h2o environment

memory.limit(1e+09)

h2o.shutdown()

h2o.init(nthreads=-1, max_mem_size="4g")

Read the model and the data to be estimated (it is assumed that the data comes

in the same format as the training data - same measurements, same field names),

except for the Mosimann transformation (which is performed below); here, just

to explain how the process works, we use some example data from the Howell

dataset

mod<-h2o.loadModel("BestModel_hidden11_L2reg1e-04")

newdat<-read.csv("example_new_data.csv")

```
# Transform data (add Geometric Mean and apply Mosimann transformation)
newdat$GM<-apply(newdat,1,gmean)

newdat[,-ncol(newdat)]<-t(apply(newdat[,-ncol(newdat)],1,mosimann))
newdat<-round(newdat,3)


# For consistency with the package 'h2o', the data is transformed into an object
# of class 'H2OFrame'
newdat<-as.h2o(newdat)


# Predict the sex of the individual crania measured in 'newdat'; the model produces
# a best estimate at a probability threshold that can be different from 0.5, but
# having trained the model with exactly equal number of females and males, we
# decide to assume a prior equal probability for each sex (thus we re-compute the
# estimated sex based on a 0.5 threshold)
pred<-h2o.predict(mod,newdat)
  pred<-as.data.frame(pred)
    pred$predict<-ifelse(pred$'F'>0.5,"F","M")



############################################## END OF SCRIPT
#############################################################
#
```

UNIVERSITAT ROVIRA I VIRGILI
A COMPUTATIONAL RE-ASSESSMENT OF SEXUAL DIMORPHISM IN THE HUMAN CRANIUM BEYOND TRADITIONAL MORPHOMETRICS: GEOMETRIC MORPHOMETRIC METHODS AND NEURAL NETWORK ANALYSIS
Antonietta Del Bove

8.2 Other Publications

A COMPUTATIONAL RE-ASSESSMENT OF SEXUAL DIMORPHISM IN THE HUMAN CRANIUM BEYOND TRADITIONAL MORPHOMETRICS: GEOMETRIC MORPHOMETRIC METHODS AND NEURAL NETWORK ANALYSIS
Antonietta Del Bove

Poster Presentation Number 107, Session 2, Friday 18:15

Exploring the impact of sexual dimorphism on cranial asymmetry in a worldwide modern human collection

Antonietta Del Bove[1,2], Antonio Profico[3], Marina Melchionna[4], Pasquale Raia[4], Carlos Lorenzo[1,2]

1 - Department of History, University Rovira i Virgili, Avinguda de Catalunya 35, 43002 Tarragona, Spain · 2 - Department of Quaternary and Prehistory, Institut Català de Paleoecologia Humana i Evolució Social (IPHES_CERCA), Zona Educational 4, Campus Sescelades URV (Edifici W3), 43007 Tarragona, Spain · 3 - Department of Biology, University of Pisa, via Luca Ghini, 13 56126 Pisa Italy · 4 - Department of Earth, Environmental and Sciences, University Federico II, 80126 Napoli, Italy

The human cranium exhibits a certain level of asymmetry. Previous studies in primates, fossil hominins and modern human have indicated a relationship between cranial asymmetry and environmental, genetic, and functional factors. In this communication, we applied a geometric morphometric protocol to the quantification and mapping of cranial asymmetry in a worldwide collection in relation to sexual dimorphism. Largest part of cranial morphological information is symmetric on the left and right side with respect to the midsagittal plane. A certain portion of cranial shape information is attributable to fluctuant asymmetry. Here, we used a large world-wide sample of modern humans (N=181; 89 females and 92 males) to measure the magnitude and pattern of asymmetry in the cranium. On each individual, we defined 50 fixed landmarks and a symmetric patch of 1000 surface semilandmarks. We have used Arothron R package [1-2] to quantify shape asymmetry. Our protocol splits each landmark and semilandmark configuration in a left (L) and a right (R) half. One side is mirrored, and the entire sets of landmarks and semilandmarks is superimposed via Generalized Procrustes Analysis followed Klingenberg [3]. Eventually, the configurations after generalised Procrustes analysis are processed by means of Principal Component Analysis (PCA). The variance associated to the asymmetric component is decomposed in two parts describing the percentage of asymmetric variation attributed respectively to Directional Asymmetry (DA, mean difference between sides) and Fluctuant Asymmetry (FA, average differences around mean of asymmetry). We found that the 18.00% of the total variance is associated to bilateral asymmetry. The asymmetric component is composed of 44.44% of directional asymmetry and 55.56% of fluctuant asymmetry. The pattern of cranial asymmetry (directional asymmetry) in females and males is largely overlapped. In both sexes the left posterior portion of the neurocranium is expanded and the left zygomatic region contracted. Neutral variations of cranial symmetry (fluctuant asymmetry) are found in the upper portion of the occipital bone and on the anterior part of the neurocranium. Our findings in contrast with previous literature demonstrate that the pattern of cranial asymmetry is not related to sex nor to cranial size. One of the novelty elements shown in this communication is the possibility to map the pattern of asymmetry based on geometric morphometric and virtual anthropology methods. Future investigations will focus on the study of cranial and brain asymmetry in living and fossil primates.

This research has received funding from the Martí i Franquès fellowship program, under grant agreement 2020PMF-PIPF-43 managed by Andreu Ollé Cañellas.

References: [1] Antonio, P., Costantino, B., Silvia, C., Marina, M., Paolo, P., Alessio, V., Pasquale, R., 2021. Arothron: An R package for geometric morphometric methods and virtual anthropology applications. American Journal of Physical Anthropology 176(1), 144-151. [2] Melchionna, M., Profico, A., Buzi, C., Castiglione, S., Mondanaro, A., Del Bove, A., Sansalone G. Piras P., Raia, P., 2021. A New Integrated Tool to Calculate and Map Bilateral Asymmetry on Three-Dimensional Digital Models. Symmetry 13(9), 1644. [3] Klingenberg, C. P., 2015. Analyzing fluctuating asymmetry with geometric morphometrics: concepts, methods, and applications. Symmetry 7(2), 843-934.

Exploring the impact of sexual dimorphism on cranial asymmetry in a worldwide modern human collection

Antonietta Del Bove[1,2], Antonio Profico[3], Marina Melchionna[4], Pasquale Raia[4], Carlos Lorenzo[1,2]

1 - Department of History, University Rovira i Virgili, Tarragona, Spain -
2 - Department of Quaternary and Prehistory, Institut Català de Paleoecologia Humana i Evolució Social (IPHES_CERCA), Tarragona, Spain -
3 – Department of Biology, University of Pisa, Pisa, Italy -
4 - DiSTAR, University of Naples Federico II, Naples, Italy -

BILATERAL ASYMMETRY

RESULTS

Total Variance

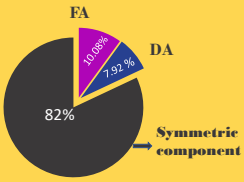

- Fluctuant Asymmetry (FA): differences between sides produced by "developmental noise" in the form of environmental and/or genetic stress;
- Directional Asymmetry (DA): refers to a skewed distribution of asymmetry when comparing the left to the right side of the cranium [4].

Shape variations

Associated with directional asymmetry

Associated with fluctuant asymmetry

Associated with fluctuant asymmetry

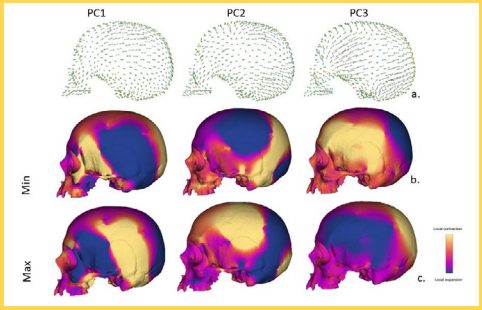

Shape variations associated with the first three PC scores: a) semilandmark displacement on the negative (red) and positive (green) values. Local differences in the area are shown from the mean shape to negative (b) and positive values (c).

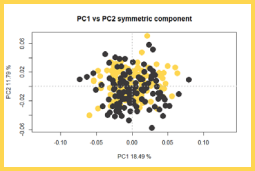

Plot of the first two Principal Components (symmetric component).
Yellow = females; dark gray = males.

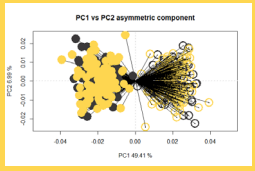

The plot of the first two Principal Components (asymmetric components).
Yellow = females; dark gray = males.
Full and empty dots represent the left and right sides, respectively.

INTRODUCTION

The human cranium exhibits a certain level of asymmetry. Previous studies in primates, fossil hominins and modern human have indicated a relationship between cranial asymmetry and environmental, genetic, and functional factors [1].
In this communication, we applied a geometric morphometric protocol to the quantification and mapping of cranial asymmetry.
In detail, we used a large world-wide sample of modern humans to measure the magnitude and pattern of asymmetry in the cranium.

Is cranial asymmetry related to sexual dimorphism?

Which are the main asymmetric components related to cranial asymmetry?

MATERIALS & METHODS

181 individuals worldwide (89 females & 92 males):

50 fixed landmarks and a symmetric patch of 1000 surface semilandmarks;

analysis was performed in R, with the use of Arothron and Morpho packages [2,3,4]:

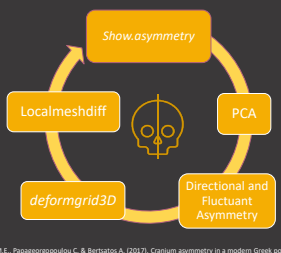

1. Chovalopoulou M.E., Papageorgopoulou C. & Bertsatos A. (2017). Cranium asymmetry in a modern Greek population sample of known age and sex. International journal of legal medicine, 131(3), 803-812.
2. Profico A., Buzi C., Castiglione S., Melchionna M., Piras P., Veneziano A. & Raia P.(2021). Arothron: An R package for geometric morphometric methods and virtual anthropology applications. *American Journal of Physical Anthropology*, 176(1), 144– 151.
3. Melchionna M., Profico A., Buzi C., Castiglione S., Mondanaro A., Del Bove A., Sansalone G., Piras P. & Raia P. (2021). A New Integrated Tool to Calculate and Map Bilateral Asymmetry on Three-Dimensional Digital Models. *Symmetry*, *13*, 1644.
4. Schlager S., (2017) "Morpho and Rvcg–Shape Analysis in R: R-Packages for geometric morphometrics, shape analysis and surface manipulations." *Statistical shape and deformation analysis*. Academic Press, 217-256.
5. Klingenberg C.P. (2015) Analyzing fluctuating asymmetry with geometric morphometrics: concepts, methods, and applications. *Symmetry* 7.2 , 843-934.

DISCUSSION & CONCLUSION

We found that the 18.00% of the total variance is associated to bilateral asymmetry. The asymmetric component is composed by 44.44% of directional asymmetry and 55.56% by fluctuant asymmetry. The pattern of cranial asymmetry (directional asymmetry) in females and males is largely overlapped. In both sexes the left posterior portion of the neurocranium is expanded and the left zygomatic region contracted. Neutral variations of cranial symmetry (fluctuant asymmetry) are found in the upper portion of the occipital bone and on the anterior part of the neurocranium. In contrast with previous literature, our results show how the pattern of cranial asymmetry is not related to sex nor to cranial size. One of the novelty elements shown in this communication is the possibility to map the pattern of asymmetry based on geometric morphometric and virtual anthropology methods. Future investigations will focus on the study of cranial and brain asymmetry in modern humans and fossil hominins.

Acknowledgments
This research has received funding from Martí i Franquès fellowship program, under grant agreement 2020PMF-PIPF-43

heritage

MDPI

Article

Enhancement and Communication of Ancient Human Remains through VR: The Case Study of Sexual Dimorphism in the Human Skull

Roberta Manzollino [1], Saverio Giulio Malatesta [1], Danilo Avola [2], Luigi Cinque [2], Antonietta Del Bove [3,4], Laura Leopardi [1] and Marco Raoul Marini [2,*]

[1] Interdepartmental Research Center DigiLab, Sapienza University of Rome, 11085 Rome, Italy; roberta.manzollino@uniroma1.it (R.M.); saveriogiulio.malatesta@uniroma1.it (S.G.M.)
[2] Department of Computer Science, Sapienza University, 00198 Rome, Italy
[3] Department of History and History of Arts, University Rovira I Virgili, Avinguda de Catalunya 35, 43002 Tarragona, Spain
[4] Catalan Institute of Human Paleoecology and Social Evolution (IPHES-CERCA), Edifici W3, Campus Sescelades URV, Zona Educational 4, 43007 Tarragona, Spain
* Correspondence: marini@di.uniroma1.it or marcoraoul.marini@uniroma1.it

Abstract: Over the last years, the exponential progress of technology introduced a broader population of researchers and developers to the use of Virtual Reality (VR) devices in numerous contexts, e.g., gaming, simulations, and culture dissemination. Recently, cultural heritage has also been supported by motivational experiences and other improvements designed explicitly for specific users (visitors, researchers, and domain experts). In this context, we propose a protocol within a digital environment, using innovative, non-invasive, and non-destructive methods for the technological enhancement, education, and dissemination of ancient human remains. The presented case study is focused on sexual dimorphism in the human skull; several 3D models are digitally generated from female and male skull references exploiting an algorithmic approach with statistical analysis, e.g., Principal Component Analysis (PCA); then, the models are made available in a virtual environment with a Head Mounted Display (HMD) and can also be interacted with via a touchless approach (hands-free). Tests conducted with segmented populations provided promising results.

Keywords: virtual anthropology; sexual dimorphism; BioAnthropology; VR; user experience

Citation: Manzollino, R.; Malatesta, S.G.; Avola, D.; Cinque, L.; Del Bove, A.; Leopardi, L.; Marini, M.R. Enhancement and Communication of Ancient Human Remains through VR: The Case Study of Sexual Dimorphism in the Human Skull. *Heritage* **2023**, *6*, 4120–4133. https://doi.org/10.3390/heritage6050217

Academic Editors: Bruno Fanini, Daniele Ferdani and Alfonsina Pagano

Received: 2 April 2023
Revised: 28 April 2023
Accepted: 3 May 2023
Published: 4 May 2023

1. Introduction

Biological anthropology is the discipline that studies archaeological human remains to obtain information about the lifestyle of ancient populations. Skeletons represent the most direct evidence of past populations [1]. The anthropologist is a highly specialized person who routinely handles human remains, such as skeletons or mummies, to perform the necessary analyses. In particular, bone manipulation is sometimes very important; the rotation and the visualization from all perspectives could help better understand the morphology of a skull, for example. One of the tasks of the anthropologist is to determine the biological sex of the individual. The skeletal regions with the most significant degree of sexual dimorphism, having the most pronounced morphological variation between the sexes, are the skull and the pelvis [2]. While this might seem obvious to professionals in medicine and human anatomy, it is not to an audience of children, teenagers, or ordinary museum visitors. Moreover, understanding this kind of topic could be complex in a specific context; museums that display human remains offer visitors a non-interactive experience, usually limited to simple observation. The specimens are placed behind glass with no opportunity to interact with, touch, or manipulate them for conservation purposes, as with any museum exhibit, as well as ethical concerns [3]. Ancient human remains have high symbolic, emotional, cultural, and religious value, and therefore, they are considered

biology

MDPI

Article

Digital Reconstructions Using Linear Regression: How Well Can It Estimate Missing Shape Data from Small Damaged Areas?

Ana Bucchi [1], Antonietta Del Bove [2,3], Sandra López-Lázaro [1,4], Fernanda Quevedo-Díaz [1] and Gabriel M. Fonseca [1,*]

[1] Centro de Investigación en Odontología Legal y Forense (CIO), Facultad de Odontología, Universidad de La Frontera, Avenida Francisco Salazar 01145, Temuco 4780000, Chile
[2] Departament d'Història i Història de l'Art, Universitat Rovira i Virgili, Avinguda de Catalunya 35, 43002 Tarragona, Spain
[3] Institut Català de Paleoecologia Humana i Evolució Social (IPHES-CERCA), Zona Educacional 4, Campus Sescelades URV (Edifici W3), 43007 Tarragona, Spain
[4] Departamento de Antropología, Facultad de Ciencias Sociales, Universidad de Chile, Santiago 7800284, Chile
* Correspondence: gabriel.fonseca@ufrontera.cl; Tel.: +56-45-232-5000

Simple Summary: Paleontologists, anthropologists and forensic scientists work with skeletal evidence that is often damaged or fragmented. Inferring what the original morphology of the bones was like is important for reconstructing fossils or identifying individuals. In this paper, we evaluate how accurate a statistical method (linear regression) is for estimating missing shape data. For this purpose, we worked with 3D models of complete human zygomatics (a face bone) that were altered to simulate damage, and reconstructed them using this method. We then evaluated how closely the original morphology resembled the reconstructed one. We conclude that this method can faithfully estimate the original anatomical data, especially when the damage is small, but the error increases significantly with increasing damage size.

Abstract: Skeletal remains analyzed by anthropologists, paleontologists and forensic scientists are usually found fragmented or incomplete. Accurate estimations of the original morphologies are a challenge for which several digital reconstruction methods have been proposed. In this study, the accuracy of reconstructing bones based on multiple linear regression (RM) was tested. A total of 150 digital models from complete zygomatics from recent past populations (European and African American) were studied using high-density geometric morphometrics. Some landmarks (i.e., 2, 3 and 6) were coded as missing to simulate incomplete zygomatics and the missing landmarks were estimated with RM. In the zygomatics, this simulated damage affects a few square centimeters or less. Finally, the predicted and original shape data were compared. The results indicate that the predicted landmark coordinates were significantly different from the original ones, although this difference was less than the difference between the original zygomatic and the mean zygomatic in the sample. The performance of the method was affected by the location and the number of missing landmarks, with decreasing accuracy with increasing damaged area. We conclude that RM can accurately estimate the original appearance of the zygomatics when the damage is small.

Keywords: geometric morphometrics; accuracy; cranial reconstruction; craniofacial approximation

Citation: Bucchi, A.; Del Bove, A.; López-Lázaro, S.; Quevedo-Díaz, F.; Fonseca, G.M. Digital Reconstructions Using Linear Regression: How Well Can It Estimate Missing Shape Data from Small Damaged Areas? *Biology* **2022**, *11*, 1741. https://doi.org/10.3390/biology11121741

Academic Editor: Eugénia Cunha

Received: 22 July 2022
Accepted: 26 September 2022
Published: 30 November 2022

Publisher's Note: MDPI stays neutral with regard to jurisdictional claims in published maps and institutional affiliations.

1. Introduction

Digital methods that recreate the anatomy of incomplete bones are relevant for sciences that often work with damaged or fragmentary materials that cannot be replaced, such as fossils or unidentified persons in forensic sciences [1–7]. Digital reconstructions are more automatic and reproducible than manual reconstructions, but it is necessary to know the error associated with these virtual methods to know how accurate the reconstructions are.

Archaeological and Anthropological Sciences (2022) 14: 38
https://doi.org/10.1007/s12520-021-01499-7

ORIGINAL PAPER

Identifying biological affinities of Holocene northern Iberian populations through the inner structures of the upper first molars

Beatriz Gamarra[1,2] · Marina Lozano[1,2] · Antonietta Del Bove[2,1] · M. Eulàlia Subirà[3] · Manuel Edo[4,5] · Concepció Castellana[4] · Josep Maria Vergès[1,2] · Juan Ignacio Morales[1,2,6] · Artur Cebrià[6] · F. Xavier Oms[6] · Carlos Tornero[1,2] · Anna Gómez-Bach[7]

Received: 21 July 2021 / Accepted: 27 December 2021 / Published online: 3 February 2022

Abstract
Neolithisation was a relatively fast process that affected both the interior and coastal zones of the Iberian Peninsula, but it was also a heterogeneous process that had diverse impacts on genomic and cultural diversity. In the Late Neolithic–Chalcolithic, a change in funerary practices, cultural material and trade networks occurred, and genomic heterogeneity decreased, suggesting human mobility and genetic admixture between different Iberian populations. Dental morphology has emerged as an effective tool for understanding genomic variability and biological affinities among ancient human populations. But, surprisingly, less attention has been paid to the morphological traits of inner dental tissues in Holocene European populations and their utility for the study of population dynamics. We applied 3D geometric morphometric methods on the enamel-dentine junction (EDJ) of the first upper molars to explore the biological affinities of north-eastern Iberian Peninsula populations from the Late Neolithic–Chalcolithic to the Bronze Age. Our results show that the EDJ morphologies of the northern Iberian Peninsula populations were generally homogeneous, indicative of genetic admixture as a result of human mobility and exchange networks. However, differences in the EDJ traits in remains from the Can Sadurní site are indicative of distant biological affinities with nearby populations. Additionally, the hypocone associated dentine area and the position of the trigon dentine horns relative to each other on the occlusal surface best describe the variability found among the samples studied. This study highlights the utility of EDJ morphology as a genetic proxy in Holocene population dynamic studies when paleogenomic studies are absent.

Keywords Late Neolithic–Chalcolithic · Iberian Peninsula · Enamel-dentine junction · 3D geometric morphometrics · Upper molar

✉ Beatriz Gamarra
beagamarra@gmail.com

[1] Institut Català de Paleoecologia Humana i Evolució Social (IPHES-CERCA), Zona Educacional 4, Campus Sescelades URV (Edifici W3), 43007 Tarragona, Spain

[2] Departament d'Història i Història de l'Art, Universitat Rovira i Virgili, Avinguda de Catalunya 35, 43002 Tarragona, Spain

[3] Unitat d'Antropologia Biològica, Departament BABVE, Facultat Biociències, Universitat Autònoma de Barcelona, 08193 Bellaterra, Spain

[4] CIPAG, Col·lectiu per a la Investigació de la Prehistòria I l'Arqueologia de Garraf-Ordal. , Passeig de l'Església, 1, 08859 Begues, Barcelona, Spain

[5] Institut d'Arqueologia, Universitat de Barcelona, Gran Via de Les Corts Catalanes, 585, 08007 Barcelona, Spain

[6] Seminari d'Estudis i Recerca Prehistòriques (SERP), Secció de Prehistòria i Arqueologia, Department Història i Arqueologia, Universitat de Barcelona, C/ Montealegre 6-8, 08001 Barcelona, Spain

[7] Departament de Prehistòria, Edifici B Facultat de Filosofia i Lletres, Universitat Autònoma de Barcelona, 08193 Bellaterra, Spain

symmetry

MDPI

Article

A New Integrated Tool to Calculate and Map Bilateral Asymmetry on Three-Dimensional Digital Models

Marina Melchionna [1,*,†], Antonio Profico [2,†], Costantino Buzi [3], Silvia Castiglione [1], Alessandro Mondanaro [4], Antonietta Del Bove [5,6], Gabriele Sansalone [7], Paolo Piras [8] and Pasquale Raia [1]

1 Dipartimento di Scienze della Terra, dell'Ambiente e delle Risorse, Università di Napoli Federico II, 80126 Napoli, Italy; silvia.castiglione@unina.it (S.C.); pasquale.raia@unina.it (P.R.)
2 PalaeoHub, Department of Archaeology, Hull York Medical School University of York, Heslington YO10 5DD, UK; antonio.profico@york.ac.uk
3 DFG Centre for Advanced Studies 'Words, Bones, Genes, Tools', Eberhard Karls University of Tübingen, 72070 Tübingen, Germany; costantino.buzi@uni-tuebingen.de
4 Dipartimento di Scienze della Terra, Università degli Studi di Firenze, 50121 Firenze, Italy; alessandro.mondanaro@unifi.it
5 Departament d'Història i Història de l'Art, Universitat Rovira i Virgili, 43002 Tarragona, Spain; adelbove@iphes.cat
6 Institut Català de Paleoecologia Humana i Evolució Social (IPHES-CERCA), 43007 Tarragona, Spain
7 Function, Evolution & Anatomy Research Lab, Zoology Division, School of Environmental and Rural Science, University of New England, Armidale, NSW 2351, Australia; gabriele.sansalone@uniroma3.it
8 Dipartimento di Scienze Cardiovascolari, Respiratorie, Nefrologiche, Anestesiologiche e Geriatriche, Università degli Studi di Roma La Sapienza, 00185 Rome, Italy; paolo.piras@uniroma3.it
* Correspondence: marina.melchionna@unina.it
† Co-first authorship.

check for updates

Citation: Melchionna, M.; Profico, A.; Buzi, C.; Castiglione, S.; Mondanaro, A.; Del Bove, A.; Sansalone, G.; Piras, P.; Raia, P. A New Integrated Tool to Calculate and Map Bilateral Asymmetry on Three-Dimensional Digital Models. *Symmetry* **2021**, *13*, 1644. https://doi.org/10.3390/sym13091644

Academic Editor: Antoine Balzeau

Received: 22 July 2021
Accepted: 4 September 2021
Published: 7 September 2021

Publisher's Note: MDPI stays neutral with regard to jurisdictional claims in published maps and institutional affiliations.

Abstract: The observation and the quantification of asymmetry in biological structures are deeply investigated in geometric morphometrics. Patterns of asymmetry were explored in both living and fossil species. In living organisms, levels of directional and fluctuating asymmetry are informative about developmental processes and health status of the individuals. Paleontologists are primarily interested in asymmetric features introduced by the taphonomic process, as they may significantly alter the original shape of the biological remains, hampering the interpretation of morphological features which may have profound evolutionary significance. Here, we provide a new R tool that produces the numerical quantification of fluctuating and directional asymmetry and charts asymmetry directly on the specimens under study, allowing the visual inspection of the asymmetry pattern. We tested this *show.asymmetry* algorithm, written in the R language, on fossil and living cranial remains of the genus *Homo*. *show.asymmetry* proved successful in discriminating levels of asymmetry among sexes in *Homo sapiens*, to tell apart fossil from living *Homo* skulls, to map effectively taphonomic distortion directly on the fossil skulls, and to provide evidence that digital restoration obliterates natural asymmetry to unnaturally low levels.

Keywords: asymmetry; *show.asymmetry*; fossil; virtual anthropology; geometric morphometrics; Arothron

1. Introduction

Most living organisms present bilateral symmetry, meaning that the left and right sides of the body represent an almost perfect reflection of one another about the medial plane. However, perfect symmetry is virtually absent in nature, and minor, localized deviations from perfect symmetry are common. Asymmetry can thus be defined as a deviation of the shape from a perfectly mirrored image of the counter-side of a bilateral object. The observation and quantification of asymmetry patterns in biological structures are keenly studied by evolutionary and developmental biologists, anthropologists, and paleontologists. There are three different types of asymmetries in living organisms: (i) fluctuating asymmetry,

Received: 15 June 2019 | Revised: 13 July 2020 | Accepted: 15 July 2020
DOI: 10.1002/ajpa.24127

RESEARCH ARTICLE

American Journal of PHYSICAL ANTHROPOLOGY WILEY

Insertion sites in manual proximal phalanges of African apes and modern humans

Ana Bucchi[1,2] | Javier Luengo[1,2] | Antonietta Del Bove[1,2] | Carlos Lorenzo[1,2]

[1]Departament d'Història i Història de l'Art, Universitat Rovira i Virgili, 35 Avinguda de Catalunya, Tarragona, Spain

[2]Institut Català de Paleoecologia Humana i Evolució Social (IPHES), 4 Zona Educacional, Campus Sescelades URV (Edifici W3), Tarragona, Spain

Correspondence
Ana Bucchi, Departament d'História i História de l'Art, Universitat Rovira i Virgili, 35 Avinguda de Catalunya, Tarragona, 43002, Spain.
Email: anabucchi@gmail.com

Funding information
Agència de Gestió d'Ajuts Universitaris i de Recerca, Grant/Award Number: 2017 SGR 1040; Consejo Superior de Investigaciones Científicas, Grant/Award Number: PGC2018-093925-B-C32; Fondo de Fomento al Desarrollo Científico y Tecnológico

Abstract

Objectives: The primary aim of this study was to describe the insertion sites of the ligaments holding the *flexor digitorum profundus* and *superficialis* muscles (flexor ridges) in proximal phalanges 2–5 of African apes and modern humans. To interpret differences in flexor ridge size based on general behavioral differences among taxa.

Materials and methods: We analyzed 3D models of manual proximal phalanges 2–5 from 29 gorillas (*Gorilla beringei* and *Gorilla gorilla*), 30 chimpanzees (*Pan troglodytes*) and 36 recent modern humans. Flexor ridges (mm^2) were compared within and across genera.

Results: Gorillas and chimpanzees had larger flexor ridges for phalanges 2–4 than humans and this difference subsists when controlling for body size. Each genus had a unique insertion size pattern across the digits, with the most heterogeneous pattern found in chimpanzees, followed by humans, and lastly gorillas. These patterns corresponded strongly to the differences in the size of the phalanges within each genus, except for phalanx 5 in humans, which had a larger flexor ridge than expected.

Discussion: When comparing these genera, the flexor ridges signal differences between taxa that use their hands for manipulation and locomotion (gorillas and chimpanzees) and taxa that use them exclusively for manipulation (humans). This functional signal was also apparent in the PP5 of humans, whose larger FR may be indicating the high recruitment of this digit during forceful precision grip characteristic of humans.

KEYWORDS
flexor ridges, functional morphology, insertion areas, manipulation

1 | INTRODUCTION

The flexor ridges are the insertion areas of the ligaments of the fingers which hold the synovial sheaths of the tendons of both the *flexor digitorum profundus* (FDP) and *superficialis* (FDS) muscles, the main flexors of the digits. During climbing and suspension both muscles are strongly recruited (Susman & Stern, 1979) and are also slightly active during knuckle-walking (Susman & Stern, 1979; Tuttle, Shine, Basmajian, & Regenos, 1972), the most frequent form of locomotion in African apes (Table 1).

Here we analyzed the areas of the flexor ridges (FR, in mm^2) in the proximal phalanges of adult gorillas (*Gorilla beringei* and *Gorilla gorilla*), chimpanzees (*Pan troglodytes*), and recent modern humans (*Homo sapiens*) (Table 2). We did this in order to (a) compare the FR of proximal phalanges 2–5 (PP2–PP5) between African apes and modern humans, and (b) determine whether variation in the FR patterns indicates functional differences in the use of the hands.

Humans use their hands exclusively for manipulation while African apes use them for manipulation and travel, which may have an effect on FR size. We expect that African apes will have larger FR than humans in all phalanges, since locomotion and manipulation require generation of higher manual forces than manipulation alone. This expectation is founded on previous electromyographic research that showed that FDP and FDS muscles are active during manipulation of

8.3 Curriculum Vitae

Antonietta Del Bove CV

CV date	05-10-23

Personal information

First name	Antonietta		
Family name	Del Bove		
Gender	Female	Birth date	18/06/87
Passport Number	YB5284844		
Professional address	IPHES-CERCA. Zona Educacional 4 – Campus Sescelades URV (Edifici W3). 43007 – Tarragona, Spain.		
E-mail and URL	antoniadelbove@gmail.com www.researchgate.net/profile/Antonietta-Del-Bove		
ORCID https://orcid.org/0000-0001-6620-4514			

According to law 679/2016 of the Regulation of the European Parliament of 27th April 2016, I hereby express my consent to process and use my data provided in this CV and application for recruiting purposes.

Current position

Position	Martí-Franquès Research PhD Grant Programme. Universitat Rovira i Virgili 2020PMF-PIPF-43.		
Initial date	2021		
Institution	Universitat Rovira i Virgili (Spain)		
Department/Center	(IPHES-CERCA) Institut Català de Paleoecologia Humana i Evolució Social		
Country	Spain	Tel. number	+34 653526221 +39 3290653115
Keywords	*Paleoanthropology, Prehistory, Geometric Morphometrics, Virtual Anthropology, Archaeology*		

Education

Period	Degree
2021 - 2023	PhD student Martí-Franquès Research PhD Grant Programme. 2020PMF-PIPF-43. Universitat Rovira i Virgili (Spain). “Sexual dimorphism in human modern crania with GM and NNA approach”. Supervised by Antonio Profico Ph.D. and Professor Carlos Lorenzo.

2015	Master in Archaeology (Prehistory) Universita degli Studi di Firenze (Italy). Full score with Laude 110 / 110. "Scoglietto's cave (Alberese Tuscany): revision of the remains excavations of Cardini and Rittatore Vonwiller (1948-1952)". Supervised by Prof. Fabio Martini and Prof. Jacopo Moggi Cecchi.
2011	Degree in History and Protection of Archaeological Heritage. Universita degli Studi di Firenze (Italy). "Evolution of manipulative capability from Hominini fossils to Homo sapiens". Supervised by Prof. Fabio Martini and Prof. Jacopo Moggi Cecchi.

CV summary

Currently, I am a Ph.D. candidate specializing in **palaeoanthropology** at the University Rovira i Virgili, Tarragona (Spain) and associate researcher at IPHES-CERCA. My Ph.D. research is focused on advancing our understanding of sexual dimorphism of the human modern cranium through the application of diverse techniques as **Geometric Morphometrics**, with a particular emphasis on virtual anthropology. My research direction is anchored in prehistoric research and encompasses other human species than modern ones, as well as in the study of long bones from the appendicular skeleton. In addition, I am familiarised with microtomographic acquisitions (see in following section about the paper: Gamarra et al., 2022) and, in the **development of methodological tools** for automatic identification, driving innovation at the intersection of new approaches to solving old questions in physical anthropology. Despite my formation being about **traditional anthropology**, in fact, during my training years at the University of Florence (Italy) and while working with the Superintendence of Florence (Italy) at the Bioarchaeology laboratory, I enriched my knowledge of traditional anthropology with the analysis and study of two important caves of Chalcolithic and Bronze Age chronology (Grotta dello Scoglietto MNI= 42 individuals, Grotta della Spinosa MNI= 41 individuals). These prior experiences and the knowledge of skeletal anatomy in a traditional manner were undoubtedly a source of enrichment for the development of my skills in my research focused on virtual anthropology and its application. I explored different approaches such as **GMM analysis and Neural Network Analysis** (Del Bove, Veneziano; 2022).

To date, I have a total of 10 publications (2017-2020), **9 of which were indexed publications** (SCOPUS). In 4 out of these 10 publications, I was the first author or corresponding author. All my data and analysis are published in open repositories. Also, I am an editor and board member of the **Data in Brief** journal for Elsevier.

Publications

2023 R. Manzollino, S.G. Malatesta, D. Avola, L. Cinque, **A. Del Bove**, L. Leopardi and M. R. Marini.Enhancement and Communication of Ancient Human Remains through VR: The Case Study of Sexual Dimorphism in the Human Skull. Heritage, 6(5), pp. 4120-4133 https://doi.org/10.3390/heritage6050217

2022 Bucchi, A., **Del Bove, A.**, Lopez-Lazaro, S., Quevedo-Diaz, F., Fonseca, G.M. Digital Reconstructions Using Linear Regression: How Well Can It Estimate Missing Shape Data from Small Damaged Areas? Biology,11(12), 1741 https://doi.org/10.3390/biology11121741

2022 **Del Bove, A.**, Veneziano, A. A Generalised Neural Network Model to Estimate Sex from Cranial Metric Traits: A Robust Training and Testing Approach. Applied Sciences, 2022, 12 (18), 9285 https://doi.org/10.3390/app12189285

2022 Gamarra, B., Lozano, M., **Del Bove, A.**, (…) Gomez-Bach, A. Identifying biological affinities of Holocene northern Iberian populations through the inner structures of the upper first molars. (3/12) Archaeological and Anthropological Sciences. 2022, 14(3), 38 https://doi.org/10.1007/s12520-021-01499-7

2021 M. Melchionna, A. Profico, C. Buzi, S. Castiglione , A. Mondanaro, **A. Del Bove**, G. Sansalone, P. Piras, P. Raia. A new integrated tool to calculate and map bilateral asymmetry on three-dimensional digital models, Symmetry, 2021, 13(9), 1644, https://doi.org/10.3390/sym13091644

2020 **Del Bove, A.**, Profico, A., Riga, A., Bucchi, A., Lorenzo, C A geometric morphometric approach to the study of sexual dimorphism in the modern human frontal bone.. American Journal of Physical Anthropology, 2020, 173(4), pp. 643-654 https://doi.org/10.1002/ajpa.24154

2020 Bucchi, A., Luengo, J., **Del Bove, A.**, Lorenzo, C. Insertion sites in manual proximal phalanges of African apes and modern humans. American Journal of Physical Anthropology, 2020, 173(3), pp. 556-567 https://doi.org/10.1002/ajpa.24127

2020 **A. Del Bove**, B. Aranguren.L'utilizzo di grotte funerarie nell'Italia centrale in eta protostorica. Il caso studio di Grotta della Spinosa (Massa Marittima). XV Incontro di studi di Preistoria e Protostoria2019 Detection of sexual dimorphism in the human neurocranium at local scale.

2019 **Del Bove, A.**, Profico, A., Lorenzo, C. 2019 IMEKO TC4 International Conference on Metrology for Archaeology and Cultural Heritage, MetroArchaeo 2019, pp. 571-575. https://www.imeko.org/publications/tc4-Archaeo-2019/IMEKO-TC4-METROARCHAEO-2019-111.pdf

2019 Antonio Profico, Paolo Piras, Costantino Buzi, **Antonietta Del Bove**, Marina Melchionna, Gabriele Senczuk, Valerio Varano, Alessio Veneziano, Pasquale Raia, Giorgio Manzi Seeing the wood through the trees. Combining shape information from different landmark configurations. Hystrix It. J. Mamm. 2019;30(2):157-165

https://doi.org/10.4404/hystrix-00206-2019

2018 **A. Del Bove**, E. Pacciani, M. Aranguren. Human skeletal remains from the eneolithic of Spinosa Cave (Grosseto, Tuscany) Italy. Proceedings of UISPP 2018.

Dataset

Ana Bucchi**, Antonietta Del Bove,** Sandra López-Lázaro, Fernanda Quevedo-Diaz and, Gabriel M. Fonseca is published in *Biology* **2022,** *11*(12), 1741. The landmarks dataset that support the findings of this study are openly available in **Zenodo** at **https://doi.org/10.5281/zenodo.6857007.**

Del Bove, A., Veneziano, A. 2022. A Generalised Neural Network Model to Estimate Sex from Cranial Metric Traits: A Robust Training and Testing Approach

Applied Sciences (Switzerland), 2022, 12(18), 9285. The code to reproduce the analysis, the model generated, and the script to use the model are made publicly available on **GitHub** at the following link: **https://github.com/AlessioVeneziano/Papers/tree/main/DelBove_%26_Veneziano_2022.**

Gamarra, B. & **Del Bove, A.** 2022

Identifying biological affinities of Holocene northern Iberian populations through the inner structures of the upper first molars. The data that support the findings of this study is available at **https://zenodo.org/record/5891983#.Y5S4lXb-MI2w**. and the surface are available at **MorphoSource.org.**

Editor of Journal

10-08-2023 Editorial Board Member with Data in Brief journal, multidisciplinary, open access, peer-reviewed journal, Elsevier

Congresses (last 5)

I've participated with poster or oral presentations at more than **20 congresses** (ESHE 2022,2021, 2020, SAP 2021, 2020, AAI 2022, AABA 2022, Uispp 2018 etc.).

Following last 5 contributions to congresses:

2023 29th EAA (Annual Meeting of the European Association of Archaeologists), Belfast (Northern Ireland).

1)Poster: "From the prehistoric site to the cloud: The IPHES-CERCA Open Data approach", session "Replicable Archaeology: Looking for Workflows and Data Management Strategies. Fostering Data Reuse and Methodological Transferability in Archaeological Science". Marta Fontanals, Javier Sopesens, Amèlia Bargalló, **Antonietta Del Bove**, Bruno Gómez de Soler, Jordi Revelles, Antonio Rodríguez, Ignasi Pastó.

2) Poster: "It Takes a Village: Interdisciplinary Bioarchaeological Research on the Role of Children in the Past". Sara Bernardini, Gwenaëlle Goude, Kerry L. Sayle, Caroline Gauthier, Eric Douville, Biancamaria Aranguren, **Antonietta Del Bove** , Mary Anne Tafuri.

2022 Congress ESHE XII meeting (European Society for Human Evolution)."Exploring the impact of sexual dimorphism on cranial asymmetry in a Worldwide modern human collection". **Antonietta Del Bove**, Antonio Profico, Marina Melchionna, Pasquale Raia, Carlos Lorenzo.

2022 AAI (Italian Anthropological Association). "A comparison of endocranial occipital bone morphology in modern human and fossil hominins". Riccardo Frittitta, Antonio Profico, **Antonietta del Bove**, Dominique Grimaud-Hervé, Julie Arnaud.

2022 AABA 2022 (communication) "Bilateral asymmetry and sexual dimorphism in the human cranium". Del Bove Antonietta, Profico Antonio, Melchionna Marina, Raia Pasquale, Carlos Lorenzo.

Research grants and awards

2023 ***Wenner*-Gren Foundation** Grant for Conference ($18.570,00 for AHEAD meeting 2023 -Tarragona https://ahead-meeting.org/).

2022 Poster Prize co-author ESHE2022.

2022 Travel Grant ESHE.

2021-2023 Martí-Franquès Research Grants Programme. Doctoral Grants. 2021. 2020PMF-PIPF-43.

2019 Scholarship by Atapuerca Foundation to excavate to Dmanisi (Georgia).

2019 Poster prize AAI (Italian Association of Anthropology).

2018 Scholarship “Course of Anatomical Network Analysis (AnNA)” Transmitting Science Ltd.

2017 “Tornosubito” Project. Lazio fellowship 10.291,29 €.

Research projects and affiliations

Social, cultural and Biological Evolution during the pleistocene (StEP), coord.: Dr. Andreu Olle (AGAUR), 2022-2024. Ref. Code: 2021 SGR01239.

Eco-Social behaviour of the Sierra de Atapuerca Hominins during Quaternary, VI. PI: Dr. M. Mosquera, Dr E. Carbonell. Ministerio de Ciencia e Innovacion, 2022-2025. Code: PID2021-122355NB-C32.

Arrels prehistoriques de la transhumancia a l’Alt Ripolles: project Arqueològic 2022-2025. PI: Carlos Tornero. Departament de Cultura. Generalitat de Catalunya. 2022-2025 Ref. Code: CLT009/ 22/00042.

Affiliated Italian Anthropologist (III level). From 2019.

Member ESHE, European Society for the Study of human Evolution. From 2017.

Member 3P, Progetto preistoria Piemonte. From 2016.

Participation in archaeological and anthropological excavations

2023-2018 Sierra de Atapuerca (Burgos, Spain)

2022 Barranc de la Boella (Tarragona, Spain)

2021-2022 Cova de la Villa (Catalunya-Spain)

2019-2023 Cova de Xaragalls (Catalunya-Spain)

2018 Dmanisi (Georgia)

2015 Ciota Ciara Cave (Italy)

2013 Erimi - Laonin tou Porakou (Cyprus, Limassol)

2011 Olduvai (Tanzania)

2011 Drimolen (South Africa)

2007-2015:

• Romito cave (CS, Italy)

• Isolino di Varese (VA, Italy)

• Scoglietto cave (GR, Italy)

- Isola del Lazzaretto Nuovo (VE, Italy)
- Sesto Fiorentino (FI, Italy)
- Firenzuola (FI, Italy)
- Balzi Rosssi (GE, Italy)
- Poggio Uccellaia (FI, Italy)

Board Memberships

Next 15/16/17-11-2023 Co-organizer of the International Congress AHAED. Advances in Human evolution and diversity. Venue: Tarragona (Spain). Number of attendants: 120. https://ahead-meeting.org/

03-02-2023 Scientific Commission of UISPP for the Biological Anthropology committee.

07-12-2022 Organizer workshop with Ana Bucchi Ph.D. Workshop Title: “Workshop introducción a la Morfometría geométrica en 2D y 3D.”. Venue: Universidad de la Frontera (Chile) (online). Approximate number of attendants: 12.

2022 Member of RRI Open Science Working Group of IPHES-CERCA.

30 and 31 -01-2020 Organizer workshop with Prof. Carlos Lorenzo. Title: “R-workshop for the study of Human Evolution” Venue: IPHES (Tarragona, Spain). Approximate number of attendants: 25. Researchers: Antonio Profico Ph. D. and Alessio Veneziano Ph.D.

Visiting experience

From 4-03-219 to 30-09-2019 (7 months) international Mobility to the Anthropologica Museum of Rome La Sapienza, director of project Prof. Giorgio Manzi.

From 28-06-2018 to 30-07-2018 (1 month) International al Mobility to the Anthropological Museum of Florence (It aly), director of osteological collection Dr. Monica Zavattaro and Prof. Jacopo Moggi Cecchi.

Academic supervision

19-07-2022- Co-supervisor: Master thesis , “An ontogenetic perspective on the emergence of sexual dimorphism in the modern human cranium.” Candidate: Jessica Armando. Full score with laude. M. Sc. in Quaternary, Prehistory and Archaeology at University of Ferrara (Italy).

Attended courses certified

21/30-01-2019 Advanced course of Statistics on the use of software R.

Department of Environmental Biology, Sapienza University of Rome, Italy.

22/26-10-2018 Course of Anatomical Network Analysis (AnNA), coord.: Dr. Diego Rasskin-Gutman (Cavanilles Institute of Biodiversity and Evolution Biology, Spain) and Dr. Esteve-Altava (Pompeu Fabra University, Spain).

26/30-05-2017 Examples of multivariate data analysis in bio-archaeology. University of Pisa (Italy) Department of Medicine.

26/30-06-2017 Summer school of “Acquiring and post- processing 3D data in anthropology”. Organized by University of Bologna (Italy). Lectures: Dr. Stefano Benazzi & Dr. Timothy M. Ryan.

20-09-2017 EVAN Toolbox Training Day - Form and shape analysis of complex geometries. EVAN Society, Vienna, Austria.

20/25-02-2012 Perugia School of Paleoanthropology (Winter School) - 2nd level. University of Perugia, Italy.

14/18-02-2011 Perugia School of Paleoanthropology (Winter School) - 1st level. University of Perugia, Italy.

Invited Talks- Lectures

24-02-2022 “Walking into the future. New technologies, new approaches and new limitations to study human evolution”. Authors: Del Bove A. and Rodriguez. A. Organizer: Open Science Working Group IPHES-CERCA.

10-06-2022 “New frontiers in biological anthropology: sexual dimorphism in skeletal remains”. Field school of Orozmani (Dmanisi-Georgia). Organizer: Giorgi Bidzinashivili.

13-09-2022 “New solution for old problems: a case of study of sexual dimorphism

in the human cranium". Field school of Orozmani (Dmanisi-Georgia). Organizer: Giorgi Bidzinashivili.

11-02-2021 Dia Internacional de les Dones i les Nenes en la Ciencia. Projecte #100tifiques. Organizers: Fundació Catalana per la Recerca and Barcelona Institute of Science and Technology (BIST).

Work Experiences

2020- feb-2024 Martí-Franquès Research Grants Programme. Doctoral Grants. Universitat Rovira i Virgili Tarragona (Spain).

2017- 2018 Project "Torno Subito" between the Anthropological Museum of Rome La Sapienza (Roma, Italy) and Universitat Rovira i Virgili (Tarragona, Spain). "Study of modern cranial collection from Lazium".

April - May 2018 Kids Workshop of Prehistory at School (for children between 8 -10 years old) School "Don Bosco", ITRI (LT, ITALY).

2016 Supervisor of anthropological excavation for ancient Roman burial, Rome (ITALY).

2015-2018 Anthropologist freelance for the lab of Bio-archaeology of the Archaeological and Heritage Superintendence of Florence (ITALY). Directed by Dr. Elsa Pacciani.

from 29-10-2015 to 28-11-2016 Cataloguer and Librarian at Italian Institute of Prehistory and Protohistory of Florence (Italy) contracted by national office of the Italian civilian service.

from 01-05-2011 to 30-07-2011 Traineeship as Librarian at Humanities Library of Universita degli Studi di Firenze (Italy).

--08-2007 Archaeologist at prehistory excavation of Sesto Fiorentino (Florence, Italy).

Technical Skills

Due to different course and collaborations with other researchers along my carrer. I am an advanced user in main **software and computer languages** used in paleoanthropology. In addition, as a member of the Open **Science Working Group** at my current institution, I am also proficient in managing different types or data and code repositories (i.e. Github or open repositories of Zenodo, Morphosource, etc.). I am a user of a lot of packages of R language for Geometric Morphometrics as Arothron (used it to analyse the Landmarks formatted by Amira or Avizo software), Morpho and geomorph (for Multivariate Analysis) rgl (for 3D

modeling) and Morphomap (Extract cross sections from long bone meshes at specified intervals along the diaphysis) and Endomaker (to extract the internal surface of bones).

Programming Language

R(packages: Arothorn, Morpho, geomorph, rgl, stringr, ggplot2… etc)

Python (Library: Pandas, Biophyton)

Software Expertise

Amira / Avizo (for landmarks configuration, segmentation, 3D visualization, movie maker etc...)

Materialize (segmentation)

Geomagic, Meshmixer (mesh repair and mesh analysis)

MorphoJ (analysis)

3D slicer (segmentation)

Agisoft photoscan (3d Model)

Viewbox (semilandmark configuration)

Meshlab (visualization)

Artec3D (surface scanner 3D)

Languages

Italian mother tongue

English (B2 UNIFI)

Spanish (B2.1 URV)

French (B2 UNIFI)

German (A2)

UNIVERSITAT ROVIRA I VIRGILI
A COMPUTATIONAL RE-ASSESSMENT OF SEXUAL DIMORPHISM IN THE HUMAN CRANIUM BEYOND TRADITIONAL MORPHOMETRICS: GEOMETRIC MORPHOMETRIC METHODS AND NEURAL NETWORK ANALYSIS
Antonietta Del Bove

Acknowledgements

- I would like to express my deepest gratitude to the following institutions, the URV for accepting my Ph.D. candidate these years, and the program Martí-Franquès Research Grant Programme (code 2020PmF-PIPF-43).
- The Catalan Institute of Human Paleoecology and Social Evolution IPHES-CERCA to host me as an associate researcher, the Director Dr. Robert Sala Ramos, the research director Dr. Xosé Pedro Rodríguez Alvarez, and the Research Career Development Dr. Ignasi Pastó Marin. Special thanks to Dr. Marina Lozano, head of the Laboratory of Palaeoanthropology.

The institutions and collection managers who provided access to the samples I needed for my research:

- Prof. Giorgio Manzi of the University of Rome La Sapienza;
- Prof Jacopo Moggi-Cecchi, University of Florence
- Dr. Lumila Menéndez of University of Bonn.
- Dr. Josep Maria Vergès, IPHES
- Dr. Carlos Tornero, University Autonoma Barcelona.

The University of Rome La Sapienza, the Museum of Anthropology "G. Sergi", the Museum of Anthropology of Florence University, and Prof. Giorgio Manzi for their support during my mobility. The "Torno Subito program" funded by Regione Lazio supported my mobility to Rome. I am also thankful to Prof. Mary Anne Tafuri, Prof. Robert Paine, Dr. Micarelli Ileana, Dr. Sara Bernardini, and Dr. Carlotta Zeppilli of the Lab of Anthropology at Rome La Sapienza.

Moreover, during those years of Ph.D. I also was part of three research projects and research groups:

- Eco-Social behaviour of the Sierra de Atapuerca Hominins during Quaternary, VI, IP: Dr M. Mosquera, Dr E. Carbonell, funder: Ministerio de Ciencia e Innovación. Reference Code: PID2021-122355NB-C32
- Social, Cultural and Biological Evolution during the Pleistocene (StEP)
  Coordinator: Dr. Andreu Ollé, Funder: Agència de Gestió d›Ajuts Universitaris i de Recerca (AGAUR)
  Reference Code: 2021 SGR 01239 (double filiation IPHES-URV Group)
- Arrels prehistòriques de la transhumància a l'Alt Ripollès: Projecte Arqueològic 2022-2025
  Principal Investigator: Dr Carlos Tornero, Funder: Departament de Cultura, Generalitat de Catalunya, Reference Code: CLT009/22/00042

I would like to extend my heartfelt gratitude to my directors Prof. Carlos Lorenzo and Dr. Antonio Profico.

I want to express my gratitude to Carlos for accepting this challenge even before we met, a testament to his trust in me. I hope I have repaid that trust and not disappointed. Throughout my time in Tarragona, working with Carlos has been a pleasure. He has provided unwavering support, backing, and invaluable advice, always delivered with a diplomatic touch. I am thankful for the times he stood by me, providing a sense of security that served as an incentive to excel and improve. Our meetings, often centered around topics like statistics and software, have been learning experiences. I also appreciate the freedom he granted me to direct my research, collaborations, and even the occasional escape from my responsibilities to participate in excavation work. Carlos, you have been an exceptional mentor, and I hope to have the opportunity to work together again in the future as a Doctor.

I met Antonio one day in Rome at the university, and I believe his first words were, 'Interesting, we could study this and this...'. Antonio, thank you for everything.

Before expressing my gratitude to Antonio for his daily assistance, support, and occasional tolerance of my emails as I worked through results independently, I must thank him for instilling in me the ethics and fundamental respect required in the research world. Respecting others' work and ideas and presenting one's results with humility are essential aspects of our field. Antonio emphasized that in the academic world, no one should be seen as a rival, and our only path to progress is through collaboration.

Of course, I wouldn't even know what a landmark is without Antonio! My academic path had always leaned more toward traditional anthropology, but he opened up a new world for me with GM. With his patience and dedication to developing me as a researcher, I understand that I have a responsibility to invest in my own growth, and I hope in the future to be as generous a mentor to others as Antonio has been to me.

Thank you to the Atapuerca Foundation for funding my excavation fieldwork at Dmanisi. The entire team of Dmanisi to host me, in particular Dr. Ann Margvelashvili, Giorgi Bidzinashvili, and Giorgi, Khatuna, Sopho, and in memoriam of Gocha.

Now I apologize to the readers, but I have decided to write the rest of the acknowledgments in Spanish, the language of my last 5 years.

El IPHES, no ha sido solo una institución ha sido un hogar, gracias a todos, seguro que alguno me lo voy a olvidar pido disculpa.

Como he dicho antes, el laboratorio de paleoantropología, la Doctora Marina Lozano, Carlos y los investigadores que en estos años han estado: Ana Bucchi, Mikel Arlegi, Beatriz Gamarra, Raquel Hernando, Alfredo Suesta, Costantino Buzi, Federica Landi y Alessio Veneziano.

Estos años he trabajado viendo trabajar a muchos del Iphes y tengo que admitir que sois increíbles, esta oportunidad de estar al lado de algunos de los mejores investigadores de Prehistorias ha sido una de la oportunidad más grande que he tendido de crecer a nivel profesional y personal.

In primis, agradezco el Dr. Andreu Olle por ser no solo el jefe del Sgr a que pertenezco si no también el tutor de mi beca doctoral. A la Dr. Marina Mosquera por el proyecto Atapuerca. A Eudald Carbonell por haber creído en tiempo inmemorables en algo de tan grande y haberlo realizado.

En el Iphes puedes hacer una tesis o decidir de hacer una tesis y vivir un experiencia de vida, yo hice la segunda..

A Ignasi Pastò, para haber sido el verdadero supervisor de mi carrera y de mi doctorado, para haberme dicho siempre que era posible, como algunas ideas un poco pretenciosas como organizar un congreso en el último año de un doctorado, pues gracias. Gracias para haberme explicado cómo se escribe un proyecto, como se hace una entrevista y contado donde se puede ir a cenar arroz del Delta en Tarragona. Espero de escribir muchos proyectos contigo y que sean todos ganadores.

Ya, que voy por el sentimental, la Doctora Gema Chacón, guerrera incansable, mientras los escribo me imagino la sonrisa del Doctor Florent Rivals de aprobación. Yo por ti no tengo palabras más de gracias. Un día de hace 5 años llegué al Iphes y me dijiste: “si necesitas ayudas pide!” lo hice y abriste hasta tu casa. La generosidad no se puede explicar es algo con mucha humildad se reconoces y se valora con lealtad. Lo digo siempre yo de adulta quiero ser una Gema ¡ojalá ¡

Esta progresión por lo sentimientos me lleva a mi director de excavación. He excavado con muchos, nos os ofendéis llegas también vuestra ronda, pero aquí es destacar una persona con queiría a excavar hasta la luna, y se lo pidiera iría también a palear por días o abrir puertas imaginarías en cueva picando por un par de campañas de excavaciones. El Dr. Josep Vallverdú, ¡Pep gracias! nos has cuidado con un amor increíble, es un placer trabajar en tus excavaciones, siempre se aprende de geología y cocina típica, y la verdad que me encanta hacer parte del team “duro”. P.s. cuando vamos a Xaragalls?

Vale, ha llegado vuestro turno, Galeria de Atapuerca: mis jefas Isabel Casares y Paola Medrano. Que decir ¿Como lo pasamos bien ¡La calidad hace que todo sea fácil, por calidad quiero también incluir mis días en el que el ser rubia me impone de resetear la estación total tres veces!. Por completar esta ronda de Galería no podría no agradecer también Paula, Hector y Irene, hasta siempre rubias ¡

Palmira Saladìe gracias ¡cuántas paciencia se puede tener para organizar todo a la perfección y tener también la capacidad de acordarse mis alergia a cada excavación. y también a nivel de investigación he aprendido muchos sobre tafonomía gracias a vuestro grupo¡ gracias Palmi!

En el iphes aprendí mucho da dos investigadores respecto a los cuales la profesión se mezcla a la amistad: Antonio Rodriguez y Mikel Arlegi. No creo hace falta escribirlo en una tesis cuanto sois importantes y que tengo un aprecio profesional y humano increíble para vosotros dos.

El grupo de Open Science: Ignasi, Marta, Javier, Bruno, Amelia, Sandra, Antonio, Ana, Miguel, Jordi.

A todos los investigadores con que he tenido la oportunidad de conocer y que han influenciado mis decisiones:

Gracias a Rosas Huguets, Juan Manuel Lopez Garcia, Hugo Blain, Diego Lombao, Aitor Burguet, Monica Fernendez, Sandra Bañuls, Jose Ramon Rabuñal, Roser Marsal, Alessandra Varalli, Irene Dori, Julie Aranaud, Marta Arzarello, Carmen Nuñez, Ivan Rey, Florent Rivals, Deborah Barsky, Stefania Titton, Marta Modolo, Juan Marin, Juan Ignacio Morales, Maria Soto, Emiliano Bruner, Vitale Sparacello, Alessandro Riga, Nohemi Sala, Adrian Pablo, Davide Bertè, Asier Gomez, Rolf Quam, Helena Santos, Jhon Wilmann, Tommaso Mori, Marco Cherin, Alessio Veneziano, Julia Aramendi, Julia Galan, Giulia Ricci, Silvia Florindi, Bianca Maria Aranguren, Pasquale Raia y muchos más.

Mis compañeros: Hector, Paula, Irene, Andion, Mary Pictures, Filippo, Gorkem, Clara, Mario, Francesc, Celia, Edgar, Toni, Sabrina, Lloyd, Pam, Almudena, Chiara, Valentina, Adrian, Esther, Elena, Riccardo frittita, Ibi, Maria Boada, Anna Paola y Maria Silva (que no son iphes pero lo son de corazon) y Ivan R.

Chiara, grazie per avermi accompagnato in questa avventura, fatta di dialoghi in spagnolo e sentimenti italiani. .

Alfredo, has ido un placer compartir contigo todo este momento. Ya se que no te lo vas a creer pero vuelve pronto que me aburro sola y aunque no lo vuelveré a repetir te agradezco mucho estos años bonitos.

El Iphes no sería lo mismo sin Felix, Vanessa, y Marta esenciales.

A todos aquello que están conmigo en este momento organizando el AHEAD: estaìs haciendo real un sueño que tenía desde muchos años.

Del lo organizadores del AHEAD, querìa distacar Garcia Latorre por la ayuda del congreso y la charlas bonitas via twitter!

A mis grupos de italiano de paleoantropologia: Federica, Costantino, Alessio... cuantos años y cuantas historias se podrìan contar ! vi voglio bene !
LA 3P: progetto Preistoria Piemonte a tutti voi grazie!

A mi familia no aquella de verdad, aquella que la vida te impone por pobreza de tener que compartir pisos: a la primera compañera de piso Raquel Hernando, siempre lo digo vivir contigo ha sido fácil a parte por el inglés.

Mientras no puedo decir lo mismo de la segunda familia: los “niños”: Miguel Noè y Andrea.

Miguel, eres estupendo no tengo nada que decirte, me acuerdo de aquella conversación en la cocina recién llegada en casa y desde entonces fue solo amor. (un besito a mi mi suegra tb). Acabar la tesis contigo ha sido un regalo de la vida !

Noè, sé que te trato mal pero no haces nada para que no sea así!es broma, cuantas conversaciones aún faltan para tener sobre cine, cervezas y música, peque que voy a ser Doctora Spaghetti!

Andrea, es que tú y yo no somos capaz de decirnos que nos apreciamos verdad? pero siempre contigo a tu lado… a ver a veces demasiado contigo un poco de privacy en Atapuerca no sería mal.

Ultima, Ana, gracias para haberme dejado el amor por la montaña pequeño d… y por los

abrazos sinceros y espontáneos que te he proibido de darme!

Héctor, no eres mi compañero de piso, pero da igual estas más metido en mi vida que cualquiera, apúntate a spinning anda!

Al grupo de espeleología de Tarragona, gracias: Ari, Dani, Cristina, Ángel, Estivill, Jordi (el presidente), Javi, Oscar y Xavi.

A Nuria y Jaime otra familia.

Ai miei amici di Firenze, Fidenti, Edo, Enrico, Giulia, Emina e la Jay.

A Martina, Chiara, Silvia, Andrea.

Alla mia famiglia tutta, vi amo follemente.

UNIVERSITAT ROVIRA I VIRGILI
A COMPUTATIONAL RE-ASSESSMENT OF SEXUAL DIMORPHISM IN THE HUMAN CRANIUM BEYOND TRADITIONAL MORPHOMETRICS: GEOMETRIC MORPHOMETRIC METHODS AND NEURAL NETWORK ANALYSIS
Antonietta Del Bove

UNIVERSITAT ROVIRA I VIRGILI
A COMPUTATIONAL RE-ASSESSMENT OF SEXUAL DIMORPHISM IN THE HUMAN CRANIUM BEYOND TRADITIONAL MORPHOMETRICS: GEOMETRIC MORPHOMETRIC METHODS AND NEURAL NETWORK ANALYSIS
Antonietta Del Bove

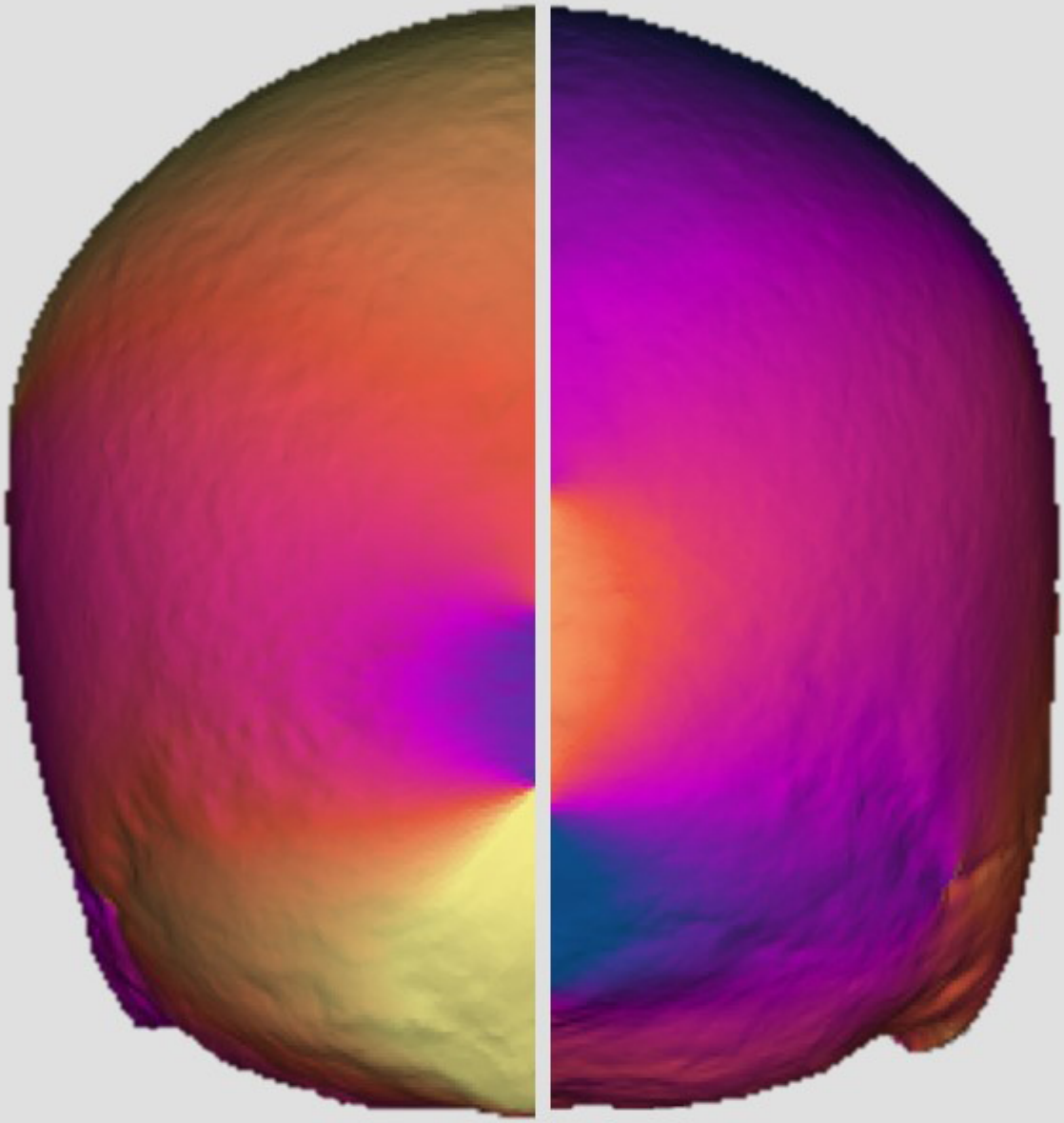

UNIVERSITAT ROVIRA i VIRGILI

IPHES
Institut Català de Paleoecologia Humana i Evolució Social